



HAL
open science

Convective memory, and the role of cold pools

Maxime Colin

► **To cite this version:**

Maxime Colin. Convective memory, and the role of cold pools. Meteorology. Sorbonne Université, 2018. English. NNT: 2018SORUS312 . tel-02864797

HAL Id: tel-02864797

<https://theses.hal.science/tel-02864797>

Submitted on 11 Jun 2020

HAL is a multi-disciplinary open access archive for the deposit and dissemination of scientific research documents, whether they are published or not. The documents may come from teaching and research institutions in France or abroad, or from public or private research centers.

L'archive ouverte pluridisciplinaire **HAL**, est destinée au dépôt et à la diffusion de documents scientifiques de niveau recherche, publiés ou non, émanant des établissements d'enseignement et de recherche français ou étrangers, des laboratoires publics ou privés.

Convective memory, and the role of cold pools

Maxime Colin

Supervisor: Professor Steven Sherwood
Co-supervisors: Dr Sandrine Bony, Professor Jason Evans

A dissertation submitted in fulfilment
of the requirements for the degree of
Doctor of Philosophy



UNSW
AUSTRALIA



**SORBONNE
UNIVERSITÉ**
CRÉATEURS DE FUTURS
DEPUIS 1257

**Climate Change Research Centre
and ARC Centre of Excellence for Climate System Science
School of Biological, Earth and Environmental Sciences
Faculty of Science
The University of New South Wales**

in a cotutelle agreement with

**Laboratoire de Météorologie Dynamique - IPSL
Ecole Doctorale des Sciences de l'Environnement d'Ile-de-France
Université Pierre et Marie Curie, Sorbonne Université**

21 August 2018

PLEASE TYPE

THE UNIVERSITY OF NEW SOUTH WALES
Thesis/Dissertation Sheet

Surname or Family name: COLIN

First name: MAXIME

Other name/s: JULIEN

Abbreviation for degree as given in the University calendar:
Doctor or Philosophy (PhD)

School: School of Biological, Earth and Environmental Sciences

Faculty: Faculty of Science

Title: Convective memory, and the role of cold pools

Abstract 350 words maximum: (PLEASE TYPE)

Convective parameterizations struggle to represent the spatial and temporal variability of convection. This may be because they wrongly assume that convection can be diagnosed from the large-scale state, without knowing the convective history. The concept of convective memory, which states that convection depends on its own history, could be used to overcome this issue. This thesis proposes a new framework for convective memory, with a distinction between microstate (unresolved) memory and macrostate (large-scale) memory.

The thesis uses a hierarchy of models either in Radiative-Convective Equilibrium or under fixed-macrostate conditions, and analyses the recovery to homogenisation perturbations. It exploits three types of models: a Cloud-Resolving Model, a General Circulation Model (GCM) in 1D and in 3D, and a simple predator-prey model.

The results show that convective memory plays a role on time scales between an hour and a day. Convective memory in time is dramatically enhanced by convective organisation in space. Microstate memory is found to be mostly stored in boundary layer microstate structures of water vapour and temperature, with a dominant water vapour memory. Furthermore, the convective microstate is shown to be inherently unstable, which confirms that knowledge of the macrostate conditions is not sufficient to predict convection. The standard version of the GCM already shows a reasonable level of convective persistence. A simple modification of the GCM convection scheme, meant to improve cold pools over oceans, improves some aspects of memory but deteriorates others. With this modification, the GCM cold pools become less cold and thus weaker to trigger convection. This leads to more intermittent precipitation, partly correcting a typical GCM bias.

Overall the thesis fosters the idea of introducing prognostic variables into GCMs and suggests ways to do it. It reveals the potential of microstate memory to improve GCM large-scale properties.

Declaration relating to disposition of project thesis/dissertation

I hereby grant to the University of New South Wales or its agents the right to archive and to make available my thesis or dissertation in whole or in part in the University libraries in all forms of media, now or here after known, subject to the provisions of the Copyright Act 1968. I retain all property rights, such as patent rights. I also retain the right to use in future works (such as articles or books) all or part of this thesis or dissertation.

I also authorise University Microfilms to use the 350 word abstract of my thesis in Dissertation Abstracts International (this is applicable to doctoral theses only).

Maxime Colin

Lianmei Jiang

28/08/2018

.....
Signature

.....
Witness Signature

.....
Date

The University recognises that there may be exceptional circumstances requiring restrictions on copying or conditions on use. Requests for restriction for a period of up to 2 years must be made in writing. Requests for a longer period of restriction may be considered in exceptional circumstances and require the approval of the Dean of Graduate Research.

FOR OFFICE USE ONLY

Date of completion of requirements for Award:



UNSW
AUSTRALIA



SORBONNE
UNIVERSITÉ
CRÉATEURS DE FUTURS
DEPUIS 1257



ARC CENTRE OF EXCELLENCE FOR
CLIMATE SYSTEM SCIENCE



UNIVERSITY OF NEW SOUTH WALES
en cotutelle avec SORBONNE UNIVERSITÉ

École doctorale des Sciences de l'Environnement d'Ile-de-France

Climate Change Research Centre and
ARC Centre of Excellence for Climate System Science

Laboratoire de Météorologie Dynamique - IPSL

La mémoire de la convection, et le rôle des poches froides

Convective memory, and the role of cold pools

Maxime COLIN

Thèse de doctorat en Sciences de la Météorologie et du Climat
Dirigée par Steven Sherwood et Sandrine Bony

Présentée et soutenue le 15 Novembre 2018

Devant un jury composé de :

Mme. Laurence PICON	Professeur, LMD-UPMC	Président du Jury
M. Jean-Philippe LAFORE	Senior Scientist, Météo-France	Rapporteur
M. Robert PLANT	Associate Professor, University of Reading	Rapporteur
M. Kerry EMANUEL	Professor, MIT	Examineur
M. Jean-Yves GRANDPEIX	Chercheur émérite CNRS, LMD-UPMC	Co-Directeur de thèse
M. Jason EVANS	Professor, UNSW	Co-Directeur de thèse
Mme. Sandrine BONY	Directeur de recherche CNRS, LMD-UPMC	Directeur de thèse
M. Steven SHERWOOD	Professor, UNSW	Directeur de thèse

ORIGINALITY STATEMENT

'I hereby declare that this submission is my own work and to the best of my knowledge it contains no materials previously published or written by another person, or substantial proportions of material which have been accepted for the award of any other degree or diploma at UNSW or any other educational institution, except where due acknowledgement is made in the thesis. Any contribution made to the research by others, with whom I have worked at UNSW or elsewhere, is explicitly acknowledged in the thesis. I also declare that the intellectual content of this thesis is the product of my own work, except to the extent that assistance from others in the project's design and conception or in style, presentation and linguistic expression is acknowledged.'

Signed Maxime Colin

Date 28/08/2018

INCLUSION OF PUBLICATIONS STATEMENT

UNSW is supportive of candidates publishing their research results during their candidature as detailed in the UNSW Thesis Examination Procedure.

Publications can be used in their thesis in lieu of a Chapter if:

- The student contributed greater than 50% of the content in the publication and is the “primary author”, ie. the student was responsible primarily for the planning, execution and preparation of the work for publication
- The student has approval to include the publication in their thesis in lieu of a Chapter from their supervisor and Postgraduate Coordinator.
- The publication is not subject to any obligations or contractual agreements with a third party that would constrain its inclusion in the thesis


Please indicate whether this thesis contains published material or not.

- This thesis contains no publications, either published or submitted for publication (if this box is checked, you may delete all the material on page 2)*
- Some of the work described in this thesis has been published and it has been documented in the relevant Chapters with acknowledgement (if this box is checked, you may delete all the material on page 2)*
- This thesis has publications (either published or submitted for publication) incorporated into it in lieu of a chapter and the details are presented below*

CANDIDATE'S DECLARATION

I declare that:

- I have complied with the Thesis Examination Procedure
- where I have used a publication in lieu of a Chapter, the listed publication(s) below meet(s) the requirements to be included in the thesis.

Name	Signature	Date (dd/mm/yy)
Maxime Colin		31/07/2018

Postgraduate Coordinator's Declaration (to be filled in where publications are used in lieu of Chapters)

I declare that:

- the information below is accurate
- where listed publication(s) have been used in lieu of Chapter(s), their use complies with the Thesis Examination Procedure
- the minimum requirements for the format of the thesis have been met.

PGC's Name	PGC's Signature	Date (dd/mm/yy)



Figure 1 Picture of organised deep convective clouds, with visible rain shafts, over the ocean. This is the kind of convective system we aim to study. Credit: Alphacoders



Figure 2 Picture of a diverse population of clouds over the Warm Pool in the tropical Pacific: shallow clouds, congestus clouds, cirrus clouds. A deep convective cloud under wind shear condition can even be seen on the top-right-hand corner. This epitomizes one of the main challenges for a convective parameterization: how to represent such a wide population of clouds, each with their own life cycle? Photo by Maxime Colin.

Introductory poems

L'Étranger, by Charles Baudelaire

in *Petits Poèmes en prose*,

from “*Œuvres complètes de Charles Baudelaire*, Michel Lévy frères, 1869, IV. Petits Poèmes en prose, Les Paradis artificiels (p. 7).”

- Qui aimes-tu le mieux, homme énigmatique, dis ? ton père, ta mère, ta sœur ou ton frère ?
- Je n'ai ni père, ni mère, ni sœur, ni frère.
- Tes amis ?
- Vous vous servez là d'une parole dont le sens m'est resté jusqu'à ce jour inconnu.
- Ta patrie ?
- J'ignore sous quelle latitude elle est située.
- La beauté ?
- Je l'aimerais volontiers, déesse et immortelle.
- L'or ?
- Je le hais comme vous haïssez Dieu.
- Eh ! qu'aimes-tu donc, extraordinaire étranger ?
- J'aime les nuages... les nuages qui passent... là-bas... les merveilleux nuages !

Series of short quotes

“Clouds come floating into my life, no longer to carry rain or usher storm, but to add color to my sunset sky.” Rabindranath Tagore, Indian polymath from Kolkata, late 19th and early 20th centuries. Verse 292, *Stray Birds*, 1916.

“Try to be a rainbow in someone’s cloud.” Maya Angelou, American poet.

“Clouds in the sky very much resemble[s] the thoughts in our minds! Both change[s] perpetually from one second to another!” Mehmet Murat ildan, Contemporary Turkish writer.

“Behind every cloud is another cloud.” Judy Garland, American actress and singer, who played in *The Wizard of Oz*.

“Clouds are on top for a reason. They float so high because they refuse to carry any burden!” Jasleen Kaur Gumber, Young Indian poet.

“I planted my self in the middle of a great many Glasses full of Dew, tied fast about me, upon which the Sun so violently darted his Rays, that the Heat, which attracted them, as it does the thickest Clouds, carried me up so high, that at length I found my self above the middle Region of the Air.” Cyrano de Bergerac, French playwright from the 17th century, in *A Voyage to the Moon*.

Clouds in Chinese poetry

1. 樂府

《出塞》王之渙： “Going far away”, by Wáng Zhihuàn
黃河遠上白雲間， Far up the yellow river lies in between white clouds
一片孤城萬仞山。 A lonely city with 10 000 mountains.
羌笛何須怨楊柳？ Why do you have to blame the willow?
春風不渡玉門關。 The spring breeze does not blow in Jade Gate Gorge.

《關山月》李白：
明月出天山，
蒼茫雲海間。
長風幾萬里，
吹度玉門關。
漢下白登道，
胡窺青海灣。
由來征戰地，
不見有人還。
戍客望邊色，
思歸多苦顏。
高樓當此夜，
歎息未應閒。

《送友人》李白：
青山橫北郭，
白水繞東城。
此地一為別，
孤蓬萬里征。
浮雲遊子意，
落日故人情。
揮手自茲去，
蕭蕭班馬鳴。

2. 五言絕句

《終南望餘雪》祖詠：
終南陰嶺秀，
積雪浮雲端。
林表明霽色，
城中增暮寒。

《尋隱者不遇》 賈島：
松下問童子，
言師採藥去。
只在此山中，
雲深不知處。

3.五言律詩

《終南山》 王維：
太乙近天都，
連山到海隅。
白雲迴望合，
青靄入看無。
分野中峰變，
陰晴衆壑殊。
欲投人處宿，
隔水問樵夫。

《夜泊牛渚懷古》 李白：
牛渚西江夜，
青天無片雲。
登舟望秋月，
空憶謝將軍。
余亦能高詠，
斯人不可聞。
明朝掛帆去，
楓葉落紛紛。

<https://tw.answers.yahoo.com/question/index?qid=20060927000011KK00448&p=%E9%9B%B2%20%E8%A9%A9%20%E4%B8%AD%E6%96%87>

Relevant Publications and Presentations

The following publications and presentations have been developed over the course of writing this thesis.

Publications

- Maxime Colin, Steven Sherwood, Olivier Geoffroy, Sandrine Bony, David Fuchs (2018). Identifying the sources of convective memory in cloud-resolving simulations. *Journal of the Atmospheric Sciences* (revised manuscript submitted)
- Maxime Colin, Jean-Yves Grandpeix, Sandrine Bony, Steven Sherwood. Impact of cold pools on the intermittence of precipitation in a General Circulation Model. *Journal of Advances in Modeling Earth Systems* (in prep)

Presentations

- November 2014: Hunter Valley, Australia. **Poster**. ARCCSS Annual workshop.
- May 2015: Melbourne, Australia. **Talk**. ARCCSS Convection workshop.
- July 2015: Brisbane, Australia. **Talk**. AMOS Conference.
- November 2015: Paris, France. **Talk**. Young Physicist Annual Meeting (RJP)

-
- January 2016: Toulouse, France. **Talk.** Atmospheric Modelling workshop (DEPHY2).
 - February 2016: Berlin, Germany. **Poster.** High-Definition Cloud and Precipitation for advancing Climate Prediction (HD(CP)2) conference.
 - June 2016: Paris, France. **Talk.** Atmospheric Modelling workshop (DEPHY2).
 - November 2016: Lorne, Australia. **Invited talk and poster.** ARCCSS Annual workshop.
 - July 2017: Delft, The Netherlands. **Talk and poster.** The future of cumulus parametrisation workshop.
 - November 2017: Sydney, Australia. **Talk.** WRF Workshop.
 - February 2018: Sydney, Australia. **Lightning lecture and poster.** AMOS-ICSHMO conference.
 - February 2018: Lorne, Australia. **Presentation given by S. Sherwood on my behalf.** Pan-GASS conference.
 - June 2018: Melbourne, Australia. **Presentation.** ARCCSS Convection workshop.

Acknowledgements

This joint “cotutelle” PhD has been an exciting and challenging journey, and I would like to thank all those who contributed to my scientific and personal development, those who supported me when progress was slow, those who provided technical, scientific, personal assistance, those who made me feel welcome and happy in various places, and those who made sure I kept practising sports and joining other activities.

Most importantly, I am deeply grateful to Steven Sherwood for taking me along for this journey, for suggesting such a stimulating research topic, for providing guidance and ideas throughout the project, and for funding my scholarship. He has been fantastic at supporting me, and I have tremendously enjoyed working with him both for scientific and personal reasons. Meanwhile, I would like to deeply thank Sandrine Bony for immediately accepting the joint PhD idea, for the many scientific discussions during my stay at LMD, for providing insightful comments and suggesting alternative approaches, and for always being very supportive. Both Steven Sherwood and Sandrine Bony have been inexhaustible sources of ideas, in particular for the methodologies and the result interpretations, and their logical and physical criticisms have been very helpful to draw more refined conclusions. Their kindness has been very much appreciated. I feel privileged that I had the opportunity to work with both of them. Jean-Yves Grandpeix has been of the greatest assistance, in particular to set up and to analyse the work with LMDZ and to challenge my thinking countless times. I am thankful for the time he spent to help me through the PhD, and for his discerning eye. I would also like to thank Jason Evans for always being available for me when I needed it, in particular to discuss WRF setups and general planning.

All along the PhD, my thesis committees have been particularly supportive and

helpful, so special thanks go to Katrin Meissner, Matt England, Donna Green, Andrea Taschetto, Romain Roehrig, Steven Phipps, and Alex Sen Gupta. I would like to express my deepest gratitude to Angela Maharaj for giving me a few opportunities to teach, and many opportunities to take part in outreach activities, which I keep unforgettable memories from.

Given my interest for debate on a wide range of topics, I would like to thank Olivier Geoffroy, Vishal Dixit, Alain Lahellec, Bao Jiawei, and others, for many endless discussions not only about science, but about geopolitics, languages, culture, environmental issues, and societal issues as well. I thank them for fantastic knowledge exchange, and for wonderful moments of logics, wisdom, creativity, problem re-framing, and sometimes solution proposals.

Life in Sydney has been utterly happy and colourful thanks to Vishal Dixit, Bao Jiawei, Olivier Geoffroy, Steefan Contractor, Steven Sherwood, Katrin Meissner, Matt England, Alejandro Di Luca, Margot Bador, Ryan Holmes, Swa Rath, Laurie Menviel, Gab Abramowitz, Angela Maharaj, Alex Sen Gupta, Esteban Abellan Villardon, Oliver Angelil, Nadja Herger, Laurence Garcia-Villada, Peter Gibson, Kaitlin Naughten, Willem Huiskamp, Nick Herold, Shirley Qin, Joe Scutt Phillips, Amandine Schaeffer, Nidhi Nishant, David Fuchs, Abhnil Prasad, Damianos Mantzis, Daniel Hernández-Deckers, Jason Evans, Donna Green, Lisa Alexander, Chris Turney, Melissa Hart, Martin Jucker, Zoë Thomas, Anna Ukkola, Chris Bull, Mat Lipson, Markus Donat, Jatin Kala, Nicola Maher, Acacia Pepler, Jules Katjar, Sarah Perkins-Kirkpatrick, Paul Spence, Martin De Kauwe, Veronique Lago, Earl Duran, Sanaa Hobeichi, Li Yue, Liu Yiling, Tamas Loughran, Helen Millman, Marco Kulüke, Steffie Ypma, the rest of the CCRC team, the UNSW International House friends from 2010, 2015, and 2017, and many others. Life in Paris was as amazing and fun and I would like to thank Binta Diallo, Karine Marquois, Venance Journé, Marie-Pierre Lefebvre, Geneviève Sèze, Ehouarn Millour, Sofia Protopapadaki, Martin Turbet, Jean-Yves Grandpeix, Alain Lahellec, Caroline Muller, Frédéric Hourdin, Jean-Louis Dufresne, Michel Capderou, François Forget, Jean-Baptiste Madeleine, Claudia Stubenrauch, Sandrine Bony, Li Shan, Florentin Lemonnier, Sylvain Lasseonde, Tanguy Bertrand, Maxence Lefevre, Lluís Fita Borrell, Margaux Vals, Wang Fuxing, David Coppin, Aymeric Spiga, Ionela Musat, Camille Risi, Artem Feofilov,

Vladimir Zakharov, and many others.

The admin and professional staff were fantastic at putting science on a smooth trajectory, so I would also like to thank Bronwen Smith, Swa Rath, Stephen Gray, Simone Purdon, Chris Cannon, Vilia Co, Karine Marquois, Martine Maherou, Franck Guyon and all others.

I am grateful to Catherine and Didier Goubert who kindly offered me to stay at their house during my time at LMD, which was extremely helpful and warmed up my heart. I also acknowledge all friends and family, including Mélanie Jambeau, Pierre Gégout, Li Jhih-Huang, Zhang Yu-Ju, Amy Lin, Abeer Mahendroo, Emily Uni Nogeh, Lloyd Fournier, Soheil Salimi, and Jiang Lianmei. I also feel indebted to all friends with who I played tennis, did ocean swims, runs, hikes, played badminton, etc. . .

People who put me on this life track deserve a special mention. Bernard Legras was my unofficial mentor and role model, and I am deeply grateful that he initiated my passion for climate and weather science, and that he nurtured it. I will always be obligated to him. Jean-Philippe Duvel, Valerian Jewtoukoff, and Amy Lin have also been crucial in that regard.

Special thanks also go to Koo Moduk for providing fantastic poems about clouds from French and Korean literature. Likewise, many thanks to all my friends who have kept my thirst for languages active and fulfilled at the same time.

Finally, I would like to thank the Centre of Excellence (ARCCSS) for providing support, career development opportunities, and funding for travels and conferences. I extend my thanks to the WCRP, Michel Rixen, Christian Jakob, Steven Sherwood, and the team of scientists around them, who allowed me to join the 1st WCRP Summer School on Climate Model Development “Atmospheric Moist Processes”. It is undoubtedly one of the best memories of my PhD: I had the chance to meet prestigious scientists as well as young scientists from around the world, to build many new international friendships, and to learn some of the bases about climate model development.

Since I cannot mention everyone here, I would like to thank all others that are close

to my heart.

Abstract

Convective parameterizations struggle to represent the spatial and temporal variability of convection. This may be because they wrongly assume that convection can be diagnosed from the large-scale state, without knowing the convective history. The concept of convective memory, which states that convection depends on its own history, could be used to overcome this issue. This thesis proposes a new framework for convective memory, with a distinction between microstate (unresolved) memory and macrostate (large-scale) memory.

The thesis uses a hierarchy of models either in Radiative-Convective Equilibrium or under fixed-macrostate conditions, and analyses the recovery to homogenisation perturbations. It exploits three types of models: a Cloud-Resolving Model, a General Circulation Model (GCM) in 1D and in 3D, and a simple predator-prey model.

The results show that convective memory plays a role on time scales between an hour and a day. Convective memory in time is dramatically enhanced by convective organisation in space. Microstate memory is found to be mostly stored in boundary layer microstate structures of water vapour and temperature, with a dominant water vapour memory. Furthermore, the convective microstate is shown to be inherently unstable, which confirms that knowledge of the macrostate conditions is not sufficient to predict convection. The standard version of the GCM already shows a reasonable level of convective persistence. A simple modification of the GCM convection scheme, meant to improve cold pools over oceans, improves some aspects of memory but deteriorates others. With this modification, the GCM cold pools become less cold and thus weaker to trigger convection. This leads to more intermittent precipitation, partly correcting a typical GCM bias.

Overall the thesis fosters the idea of introducing prognostic variables into GCMs and suggests ways to do it. It reveals the potential of microstate memory to improve GCM large-scale properties.

Résumé

Les paramétrisations représentent encore mal la variabilité spatio-temporelle de la convection. Cela peut provenir du fait que les paramétrisations supposent, à tort, que la convection peut être diagnostiquée à partir des conditions de grande échelle. Le concept de mémoire de la convection, signifiant que la convection dépend de sa propre histoire, pourrait permettre de résoudre ce problème. Cette thèse propose un nouveau cadre d'étude faisant la distinction entre la mémoire micro-état (non résolue) et la mémoire macro-état (de grande échelle).

La thèse a recours à une hiérarchie de modèles: un modèle résolvant les nuages, un Modèle de Circulation Générale (GCM) en 1D et en 3D, et un modèle simple proie-prédateur. Ils sont placés soit en Equilibre Radiatif-Convectif soit en condition de macro-état fixé, et on analyse leur réponse à des perturbations d'homogénéisation.

La mémoire de la convection a un temps typique compris entre une heure et un jour, et elle apparaît fortement liée à l'organisation convective dans l'espace. La mémoire du micro-état est essentiellement stockée dans les structures micro-état de couche-limite de la vapeur d'eau et de la température, la mémoire de la vapeur d'eau étant dominante. De plus, le micro-état convectif est intrinsèquement instable, ce qui confirme que la connaissance de l'état de grande échelle n'est pas suffisante pour prédire la convection. On montre ensuite que le GCM de référence a déjà des formes encourageantes de mémoire. Par une modification simple du GCM, on améliore certains aspects de la mémoire, mais en détériore d'autres. Cette modification rend les poches froides moins froides et ainsi moins aptes à déclencher la convection. La pluie du GCM modifié devient ainsi plus intermittente, résolvant un biais typique des modèles.

Cette étude promeut l'introduction de variables pronostiques dans les GCMs pour représenter la mémoire du micro-état, permettant ainsi d'améliorer les propriétés de grande échelle des GCMs.

Contents

Abstract	xvii
Résumé	xix
1 Introduction	1
1.1 The nature of convection	1
1.1.1 What is convection?	1
1.1.2 Convective processes and structures	6
1.1.3 The role of deep convection in the water and energy cycles . .	10
1.2 Convection in General Circulation Models	11
1.2.1 The grand challenge of convection	11
1.2.2 Representation of convective processes by parameterizations of convection	11
1.2.3 Issues with convective parameterizations	14
1.2.4 Quasi-Equilibrium	16
1.3 The origins of the convective memory issue	22
1.3.1 The diagnostic assumption	22
1.3.2 The diagnostic assumption problem: why it may be inaccurate	24
1.3.3 Solution: a prognostic formulation	24
1.4 Convective memory	26
1.4.1 Definition	26
1.4.2 Memory vs Persistence	27
1.4.3 Three types of memory storage	27
1.4.4 Processes inducing convective memory	30
1.4.5 Examples of introduction of convective memory into GCMs . .	31

1.4.6	Time scales of convective memory	35
1.4.7	Simple models of memory	36
1.5	The relationship between memory and organisation	36
1.5.1	Why such a link?	36
1.5.2	Convection organisation and convective self-aggregation	39
1.5.3	The role of cold pools in organisation	43
1.5.4	Representation of cold pools in GCMs	46
1.5.5	Case of LMDZ: deep convection scheme, cold pool scheme, and thermal-plume scheme	48
1.6	Aim of the thesis	51
1.7	Overview of the thesis	52
2	Identifying the sources of convective memory	55
2.1	Abstract	55
2.2	Introduction	56
2.3	Methods	61
2.3.1	The simulations	61
2.3.2	Model and setup	63
2.3.3	Other simulation settings	65
2.3.4	Design of perturbation experiments	65
2.4	Supplementary information on the methods	67
2.4.1	Methods for the preliminary 2D tests	67
2.4.2	Methods for the 3D simulations	68
2.5	Exploration by 2D test simulations	70
2.5.1	Convective memory attributed to microstate structures	71
2.5.2	Which variables are the main sources of convective memory?	72
2.5.3	Role of convective self-aggregation in 2D	73
2.5.4	Uncertainty estimate for the 2D results	75
2.5.5	Sensitivity to the microphysical scheme	76
2.6	Results from 3D simulations	78
2.6.1	In which variables is convective memory stored?	78
2.6.2	Interpreting the response to homogenisation of temperature	83
2.6.3	Which layer of the atmosphere carries most memory?	85

2.6.4	Role of convective organisation	87
2.6.5	Negligible role of surface fluxes	88
2.6.6	Secondary response: a microstate-macrostate feedback	89
2.6.7	General caveats	91
2.6.8	Implications for parameterizations	93
2.6.9	Why does memory come from near the surface?	94
2.7	Supplementary results	95
2.7.1	Which layer of the atmosphere carries most memory?	95
2.7.2	Existence of structures vs detailed description of them	96
2.8	Supplementary discussion	98
2.8.1	RCE state and method validation	98
2.8.2	Role of perturbation scale	99
2.9	Conclusion	99
3	Isolating microstate memory: CRM & toy model	103
3.1	Introduction	103
3.2	Isolating the microstate memory in WRF	107
3.2.1	Method	107
3.2.2	Description of the instability that appears in the fixed-macrostate experiments in WRF: growth and decay	114
3.2.3	Mechanisms explaining the instability development	122
3.3	Stochastic toy model of convection with memory	131
3.3.1	Description of the toy model	131
3.3.2	Analytical analysis of the toy model	142
3.3.3	Numerical integration of the toy model: RCE runs	149
3.3.4	Oscillations in the free RCE experiments	150
3.3.5	The stochastic toy model reproduces well the key memory aspect of the CRM	152
3.3.6	Interpretation of the CRM instability to fixed macrostate ex- periments by a Markov chain	156
3.4	Conclusion	162
4	Comparing convective memory in GCM and CRM	167

4.1	Introduction	167
4.2	Presentation of LMDZ	168
4.2.1	Overview of the cold pool scheme in the LMDZ model	168
4.2.2	Potential sources of memory in LMDZ: key variables and parameters	170
4.3	Preliminary experiments on cold pool parameters	171
4.4	Methods	176
4.5	Does LMDZ have the same sources of memory as WRF?	177
4.6	Does modified LMDZ have the same memory sources?	184
4.7	Conclusion	190
5	Cold pools and precipitation intermittence	193
5.1	Introduction	193
5.2	Methods	197
5.2.1	Overview of the cold pool scheme in the LMDZ model	197
5.2.2	Experimental approach with the LMDZ 1D and 3D simulations	198
5.3	Results	199
5.3.1	Insights on cold pool properties from a Cloud-Resolving Model simulation over ocean	199
5.3.2	Comparison with the cold pools over land	201
5.3.3	Sensitivity of cold pool thermodynamic and dynamic properties to cold pool number density in 1-D LMDZ	202
5.3.4	Sensitivity of the cold pool - convection interaction to cold pool number density in 1-D LMDZ	204
5.3.5	Higher precipitation frequency over oceans with a higher cold pool number density in 3-D LMDZ	207
5.4	Conclusion	216
6	Conclusion	219
6.1	Summary	219
6.2	Implications	223
6.2.1	Understanding of convection	223
6.2.2	Development of GCM convective parameterizations	223

6.2.3	Extended meaning of memory	225
6.3	Limitations	226
6.4	Future work	228
6.4.1	Need for observations	228
6.4.2	Need for high-resolution simulations	229
6.4.3	Need for low-resolution climate simulations	230
6.4.4	Need for theoretical framework, and simplified models	232
6.5	Final words: what to remember?	234
	Bibliography	237
	Appendices	259
	A Defining convective memory	259
A.1	Several ways of defining convective memory	259
A.2	A statistical definition of convective memory	261
	B Exploring convective self-aggregation with various WRF setups: what controls self-aggregation?	263
	C Statistics of water vapour, in particular for the transformation from dry to humid states	267
	D Table of homogenisation experiments performed in WRF	275

List of Figures

- 1 Picture of organised deep convective clouds, with visible rain shafts, over the ocean. This is the kind of convective system we aim to study. Credit: Alphacoders vi
- 2 Picture of a diverse population of clouds over the Warm Pool in the tropical Pacific: shallow clouds, congestus clouds, cirrus clouds. A deep convective cloud under wind shear condition can even be seen on the top-right-hand corner. This epitomizes one of the main challenges for a convective parameterization: how to represent such a wide population of clouds, each with their own life cycle? Photo by Maxime Colin. vi
- 1.1 Rayleigh-Benard convection, with a fluid placed between two plates, the bottom plate being maintained at a higher temperature than the top plate. Convection spontaneously appear in the fluid when the temperature difference between the two plates is large enough, with the convective cells being spatially organised, a clockwise cell alternating with a counter-clockwise one. From <https://www.mis.mpg.de/applan/research/rayl>
- 1.2 (left) Experimental setup for Benard-Marangoni convection, with energy transfers symbolised by red arrows (for high energy transfer) and cold arrows (for low energy transfer). Motion is the fluid organises as convective cells. From <https://www.esrl.noaa.gov/psd/outreach/education/science/con>
(right) Image representing the hexagonal patterns observed from the free top in the Benard-Marangoni experiment. From Wikipedia. . . . 4

LIST OF FIGURES

1.3	Perfectly symmetric cumulonimbus surrounded by its army of lower clouds. These lower clouds become increasingly higher as they are located closer to the cumulonimbus itself. We can also see the anvil around cloud top, as well as the cloud overshoot. From http://tpevolavoile.e-monsite.com/pages/meteo/cumulonimbus.html	5
1.4	Schematic of the basic convective processes occurring in deep convective clouds. From <i>Arakawa</i> [2004].	6
1.5	Schematic of the different structures appearing in a deep convective cloud (cumulonimbus): updraft, downdraft, and cold pool. The updraft and the detrained air are embodied by the red arrows, the downdraft is represented by the blue arrows, and the cold pool boundary is shown by the blue curve with blue triangles near the surface. The cold pool edge is located near the updraft location, because of their interplay. From UCAR and NOAA National Weather Service.	9
1.6	Schematic of vertical mass flux and entrainment of environmental air into a rising cloud. This particular schematic is the three-layer model representing tropical cyclone development which was developed by <i>Ooyama</i> [1969]. Figure from <i>Arakawa</i> [2004].	13
1.7	Schematics of the three repositories of convective memory (in red): the microstate, the macrostate and the synoptic state. A few key processes are added in blue: convection and solar radiation. The impact of one element on another is symbolised by a black arrow. The green dotted line separates the elements that we will not be able to simulate in a small domain model with periodic boundary conditions.	29
1.8	Convection scheme with prognostic organisation variable “org” as implemented by <i>Mapes and Neale</i> [2011]. Rain evaporation is a source for org, which then influences the width of the cloud (and therefore entrainment rate), and a few other variables. This positive feedback is a process that leads to convective memory. From <i>Mapes and Neale</i> [2011]	33
1.9	Photo of a squall line from Nebraska, United States. From <i>Business insider</i>	40

1.10	Schematic of four types of organised convection, for different wind shear profiles and consequently different dynamical regimes, entailing different qualitative transport of momentum. From <i>Miller and Moncrieff</i> [1983]	41
1.11	Cold pools over the tropical Indian ocean, as seen by the absence of reflectivity from radar observations, during the AMIE/DYNAMO field campaign. The cold pools are subjectively identified and marked by white dashed circles, at (a) 1100 UTC (b) 1130 UTC (c) 1200 UTC (d) 1230 UTC. The spatial scale is given by the concentric circles centred around the radar: there is one circle every 25 km. From <i>Feng et al.</i> [2015].	45
1.12	Schematic of upscale growth of convection due to cold pools, for different phases of the Madden-Julian Oscillation. New convection is triggered around cold pool edges, and this allows for convective organisation, and development of a Mesoscale Convective System (MCS). From <i>Rowe and Houze</i> [2015].	46
1.13	Representation of cold pools in a GCM grid cell, as seen from above, for the cold pool parameterization used in the LMDZ GCM. From <i>Grandpeix and Lafore</i> [2010].	49

2.1 Schematic of the three different types of memory that can emerge with respect to a mesoscale λ (which may be a finite model resolution, but also more generally any length scale). Limited resolution stems from the GCM grid cell (equivalent to a full CRM domain). (1) refers to synoptic state memory: it arises from processes that involve several GCM grid cells, such as synoptic-scale convergence/divergence, the Hadley circulation or Convective Instability of the Second Kind. (2) refers to macrostate memory: it arises from processes that impact the local profiles of a single GCM grid cell, i.e. the mean profiles of the full CRM box (for example the mean profiles of specific humidity and potential temperature). And (3) refers to microstate memory: it arises from GCM sub-grid scale processes, i.e. resolved CRM processes (for example rain evaporation, cold pools, secondary triggering of convection by cold pools, cloud entrainment, convergence under cloud base). Current GCMs resolve the synoptic state memory through circulation, and the macrostate memory through convective parameterization. However, they are generally blind to microstate memory. 59

2.2 Snapshots of Outgoing Longwave Radiation (OLR) in the domain, in the Radiative-Convective Equilibrium state, towards day 80 or 81 of the control runs, for three convective types with different convective organisation: (a) unorganised case, (b) wind shear organised case, with the wind shear being positive and along the x-axis, (c) self-aggregated case. 62

2.3 (left) Instantaneous snapshot of Outgoing Longwave Radiation (OLR) during the 90th day into the 3D control simulation, showing unorganised convection (right) Instantaneous vertical section of the 3D cloud fraction for the same simulation during the 90th day. Note that the y-axis is model levels, which are not linear with height nor pressure. 62

2.4	Horizontally-averaged equilibrium profiles for the 3D unorganised control simulation (3D-Ctrl) (see table D.1), computed on the last month of the simulation. (a) Relative Humidity. (b) Cloud fraction as defined on 3D grid cells. (c) Equivalent potential temperature.	63
2.5	Time series of horizontally-averaged precipitable water (PW), for the 3D "normal" control simulation. Statistical equilibrium seems to be reached after 30-40 days, so that afterwards, the atmosphere is in Radiative-Convective Equilibrium (RCE) state.	69
2.6	Schematic of the perturbations added in the model during restart: horizontal homogenisation of some variables at an instantaneous (pseudo-initial) time.	70
2.7	Time series of horizontally-averaged precipitation rate for different 2D Control and "Maximum effects" experiments (see table D.4), for the first 24h after restart. These results have been averaged over an 18-member ensemble of 2D simulations with warm rain microphysics (Kessler scheme), with members selected only when convection was considered clearly disorganised.	72
2.8	Response of horizontally-averaged precipitation rate after homogenisation and model restart, for the "Additional impact to base" 2D experiments (see table D.4). (left) and (right) respectively show ensemble averages over 9 and 18 members. (left) With the warm rain (Kessler) microphysics scheme, where there was clear convective organisation. (right) With the warm rain (Kessler) microphysics scheme, where there was no convective organisation.	73
2.9	Organised and disorganised convection in the 2D control simulation with warm rain microphysics (Kessler scheme). (a) Instantaneous vertical section of water vapour mixing ratio at the 31st day, showing a dry and a humid region. (b) Hovmuller plot of Outgoing Long-wave Radiation (OLR) during the organised phase (35th day). (c) Hovmuller plot of OLR during the disorganised phase (60th day). . .	74

2.10 Time series of the horizontal standard deviation of precipitable water (PW), for the 2D control simulation with warm rain microphysics (Kessler scheme). The standard deviation of PW is a measure of convective organisation. There is an increase in convective organisation up to day 30, followed by a decrease. So we can split the simulation between the most organised days and the least organised days. 75

2.11 Response of horizontally-averaged precipitation rate after homogenisation and model restart, for the "Single set" 2D experiments (see table D.4). (left), (middle) and (right) respectively show ensemble averages over 5, 9 and 18 members. (left) With the normal (WSM6) microphysics scheme used in this study, in which there was no particular convective organisation. (middle) With the warm rain (Kessler) microphysics scheme, when there was clear convective organisation. (right) With the warm rain (Kessler) microphysics scheme, when there was no convective organisation. 75

2.12 Same as Figure 2.11 (middle), but with error bars. The error bars were computed as the standard error of the mean, based on the ensemble of several members we have for each plotted line. 76

2.13 Same as Figure 2.14(a) but with a measure of the uncertainty. The standard error of the mean, for each type of homogenisation, is represented by lighter colors as the width of the lines representing the ensemble mean by darker colors. In practice, the standard error of the mean is smaller than the thickness of the lines, so that it is subtle to distinguish. This shows high statistical significance. 79

2.14	Response of horizontally-averaged precipitation rate after homogenisation and model restart, for the control run and for experiments on a single variable; colors indicate different experiments, and the legend indicates the variable homogenised in each experiment (see table 2.1). These are ensemble averages over 19 or 20 members. The panels represent experiments conducted on different convective types: (a) unorganised convection, (b) convection organised by wind shear, (c) self-aggregated convection. The peak precipitation rate following homogenisation of temperature in the self-aggregated case (off scale) is 32 mm/day.	80
2.15	Same as Figure 2.14 but for the first 24 h after homogenisation instead of 6 h.	80
2.16	Snapshots of the OLR response to various homogenisation in the unorganised case. (a) Control run. (b) Water vapour homogenisation. (c) Potential temperature homogenisation. (d) Water vapour and potential temperature homogenisation. Time flows from top to bottom: at $t = 0, 1 \text{ h}, 3 \text{ h}$ after homogenisation.	81
2.17	Same as Figure 2.16 but for the wind shear organised case. Time flows from top to bottom: at $t = 0, 1 \text{ h}, 3 \text{ h}, 6 \text{ h}$ after homogenisation.	82
2.18	Same as Figure 2.16 but for the self-aggregated case. Time flows from top to bottom: at $t = 0, 1 \text{ h}, 3 \text{ h}, 6 \text{ h}, 12 \text{ h}$, and about 24 h after homogenisation.	83
2.19	Response of horizontally-averaged precipitation rate after homogenisation and model restart, for the control run and for experiments on a double set of variables (dashed), compared to the single-variable temperature and humidity results (solid). Different experiments are indicated by different colors (see legend and Table 2.1). These are ensemble averages over 19 or 20 members. The panels represent experiments conducted on different convective types: (a) unorganised convection, (b) convection organised by wind shear, (c) self-aggregated convection.	84

LIST OF FIGURES

2.20 Same as Figure 2.19 but for the first 24 h after homogenisation instead of 6 h. 84

2.21 Response of micro-scale structures, for different 3-D experiments in the unorganised convection case. Different experiments are indicated by different colors (see legend and Table 2.1). Both panels show ensemble averages for 19 members. (a) Sub-cloud layer average of the horizontal standard deviation of Moist Static Energy (MSE). (b) Horizontal standard deviation of Moist Static Energy (MSE) at 500hPa. 85

2.22 Response of horizontally-averaged precipitation rate after homogenisation and model restart, for the control run and for experiments on specific layers only: homogenisation before the restart is conducted over different atmospheric layers: sub-cloud layer (surface-940hPa), mid layer (940hPa-700hPa), high layer (700hPa-tropopause). Different experiments are indicated by different colors (see legend and Table 2.1). These are ensemble averages over 19 or 20 members. Different panels represent experiments conducted on different convective types: (a) unorganised convection, (b) convection organised by wind shear, (c) self-aggregated convection. 86

2.23 Same as Figure 2.22 but for the first 6 h after homogenisation instead of 24 h. 86

2.24 With fixed surface fluxes. Response of horizontally-averaged precipitation rate after homogenisation and model restart, for different 3D experiments (see table D.1). These are ensemble averages over 8 members, for control, blank, and single set experiments. 89

- 2.25 Response after homogenisation of variables given by the legend (colors, see Table 2.1) and model restart, on longer time scale (24 h), for unorganised convection. These are ensemble averages over 19 members. The response of different variables is presented: (a) Horizontal average of precipitation rate, (b) Horizontal average of CAPE, (c) Horizontal average of MSE at 500 hPa, (d) Standard deviation of MSE at 500 hPa, (e) Horizontal average of the total wind at 500 hPa, (f) Standard deviation of the total wind at 500 hPa. As shown by the legend, the lines show the control run (black), single set homogenisation experiments on water vapour, potential temperature, winds, hydrometeors (respectively green, red, dark blue, orange), and a double set homogenisation experiment on water vapour and potential temperature together (dashed cyan). The total wind is computed as the amplitude of the 3D wind vector. The standard deviation of the total wind is very similar to the Convective Kinetic Energy (CKE). CAPE and MSE respectively stand for Convective Available Potential Energy and Moist Static Energy. Note that here CKE refers to the CKE defined at each point by the velocities resolved by the CRM, which is different from the parameterized sub-grid TKE used by the CRM. . . . 90
- 2.26 With Thompson microphysics, but a very small domain (31 km * 31 km), so that convection is not very organised (almost unorganised). Response of horizontally-averaged precipitation rate after homogenisation and model restart, for different 3D experiments (see table D.1). These are ensemble averages over 22 members. For homogenisation of control, and (a) single set experiments, (b) double set experiments. 92
- 2.27 Response of horizontally-averaged precipitation rate after homogenisation and model restart, for different 3D experiments performed by layers (see table D.2) in the unorganised case. Homogenisation before the restart is conducted over different atmospheric layers: sub-cloud layer (surface-940hPa), mid layer (940hPa-700hPa), high layer (700hPa-tropopause). All panels show ensemble averages over 8 members. For homogenisation of (left) q_v and θ (middle) q_v (right) θ . . . 95

2.28 Response of horizontally-averaged precipitation rate after homogenisation and model restart, for different 3D experiments performed by layers and on specific points only (see table D.3) in the unorganised case. Homogenisation before the restart is conducted over the sub-cloud layer (surface-940hPa), and over specific areas only: where values are above the horizontal mean (without touching values below the mean), or when values are below the horizontal mean (without touching values above the mean). All panels show ensemble averages over 8 members. For homogenisation of (left) q_v and θ (middle) q_v (right) θ 97

3.1 Response after homogenisation and model restart on a time scale of 24 h, for different experiments where different variables have been homogenised, for unorganized convection. The variables homogenised are given by the legend (colors, see table 2.1). These are ensemble averages over 19 members. The response of different variables is presented: (a) Horizontal average of precipitation rate, (b) Horizontal average of CAPE, (c) Horizontal average of MSE at 500 hPa, (d) Horizontal average of MSE in the sub-cloud layer, (e) Horizontal average of the total wind at 500 hPa, (f) Horizontal average of temperature in the subcloud layer. As shown by the legend, the lines show the control run (black), single set homogenization experiments on water vapor, potential temperature, winds, hydrometeors (respectively green, red, dark blue, orange), and a double set homogenization experiment on water vapor and potential temperature together (dashed cyan). The total wind is computed as the amplitude of the 3D wind vector. CAPE and MSE respectively stand for Convective Available Potential Energy and Moist Static Energy. 104

3.2	Vertical profiles of water vapour mixing ratio, for different simulations: (a) With homogenisation of water vapour and temperature (HOMOG EXP) (b) Control (c) For the difference HOMOG EXP minus CONTROL. The black lines correspond to the average for the first 24 h after homogenisation and restart. The red lines correspond to the average over the first 3 h after homogenisation and restart, while the blue lines correspond to the last 3 h of the first 24 h after homogenisation.	105
3.3	Same as 3.2 but for temperature instead of water vapour mixing ratio	105
3.4	Same as 3.2 but for relative humidity instead of water vapour mixing ratio	106
3.5	Same as 3.2 but for cloud fraction instead of water vapour mixing ratio	106
3.6	Extract of the implementation of the strong nudging method in WRF code	110
3.7	Two major behaviours of simulations with strong nudging for different initial conditions: (1) instability growth up to an unphysical and highly convective state, and (2) a slow decay of convection up to a quiet state with no convection.	114
3.8	Snapshots of Outgoing Long-wave Radiation (OLR) in a simulation with strong nudging which developed an instability. Each panel corresponds to a different time into the simulation after we started to apply the strong nudging method: (a) 0 h, output=0 (b) 2.5 h, output=10 (c) 5 h, output=20 (d) 7.25 h, output=29 (e) 8 h, output=32 (f) 8.75 h, output=35 (g) 9.5 h, output=38 (h) 10.25 h, output=41 (i) 12.5 h, output=50 (j) 15 h, output=60 (k) 17.5 h, output=70 (l) 20 h, output=80. Blue corresponds to high clouds (low OLR) and red to the surface (high OLR).	115

3.9 Vertical cross-section snapshots of cloud fraction (a,c,e,g) and U wind (b,d,f,h) in the same unstable simulation as figure 3.8. Note that this shows the 3-D cloud fraction, and that U wind is the wind along the horizontal x-axis. Each panel corresponds to a different time into the simulation after we started to apply the strong nudging method: (a,b) 0 h, output=0 (c,d) 7.5 h, output=30 (e,f) 10 h, output=40 (g,h) 20 h, output=80. 116

3.10 Time series comparing the control simulation without strong nudging (blue) and with strong nudging, i.e., the same unstable control simulation as figure 3.8 (red). (a) Domain-mean Precipitable Water (b) Domain-mean relative humidity at 500 hPa (c) Domain-mean potential temperature at model level number 30 (about 500 hPa). The red curves only start from day 61, when strong nudging is activated. The blue curves show RCE fluctuations. 117

3.11 Time series and vertical profiles of the control simulation with strong nudging which developed an instability (same unstable simulation as figure 3.8), during the first day of simulation after we started to apply the strong nudging method. (a) Time series of the domain-mean Precipitable Water (b) Time series of the domain-mean rain rate (c) Domain-mean temperature profiles (d) Time series of domain-mean OLR (e) Domain-mean total (short-wave + long-wave) radiative heating profiles (f) Domain-mean relative humidity profiles (g) Time series of the horizontal standard deviation of Precipitable Water (h) Time series of domain-mean 500 hPa temperature (i) Domain-mean 3-D cloud fraction as a function of time and model level. 119

3.12	Vertical profiles of water vapour mixing ratio, for different cases: (a) The target to be imposed by the strong nudging method (b) The control simulation with strong nudging (same unstable simulation as figure 3.8) (c) For the difference (b)-(a). The black lines correspond to the average for the first 24 h after strong nudging activation. The red lines correspond to the average over the first 3 h after strong nudging activation, while the blue lines correspond to the last 3 h of the first 24 h after activation.	120
3.13	Same as figure 3.12 but for relative humidity	120
3.14	Same as figure 3.12 but for potential temperature	121
3.15	Same as figure 3.12 but for total pressure	121
3.16	Vertical profiles of (a) water vapour mixing ratio (b) relative humidity (c) temperature, for: (left) The target to be imposed by the strong nudging method (middle) The control simulation with strong nudging (same unstable simulation as Figure 3.8), at time $t=8.75$ h after strong nudging activation (right) The difference (middle)-(left) between the control simulation at $t=8.75$ h and the target.	123
3.17	Same as Figure 3.16, but for (a) potential temperature (b) total pressure.	124
3.18	Vertical profiles of the difference between a variable and its strong nudging target, at different times of the control simulation with strong nudging (same unstable simulation as Figure 3.8). Time evolves in each panel from left to right: 6 h, 8 h, 10h, 12 h after strong nudging activation. The variable anomaly presented are (a) water vapour mixing ratio (b) relative humidity (c) temperature (d) potential temperature (e) total pressure.	125

LIST OF FIGURES

3.19 Time series of different variables (as indicated by legend), rescaled to evolve from 0 to 1 throughout 1 day of the control simulation with strong nudging (same unstable simulation as Figure 3.8). If a variable v was originally decreasing with time, we plot $1-v$ so that it can be compared with the other variables. The solid lines refer to standard deviations (microstate, std) and the dotted lines refer to domain averages (macrostate, ave). Different colours stand for different variables. $T_{500\text{hPa}}$ is the temperature at 500 hPa, MSE_{subcloud} is the Moist Static Energy in the sub-cloud layer, PW is the Precipitable Water, $CAPE$ is the Convective Available Potential Energy, T_2 is the 2-metre temperature, $W_{700\text{hPa}}$ is the vertical velocity at 700 hPa. 127

3.20 Same as Figure 3.19 but zoomed between 4 h and 10 h after strong nudging activation. 128

3.21 Same as Figure 3.19 but for different variables (as indicated by legend). CIN is Convective Inhibition, OLR is Outgoing Longwave Radiation, vel_{1st_lay} is the velocity in the lowest model layer, THF is the total surface heat flux (latent + sensible), Q_2 is the 2-metre humidity, and T_2 is the 2-metre temperature. 129

3.22 (left) Normalised PDF of the additive stochastic term in the V equation (right) Normalised PDF of the multiplicative stochastic term in the P equation. 134

3.23 Schematic of the physics behind the toy model: the atmospheric humidity represented by a single variable r has a source term, evaporation E_0 (denoted by E here), and a sink term, precipitation P . The key variable in this model is the variance V , representing the microstate turbulence or microstate variability/heterogeneity. 134

-
- 3.24 Responses of (left) P, (middle) r, and (right) V, for the toy model under usual RCE conditions, i.e, without strong nudging (“Free” runs). The top row presents the first 25 time units after homogenisation, and the bottom row the first 400 time units. The black line shows the RCE time series if no homogenisation is performed (Control), the blue line shows the time series after homogenisation (V=0). All simulations have been done with $\alpha_{damp} = 0.3$. Plots show the ensemble average over 100 members. 150
- 3.25 Responses of P to homogenisation in the toy model under RCE conditions, i.e, without strong nudging (“Free” runs). (a) For a toy model in the default configuration. (b) For a toy model where all stochastic terms have been turned off. Each row is for a different value of α_{damp} , from 0.1 at the top to 0.9 at the bottom. The black line shows the RCE time series if no homogenisation is performed (Control), the blue line shows the time series after homogenisation (V=0). Plots show the ensemble average over 1000 members. 151
- 3.26 Same as Figure 3.25 but with the spread between ensemble members added in gray, relative to the ensemble average in blue. (a) For a toy model in the default configuration except that the RCE state was computed over 1000 time units instead of 200. (b) For a toy model in which the stochastic terms were calculated in an alternative way (each member having a different stochastic time series), and in which the RCE state was also computed over 1000 time units instead of 200. 153
- 3.27 Comparisons of the responses to homogenisation of different variables in WRF (top row, see chapter 2) and in the toy model (bottom row). (left) Precipitation rate, (middle) Horizontally-averaged water vapour mixing ratio in the sub-cloud layer (humidity macrostate), (left) Standard deviation of water vapour mixing ratio in the sub-cloud layer (humidity microstate). The black line shows the response if no homogenisation is performed (Control, RCE state), the blue line shows the response after homogenisation (V=0 in the toy model, homogenisation of potential temperature and water vapour in WRF). 154

3.28 Same as Figure 3.27, but for different variables in WRF to be compared to the toy model’s r and V : (left) Precipitation rate, (middle) Horizontally-averaged CAPE (CAPE macrostate), and (right) Standard deviation of CAPE (CAPE microstate). In the WRF plots, additional lines have been left where different variable subsets are homogenised (see legend). It is still the homogenisation of both potential temperature and water vapour that compares best to the toy model. 155

3.29 Same as Figure 3.24 but for a toy model under fixed-macrostate conditions (“strong nudging” runs). The top row presents the first 25 time units after homogenisation, and the bottom row the first 800 time units. The black line shows the RCE time series if no homogenisation is performed (Control) and with free macrostate; the blue line shows the time series after homogenisation ($V=0$) and under fixed-macrostate conditions. Stochastic terms are activated, and plots show the ensemble average over 1000 members. 157

3.30 Same as Figure 3.25 but for a toy model under fixed-macrostate conditions (“strong nudging” runs). (left) For a toy model in the default configuration. (right) For a toy model where all stochastic terms have been turned off. 158

3.31 Same as Figure 3.26 but for a toy model under fixed-macrostate conditions (“strong nudging” runs). (left) For a toy model in the default configuration. (right) For a toy model in which the stochastic terms were calculated in an alternative way (each member having a different stochastic time series), and in which the RCE state was also computed over 1000 time units instead of 200. 160

3.32 Schematic representation of the toy model equations as a combination of positive and negative feedbacks, depending on the term sign on the right-hand side of the equations. (top) For the “free” runs, i.e., without strong nudging. (bottom) For the “nudged” runs, i.e., with strong nudging. In a toy model with strong nudging, one negative feedback has been removed, allowing for instability to occur. 161

-
- 4.1 Impact of the gravity wave parameter (which acts to damp cold pools) on several variables. (a) Available Lifting Power (ALP, related to convective intensity) for different values of the multiplicative factor to the gravity wave parameter (1 means default, 100 means 100 times greater). Red is for ALP due to cold pools, blue is for ALP due to thermals, and green is the total ALP (sum of the ALP due to each). (b) Convective heating profiles (excluding cold pools) for different values of the multiplicative factor to the gravity wave parameter. Colours (see legend) indicate the value of the multiplicative factor (yellow means high value). The horizontal lines indicate the Lifting Condensation Level. (c) Same as (b) but for the cold pool heating profile. 172
- 4.2 Impact of the upper bound parameter for cold pool fractional surface area on several variables. (a) Vertical profiles of cold pool temperature anomaly. Colours (see legend) indicate the value of the cold pool fractional area upper bound (red means small, purple means large) (b) Same as (a) but for the vertical profiles of cold pool humidity anomaly. (c) Available Lifting Energy (ALE, related to convective triggering) for different values of the cold pool fractional area upper bound. Red is for ALE due to cold pools, blue is for ALE due to thermals. (d) Same as (c) but for Available Lifting Power (ALP, related to convective intensity). Green is for the total ALP. At the bottom, cartoons show the meaning of low, default and high cold pool fractional area upper bound, viewed from the top and with cold pools being blue. 173
- 4.3 Impact of the 1D simulation grid area on several variables. (a) Time series of the precipitable water for the 90 days of simulation (spin-up then RCE).(b) Time series of the cold pool fractional surface area, for the first 50 hours of the simulation. Colours (see legend) indicate the value of the grid area (red means small, purple means large). . . . 175

- 4.4 Responses of precipitation rate to different types of initial homogenisation (see colours and legend: control (black), no homogenisation (grey), temperature homogenisation (red), water vapour homogenisation (green), both water vapour and temperature homogenisation (light blue), wind homogenisation (dark blue), condensate homogenisation (orange)). (a) In the CRM, for the first 6 h after homogenisation (as in Figure 2.14(a) but modified to include the response to homogenisation of both temperature and humidity, and the response to a blank restart with no homogenisation at all). (b) In the CRM, for the first 24 h after homogenisation (as in Figure 2.25(a)). (c) In the SCM, for the first 6 h after homogenisation. (d) In the SCM, for the first 24 h after homogenisation. (e) In the predator-prey model, for what seems equivalent to the first 6 h after homogenisation (as in Figure 3.25(a)). The CRM responses are averaged over 19 members, the GCM ones over 60 members, and the predator-prey model ones over 1000 members. 178
- 4.5 Responses of different cold pool properties (microstate) in the SCM to different types of initial homogenisation (colours and legend: see Figure 4.4). (a) Cold pool temperature anomaly, with high frequency output (every 5 min), for the first 6 h after homogenisation. (b) Same as (a) but for the first 24 h after homogenisation. (c) Same as (b) but with hourly output. (d) Cold pool humidity anomaly, with high frequency output, for the first 6 h after homogenisation. (e) Same as (d) but for the first 24 h after homogenisation. (f) Same as (e) but with hourly output. (g) Cold pool fractional surface area, with high frequency output, for the first 6 h after homogenisation. (h) Same as (g) but for the first 24 h after homogenisation. (i) Same as (h) but with hourly output. The responses are averaged over 60 members. For cold pool temperature and humidity anomalies, lines only show the time series at the first model level (near surface). 179

-
- 4.6 Responses of different macrostate variables in the SCM to different types of initial homogenisation (colours and legend: see Figure 4.4). (a) Precipitation rate, with high frequency output (every 5 min), for the first 6 h after homogenisation (as in Figure 4.4(c)). (b) Same as (a) but for the first 24 h after homogenisation (as in Figure 4.4(d)). (c) Same as (b) but with hourly output. (d) Available Lifting Power (convective intensity due to cold pools), with high frequency output, for the first 6 h after homogenisation. (e) Same as (d) but for the first 24 h after homogenisation. (f) Same as (e) but with hourly output. (g) Precipitable water, with high frequency output, for the first 6 h after homogenisation. (h) Same as (g) but for the first 24 h after homogenisation. (i) Same as (h) but with hourly output. The responses are averaged over 60 members. 180
- 4.7 Responses of precipitation rate (a,d,g), a typical macrostate variable (b,e,h), and a typical microstate variable (c,f,i), to different types of initial homogenisation (colours and legend: see Figure 4.4), for the first 6 h after homogenisation, in different models. (a) Precipitation rate in the CRM (as in Figure 4.4(a)). (b) Average of water vapour mixing ratio in the sub-cloud layer (macrostate), in the CRM. (c) Standard deviation of water vapour mixing ratio in the sub-cloud layer (microstate), in the CRM. (d) Precipitation rate in the SCM (as in Figure 4.4(c)). (e) Mean humidity (macrostate), at first model level, in the SCM. (f) Cold pool humidity anomaly (microstate), at first model level, in the SCM (as in Figure 4.5(d)). (g) Precipitation rate P in the predator-prey model. (h) Average humidity r (macrostate) in the predator-prey model. (i) Boundary-layer heterogeneity V (microstate) in the predator-prey model. The CRM responses are averaged over 19 members, the GCM ones over 60 members, and the predator-prey model ones over 100 members. The predator-prey model panels are reproduced from Figure 3.24. 181

4.8 Responses of precipitation rate to different types of initial homogenisation (colours and legend: see Figure 4.4). (a) In the CRM, for the first 6 h after homogenisation (as in Figure 4.4(a)). (b) In the CRM, for the first 24 h after homogenisation (as in Figure 4.4(b)). (c) In the SCM with default cold pool number density (D_{CP}), for the first 6 h (as in Figure 4.4(c)). (d) In the SCM with default D_{CP} , for the first 24 h (as in Figure 4.4(d)). (e) Same as (c), but for a SCM with D_{CP} 100 times greater than the default (f) Same as (d), but for a SCM with D_{CP} 100 times greater than the default (g) In the predator-prey model, for what seems equivalent to the first 6 h after homogenisation (as in Figure 4.4(e)). The CRM responses are averaged over 19 members, the GCM ones over 60 members, and the predator-prey model ones over 1000 members. 185

4.9 Responses of different microstate (or cold pool) properties to different types of initial homogenisation (colours and legend: see Figure 4.4), in the CRM (a,b), in the default SCM (c,d,e) and in the modified SCM (f,g,h), for the first 6 h after homogenisation. (a) Standard deviation of temperature in the sub-cloud layer in the CRM, to be compared to (c) and (f). (b) Standard deviation of water vapour in the sub-cloud layer in the CRM, to be compared to (d) and (g) (as in Figure 4.7(c)). (c) Cold pool temperature anomaly (in absolute value) in the default SCM (as in Figure 4.5(a) but in absolute value). (d) Cold pool humidity anomaly in the default SCM (as in Figure 4.5(d)). (e) Cold pool fractional surface area in the default SCM (as in Figure 4.5(g)). (f) Same as (c) but for the modified SCM. (g) Same as (d) but for the modified SCM. (h) Same as (e) but for the modified SCM. The responses are averaged over 19 members for the CRM, over 60 members for the SCM. We use high frequency output (every 5 min). For cold pool temperature and humidity anomalies, lines only show the time series at the first model level (near surface). 186

4.10 Responses of different macrostate variables to different types of initial homogenisation (colours and legend: see Figure 4.4), in the CRM (a,b,c), in the default SCM (d,e,f) and in the modified SCM (g,h,i), for the first 6 h after homogenisation. (a) Precipitation rate in the CRM, to be compared to (d) and (g) (as in Figure 4.4(a)). (b) Mean Convective Available Potential Energy (CAPE) in the CRM, to be compared to (e) and (h). (c) Mean Precipitable Water, in the CRM. (d) Convective precipitation in the default SCM (as in Figure 4.4(c)). (e) CAPE in the default SCM. (f) Precipitable Water in the default SCM (as in Figure 4.6(g)). (g) Same as (d) but for the modified SCM. (h) Same as (e) but for the modified SCM. (i) Same as (f) but for the modified SCM. The responses are averaged over 19 members for the CRM, over 60 members for the SCM. We use high frequency output (every 5 min).	187
---	-----

4.11 Responses of precipitation rate (a,d,g,j), a typical macrostate variable (b,e,h,k), and a typical microstate variable (c,f,i,l) to different types of initial homogenisation (colours and legend: see Figure 4.4), in the CRM (a,b,c), in the default SCM (d,e,f), in the modified SCM (g,h,i), and in the predator-prey model (j,k,l), for the first 6 h after homogenisation. (a) Precipitation rate in the CRM. (b) Mean water vapour mixing ratio in the sub-cloud layer (macrostate), in the CRM. (c) Standard deviation of water vapour mixing ratio in the sub-cloud layer (microstate), in the CRM. (d) Precipitation rate in the default SCM. (e) Mean humidity (macrostate) in the default SCM. (f) Cold pool humidity anomaly (microstate), at first model level, in the default SCM. (g) Same as (d) but for the modified SCM. (h) Same as (e) but for the modified SCM. (i) Same as (f) but for the modified SCM. (j) Precipitation rate P in the predator-prey model. (k) Mean humidity r (macrostate) in the predator-prey model. (l) Boundary-layer heterogeneity V (microstate) in the predator-prey model. The responses are averaged over 19 members for the CRM, over 60 members for the SCM, and over 100 members for the predator-prey model. We use high frequency output (every 5 min). Panels (a,b,c,d,e,f,j,k,l) are all taken from Figure 4.7. 188

4.12 Same as Figure 4.11 but for the first 24 h after homogenisation, and without the last three plots on the predator-prey model. 189

- 5.1 Snapshots of cold pools in a CRM simulation in Radiative-Convective Equilibrium. (a) Vertical cross-section of water vapour mixing ratio (kg/kg), in an (x,z) plane. (b) Vertical cross-section of potential temperature anomaly (K) compared to a fixed 300 K value, in an (x,z) plane. (c) View from the top of the potential temperature averaged in the sub-cloud layer, in an (x,y) plane, which allows to visualise the horizontal distribution of cold pools. (d) Same as (a) but zoomed over the region where cold pools are the strongest. (e) Same as (b) but zoomed over the region where cold pools are the strongest. x_0 denotes the x-axis location of a cold pool at its apex. The red zig-zag in (c) denotes the y-axis location of the vertical cross-sections showed in (a),(b),(d),(e). The vertical black lines in (d),(e) denote the x-axis boundaries of two particular strong cold pools in the cross-sections presented here. 200
- 5.2 Sensitivity of cold pool properties to the cold pool number density. (a) Vertical profiles of cold pool temperature anomaly for simulations where the “splitting” option is deactivated. (b) Vertical profiles of cold pool humidity anomaly for simulations where the “splitting” option is deactivated. (c) Same as (a) but with the “splitting” option activated. (d) Same as (b) but with the “splitting” option activated. The cold pool number density is denoted by `wdens`, shown by the colours, and values are given in the legend (red related to sparse cold pools, i.e. low cold pool number density, and purple to numerous cold pools, i.e. high cold pool number density), relatively to the default value which is written `wdens_ref`. On the right-hand side, cartoons show the meaning of low, medium and high cold pool number density, viewed from the top and with cold pools being blue. 203

5.3 Sensitivity of the impact of cold pool on convection to the cold pool number density. (a) Available Lifting Energy (ALE, triggering) with respect to cold pool number density, with “splitting” option deactivated. (b) Available Lifting Power (ALP, closure) with respect to cold pool number density, with “splitting” option deactivated. (c) Same as (a) but with “splitting” option activated. (d) Same as (b) but with “splitting” option activated. Colours refer to ALE or ALP due to cold pools (red), to thermals (blue) and to the association of both cold pools and thermals eventually seen by the convection scheme (green), as per the legend. The cold pool number density, denoted by w_{dens} , is shown on the x-axis as a multiplying coefficient with respect to the default value (the multiplying value is 1 for the default cold pool number density, and 100 when the cold pool number density is 100 times larger than its default value). At the bottom, cartoons show the meaning of low, medium and high cold pool number density viewed from the top and with blue cold pools. 205

5.4 Global maps of the number of convectively rainy days in a year (number of days in a year for which convective rain exceeds a threshold of 10^{-6} mm.day $^{-1} \approx 4.10^{-8}$ mm.h $^{-1}$). Each map corresponds to a different value of the cold pool number density: (a) 10 times less than default (b) default (c) 10 times more than default (d) 100 times more than default (e) 250 times more than default. 208

5.5 Similar maps as Figure 5.4 but expressed as a difference to the default. Maps show the difference between (1) the number of convectively rainy days in a year for the cold pool number density used in a given experiment, and (2) the number of convectively rainy days for the default cold pool number density. Cold pool number density in the experiment is (a) 10 times less than default (b) 10 times more than default (c) 100 times more than default (d) 250 times more than default. 209

5.6 Same maps as Figure 5.4 but for the amount of convective precipitation. 210

5.7	Same maps as Figure 5.4 but for the difference between the triggering energy of cold pools and the triggering energy of boundary layer thermals ($ALE_{wk} - ALE_{bl}$), showing which sub-cloud process dominates the triggering between cold pools and thermals.	210
5.8	Same maps as Figure 5.4 but for the cold pool surface area fraction (surface occupied by cold pools in each grid cell, capped at a maximum of 0.4 by LMDZ scheme)	211
5.9	Same maps as Figure 5.4 but for the number of days with total precipitation (convective + stratiform)	211
5.10	Same maps as Figure 5.4 but for the amount of total precipitation (convective + stratiform)	212
5.11	Annual mean of the percentage time precipitation occurs above a given threshold of 0.02 mm/h in observations at 0.25° spatial resolution for (left) daily data (right) hourly data. Adapted from Figure 4 in <i>Trenberth and Zhang</i> [2018].	213
5.12	Observed global distribution of the frequency of occurrence of precipitation with an approximate 2° resolution. Adapted from Figure 6d in <i>Stephens et al.</i> [2010].	213
5.13	Mean JJA precipitation frequency (%) for light precipitation (1-10 mm/day), from daily data, from gridded GTS (Global Telecommunications System) observations (b) on a 1° grid (c) on a 3° grid. Adapted from Figure 3 in <i>Sun et al.</i> [2006].	214
5.14	Same as in Figure 5.13 but for the frequency (%) of heavy precipitation (> 10 mm/day). Adapted from Figure 4 in <i>Sun et al.</i> [2006].	214
5.15	Same as in Figure 5.13 but for the number of rainy days contributing to 67% of the annual precipitation. Adapted from Figure 8 in <i>Sun et al.</i> [2006].	214

- 5.16 Time series of convective rain, for different values of cold pool number density: either the default (top, (a),(b),(c),(d)) or 100 times the default (bottom, (e),(f),(g),(h)). These plots are taken for either an Eastern tropical Pacific location, -110° longitude and 12° latitude (left, (a),(b),(e),(f)) or a Western tropical Pacific location, 150° longitude and 5° latitude (right, (c),(d),(g),(h)). There are two different time periods: either over a month, 4 Dec 1984 to 3 Jan 1985 ((a),(c),(e),(g)) or over a year, 4 Dec 1984 to 3 Dec 1985 ((b),(d),(f),(h)). 215
- 6.1 Schematics of the meaning of microstate memory and macrostate memory for (a) a parameterization which only has macrostate memory (b) a parameterization which has both microstate memory and macrostate memory. These two schematics are presented as an evolution of the quasi-equilibrium schematic presented in *Arakawa [2004]*'s figure 7 to incorporate convective memory. The x-axis is the lapse rate, the y-axis is the relative humidity of the boundary layer, and A is the cloud work function. $A > 0$ means the atmosphere is conditionally stable, and $A < 0$ conditionally unstable. The large-scale forcings at $t-1$ and at t are represented by green arrows. The resulting instantaneous adjustments (based on quasi-equilibrium or not) are the blue arrows. Note that green and red arrows are considered as vectors, so that their initial point is not important. The red dot represents the current state of the system. In (a), the actual trajectory is following a weighted mean of the adjustments at t and at $t-1$, so the macrostate at $t-1$ is remembered, which gives the system some macrostate memory. In (b), the weighted mean of the adjustments at t and $t-1$ gives a tendency due to macrostate memory, but there is also a tendency due to microstate memory, since the system now has some microstate inertia and tends to follow the tangent to its trajectory in the phase space. In this case, the actual trajectory followed by the system is the combination of both macrostate tendency and microstate tendency, as represented by the composition of the two vectors. 235

-
- B.1 Table of various WRF setups and their impact on self-aggregation. Each setup (each row) is defined by its grid spacing, domain size, Sea Surface Temperature (SST), turbulence scheme, microphysical scheme, as specified by the columns. The impact on convective organisation is (1) measured by two Outgoing Longwave Radiation (OLR) snapshots on the right-hand side: after 21 days of simulation, and after 39 days, and (2) summarised by a subjective comment in the last column. The two OLR snapshots for each setup are placed in staggered rows, either slightly more to the right, or slightly more to the left: the results for each setup are always horizontally aligned. Green highlighting shows the reference unorganised setup used in the whole thesis (e.g. Chapter 2). Red or blue highlighting indicates changes to this reference setup. Yellow highlighting indicates the most aggregated setup. 265
- C.1 PDFs of water vapour fields at different pressure levels (different panels), for all instants when the horizontal mean is higher than the 90th percentile (red) or lower than the 10th percentile (green) of the time series (based on the last 50 days of RCE unorganised control run). The vertical solid red (resp. green) lines indicate the minimum and maximum values of the water vapour fields when the mean is higher than the 90th percentile (resp. when the mean is lower than the 10th percentile). The vertical dotted red (resp. green) lines show the value of the 90th percentile (resp. 10th percentile) of the time series of horizontal mean water vapour (in practice they are almost co-located). The scales on the x-axis (water vapour range) and y-axis (normalised PDF) are different in each panel. 270
- C.2 PDFs of water vapour fields at different pressure levels, based on the last 50 days of RCE unorganised control run. The red and green PDFs are the same as on Figure C.1. The blue PDF is calculated on the time series of the horizontal mean water vapour mixing ratio at that pressure level. The horizontal mean does not vary much with time compared to the spatial variations. 271

C.3 Difference between the two PDFs of water vapour mixing ratio field, calculated for all instants when the horizontal mean is higher than the 90th percentile on the one hand, and when the horizontal mean is lower than the 10th percentile on the other hand, at different pressure levels (based on the last 50 days of RCE unorganised control run). In other words, it is the difference between the red and the green PDFs from Figure C.1. The number of bins we choose to compute the PDFs influences somewhat the amount of noise that appears. 272

C.4 Transformation function $dq_vapour(q)$ to go from the relatively "dry" states (x,y,t variations for a mean value <10 th percentile) to the relatively "humid" states (x,y,t variations for a mean value >90 th percentile). The x,y,t variations were used to build two single-dimension ordered lists, one for the dry states and one for the humid states. dq_vapour represents the difference between the humid ordered list and the dry ordered list of points. The x-axis q is the mean water vapour mixing ratio between the values in the two ordered lists. This was done at different pressure levels (different panels). The colours indicate the PDF of the x-axis, so that the density of points in the scatter plots becomes obvious. Thus, the transformation function is just an abstract representation of a shift from an equilibrated 2D dry state to an equilibrated 2D humid state. 273

List of Tables

- 2.1 List of variables averaged in the homogenisation experiments. The model is restarted from different horizontally homogenised conditions of combinations of these variables. q_c, q_r, q_i, q_s, q_g respectively refer to the mixing ratios of cloud liquid water, rain, ice, snow and graupel. . . . 66
- D.1 List of homogenisation experiments performed in 3D on different variables: "single" set impact and "double" set impact. The model is restarted from different horizontally homogenised conditions. 275
- D.2 List of 3D homogenisation experiments performed by layers. The sub-cloud layer corresponds to the layer between the surface and 940hPa (600m). Mid layer refers to the layer between 940hPa and 700hPa. And high layer refers to the layer between 700hPa and the tropopause. 276
- D.3 List of 3D homogenisation experiments on layers performed on specific areas of the domain. When homogenisation is performed only *below* the mean values: the horizontal mean is computed for each variable, at each vertical level, and only the values *below* the mean are averaged out together, values *above* the mean are left untouched. When homogenisation is performed only *above* the mean values, the same process applies but on values *above* each horizontal mean. . . . 276
- D.4 List of homogenisation experiments performed in 2D. The model is restarted from different horizontally homogenised conditions. 277

Chapter 1

Introduction

1.1 The nature of convection

1.1.1 What is convection?

Defining convection is already a challenge: it has different meanings in different fields. Firstly, the widest definition for convection given by physicists in fluid mechanics is perhaps the following: the general motion of a fluid due to the collective effect of all the movements of its molecules. In this view, convection is seen as one of the three basic mode of energy transfer, alongside thermal conduction (diffusion) and radiation. Sometimes, convection refers more to the transport of energy by the general motion of a fluid rather than to the motion of the fluid itself. In some cases, convection is even taken to include any motion of the fluid, whether it is a bulk motion (advection) or the motion of individual particles (diffusion), so that it includes two of the three previously mentioned modes of energy transfer. Secondly, in thermodynamics, convection may have a stricter meaning: the general motion of a fluid due to a gradient of temperature or a gradient of other properties of the fluid. This is somewhat similar to the general definition proposed by *Emanuel* [1994] which states that convection is the ensemble of motions resulting from the action of a steady gravitational field upon variations of density in a fluid. Thirdly, in meteorology and other geosciences, the meaning of convection is restricted even further to the vertical motion of a fluid, usually associated with gradients of density or temper-

ature. In the rest of the manuscript, convection will refer to the "collective" vertical motions of the air, where the term "collective" can refer to any scale, as long as it includes a large number of fluid molecules. Most of the time, the scale of convection will be taken as the scale of clouds, excluding some smaller-scale convection (such as laboratory-scale convection) and some larger-scale convection (such as the Hadley cell).

Convection bears an interesting contradiction: it is based on very simple physical laws, yet it is responsible for acute complexity in fluid dynamics and thermodynamics. So let us start with one of the most typical examples of convection: Rayleigh-Benard convection [*Bergé and Dubois*, 1984]. Rayleigh-Benard convection is the buoyancy-driven flow that occur in a horizontal fluid layer heated from below and cooled from above. The usual experimental setup is such that the fluid is placed between two plates maintained at fixed temperatures, with the temperature of the bottom plate being higher than the temperature of the top plate. Below a critical temperature difference, the energy transfer is done by heat diffusion, and there is no convection. Above a critical temperature difference (or adimensional number called Rayleigh number), convection occurs, the fluid has a general motion carrying energy from the bottom to the top, with a spatial organisation into rolls or cells (see figure 1.1). When there is no cold top plate and cooling is done by the air, these convective cells tend to self-organise as polygons (usually hexagons): in this case one talks about Benard-Marangoni convection (figure 1.2). In the typical setup with two plates, the size of the cells, and the velocity in the fluid is related to the temperature difference imposed by the two plates as boundary conditions. Further discussions in light of atmospheric science are presented in *Emanuel* [1997].

In atmospheric science, dry convection is the first illustration of convection, and is also the closest to Rayleigh-Benard convection. Dry convection means there is no phase change of water involved in the air motion, so no clouds. Dry convection is usually observed in the lower part of the atmosphere, that is in the atmospheric boundary layer, and gives birth to boundary layer thermals, and what is called "dry turbulence" in meteorology and aviation. With dry convection, the first law of thermodynamics only involves work against the pressure forces for expansion, and heat from external sources (e.g., radiation). When there is no water vapour, the

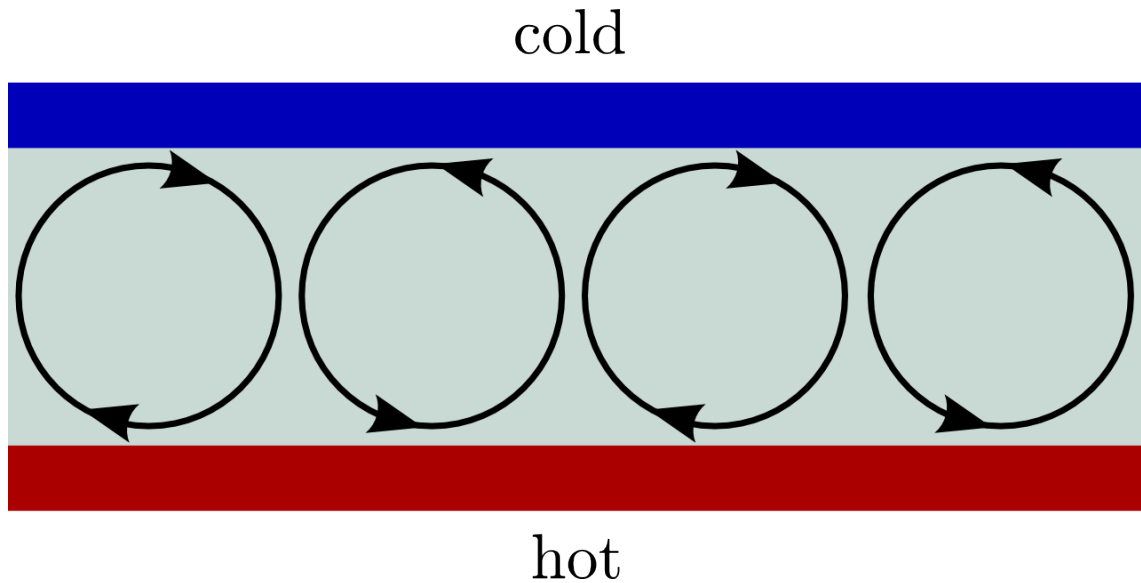


Figure 1.1 Rayleigh-Benard convection, with a fluid placed between two plates, the bottom plate being maintained at a higher temperature than the top plate. Convection spontaneously appear in the fluid when the temperature difference between the two plates is large enough, with the convective cells being spatially organised, a clockwise cell alternating with a counter-clockwise one. From <https://www.mis.mpg.de/applan/research/rayleigh.html>

conserved variable is potential temperature, defined in equation 1.1. When there is water vapour (but still without phase change), the same potential temperature is only approximately conserved, and one may prefer to use a different and more accurate formula for the conserved variable (potential temperature in the humid case). In the case without any water vapour, potential temperature reads:

$$\theta = T \left(\frac{p_0}{p} \right)^{\frac{R_d}{c_P}} \quad (1.1)$$

with T the temperature, p the pressure, c_P the specific heat of air at constant pressure per unit of mass, R_d the gas constant for dry air, and $p_0 = 1000$ hPa a reference pressure.

Since convection is made up of vertical movements, pressure decreases exponentially with height, and water vapour is ubiquitous in the atmosphere, water phase changes are often involved in convective processes: this is moist convection. When some air is less dense than its environment, it moves upward according to Archimedes' principle, carrying water vapour along. Along the upward motion, pressure drops, and at a certain height the air reaches the saturation water vapour pressure: the water vapour starts to condense, thus releasing latent heat, and modi-

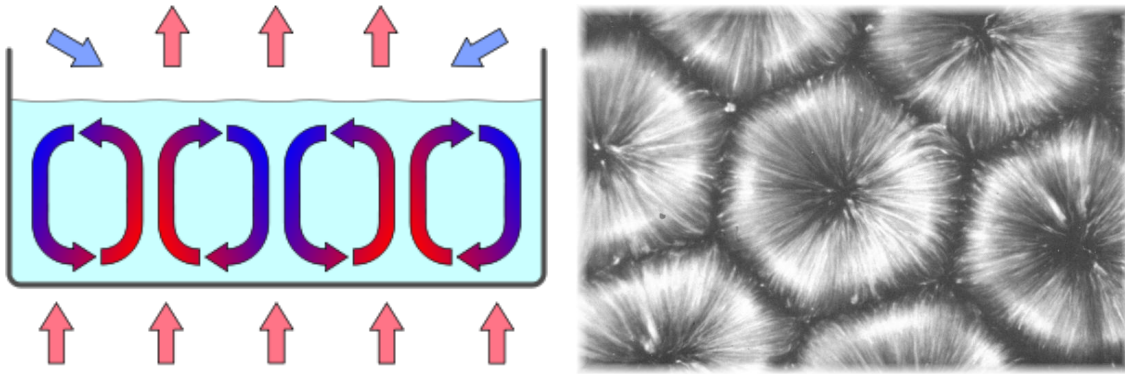


Figure 1.2 (left) Experimental setup for Benard-Marangoni convection, with energy transfers symbolised by red arrows (for high energy transfer) and cold arrows (for low energy transfer). Motion is the fluid organises as convective cells. From <https://www.esrl.noaa.gov/psd/outreach/education/science/convection/RBCells.html> (right) Image representing the hexagonal patterns observed from the free top in the Benard-Marangoni experiment. From Wikipedia.

ifying the energy budget. The air becomes warmer and less dense than without water condensation, which modifies the motion itself. This positive feedback between density and motion, between thermodynamics and non-linear fluid dynamics, is one of the main reasons why moist convection is still an enigma. For moist convection, we have saturated adiabatic transformations, so the conserved variable is the equivalent potential temperature θ_e , which is defined by:

$$\theta_e = T \left(\frac{p_0}{p_d} \right)^{\frac{R_d}{c_{Pt}}} rh^{\frac{-q_v R_v}{c_{Pt}}} e^{\frac{q_v l_v}{c_{Pt} T}} \quad (1.2)$$

where T is the temperature of the parcel, p_d the partial pressure for the dry component of the air, c_{Pt} a specific heat at constant pressure taking into account dry air and water content, rh the relative humidity (water vapor content over saturated water vapor content), q_v the mixing ratio of water vapor (mass of water vapor per unit of mass of dry air), R_v the gas constant for water vapor (universal ideal gas constant over molar mass of water), l_v the latent heat of vaporization per unit of mass. See *Legras* [updated 2016] for derivations and explanations.

Moist convection is said to be shallow if it is limited to the lower free troposphere, that is if convection occurs only in the first 4 km of the atmosphere or so. In other words, shallow moist convection is associated with the formation of cumulus and stratocumulus clouds, but it excludes cumulonimbus. When convection reached

much higher in altitude, close to the tropopause, we talk about deep moist convection. Deep moist convection is associated with the formation of congestus (5-9 km) and cumulonimbus clouds (10-16 km). Deep convection is potentially more violent than shallow convection, since it is able to go higher, and generate larger clouds. In particular, deep convection will not only form liquid water, but it will also form ice particles: latent heat release is even higher, and given the large variety of condensate water particles, it is even more complicated to understand, model, and predict.



Figure 1.3 Perfectly symmetric cumulonimbus surrounded by its army of lower clouds. These lower clouds become increasingly higher as they are located closer to the cumulonimbus itself. We can also see the anvil around cloud top, as well as the cloud overshoot. From <http://tpevolavoile.e-monsite.com/pages/meteo/cumulonimbus.html>

Once convection is deep enough, it generates precipitation that is generally able to reach the surface: this is precipitating deep convection. Because precipitation reaches the surface, this kind of convection is important for humans, and it could even lead to potential risks, such as heavy storms, flooding, or precipitation-related winds. The microphysical processes involving ice and water particles leading to precipitation at ground level are numerous. They occur at very small scales ($\sim 2 \mu\text{m}$ to 2 mm) but they have a paramount influence at much larger scale (up to ~ 100 km). This also explains the inherent multi-scale multi-interaction nature of deep convection.

1.1.2 Convective processes and structures

In this thesis, we consider deep convection. It involves many processes and many convective structures, so that we only intend to present a highly simplified view of deep convection here. Even if this exercise is necessarily incomplete, we provide here a list of convective processes and structures. Note that this list would probably evolve in the future, since new concepts and new points of view on the convective processes are likely to be proposed. However, we hope that this incomplete list of key processes and structures contains most of the main ideas (see figure 1.4).

UNCERTAINTIES IN FORMULATING CLOUD AND ASSOCIATED PROCESSES

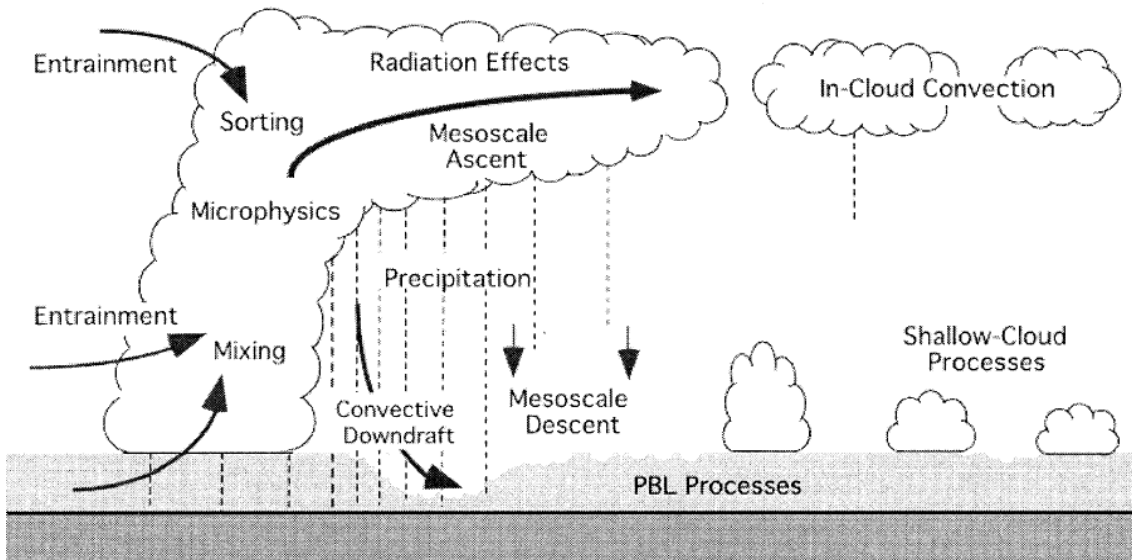


FIG. 2. Cloud and associated processes for which major uncertainties in formulation exist.

Figure 1.4 Schematic of the basic convective processes occurring in deep convective clouds. From *Arakawa* [2004].

The first structures to consider are related to the separation between the saturated part (clouds) and the unsaturated part of convection. The saturated part is made up of a spectrum of clouds of various depths and various heights: some clouds may have their base near the boundary layer top (e.g. cumulus, cumulus congestus, cumulonimbus), and some clouds may have their base higher aloft (e.g. the anvils produced by cumulonimbus clouds). Furthermore, the saturated part of convection is at least made up of updrafts and downdrafts. Precipitating downdrafts, which can be either saturated or unsaturated, are produced by the cooling resulting from evaporation of condensed water at first order and from fusion of ice particles at

second order.

The first main convective structure is the updraft. It is a volume of air that is moving higher up with the convective motion. It somehow amounts to the rising part of the Rayleigh-Benard cells. The updraft usually takes buoyant air from the surface or from the boundary layer, and brings it to the free troposphere, contributing to convective heating of the free troposphere and thus stabilisation of the vertical profile. Because they are carrying humid air upwards, updrafts are responsible for water vapour condensation, and consequently for creating convective clouds such as cumulus and cumulonimbus. Condensation of water vapour releases latent heat, which enhances the upward motion of the updraft. Because they are associated with cloud formation, and because they usually occur as early as the first stages of convection development, updrafts are always the first structure to consider to understand convection.

Updrafts are associated with mass convergence near their base, and with mass divergence near their top, though it might actually be a little more complicated. There is a direct link between the vertical motion (updraft) and the horizontal motion near the surface (mass convergence, i.e., horizontal convergence of mass flux). However, the direction of the causal link is not always clear: horizontal mass convergence can create an updraft, but an updraft generated by positive buoyancy can generate mass convergence as well. It is not always easy to disentangle which one is cause and which one is effect [*Arakawa, 2004*].

Mass convergence near the surface, where specific humidity is large, leads to humidity convergence (i.e. horizontal convergence of humidity flux). So updrafts are also associated with humidity convergence near the surface. Once again, it is difficult to know whether humidity convergence generates larger Convective Available Potential Energy (CAPE) which generates an updraft, or whether a rising updraft induces humidity convergence because of mass conservation and high humidity near the surface.

The counter-part of the updrafts are downdrafts. Downdrafts are downward-moving volume of air due to convection. They can be created as follows. Cloud water droplets created in the updraft region grow larger and larger, until they become

massive enough to fall as rain. When rain (or any other condensed water) falls into a non-saturated area, part of the rain re-evaporates, thus cooling down the air. This cooling makes the air denser and denser, until a buoyancy-driven downward motion is generated: the downdraft. The downdraft is usually found close to the updraft, so that it partially acts to guarantee mass compensation.

When downdrafts reach altitudes close to the surface, below cloud base, they can create cold pools. Cold pools are cold volumes of air created by precipitation evaporation and located close to the surface, say under cloud base. Downdrafts themselves are dense, cold air volumes. Moreover, downdrafts reaching cloud base usually still contain a lot of rain, so when the rain reaches air located under cloud base, where it is always unsaturated, rain evaporation continues to be important, which keeps cooling down the air and making it denser. This downward motion of air under cloud base reaches the surface, where vertical velocity has to be zero, and the downward motion is converted to horizontal motion: this is the cold pool spread. Cold pools are fed (in part) by downdrafts, so that at the beginning of their life cycle, cold pools may be understood as an extension of the downdrafts towards the surface (“jet spread” model). However, because cold pools quickly become buoyancy-driven, they quickly behave like density currents which spread because of their weight (“density current” model). Cold pools spread at the surface due to mass conservation, creating gust fronts at their edges, which are strong chaotic horizontal winds.

For deep moist convection, updrafts and downdrafts are not completely symmetric to each other, unlike Rayleigh-Benard convection or some dry convection. So the mass they transport vertically does not completely balance out. So there can be a general vertical motion of the convective area (usually upward for deep convection), when taking into account both updrafts and downdrafts. But mass conservation will still be valid at larger scales, so that there must be a slow non-convective downward vertical air motion to compensate for the general upward motion of the convective area. This is called the compensating subsidence. Compensating subsidence may be considered as part of the convective process, as it allows convection to satisfy mass conservation. Although it occurs at larger scales, it is important to understand convection. While compensating subsidence can be explained by mass conservation, it is also considered as a radiative process. A non-convective part of the atmo-

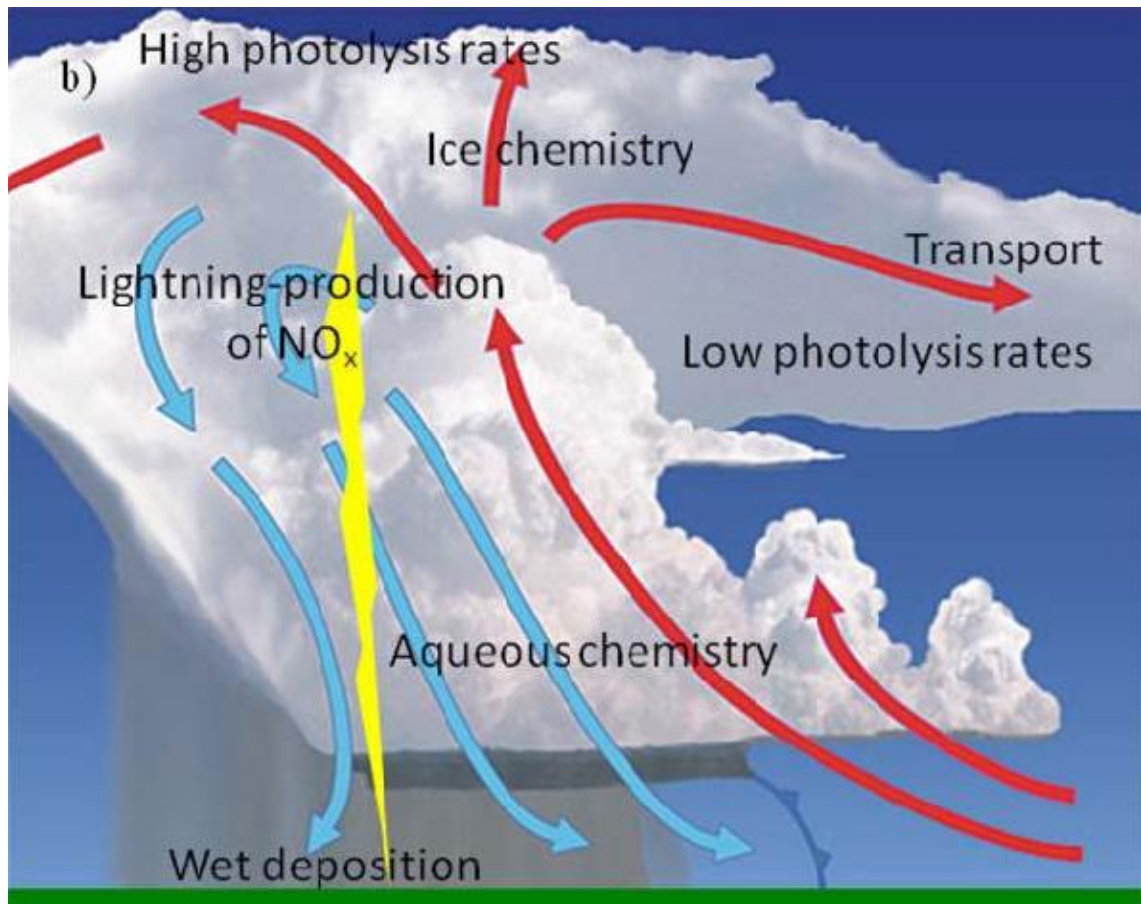


Figure 1.5 Schematic of the different structures appearing in a deep convective cloud (cumulonimbus): updraft, downdraft, and cold pool. The updraft and the detrained air are embodied by the red arrows, the downdraft is represented by the blue arrows, and the cold pool boundary is shown by the blue curve with blue triangles near the surface. The cold pool edge is located near the updraft location, because of their interplay. From UCAR and NOAA National Weather Service.

sphere undergoes radiative cooling, mostly in the long-wave spectrum, so that it slowly cools down and slowly moves downward. Sometimes this radiatively-driven subsidence can even be used as a driver for convection in a nearby location.

The question of what happens in convective columns is at the limit between the understanding of convection and its modelling. We will thus discuss it further in Section 1.2. There exist several images: either with elongated (anisotropic) updrafts, or with more isotropic bubbles. In the first case, updrafts are considered stronger structures. In the second case, bubbles are more transient, and it is the collective behaviour of bubbles that leads to an updraft-like behaviour.

There is one more aspect of convective processes that is critical: the microphysics. The microphysics is the ensemble of processes which explain water phase

changes at a micrometer scale. This includes cloud droplet formation, rain droplet formation, coalescence of liquid droplets, freezing of liquid water, collision of ice particles, evaporation of rain, and many other processes. It is a key aspect of moist convection, as the feedback between the dynamics and the microphysics completely modifies convection, as compared to dry or Rayleigh-Benard convection. It is a complex topic, because of the tiny scales involved, because of the diversity of condensed water particles, because of the interplay between radiation, dynamics, and microphysics. The wide range of scales that are involved in convection, from the microphysical scale, to the cyclone scale, via the cloud scale, brings convection at the heart of many atmospheric problems. Numerous multi-scale interactions are in the typical nature of convection.

1.1.3 The role of deep convection in the water and energy cycles

This study will focus on tropical deep convection in the atmosphere. While radiative processes tend to cool down the troposphere, leading to vertical instability, deep convection is a key process to redistribute energy and moisture along the vertical direction, bringing back the vertical stability. Thus, radiation and convection are a fundamental duo of the atmosphere. The impact of deep convection is even more important in the tropics, because there is much more moisture and heat at the surface, so that clouds reach much higher altitudes and convection creates much more precipitation. Consequently, it is in the tropics where most of the energy transfers occur in the atmosphere. Therefore, tropical deep convection is one of the most important phenomenon to understand thoroughly in the climate system.

1.2 Convection in the context of General Circulation Models

1.2.1 The grand challenge of convection

Convection remains one of the main challenges that limits our understanding in weather and climate science [Bony *et al.*, 2015]. It is thus an important focus for the research community. With better understanding of convection, we hope to be able to make better climate projections, seasonal forecasts, and weather forecasts.

General Circulation Models (GCMs) are probably the most important tool for scientists to investigate current and future climate. Given the current limits of computational resources, the typical resolution used in these climate models ranges roughly from 30 to 300km [Rio *et al.*, 2009]. At such scales, many phenomena (such as deep convection) remain unresolved, and therefore it is necessary to come up with parameterizations to represent their effects on the resolved state. A parameterization is a set of approximate equations whose objective is to express the collective effect of unresolved processes on the resolved state. These approximate equations try to capture in a realistic way the essence of unresolved processes in a pixelised world. Despite constant research efforts and progress, the representation of deep convection in these models still remains one of their major sources of uncertainty.

1.2.2 Representation of convective processes by parameterizations of convection

It is very common to conceptualise an updraft in terms of a rising plume, with carries air parcels upward. First, the concept of an air parcel assumes that it contains many molecules so that a continuous approximation can be made: the scale of a parcel is at least a few meters. Second, it assumes that there is local thermodynamic equilibrium, so that thermodynamic properties of the parcel can be defined. This means that turbulence at the scale of the parcel or even smaller scales does not lead to any gradient. Once we can apply the parcel concept, we can

schematically represent an updraft by a plume: a large vertical pipe that would pick up air from the surface to bring it and release it at the cloud top. By doing so, it is usually assumed that a single plume could represent an ensemble of updrafts, so that a plume is representing the “bulk” effect of updrafts.

But plumes are not a perfect model for updrafts and even less so for convection. A competing point of view is the bubble. Deep convection is seen as a population of bubbles, that rise up in the air. They are more transient, more updraft-like, and smaller in size. Convection can be viewed as an ensemble of transient bubbles, that spin around like duos of vortices [*Sherwood et al.*, 2013; *Yano*, 2014]. This representation is appealing because it helps explain why cumulus and cumulonimbus look so bubbly or sheep-like. However, it introduces additional degrees of freedom and calls for the use of statistics on turbulent objects. The question on whether convection is similar to a bubble or a plume has been reviewed by *Yano* [2014].

First of all, when is convection parameterizable? *Arakawa and Schubert* [1974] and *Arakawa* [2004] state that the quasi-equilibrium assumption (defined in Subsection 1.2.4) is necessary for parameterizability. Convection is considered to be parameterizable when it can be related to the past history of the large-scale forcing. In this thesis, we are looking to extend the range of convection parameterizability beyond this definition.

There have been two main traditional schools of thought to parameterize convection: one based on moisture convergence, and one based on moist-convective adjustment [*Arakawa*, 2004]. The schemes based on moisture convergence assume that low-level large-scale moisture convergence causes convection, whereas the schemes based on adjustment focus on the result post-convection and impose a post-convective profile from a family of profiles. For the adjustment school, convection is acting to reduce instability created by large-scale processes. Beyond these two schools of thought, there are two main types of schemes: pure adjustment schemes, and mass-flux schemes.

Pure adjustment schemes do not attempt to represent convective processes explicitly. They relax the atmosphere to a pre-defined type of vertical profile, using boundary layer equivalent potential temperature. In the simplest case, the adjusted

profiles are moist adiabats, whose equivalent potential temperature is the current value of the boundary layer. The *Betts and Miller* [1986] scheme is an example of such parameterizations.

Most schemes are now expressing convective vertical mass flux, as a minimal requirement to represent the details of the convective processes: we talk about mass-flux schemes. *Arakawa and Schubert* [1974], one of the first mass flux schemes, still contains very challenging components for today's models. In a mass-flux scheme, the atmosphere is typically divided into an ascending part representing the updraft, and a compensating subsidence part. In some cases, they can also include a descending part representing the downdraft. Typically, the updraft region and the downdraft region are assumed to be small compared to the grid size, which allows for useful simplifications in scheme derivations. For example, it implies that the vertical velocities in the updraft and downdraft regions are much larger than the vertical velocity in the compensating subsidence region. However, this assumption is getting less and less valid with increasing resolutions.

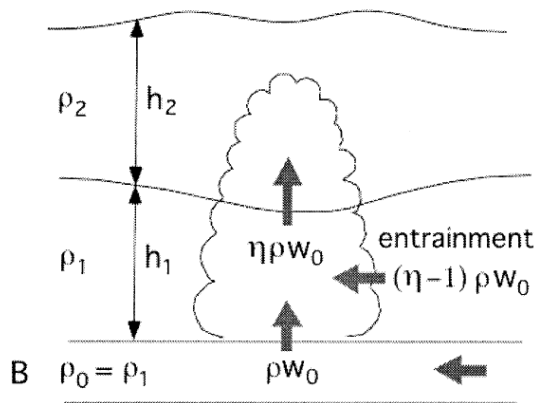


Figure 1.6 Schematic of vertical mass flux and entrainment of environmental air into a rising cloud. This particular schematic is the three-layer model representing tropical cyclone development which was developed by *Ooyama* [1969]. Figure from *Arakawa* [2004].

Most convective parameterizations require three components to build a closed system: a triggering, a cloud model, and a closure (see review by *Yano et al.* [2013]). The triggering is a switch that decides whether there is deep convection or not in the grid cell at the current time step. The triggering allows to decide when to use the convective scheme, and when to skip it. It is a key condition, which usually helps make choices between dry, shallow or deep convection. Then the cloud model

is a representation of convective processes that allows to split the amount of mass, humidity and energy provided by convection between each level of the atmosphere. It typically includes the vertical distribution of mass fluxes, entrainment, and detrainment (figure 1.6). This is where various influences on the convective processes can be included. Finally, the closure gives the intensity of convection. It imposes the absolute value of convection, for example the cloud-base mass flux, while the cloud model imposes the relative distribution of this intensity with height and between processes. The closure is where convection is scaled with the large-scale processes.

1.2.3 Issues with convective parameterizations

Many of the current atmospheric General Circulation Models (GCMs) have shortcomings, and some of them are attributed to the convective parameterizations. Here are a few ones:

- First, in terms of precipitation. GCMs rain too often and too little [*Stephens et al.*, 2010], so they are said to drizzle all the time. In reality, we observe much more heavy precipitation events. GCMs yield too much convective rain compared to stratiform rain [*Dai*, 2006].
- Second, in terms of clouds. They tend to produce too much high cloud and too little shallow cloud [*Chepfer et al.*, 2008; *Sherwood et al.*, 2013]. This problem is also related to the lack of sensitivity of convective schemes to environmental humidity [*Derbyshire et al.*, 2004].
- Third, in terms of spatial organisation of convection [*Bony et al.*, 2015]. In the real world, there are organised patterns of convection, so that convective structures are not purely random. Convection often organises spatially into propagating structures such as Mesoscale Convective Systems (MCS) [*Houze*, 2004] or the Madden-Julian Oscillation (MJO) [*CLIVAR Madden-Julian Oscillation Working Group: Waliser et al.*, 2009]. But even though GCMs may be able to represent some organised features of convection, they do not capture the upscale growth towards MCS [*Rowe and Houze*, 2015], and most of them do not capture the Madden-Julian Oscillation [*CLIVAR Madden-Julian Oscil-*

lation Working Group: Waliser et al., 2009; Jiang et al., 2015]. Worse, some GCMs show an unrealistic double Inter-Tropical Convergence Zone (ITCZ) [Dai, 2006; Oueslati and Bellon, 2013]. Also, their convective parameterizations do not consider organisation explicitly [Mapes and Neale, 2011; Tan et al., 2015].

- Fourth, in terms of diurnal cycle. The timing of parameterised convection in the tropics is usually inaccurate [Rio et al., 2009; Langhans et al., 2013; Bechtold et al., 2014]. The diurnal cycle of convection, chiefly over tropical land, is poorly captured by GCMs. Obviously insolation peaks around mid-day. Many GCMs predict a precipitation peak too early in the afternoon, sometimes even in phase with solar forcing, while observed tropical precipitation is usually maximum in the late afternoon (or even during the night over ocean). Significant improvements have already been achieved [Rio et al., 2009; Stratton and Stirling, 2012; Folkins et al., 2014], but the diurnal cycle obtained by parameterized convection is still largely unrealistic.
- The triggering of convection is another major issue of convective parameterizations. Is convective initiation mostly due to moisture convergence (large-scale forcing) or to moistening of the atmosphere by cumulus clouds (local thermodynamics)? Hohenegger and Stevens [2012] support the idea that the transition from shallow convection to deep convection (i.e. deep convection initiation) is related to large-scale forcing. Conversely, many studies show that deep convection initiation is more strongly dependant on thermodynamical factors such as Convective Inhibition (CIN) or moistening of the lower and medium free troposphere by previous clouds [Chaboureau et al., 2004; Yano et al., 2013].
- Perhaps the most striking flaw is that models differ so much from one another that in idealized configurations, they can produce cloud and precipitation responses to warming that have opposite signs [Stevens and Bony, 2013].

Among the issues that convective parameterizations still have, two of them are of particular interest for this study: the diurnal cycle, and convective organisation.

Note that these issues could be attributed to two kinds of flaws in the parameterizations of deep convection: either to the lack of representation of some important

processes, which implies that current schemes can be incrementally improved by adding new technical features (for example cold pools), or to the basic assumptions of parameterizations [Arakawa, 2004; Yano, 2014]. Or it could be attributed to both kinds. Tackling the basic assumptions is clearly much harder to achieve than to add new processes, but it may still be a necessary step for significant improvement.

1.2.4 Quasi-Equilibrium

Local convective quasi-equilibrium is an assumption which was first proposed by *Arakawa and Schubert* [1974] during an era where tremendous steps forward were made to forge convective parameterizations, in a quickly growing field of atmospheric modelling. It was also formulated in a more statistical way by *Emanuel et al.* [1994]. Quasi-equilibrium is defined as the assumption that the convective response is in equilibrium with the large-scale forcing: the response is deterministically and rapidly related to the disequilibrium introduced locally by the large-scale dynamics and by the other parameterizations. Quasi-equilibrium applies after an adjustment time whose time scale is several hours [Emanuel et al., 1994]. Quoting *Arakawa and Schubert* [1974], this assumption “means that the cumulus ensemble follows a sequence of quasi-equilibria with the current large-scale forcing. We assume that this is the case for the cumulus ensembles we wish to parameterize”. For *Emanuel* [1991], usual schemes “have somewhat different ways of calculating the cloud-base mass flux of updrafts, but (...) these differences should not affect the results of the schemes under quasi-equilibrium conditions in which the environmental forcing effectively determines the cloud-base mass flux”. *Raymond* [1995] defines the quasi-equilibrium hypothesis the following way: “convection occurs as needed to just balance the production of convective instability and (...) the timescale to establish this balance is much less than the timescales of tropical disturbances”. He also says: “Quasi-equilibrium postulates that convective destruction of instability approximately balances its non-convective creation on a short timescale compared to nonconvective timescales”. *Pan and Randall* [1998] define quasi-equilibrium as “a closure assumption based on the hypothesis that the convective clouds quickly act to convert whatever moist convective available potential energy is present in

convectively active atmospheric columns into convective kinetic energy”. They draw an analogy with team sports: with quasi-equilibrium, cumulus clouds “closely follow the large-scale forcing, quickly reacting to changes in the large-scale forcing in a very short ‘adjustment time’, like a basketball player in a man-to-man defence.” *Raymond and Herman* [2011] also have a long discussion on quasi-equilibrium: they define quasi-equilibrium by the hypothesis stating that “the time scale for convection to remove a buoyancy perturbation at any level in the atmosphere reached by the convection is of order the time required for a convective cell to pass through its life cycle, i.e., a few hours”.

In many people’s opinion, quasi-equilibrium is still one of the major assumptions made explicitly or implicitly in most convective schemes used by GCMs [*Arakawa*, 2004; *Davies et al.*, 2009, 2013a; *Bechtold et al.*, 2014]. According to *Arakawa* [2004], most convective parameterizations “are based on the quasi-equilibrium concept”. Some parameterizations assume full quasi-equilibrium, some assume a quasi-equilibrium with a non-zero relaxation time scale. However, some schemes can also be derived without this assumption. For example, without assuming quasi-equilibrium explicitly when deriving the parameterization, *Emanuel* [1991] argues the numerical applications of the convective scheme support equilibrium convection. Undoubtedly, quasi-equilibrium is a very useful assumption in order to derive successfully the scheme equations [*Mapes and Neale*, 2011] and has been helpful for GCMs to make strides.

Yet, most convective parameterizations used in current GCMs have a separate triggering function, which means that the convective adjustment is only applied under certain conditions: this is a non-linear non-equilibrium condition. A separate triggering of convection implies there is no quasi-equilibrium anymore, because a given quantity (such as CIN) has to exceed a threshold before the balance between large-scale forcing and convection can be established in a quasi-equilibrated way. This recognizes that the existence of triggering is incompatible with quasi-equilibrium. There are two reasons to explain this apparent discrepancy in the use of the word quasi-equilibrium. The first is, as pointed out by several studies [*Arakawa*, 2004], that most schemes are “**based on**” quasi-equilibrium. This is different from imposing it. It suggests that most schemes are an extension of quasi-equilibrium, but

they do not assume quasi-equilibrium. In other words, many schemes are said to be based on quasi-equilibrium because their asymptotic behaviour is quasi-equilibrium, without strictly assuming quasi-equilibrium. The second reason is that, as pointed out by *Arakawa* [2004], quasi-equilibrium is fine if the purpose is to predict general weather and climate, that is, if space and time resolutions are not too fine. If we wish to predict finer details than general weather and climate, such as localised phenomena, this is not within the scope of quasi-equilibrium. Many studies have already pointed out quasi-equilibrium does not hold at small grid spacing, and fine temporal resolution.

Other studies express the incompatibility between quasi-equilibrium and triggering function. *Yano and Plant* [2012b], which analyse the relationship between triggering and quasi-equilibrium, have a similar stance on the fact that schemes with a separate triggering function cannot be said to be in quasi-equilibrium. They say: “A strict CQE [Convective Quasi-Equilibrium] hypothesis does not work in this type of situation, and many operational schemes introduce a trigger condition for just this reason”. *Emanuel* [1991] points that a condition on instability may exist for quasi-equilibrium: “All the aforementioned schemes have somewhat different ways of calculating the cloud-base mass flux of updrafts, but (...) these differences should not affect the results of the schemes under quasi-equilibrium conditions in which the environmental forcing effectively determines the cloud-base mass flux, **given only** that the schemes turn on when the atmosphere is unstable to parcel ascent”. It goes further about quasi-equilibrium: “Naturally, these arguments do not apply to **stored energy convection** of the kind experienced occasionally in middle latitudes (particularly North America); here the rate at which stored energy is released becomes an important consideration.”

Here we mostly advocate for a change of vocabulary: most schemes do not actually assume quasi-equilibrium, they essentially do a non-linear approach towards it.

Beyond the use of vocabulary, the quasi-equilibrium assumption in itself is problematic. Even though it is thought to be widely used, at least as a base for more flexible convective parameterizations with some departure from equilibrium,

the quasi-equilibrium assumption cannot be strictly correct. Even *Arakawa and Schubert* [1974] acknowledge a weakness of quasi-equilibrium, by clarifying that cumulus will develop based on the large-scale forcing “provided that there is a triggering mechanism”. *Raymond* [1995] argues that quasi-equilibrium is not valid, and instead proposes a separate concept of boundary layer quasi-equilibrium. He states that instead of quasi-equilibrium, convection follows boundary layer quasi-equilibrium, because there is a threshold to exceed (convective inhibition) for convection to be triggered. This threshold condition can be given in terms of boundary layer equivalent potential temperature, by comparing it to conditions just above cloud base. What is in quasi-equilibrium here is the value of boundary layer equivalent potential temperature, and not the whole thermodynamic profile of the whole atmosphere as the usual quasi-equilibrium would state. *Raymond and Herman* [2011] reformulates this by saying that only the lower troposphere obeys rapid convective adjustment, while the upper troposphere adjusts much more slowly. In a similar vein, *Mapes* [1997] argues for activation control of convection rather than equilibrium control of convection. For example, a discussion of the activation control is given by *Yano and Plant* [2012b]. Current schemes tend to follow the activation control idea by representing more and more boundary layer processes and let them control convection [*Grandpeix and Lafore*, 2010; *Rio et al.*, 2013]. *Pan and Randall* [1998] also go beyond quasi-equilibrium, and already recognise that quasi-equilibrium prevents clouds from having a memory of their past history. *Arakawa* [2004] also recognizes the problem of mesoscale organisation of cumulus convection for quasi-equilibrium. “Fluctuations in cumulus activity [in these organized forms of convection are] not fully modulated by large-scale forcing. (...) These fluctuations cannot be parameterized using a quasi-equilibrium assumption, showing that there is a limit of diagnostic or deterministic parameterizability. To go beyond this limit requires the introduction of more prognostic equations to predict transient cumulus activity or stochastic components representing uncertainties on the initial conditions for those equations. The concept of quasi-equilibrium can be either implicit in the prognostic system or can be used as a weaker constraint on the system.”

More recently, quasi-equilibrium has been recognized as a drawback preventing convection schemes to become more versatile and accurate [*Mapes*, 1997; *Davies*

et al., 2009; *Raymond and Herman*, 2011; *Davies et al.*, 2013a; *Bechtold et al.*, 2014]. Indeed, convection is a response of the atmosphere to large-scale forcing. If we had equilibrium convection, convection would be in phase with the large-scale forcing, and convective precipitation may, for example, peak around midday over tropical land (in a simple example where large-scale forcing is in phase with solar forcing). However, in observations, due to the late trigger of deep convection during the day (diurnal cycle), the response of convection is out of phase: there is non-equilibrium convection. *Yano and Plant* [2012b] also point out parameterizations with triggering cannot be said to assume quasi-equilibrium. Even though parts of their formulation may be based on quasi-equilibrium, they do not in practice ensure that convection is in quasi-equilibrium with the large-scale forcing.

This particular problem of the diurnal cycle peaking at midday may be partly alleviated by moving from “hard adjustment” to “soft adjustment”. If we assume that convection consumes CAPE as fast as it is produced (hard adjustment), then convection should peak when the solar heating is greatest, which indeed would be noon. According to this assumption the CAPE would reach a limit in the morning and remain approximately constant throughout the rest of the day until sunset. But this type of hard adjustment has already been superseded. A more acceptable soft adjustment model (with a time constant characterising the rate of relaxation to the reference state) also seems “quasi-equilibrium” in the sense there is no triggering condition and the convective activity is proportional to the CAPE with no delay. But since the CAPE grows throughout the middle of the day due to ground heat capacity, the convection peaks in the afternoon or early evening.

Another reason showing that quasi-equilibrium is inaccurate is that a scale separation between parameterized convection and the resolved large-scale forcings is necessary for quasi-equilibrium to be valid [*Mapes*, 1997]. Yet, the current trend is for models to have finer grid spacing and shorter time steps. When spatial and temporal resolutions increase, inertial and stochastic effects become more important, the scale separation vanishes, and quasi-equilibrium cannot hold [*Hagos and Houze*, 2016].

Arakawa [2004] explains that, by 2004, the scientific community had not taken

on the question of quasi-equilibrium, so that it was not a mature scientific question yet. But this is probably starting to move ahead nowadays. In section 5, he explains that indeed, many convective schemes assume quasi-equilibrium (explicitly or implicitly or even virtually). However, there exists some relaxed and triggered adjustment schemes that all have a non-zero time scale for convection response to relax towards equilibrium. For example *Betts and Miller* [1986] and *Kain and Fritsch* [1990]. In this category of schemes, some non-equilibrium behaviour is likely to exist already. *Arakawa* [2004] also reports that there are a few schemes which do have a prognostic closure [*Emanuel*, 1991; *Pan and Randall*, 1998]. These schemes do require time to return to quasi-equilibrium thanks to the implementation of short-term physical processes. Can these schemes therefore be said to have memory? As shown in Section 1.3, we consider that they do only if they explicitly re-use variables from the previous time step in the convective effects of the current time step. Partial relaxation towards quasi-equilibrium is not memory, unless some measure of convection from the previous time step is reused in the current convective calculation.

To address some of the shortcomings of quasi-equilibrium convective parameterizations, some studies have tried to introduce some forms of non-equilibrium behaviour, by working without the quasi-equilibrium assumption. Several interesting pathways are currently investigated: *Hagos and Houze* [2016] draw a picture of the challenges and current directions for convective parameterization developments or for alternatives, in order to overcome the quasi-equilibrium assumption. For example: Probability Density Function (PDF)-based turbulent convective schemes [*Golaz et al.*, 2002; *Bogenschutz et al.*, 2012, 2013], superparameterization [*Grabowski and Smolarkiewicz*, 1999; *Randall et al.*, 2003; *Grabowski*, 2004; *Randall*, 2013; *Randall et al.*, 2013], global Cloud-Resolving Models [*Sato et al.*, 2008; *Miyamoto et al.*, 2013], dynamical representation of organized convection [*Khouider and Majda*, 2006; *Peters et al.*, 2013] ... Another very promising avenue to go beyond quasi-equilibrium is to add a prognostic variable into the scheme. The first approach was probably the scheme by *Pan and Randall* [1998], which was a major step forward: instead of assuming quasi-equilibrium, it contains a prognostic closure. Other prognostic schemes followed [*Piriou et al.*, 2007; *Grandpeix and Lafore*, 2010; *Mapes and Neale*, 2011; *Park*, 2014]. All these examples fall in one of two categories: either

improving parameterizations, or trying to do without them. This thesis is more relevant for the first category.

In a nutshell, there has been debate around quasi-equilibrium. Decades ago, some studies showed the importance of relaxing the strict quasi-equilibrium assumption by introducing a non-zero time lag [Emanuel, 1993]. And this approximation, even in some less strict forms, is now recognized to prevent convection schemes from tackling some modern issues, e.g. convective organization, memory, increasing resolution [Mapes, 1997; Davies *et al.*, 2009; Raymond and Herman, 2011; Davies *et al.*, 2013a; Bechtold *et al.*, 2014]. Consequently, many current convective parameterizations and theories do not assume quasi-equilibrium, and alternative pathways are being investigated [Hagos and Houze, 2016].

In this thesis, we do not argue against all quasi-equilibrium ideas, we rather advocate for a more flexible quasi-equilibrium.

1.3 The origins of the convective memory issue

1.3.1 The diagnostic assumption

A similar question to quasi-equilibrium, but perhaps more fundamental, is the “diagnostic assumption”. It is this assumption, which has received much less attention, that we examine in this study. To understand it we first define some key terms in the modelling context. State variables are the variables used by the model to compute advection and to be used in the parameterizations. State variables completely define the state of the system: knowing all the state variables is enough to know everything about the system. The phase space is the space in which evolve the state variables. A *prognostic* variable is one which is remembered for the next time step in a numerical model. In the mathematical world, this is equivalent to saying that the variable has a time derivative in its governing equation, so that its future value is calculated based on its present value. Conversely, a *diagnostic* variable does not have any time derivative in its governing equation: it does not have to be remembered by the model, and can be deduced at each time step from

other current variables. With all the prognostic variables in a model, the whole state of the system is known (in its phase space), so that all other variables can be reconstructed through diagnostic relationships.

For convection, the “diagnostic assumption” is the assumption that convective effects at a large scale can be diagnosed from the state variables at that scale, instead of following a prognostic relationship. This assumption is made almost universally in traditional convective parameterizations used in GCMs, although it is unclear from basic principles why convection would obey a diagnostic relationship with the instantaneous large-scale state. We think that the diagnostic assumption is made in most traditional convective parameterizations [see subsections 5b and 5c in *Arakawa, 2004*], observational analyses [e.g. *Masunaga, 2012; Tan et al., 2013; Davies et al., 2013b*], and many modeling studies [e.g. *Kuang, 2010*]. Examples of diagnostic schemes as per *Arakawa [2004]*’s classification are: *Tiedtke [1989]*, *Arakawa and Schubert [1974]*, *Lord et al. [1982]*, *Donner et al. [2001]*, *Grell [1993]*, *Betts and Miller [1986]*, *Gregory et al. [2000]*, *Kain and Fritsch [1990]*, *Moorthi and Suarez [1992]* (relaxed Arakawa-Schubert), *Zhang and McFarlane [1995]*. Among traditional parameterizations, notable exceptions which do not make a diagnostic assumption are *Emanuel [1991]* and *Pan and Randall [1998]*, as pointed out by *Arakawa [2004]*. We will review how newer schemes deal with this assumption in Subsection 1.3.3.

Note that, in comparison with the diagnostic assumption, quasi-equilibrium is an even stronger assumption: it states that not only can convective effects be diagnosed, but they also act in order to keep modifications of a closure variable (e.g. Convective Available Potential Energy) close to zero. So for example, convective schemes that involve a separate triggering of convection are not quasi-equilibrium schemes, since a triggering condition must be met before allowing convection to respond to the forcing [*Yano and Plant, 2012b; Emanuel, 1991*]. However, such schemes may still diagnose both the triggering and closure variables from the current grid-scale state: they may still make the diagnostic assumption.

The case of relaxed and triggered adjustment schemes requires a bit more attention. As discussed above, triggered adjustment may not really be considered as quasi-equilibrium schemes, although they may still make the diagnostic assumption.

Relaxed adjustment schemes, which have a relaxation time scale longer than the model time step, can still be said to be a softer form of quasi-equilibrium. But it does not mean they do without the diagnostic assumption, since a partial relaxation obtained in a diagnostic way is still non-prognostic. The only way for a relaxed adjustment scheme to become prognostic is to re-use a convective variable from the previous time step. In this case only can they be said not to make the diagnostic assumption. Traditionally, relaxed and triggered adjustment schemes still make the diagnostic assumption. The case of certain newer schemes will be discussed in Subsection 1.3.3.

1.3.2 The diagnostic assumption problem: why it may be inaccurate

But it is far from clear that the “diagnostic assumption” is justifiable. Because of the finite resolution of models, many unresolved processes, which generally have their own inertia and internal time scales, could bring inertia to the system. And a diagnostic relationship cannot represent this, because it automatically assumes that all such time scales are no longer than the model time step, which is typically of order 10 minutes in global atmospheric models for climate prediction. Yet the time for a single updraft to penetrate the troposphere is already longer than this. Moreover, the current trend is for models to have finer grid spacing and shorter time steps, so that this diagnostic assumption is increasingly problematic.

1.3.3 Solution: a prognostic formulation

To go beyond the diagnostic assumption one would need to add one or more prognostic variables into the scheme, which would carry information (“memory”) on the previous behaviour of unresolved processes. If convection were to be diagnosed by an equilibrium with the large-scale forcing, it would only be sensitive to the recent history of the forcing. With a prognostic formulation, not only do we have non-equilibrium convection (i.e. an approach to quasi-equilibrium), but convection is also made sensitive to its own history. Many examples already exist. To our knowledge,

the first was *Pan and Randall* [1998]. Their prognostic variable is the Cumulus Kinetic Energy (CKE), whose source is taken to be the product between the cloud work function (a measure of Convective Available Potential Energy (CAPE)) and the cloud-base mass flux. Later, in the Prognostic Condensates Microphysics and Transport (PCMT) parameterization with memory [*Piriou et al.*, 2007], the source of a prognostic memory variable is chosen to be precipitation evaporation, because downdraft-induced gust fronts are thought to be involved. The higher this variable, the lower the entrainment rate. Similarly, *Mapes and Neale* [2011] use a prognostic “ORG” variable to quantify the spatial organisation of convection. They assume that precipitation evaporation is the main source of ORG. *Willett and Whitall* [2017] also introduce some memory in the UK MetOffice model: the source of memory is surface precipitation, and the effect is also on the entrainment rate. *Grandpeix and Lafore* [2010] and *Del Genio et al.* [2015] have some memory arising from the thermodynamic properties of cold pools, although they do not remark on its role, and *Park* [2014] has memory due to both cold pools and mesoscale organized flows. While these efforts are important, they were arguably ad hoc and have not led to a consensus on whether memory needs to be explicitly included in models or how to do it. The current study is intended to establish more generally whether memory is important and how it might best be represented.

To epitomize this problem, here is an extreme example. To compute the features and effects of convection, traditional parameterizations of convection in GCMs may use large-scale variables such as temperature, moisture, and winds, etc. . . **at instant t only**. But they rarely explicitly look back in time (although they can implicitly look back in time through large-scale processes such as the sensitivity of convection to large-scale humidity. Nevertheless, we know that the previous convective states also influence the current convective state [*Mapes and Neale*, 2011]). Therefore, to solve this issue, it seems reasonable to introduce into the parameterization a prognostic variable (a variable that is carried in time by the model, in order to be used in subsequent time steps) representing the previous states of the convective atmosphere. This variable would allow the model to remember the main features of convection at previous time steps, and would then influence future convection.

1.4 Convective memory

1.4.1 Definition

We define process memory (such as convective memory) as the phenomenon where the behavior of a process (such as convection) depends on its own history, rather than just on current large-scale (i.e. external or “environmental”) conditions. This is an extension broadly consistent with the understanding of convective memory provided by *Davies et al.* [2009]. Even if they instead define convective memory via convective life cycle (and more precisely via the convective response time scale to varying forcing), our definition is consistent with the properties of memory they found for an intermediate value of their memory time scale.

Our definition can be further formulated in terms of conditional probabilities. First, one should select a length scale λ , which we select as a typical GCM grid cell ($O(100 \text{ km})$). At each time t , let us define a measure of the convective state $C(\lambda, t)$ and a measure of the “environmental” variables $\xi(\lambda, t)$. Now statistics based on Probability Distribution Functions (PDF) can be made with varying t . Convective memory is the dependence of the PDF of $C(\lambda)$ on its own history, for given environmental conditions $\xi(\lambda, t)$. If convection had no memory, the convective state $C(\lambda, t_0)$ would be conditionally independent from earlier convection $C(\lambda, t) \forall t < t_0$. But if convection has memory, then for a fixed environmental state $\xi(\lambda)$, the convective state $C(\lambda, t_0)$ is conditionally dependent on earlier convective states $C(\lambda, t) \forall t < t_0$.

There are two important concepts that should not be confused: the storage of memory (hereafter the repository), and the sources and sinks filling or consuming the repository of memory. The repository can be a prognostic variable itself, or a diagnostic function of prognostic state variables. It can be seen as a “memory bank”. Presumably, the repository is a variable that is likely to represent some form of atmospheric structure, so that it could be the variance of some relevant variables (which relates to information theory’s entropy). Because one does not necessarily know the repository, in this study we will focus on standard prognostic state variables, in order to guide the identification of the repository and its role in

memory.

1.4.2 Memory vs Persistence

Note that convective memory is more than just persistence of convection: even if $C(\lambda, t_0)$ shows persistence, this could be due to persistence of $\xi(\lambda, t)$, itself arising for whatever reason. Thus, while memory implies persistence, persistence does not necessarily imply memory (contrary to the example given by *Davies et al.* [2009]).

A supermarket analogy may help understand this distinction. If one goes to the supermarket without one's shopping list, one will be much more sensitive to the items displayed on the supermarket shelves, so that one may buy unexpected items, instead of remembering one's needs, written down consciously before entering the shop. In other words, with convective memory (a shopping list), one is not only sensitive to the environmental conditions (the supermarket's displays and marketing), but also to its own history (one's needs at home).

Even if one always forgets one's shopping list, one may still end up buying the same products every week if the shop's displays remain unchanged, via the effect of good marketing on one's buying intentions. In other words, without memory (no shopping list), there may still be persistence in the convective states (items bought) if the environmental conditions persist (supermarket shelves). This means there can be persistence without memory. Conversely, if one always remembers one's shopping list, even if the supermarket always changed the displays to lure customers into buying new products, one may not be so affected, thanks to the inertia provided by one's shopping list. In other words, with convective memory, a change in environmental conditions is not enough to generate a rapid change in convective state: memory implies persistence.

1.4.3 Three types of memory storage

In this framework, there are three important concepts that should not be confused: the storage of memory (the repository), the prognostic state variables which are used to define the repository in a diagnostic way, and the sources and sinks

filling or consuming the repository of memory. The repository can be seen as a “memory bank”. The repository is a variable that is likely to represent some form of atmospheric structure, so that the storage would be the variance of some relevant variables (which relates to information theory’s entropy). In this study, we are mostly interested in the prognostic state variables used to define the repository, since they are our best guess towards the repository.

To understand the hierarchy of spatial scales involved, an analogy can be drawn between convection and statistical physics applied to an ideal gas. A full description of the gas particles specifies the so-called microstate, while the description of the collective behavior via either statistical physics or thermodynamics gives knowledge about the macrostate (pressure, temperature, volume). By analogy, one can define a microstate (description of all elementary units) and a macrostate (description of the collective behaviour) for convection. If the particle ensemble size is large enough, the law of large numbers can be applied, so local thermodynamic equilibrium (LTE) is valid at the macrostate and governing relationships hold between macrostate quantities (e.g., the ideal gas law): there is no need to know the microstate. But when the ensemble size becomes too small, individual particle effects start to be seen at the macrostate, and local thermodynamic equilibrium does not apply: a non-equilibrium description of the microstate is needed to explain the macrostate. While in usual fluid-dynamics applications there are enough gas particles to apply LTE, the cumulus ensemble size is much smaller for convection, especially as grid sizes decrease, so that one grid cell only represents a few clouds. Note that *Yano and Plant* [2012b] also discussed a comparison between microscopic and macroscopic views, but for different purposes.

In accord with this analogy, we will refer to the state variable fluctuations below the scale λ as the *microstate* and the associated subgrid-scale processes as micro-scale processes. The state at the scale λ is referred to as the *macrostate* and processes at that scale as macroscale processes. Finally, some processes involve interaction between the local environment and more remote regions (e.g., Rossby waves or the Hadley cell). We refer to these as synoptic-scale processes, and to the atmospheric state including these remote regions as the *synoptic state*. System memory can reside at each of these three scales: we distinguish between microstate

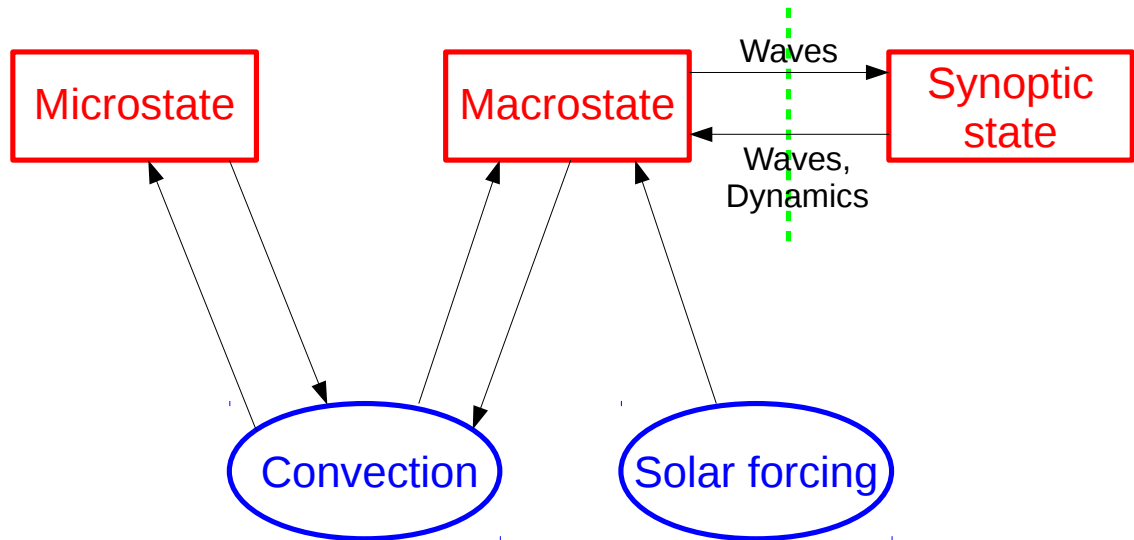


Figure 1.7 Schematics of the three repositories of convective memory (in red): the microstate, the macrostate and the synoptic state. A few key processes are added in blue: convection and solar radiation. The impact of one element on another is symbolised by a black arrow. The green dotted line separates the elements that we will not be able to simulate in a small domain model with periodic boundary conditions.

memory stored in microstate structures, macrostate memory stored in macrostate structures, and synoptic state memory stored in synoptic state structures. All three types refer to convective memory (how future convection is conditionally dependent on its own past), but with a repository done at different scales.

Feedbacks are needed for memory. Convection refers to a multi-scale process which depends on the microstate, the macrostate and the synoptic state. So convection is not unequivocally defined by its diagnostic macrostate variables, since other degrees of freedom are missing (e.g. the microstate). Macrostate convective memory relies on a reciprocal interaction between convection and the macrostate: convection influences the macrostate, which can influence convection back. This way, convection influences itself via the macrostate. For synoptic state memory, the feedback loop between convection and the synoptic state is even more obvious, because memory is stored across a large area beyond the local grid cell. In this case, convection influences itself via changes in the synoptic state. *Davies et al.* [2013a] found that macrostate memory is relatively weak compared with microstate memory, and they thus fostered the incorporation of microstate memory into GCMs.

Following this reasoning, the definition given in Subsection 1.4.1 is actually a

more appropriate definition for microstate memory. We can reformulate here the idea given in terms of conditional probabilities for microstate memory. Microstate convective memory is the dependence of the PDF of $C(\lambda, t)$ on its own history, for given environmental conditions $\xi(\lambda, t)$. If convection had no microstate memory, the convective state $C(\lambda, t_0)$ would be conditionally independent from earlier convection $C(\lambda, t) \forall t < t_0$, given the large-scale state $\xi(\lambda, t)$. Otherwise, convection has microstate memory.

A schematic summarising these ideas is presented on Figure 1.7.

1.4.4 Processes inducing convective memory

In GCMs, microstate convective memory must be represented via an additional prognostic variable, whereas macrostate and synoptic state convective memory should be captured by diagnostic representations because their memory is stored in the resolved fields. In the real world, many physical processes generate convective memory, by impacting transitions between convective states (for example between shallow and deep convection). The physical processes include:

- The preconditioning of deep convection. Before creating deep convection, it is necessary for the atmosphere to start with shallow convection, which gets deeper and deeper with time. This process is the preconditioning of deep convection [*Chaboureaud et al.*, 2004; *Stevens*, 2007; *Rio et al.*, 2009; *Hohenegger and Stevens*, 2012].
- The cold pools. When a first deep convective event is mature enough, it creates precipitation. When the precipitation fall into unsaturated air, the droplets partly evaporates, which is a sink for heat. Thus, the air becomes colder: this is a cold pool. When cold pools spread at the surface, they are likely to initiate further events of convection, bringing memory to the system. See *Rio et al.* [2009]; *Schlemmer and Hohenegger* [2014].
- The dependence of entrainment rate on the width of the cloud. When a cloud grows, it becomes wider, so its entrainment rate decreases, so that it keeps

growing even more. This positive feedback carries convective memory, as a big cloud is more likely to keep growing than a thin cloud [Romps and Kuang, 2010; Mapes and Neale, 2011; de Rooy et al., 2013; Piriou et al., 2007]. This has been used in the literature to create prognostic variables for convective memory (see subsection 1.4.5).

- Secondary initiation of convection. The mechanisms of convective development have been investigated in some observational studies, which showed triggering of convection by previous convective clusters, and suggests there is convective memory [Morcrette et al., 2006; Marsham and Parker, 2006].

These physical processes could be chosen for prognostic representations into models with microstate memory, and they have all been chosen in previous studies to incorporate convective memory in parameterizations. Note that some of these processes may act through both the microstate and the macrostate, which ideally should be disentangled before parameterizing.

The role of gravity waves in the memory process is unclear, since gravity waves transport information about temperature to adjacent locations, which can influence future convection in local and remote locations, but the gravity wave propagation time scale may be smaller than a GCM time step. For example, cloud spacing has been shown to be more important than gravity waves to determine the response time scale to macrostate perturbations [Cohen and Craig, 2004].

1.4.5 Examples of introduction of convective memory into GCMs

The first study which introduces convective memory (i.e. a prognostic variable) in convective parameterizations is probably Pan and Randall [1998]. The prognostic variable carrying the memory is the Convective Kinetic Energy, some measure of the turbulent kinetic energy related to convective motions, This prognostic variable is fed by a single source, which is the product of the cloud work function (similar to Convective Available Potential Energy (CAPE)) and the cloud-base mass flux. The

asymptotic behaviour of this scheme is the quasi-equilibrium, but it already has the ability to be out of equilibrium and more importantly, non-diagnostic.

Piriou et al. [2007] started a different branch in the recent development of convective parameterizations with prognostic variables, by relating memory to rain evaporation. They chose a different prognostic variable which is the probability of undiluted updrafts. Essentially, this is related to the entrainment rate, so that the storage of memory is done via entrainment. The higher the prognostic probability of undiluted updraft, the lower the entrainment. The source of memory, which is the source of the prognostic variable, is chosen to be precipitation evaporation. This variable is interesting since it is a vague proxy of the age of the convective system: there is more precipitation and thus more precipitation evaporation in an older or stronger convective system. They made this choice of memory source, since they anticipate a memory effect due to downdraft-related cold pools and consequently gust fronts. Note that they performed this study in a single-column model only, but they had a dramatic improvement of the diurnal cycle over land: introducing memory does seem to delay the diurnal cycle and correct one of the typical GCM weaknesses.

Mapes and Neale [2011] also implemented an idea of memory related to rain evaporation, but in a 3-D setup, although they did not explicitly talk about “memory”. They introduce a prognostic variable as well, which is a non-dimensional scalar variable meant to represent convective organisation, as will be motivated further in section 1.5. In their GCM, the prognostic variable builds a time-lagged positive feedback in the parameterization of convection. The source of this prognostic variable is rain evaporation, which is a simple representation of current convective state (figure 1.8). This prognostic organisation variable is then used to enhance convection in several ways, and in particular by reducing the entrainment rate (making wider clouds) and increasing plume base temperature. Both studies [*Piriou et al.*, 2007; *Mapes and Neale*, 2011] represented this time-lagged relationship by adding a prognostic variable to link precipitation evaporation (related to the strength of convection, so related to cloud width) and entrainment rate.

In the wake of such studies, Martin Willett, at the UK MetOffice [Willett 2014,

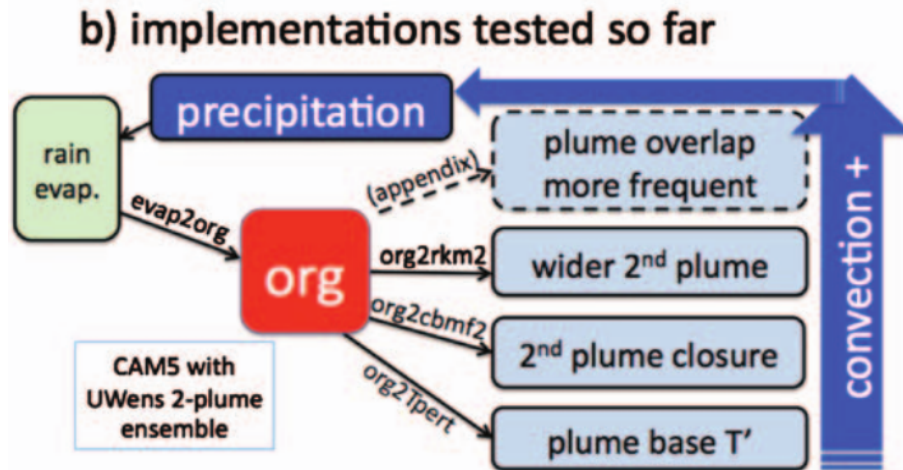


Figure 1.8 Convection scheme with prognostic organisation variable “org” as implemented by *Mapes and Neale* [2011]. Rain evaporation is a source for org, which then influences the width of the cloud (and therefore entrainment rate), and a few other variables. This positive feedback is a process that leads to convective memory. From *Mapes and Neale* [2011]

personal communication] [*Willett and Whitall*, 2017], has also tested a similar prognostic variable in the Unified Model to capture the effects of convective memory. They relate the surface precipitation (roughly related to the strength of convection, so related to cloud width) at time t , $t-1$, etc. . . with the entrainment rate at time t . We can simply think about it as the past precipitation affecting the future entrainment rate. The prognostic variable is a 3-D evolution of recent surface precipitation, so that the memory storage is done via a kind of surface precipitation bucket. The source of this prognostic variable is the actual surface precipitation. The memory variable in turns affect the entrainment rate computation, so that with a higher memory storage, the cloud is wider and there is a lower entrainment rate. This gave very promising results as well, with not only a more realistic diurnal cycle, but also better convection structures in the tropics.

These three previous studies [*Piriou et al.*, 2007; *Mapes and Neale*, 2011; *Willett and Whitall*, 2017], via a varying entrainment rate depending on previous convective conditions, have all introduced some form of convective memory. They suggest it is relevant to focus efforts on convective memory.

Other recent studies have come up with a promising pathway to introduce convective memory: via cold pools. Although it was not their main objective, *Grandpeix and Lafore* [2010] and *Del Genio et al.* [2015] introduced some memory

via their prognostic cold pool schemes. The prognostic variables are the cold pool thermodynamic properties (their temperature and humidity anomalies) and some cold pool geometric properties (such as the surface fractional area occupied by cold pools, and in *Del Genio et al.* [2015] the cold pool depth as well): the memory is stored in the cold pools. In other words, one could claim that cold pools are the memory storage. There are several sources for these prognostic variables, but in essence they are in the downdraft mass flux and downdraft properties, which entail precipitation evaporation.

There is also a scheme fully based on prognostic representation of prognostic processes: *Park* [2014]. In this scheme, there are numerous prognostic variables, so that the memory storage becomes multiple. These prognostic variables include sub-grid cold pools but also mesoscale organised flows in the boundary layer. This scheme allows not only for a better representation of the diurnal cycle, but also for a better Madden-Julian Oscillation, showing that schemes with memory can also improve spatial organisation of convection.

The main prognostic variables used in the above studies are relatively diverse: convective kinetic energy, probability of undiluted updrafts, convective organisation, recent convective precipitation, cold pools (thermodynamic and geometric properties), and mesoscale organised flows. These are the main memory repositories identified by parameterization developers. These prognostic variables also have a very diverse range of sources: CAPE, precipitation evaporation, surface precipitation, and cold pool formation processes, in particular downdraft mass flux.

Nevertheless, these studies did not bring systematic evidence, nor experimental evidence to support their hypotheses on where memory resides (memory storage) and where it comes from (sources of memory storage). They proposed such memory sources based on physical reasoning or practical purposes. The only few previous studies which have tried to demonstrate the origins of convective memory are *Davies et al.* [2013a] and perhaps *Jones and Randall* [2011]. In this thesis, we aim to determine more thoroughly where memory resides and points to where it comes from, with a systematic method based on cloud-resolving simulations. Findings could help develop prognostic closures for convective schemes with more grounded

arguments.

1.4.6 Time scales of convective memory

Convective memory effects naturally lead us to think about the time scale of this memory. Most of studies that have investigated convective memory or convective organisation have pointed out typical time scale of a few hours. For example, *Mapes and Neale* [2011] have chosen about 3 hours for 2° grid cells (for the feedback related to their organisation factor). Similarly, Martin Willett at the UK MetOffice [Willett 2014, personal communication] chose time scales ranging from an hour to a few hours to describe the lasting effect of precipitation on the atmosphere. So, in attempts to represent memory in GCMs, the time scales involved are often about a few hours. In studies that have focused on a particular aspect of convective memory, we also find very similar time scales. For instance, *Rio et al.* [2009], resorting to preconditioning of convection and cold pool effect, managed to shift the diurnal maximum of precipitation by about 4 hours. It seems that simulations by *Piriou et al.* [2007] have a phase lag ranging from 3 to 7 hours, which remains consistent with the above values.

Other investigations have completely focused on the time scales related to convective history. For example, *Davies et al.* [2009] have used a relatively simple theoretical model to investigate the consequences of choosing a memory time scale on the development and occurrence of convection. They have shown that for theoretical systems with little memory (that is, small value of memory time scale, $\simeq 1$ h), convection is tightly knit to the forcing, and thus convection is quite predictable. For systems with long memory (high value of memory time scale, $\simeq 24$ h), convection doesn't feel the variations of the forcing much, it only feels the time-averaged forcing. In this case, convection is also predictable. However, for intermediate value of the memory (between about 6h and 20h), convection becomes non-repetitive, with sometimes strong convective events and sometimes weak convective events. In the latter case, closer to reality, convection is very hard to predict, and seems to bear a strong random component. This is exactly the case that will be tackled here, in a different context. They demonstrated that it is for forcing time scales between 6h

and 20h that it is the most difficult to predict convection. These results with three distinct categories of behaviour were confirmed afterwards by a cloud-resolving modelling study by *Davies et al.* [2013a]. Note however that the numerical values from *Davies et al.* [2009] may not be totally applicable in a more realistic simulation, as these values may depend on many assumptions made to build the theoretical model, and on the parameters chosen to run it.

Note that the introduction of a small lag (a few hours to a few days) between the large-scale forcing and convection can have indirect effects on convective variability on longer time scales (intraseasonal) [*Emanuel, 1993; Bony and Emanuel, 2005*].

1.4.7 Simple models of memory

Some simple models also try to capture some aspects of convective memory [*Davies et al., 2009; Yano and Plant, 2012a*]. *Masunaga and Sumi* [2017] have a toy model of convection with moisture storage, acting as a memory repository. These studies have attempted to look at convective memory in simple models either by mentioning memory explicitly [*Davies et al., 2009*] or implicitly [*Yano and Plant, 2012a; Masunaga and Sumi, 2017*]. Mathematical aspects of memory and persistence have also been studied [*Panchev and Spassova, 2005*].

1.5 The relationship between memory and organisation

1.5.1 Why such a link?

Convective memory is for time what convective organisation is for space. They are both coherence, lag-correlation (in space or time), and more accurately dependence of convection at the point of interest on its neighbours or its history (in space or time). In crude terms, spatial convective organisation reduces the randomness of the atmosphere, so it can also be seen in terms of memory: the atmosphere keeps the memory of its previous organisation, its previous clouds and fluctuations. The organ-

isation effects of convection give memory to the system, by the fact that organisation can only entail common, coherent, and reciprocal changes (if any). But the representation of this organisation-induced or more generally structure-induced memory is still lacking in most convective parameterizations of current GCMs. . . Organisation is definitely an important component of convective memory.

Arakawa [2004] already recognises the problem of mesoscale organisation of convection for the quasi-equilibrium problem. He writes: “Fluctuations in cumulus activity [in these organised forms of convection are] not fully modulated by large-scale forcing. (...) These fluctuations cannot be parameterized using a quasi-equilibrium assumption, showing that there is a limit of diagnostic or deterministic parameterizability. To go beyond this limit requires the introduction of more prognostic equations to predict transient cumulus activity or stochastic components representing uncertainties on the initial conditions for those equations. The concept of quasi-equilibrium can be either implicit in the prognostic system or can be used as a weaker constraint on the system”. He goes even further and explains that to represent convective organisation, one needs to have a prognostic scheme, i.e., memory. Without making the connection with memory explicitly, this sentence already suggests the intimate link between organisation and memory.

Pan and Randall [1998] first introduced the idea of memory, but did not explicitly mention convective organisation. They decided the memory would reside in the Convective Kinetic Energy. Although they did not talk about organisation explicitly, they did seem to have some organised convective structures in mind, the ones carrying the kinetic energy. With *Mapes and Neale* [2011], it is the opposite: they talk about organisation, but not memory. Their goal was clearly to represent convective organisation, and since they did it in a prognostic way, they did introduce some memory. These two studies already made important steps towards linking memory and organisation. Other studies [*Mapes et al.*, 2009] have shown evidence towards the link between convective organisation (spatial systems) and memory (the timing). A previous PhD thesis first proposed the connexion between convective organisation and memory [*Davies*, 2008].

Yano and Plant [2012b] are also close to making the connection between memory and organisation. They discuss two alternative theories to quasi-equilibrium: activation control [*Mapes, 1997*], and self-organised criticality. The idea of activation control directly tackles the issue of triggering for quasi-equilibrium, and self-organised criticality relates to organisation. In their opinion, these two theories are compatible between each other, but then it is unclear whether quasi-equilibrium can hold or whether parameterizations must become prognostic. Here we state that the activation control is a non-quasi-equilibrium behaviour, because there is no direct link between the large-scale forcing and convection, since one has to check whether the activation threshold (e.g. convective inhibition) is overcome before applying any balance between the large-scale forcing and convection. The activation control, i.e., the triggering condition, clearly introduces a hysteresis in the system, so that no quasi-equilibrium idea can hold. Moreover, we state that if one really takes on both ideas of activation control and convective organisation, not only would quasi-equilibrium be invalid, but the diagnostic assumption would also have to be abandoned, because of the dependence of convection on its own history, at least through the non-linear activation threshold to overcome and the spatial coherence. So a prognostic formulation is required to fully implement both activation control and organisation theories, necessarily introducing memory into the system.

There is probably a two-way relationship between convective organisation and convective memory. In a case with more convective organisation, we have stronger structures, so that there may be more memory: organisation would imply memory. To confirm this intuition, we will investigate in details the impact of different convective organisation types on the memory (chapter 2). Reciprocally, if there is a lot of memory in the system, it must be carried by some structures (the memory repositories). This suggests a form of organisation is necessary to carry the memory from one time step to the next: memory would imply organisation as well. Thus, it is likely that organisation is both a sufficient and necessary condition for memory. Although we have no evidence of it at this stage, it is even possible that convective memory and convective organisation are actually different points of view of the same phenomenon.

For further discussion, see the comments given in Chapter 2, which is part of a

manuscript submitted for publication as: Colin et al (2018), Identifying the sources of convective memory in cloud-resolving simulations, *Journal of the Atmospheric Sciences*.

1.5.2 Convection organisation and convective self-aggregation

The organisation of convection in space is ubiquitous: it happens all around the Earth, at a wide range of scales. It can take a wide range of shapes and lots of phenomena may be involved. More importantly, there are many spatial scales of convective organisation, from 1 km to thousands of kilometres. Usually, it is understood that organised structures on scales smaller than 1 km (or larger than thousands of kilometres) may be not included in “convective organisation”, since not all convective-related structures may be called “organisation”. Convective organisation can range from cold pools to tropical cyclones, via Mesoscale Convective Systems (MCS).

Tropical cyclones [*Wang and Wu, 2004*] are an extreme form of organization at a large scale, but with different scales being involved. They lead to heavy rainfall, potentially causing flooding and landslide [*Emanuel, 2005; Chang et al., 2013*] and they have consequently been the centre of attention for a long time.

Mesoscale Convective Systems [*Houze, 2004*] are good examples of organised convection. They can be squall lines [*Houze, 1977*], supercells [*Grant and van den Heever, 2014*], and other forms of multi-cumulonimbus cloud systems which produce rain continuously over large areas. They have a non-trivial dynamics, related to interplay between scales. MCS feed back on the large-scale environment, and can even lead to tropical cyclone. Observations from satellites and scatterometers by *Mapes et al.* [2009] have shown the life cycle of wind convergence and precipitable water accumulation associated with MCS over the tropical oceans.

Squall lines are a common type of MCS, observed for example over continental West Africa [*Provod et al., 2016*] or over tropical oceans [*Houze, 1977*]. They consist in a line of convective cores, connected by a large trailing stratiform part. Low-level wind shear seems to play a key role in forming and shaping the squall line, as

formalised by *Rotunno et al.* [1988]. The sensitivity of squall line and convective organisation more generally was investigated in a more idealised configuration by *Robe and Emanuel* [2001]. These studies seem to show that the role of wind shear is connected with the cold pools created by the squall line, thus self-maintaining itself. The circulations in these squall lines is still an active topic of research [*Bryan et al.*, 2007].



Figure 1.9 Photo of a squall line from Nebraska, United States. From Business insider.

A theory to classify and model convective organisation was proposed by *Moncrieff* [1981]; *Miller and Moncrieff* [1983], based on observed convection. These models of convective organisation are important to generate understanding and improve parameterized convection. The key variable in their classification is vertical wind shear, although they recognise CAPE and downdrafts are also playing a role in organising convection. They come up with four main types of organised convection: classical, steering-level, propagating, and jump type. There is also a fifth type of organisation, which is called the cellular model, and is similar to convective self-aggregation (which will be defined below). An alternative model for convective organisation designed for parameterization was written by *Moncrieff* [1992]. This model was a combination of the jump and the steering-level models. Instead of try-

1.5. THE RELATIONSHIP BETWEEN MEMORY AND ORGANISATION

ing to be as comprehensive as the four organisation types, it was aiming to be easier to implement in GCMs. But unfortunately, this model has not been implemented in GCMs yet.

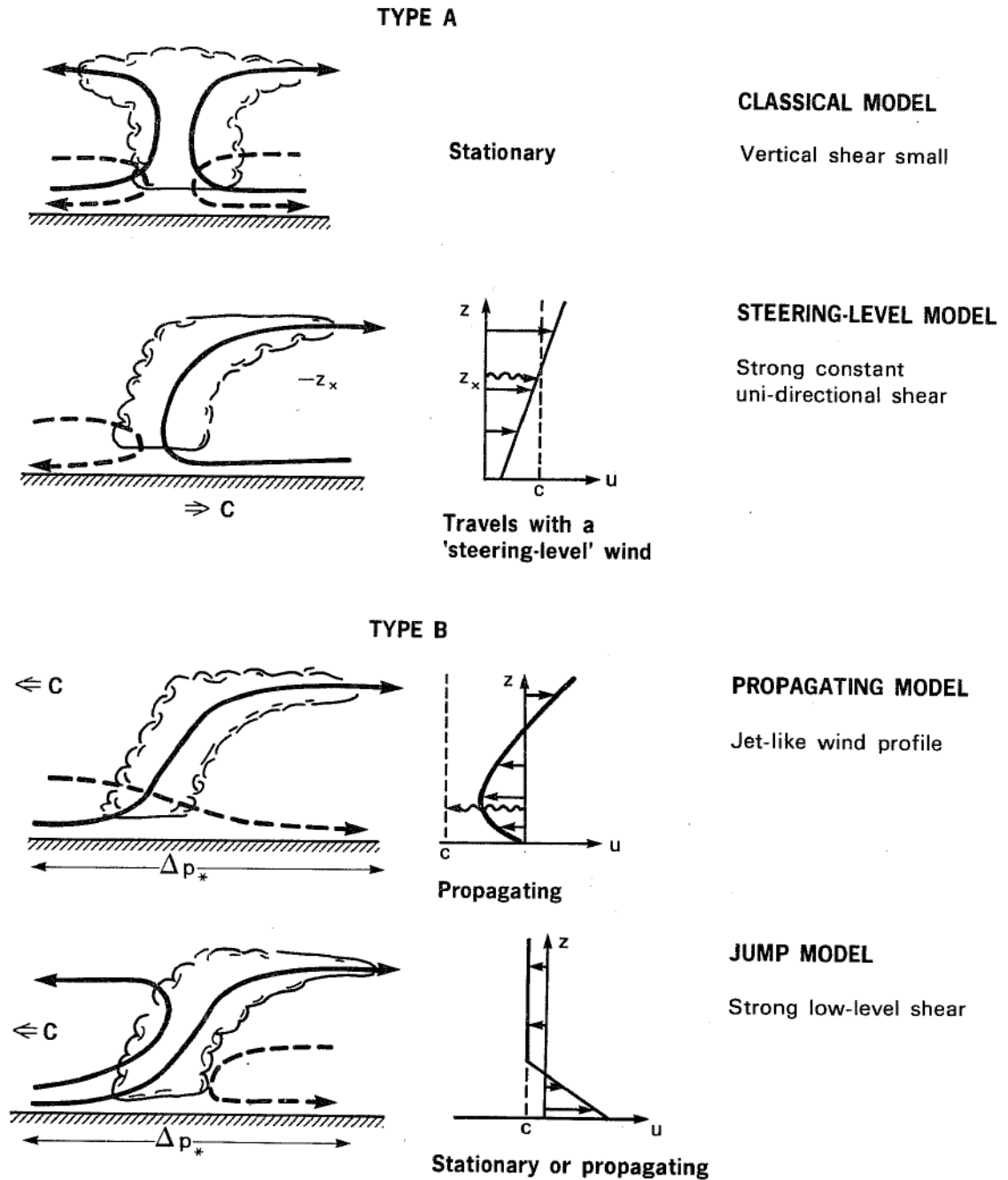


Figure 1.10 Schematic of four types of organised convection, for different wind shear profiles and consequently different dynamical regimes, entailing different qualitative transport of momentum. From *Miller and Moncrieff* [1983]

Another different kind of convective organisation is the Madden-Julian Oscillation (MJO) [Zhang, 2005; Raymond and Željka Fuchs, 2009]. The MJO is the most important component of intraseasonal variability in the tropics, and as such attracts

a lot of attention. It is a large-scale Eastward-propagating wave creating wind disturbance and enhanced convection, observed in the tropical Indian and western Pacific ocean only. Its period varies between 30 to 90 days. Since it is a persistent kind of organisation at large-scale related to larger-scale waves, it is very different from the convective organisation types mentioned above (such as MCS). Not only is convection organised longitudinally, due to the peaks and crests of the large-scale wave, but it is also organised meridionally, due to the trapping of the MJO along the Equator. The MJO is largely observed, usually through a series of indices [*CLIVAR Madden-Julian Oscillation Working Group: Waliser et al., 2009*], and it has also been reproduced in cloud-resolving models [*Wang et al., 2016*]. Although progress are being made [*Krishnamurti et al., 2016*], a consistent and accepted theory of the MJO is still lacking [*Jiang et al., 2015*].

One could also argue that the Inter-Tropical Convergence Zone (ITCZ), and the associates monsoon regimes, are also a form of convective organisation, though it is on much larger scales. The ITCZ is the region of the world where precipitation is the highest, due to heat and moisture availability and low-level large-scale wind convergence. The monsoons are still a major topic of research, since predicting when they will occur is of direct relevance to the population affected by heavy monsoon rainfall.

One particular form of convective organisation that has generated a lot of attention recently is self-aggregation. With this form of organisation, convection spontaneously aggregates to create a small dense moist and convective region, surrounded by a large dry and subsiding region. This happens without external forcing. This is mostly a behaviour that appears in Cloud-Resolving Models (CRM) [*Bretherton et al., 2005; Muller and Held, 2012; Wing and Emanuel, 2014; Tsai and Wu, 2017*] and General Circulation Models (GCM) [*Coppin and Bony, 2015; Becker et al., 2017*]. Although it is still difficult to observe aggregation in the real world, some attempts are being made and could prove increasingly insightful [*Tobin et al., 2012; Holloway et al., 2017*]. The self-aggregated state appears as an alternative equilibrium state of the models, which were originally thought to reach a simple scattered convection equilibrium state when run to a statistical radiative-convective equilibrium [*Emanuel et al., 2014*]. The possibility that models may have multiple equilibrium

states naturally generates a lot of research.

The processes that initiate and maintain convective self-aggregation are numerous and multifaceted, and recent studies try to disentangle them (see the review by *Wing et al.* [2017]). It has been shown that convective self-aggregation is related to the low cloud distribution ([*Muller and Held*, 2012]). To be more specific, they suggested a mechanism for this effect, which consists of a positive feedback between the longwave radiative cooling and the convergence circulation around low clouds. So both factors have to be taken into account when looking for organised convection in cloud-resolving simulations. But processes other than radiation may also be important for self-aggregation: *Tompkins and Semie* [2017] have shown the important role of horizontal mixing (and potentially other processes impeding convection) to generate self-aggregation.

Moreover, the conditions under which self-aggregation occurs in long-term simulations is another important enigma. *Muller and Held* [2012] show that self-aggregation of convection can occur not only when the domain is large enough (> 200 km), but also when the resolution is coarse enough (> 2 km). *Jeevanjee and Romps* [2013] proposed an explanation based on cold pools to explain the dependency on domain size. The sensitivity of convective self-aggregation to Sea Surface Temperature (SST), convection scheme, and large-scale forcing has been investigated by *Bao et al.* [2017] to understand the link between convective organisation and extreme precipitation.

1.5.3 The role of cold pools in organisation

In the real world, cold pools are not only a key element in convective organisation, but they may also partly account for its development and its maintenance. The cold pools are a defined structure of the low-level atmosphere, related to convection, so they are part of the convective organisation. They can be determined thanks to their density current property: the air volume at low levels that is denser than its environment, when this high density is related to precipitation evaporation. This means a cold pool boundary can be found by its low virtual potential temperature. However, for simplicity, it is still common to use the temperature for cold pool

detection [*de Szoeke et al.*, 2017]. A review of oceanic cold pools was written by *Zuidema et al.* [2017].

Observations of cold pools are useful, though they are usually limited to a single dimension. First, cold pools have been observed by surface stations, usually over fixed land based stations [*Provod et al.*, 2016], but also from ships [*Feng et al.*, 2015]. These only provide 0-dimension measurements since instruments usually measure the near-surface thermodynamic properties when the cold pool passes over the station. Such measurements show that when the cold pool travels over the station, temperature drops by about 1 K over ocean and by about 5 K over land, water vapour mixing ratio may increase by 0.1 g.kg^{-1} over ocean and decrease by about 1 or 2 g.kg^{-1} over land, wind speed increases by 2.5 m.s^{-1} over ocean and by 5 m.s^{-1} over land, wind direction changes by about 80° over land, and pressure increases by about 2 hPa over land. While these station observations are very insightful, they are sparse, case-dependent, and do not give a 3-dimensional view of the cold pools. 3D cold pool observation techniques from radars are developing [*Lothon et al.*, 2011; *Rowe and Houze*, 2015; *Feng et al.*, 2015], but they often require manual checks. Satellite imagery could become useful but it is not sufficient for cold pool detection yet [*Zuidema et al.*, 2017]. This generally supports efforts spent for more intensive observations of cold pools.

Cold pools are able to trigger subsequent convection, so that they may play a role in convective organisation [*Marshall and Parker*, 2006; *Rowe and Houze*, 2015]. This can be explained by two different processes: a dynamic effect and a thermodynamic effect of cold pools. The dynamic effect is related to the spread of cold pool at the surface due to their negative buoyancy (density current). The spread of cold pools mechanically lifts the air in front of the cold pools upwards since it is warmer than the cold pool. This helps bringing air aloft for convection. Moreover, cold pool spread creates gust winds near their leading edges. The resulting turbulence can also favour convection near cold pool edges. This two aspects of the dynamic effect of cold pools on subsequent convection was originally considered the main reason for convective triggering by cold pools. But there is also a thermodynamic effect due to the presence of moisture patches around the edges of cold pools [*Tompkins*, 2001a; *Schlemmer and Hohenegger*, 2014]. The moisture patches reduce convective inhib-

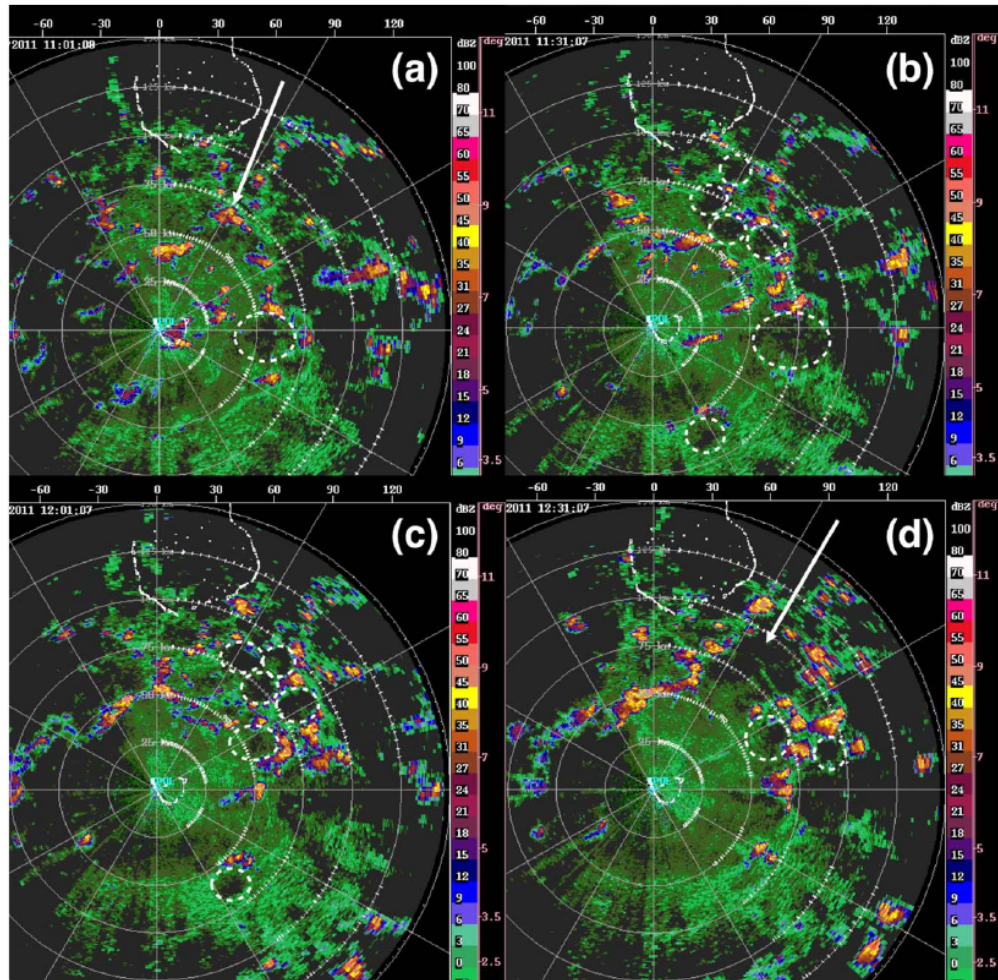


Figure 1. A sequence of S-PolKa radar-observed convective cells and cold pools (subjectively identified by white-dashed circles) over the tropical Indian Ocean on 10 October 2011 at (a) 1100 UTC, (b) 1130 UTC, (c) 1200 UTC, and (d) 1230 UTC. The S-Pol radar was deployed on Addu Atoll, Maldives during the 2011 AMIE/DYNAMO field campaign. Each concentric solid white circle increases by 25 km and the outer most circle marks the 150 km maximum range of the radar.

Figure 1.11 Cold pools over the tropical Indian ocean, as seen by the absence of reflectivity from radar observations, during the AMIE/DYNAMO field campaign. The cold pools are subjectively identified and marked by white dashed circles, at (a) 1100 UTC (b) 1130 UTC (c) 1200 UTC (d) 1230 UTC. The spatial scale is given by the concentric circles centred around the radar: there is one circle every 25 km. From *Feng et al.* [2015].

ition, thereby supporting new convection. The origin of the moisture patches, or moisture rings, is multiple: rain evaporation, surface fluxes, older moisture advected from the downdrafts, and entrainment at the boundary layer top. The contribution of each of these processes to the moisture patches has been investigated by [*Langhans and Romps, 2015; Schlemmer and Hohenegger, 2016; Torri and Kuang, 2016*]. The thermodynamic effect has been thought to be dominant over the dynamic effect, although both effects may actually play a role [*Torri et al., 2015*].

Although cold pools help trigger new convection around their edges, they are a negative feedback for self-aggregation. Indeed, the air inside the cold pool is cold and

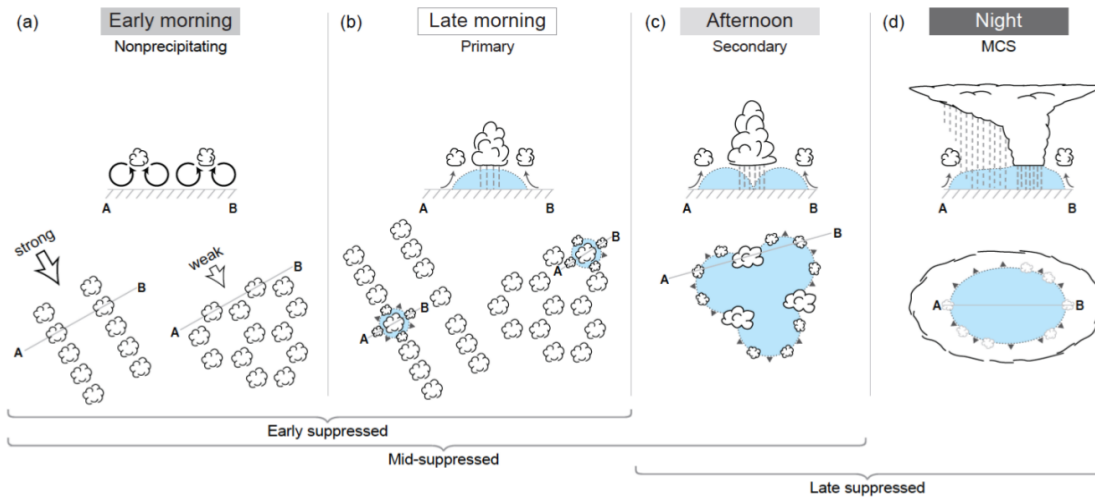


Figure 1.12 Schematic of upscale growth of convection due to cold pools, for different phases of the Madden-Julian Oscillation. New convection is triggered around cold pool edges, and this allows for convective organisation, and development of a Mesoscale Convective System (MCS). From *Rowe and Houze* [2015].

dense, so that it has a low moist static energy. This makes it less likely to generate new convection. This negative feedback of cold pools and associated downdrafts on self-aggregation has been shown by *Jeevanjee and Romps* [2013]; *Muller and Bony* [2015] and others.

This means there are two competing effects of cold pools on convection: they do trigger convection, but also make it sparser. This is simply because cold pools trigger subsequent convection around their edges, but prevent convection inside them. This trade-off could still be clarified further, which would probably help make cold pools easier to represent in GCM.

1.5.4 Representation of cold pools in GCMs

Although it is still a recent and new area of GCM parameterization, cold pool parameterizations are becoming increasingly popular. The first cold pool scheme was probably *Qian et al.* [1998]. Their cold pools, called wakes, already have detailed geometrical and thermodynamic features. The cold pool model includes special calculation of surface fluxes in the cold pools, entrainment at cold pool top, and gust front properties. By coupling this cold pool scheme with a downdraft scheme, they are able to simulate a convective life cycle, including the termination of a convective

event. This is very encouraging when thinking about improving the diurnal cycle. This scheme was tested in a 1-D GCM (the Community Climate Model, CCM3) by *Rozbicki et al.* [1999], which pointed at many difficulties when comparing with squall line observations.

It is only a decade later that cold pool scheme development really took off. *Grandpeix and Lafore* [2010] developed a cold pool scheme with prognostic thermodynamic characteristics (cold pool temperature and humidity anomalies) and prognostic cold pool surface area in the grid cell. This scheme will be further described in subsection 1.5.5. It was first implemented in 1-D [*Grandpeix et al.*, 2010]. And then it was successfully added to the 3-D model developed at Institut Pierre-Simon Laplace (IPSL): it entered the operational version B of the atmospheric component of the IPSL GCM for CMIP5 (Coupled Model Intercomparison Project Phase 5), i.e. the version LMDZ5B of the atmospheric GCM, which is part of the version IPSL-CM5B of the coupled climate model [*Hourdin et al.*, 2013]. According to the 1-D implementation, the properties of parameterized cold pools were in relative agreement with observations, and the coupling between cold pools and the convection scheme led to similar heat tendency, moisture tendency, and precipitation as a comparable situation simulated by a cloud-resolving model. The 3-D implementation of the cold pool scheme as well as other physical parameterizations led to several improvements, including the diurnal cycle [*Hourdin et al.*, 2013].

The successes of this implementation probably inspired others, and a few cold pool parameterizations exist nowadays. *Park* [2014] developed a unified convection scheme, UNICON, with prognostic cold pools and mesoscale organised flow in the boundary layer. This is a very elegant way of replacing traditional scheme by a unified convection scheme with cold pools, able to represent dry convection, shallow convection, and deep convection.

Grandpeix and Lafore [2010] cold pool parameterization is quite detailed. To take advantage of such a detailed scheme but in a more pragmatic way, *Del Genio et al.* [2015] developed a simpler cold pool scheme inspired by both detailed explicit cold pool schemes [*Qian et al.*, 1998; *Grandpeix and Lafore*, 2010; *Park*, 2014] and also by simple implicit treatments [*Piriou et al.*, 2007; *Mapes and Neale*, 2011]. This

parameterization still has prognostic cold pool thermodynamic properties (cold pool temperature and humidity) and prognostic geometric properties (cold pool surface area and depth).

Part of the community requests simpler parameterizations, with fewer details and processes, and more heuristic approaches. With this philosophy, the UK MetOffice is developing a simple cold pool representation where cold pools simply increase the Turbulent Kinetic Energy (TKE) in the boundary layer, and therefore enhance subsequent convection [Alison Stirling 2017, personal communication]. This work is based on similarity theory results by *Rooney* [2015].

Whether it is by an explicit representation of cold pool processes, or by simple semi-empirical representation of cold pool effects, there is a clear tendency to develop more and more cold pool schemes.

1.5.5 Case of LMDZ: deep convection scheme, cold pool scheme, and thermal-plume scheme

The atmospheric component of the IPSL global climate model is LMDZ (Laboratoire de Météorologie Dynamique Zoomed). In this thesis, we use a version of LMDZ which has undergone several recent developments with respect to LMDZ5B, which was one of the LMDZ version used for the Coupled Model Intercomparison Project Phase 5 (CMIP5). The version we use is almost identical to version 2420 from 2016-01-05, and it is described in this subsection.

LMDZ has a buoyancy-sorting mass flux deep convection scheme based on *Emanuel* [1991] and *Emanuel and Živković Rothman* [1999] but with subsequent modifications, as well as an ALP closure controlled by two sub-cloud processes: thermals and cold pools [*Rio et al.*, 2013]. The interplay between all these components is reviewed by *Hourdin et al.* [2013].

The cold pool scheme by *Grandpeix and Lafore* [2010] models a population of circular cold pools (or “wakes”) in each grid cell, without communication or propagation between grid cells at this point. The cold pools are assumed to be pure density currents, which all have the same size. The parameterized cold pools have separate

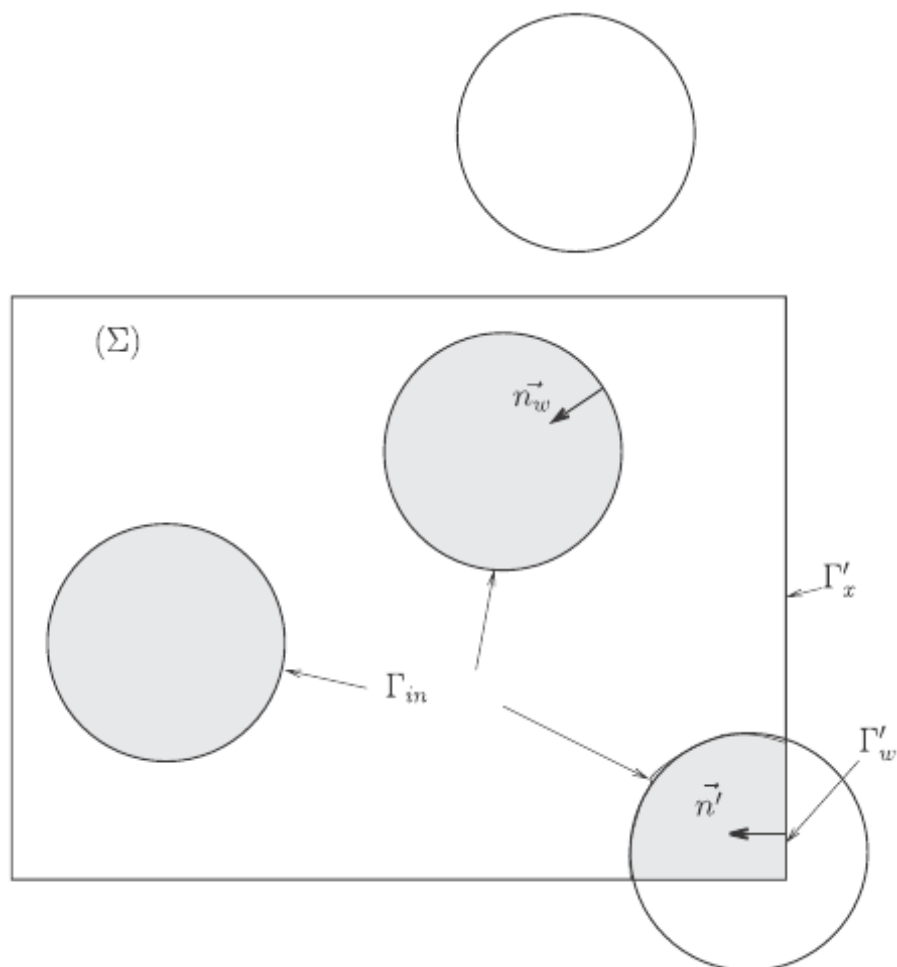


Figure 1.13 Representation of cold pools in a GCM grid cell, as seen from above, for the cold pool parameterization used in the LMDZ GCM. From *Grandpeix and Lafore* [2010].

thermodynamic variables (temperature and humidity) compared to their environment, which is one of their key properties and has a key effect in the parameterization. These cold pools are able to spread at the surface, according to their available potential energy, which is related to their negative buoyancy. They have a downward vertical velocity, and entrain air from their environment near their top. Cold pools impact convection in three ways: triggering via Available Lifting Energy (ALE), closure via Available Lifting Power (ALP), and through the warmer environment they create outside of them (convection is only triggered out of the cold pools, where the air is warmer than in the cold pools by definition). Creation of a warmer environment outside cold pools can be seen as a representation of the thermodynamic effect of cold pools, and the closure in ALP can be seen as a representation of the dynamic effect of cold pools, although the two aspects of the parameterization

probably do not match identically the two actual phenomena. The triggering of convection is decided by a comparison between the convective inhibition and the ALE due to cold pools or thermals. The ALE related to cold pools is calculated as the vertical integral of cold pool negative buoyancy, thus being like a “Wake” Available Potential Energy (WAPE), which is then converted to horizontal kinetic energy during cold pool spread, which is in turns converted to upward vertical kinetic energy at cold pool edges, thus helping in triggering. These are the three ways for cold pools to have an effect on convection. Reciprocally, convection also affects cold pools via the updrafts/downdrafts separation: the unsaturated downdrafts feed the cold pools, through their cooling and moistening tendencies, which models the fact that precipitation evaporation drives the cold pools. Conversely, the saturated updrafts remain outside the cold pools, which ensures updrafts do not affect cold pool air. There is thus a two-way interaction between the cold pool scheme and the convection scheme.

There is also a thermal-plume parameterization representing the Boundary Layer (BL) thermals [*Rio and Hourdin, 2008*]. A key impact of thermals is through the triggering of deep convection, which has been modified by recent developments (post-CMIP5) [*Rochetin et al., 2014a,b*]. The thermals are now represented by a size distribution following a double-exponential Probability Distribution Function (PDF), based on Large-Eddy Simulations (LES) results. When the thermals become large enough, their vertical velocity increases and they may be able to trigger convection under two consecutive conditions. First, the maximal vertical velocity of the strongest thermal has to exceed a given threshold, which means that the thermal-related ALE and the convective inhibition have to be compared. Second, a stochastic condition on the maximum cloud size reached by the cloud ensemble is imposed: if this condition is met, the ALE is unchanged, but if the condition is not met then the ALE is set to zero. Thus the dynamic triggering condition on vertical velocity (via the kinetic energy, i.e. ALE) is modulated by a stochastic component that interplays as an additional geometric triggering condition.

In the GCM, there are two ways to trigger convection: by cold pools, and by boundary layer thermals. There is thus a competition between thermals and cold pools to trigger convection, and the larger of their ALE has to be compared with

the convective inhibition (CIN) to decide whether or not to trigger the convection scheme. Conversely, for the convective closure, which is based on ALP, the effects of cold pools and saturated thermals add up to each other [Rio *et al.*, 2013].

1.6 Aim of the thesis

The aim of the thesis is to trace back the physical origins of convective memory and to better understand the processes involved in convective memory, in order to improve parameterizations of tropical moist convection in General Circulation Models (GCM) by introducing some elements of convective memory. Eventually, the long-term goal is to help improve future predictions in climate and weather contexts.

This general aim can be subdivided into three main objectives:

- Better understand where convective memory comes from, and better quantify it
- Analyse the memory of a GCM and assess to what extent it resembles the memory of a CRM
- Draw conclusions for future parameterization developments

This implies there are several intermediate goals:

- assessing whether convective memory is important, and evaluating its order of magnitude
- providing a framework to better understand convective memory and to analyse convective memory in a rigorous way
- determining where convective memory is dominantly stored, finding the dominant sources of convective memory, and pointing at how this can help parameterization development
- understanding the basic physical process leading to convective memory and

the extent of its impact

- building a simple model of convection with memory
- analysing the processes that may already bring some form of memory in the convection scheme of a General Circulation Model (GCM)
- comparing convective memory in a GCM and in a cloud-resolving model
- showing how better knowledge about convective memory can be used in a GCM
- testing a simple improvement of a convective parameterization (by changing its memory), and showing the improvement on process representation and climate properties

The scope of the thesis is limited in different ways. First, the thesis is not aimed at developing a convective parameterization in itself, but rather to act as a guide for understanding of convection and parameterization development. Second, we do not attempt to fully analyse each process that may lead to memory one by one, and we do not attempt to compare an infinite list of processes together to determine the proportion by which they are a source for memory. Instead, we develop a comprehensive approach which encompasses all potential processes being a source of memory, and we choose to ask where this memory resulting from many processes is physically stored. Third, we mostly analyse Radiative-Convective Equilibrium (RCE) simulations, and we do not try to compare them with a large number of non-RCE simulations or observations. We thus assume that the RCE setup is a good testbed for process understanding, so that its results would remain valid in other setups, at least qualitatively.

1.7 Overview of the thesis

We will first determine the relevance, magnitude, sensitivity, and preferred storage of convective memory (Chapter 2). We will then analyse more specifically the physical mechanisms behind microstate convective memory, and we will build a simple toy model of convection with memory to capture its essence (Chapter 3). A

comparison between the memory in a Cloud-resolving Model and a General Circulation Model (GCM) will be drawn to determine the issues related to with memory representation in convective schemes (Chapter 4). An improvement of GCM rainfall frequency thanks to changes in memory occurring via the cold pool scheme will then be presented as a simple application of the knowledge gained on memory (Chapter 5). The thesis will end by a final conclusion and discussion (Chapter 6), followed by appendices on various issues connected to the approach to memory presented here.

Chapter 2

Identifying the sources of convective memory in cloud-resolving simulations

Essential parts of this chapter form a revised manuscript which has been submitted for publication as: Maxime Colin, Steven Sherwood, Olivier Geoffroy, Sandrine Bony, David Fuchs (2018), Identifying the sources of convective memory in cloud-resolving simulations for various convective organisation types, *Journal of the Atmospheric Sciences*. I performed all the simulations, carried out all the analyses, and led the writing of this manuscript. The design of the experiments has been done with Steven Sherwood. The results have been discussed with all co-authors, and all helped in the writing of manuscript. Olivier Geoffroy and David Fuchs occasionally provided useful technical assistance.

2.1 Abstract

Most convective parameterizations diagnose convective effects from the simultaneous environmental mean state, but memory of previous convective-scale behaviour may also be important. This study proposes a new framework in which the latter, “microstate” memory, is distinguished from macrostate memory, and conducts

numerical experiments to reveal these memory types. A suite of idealized, cloud-resolving radiative-convective equilibrium simulations in a 200-km square domain is performed with the Weather Research and Forecasting (WRF) model. Three deep convective cases are analysed: unorganised, organised by low-level wind shear, and self-aggregated. The systematic responses to sudden horizontal homogenisation of various fields, in various atmospheric layers, designed to eliminate their specific microstructure, are compared in terms of precipitation change and time of recovery to equilibrium.

Results imply a substantial role for microstate memory. Across organisation types, microstructure in water vapour and temperature has a larger and longer-lasting effect on convection than in winds or hydrometeors. Microstructure in the sub-cloud layer or the shallow cloud layer has more impact than in the free troposphere. The recovery time scale dramatically increases from unorganised (2-3 hours) to organised cases (24 hours or more). Longer time scale adjustments also occur and appear to involve both small-scale structures and domain-mean fields. These results indicate that most convective microstate memory is stored in low-level thermodynamic structures, potentially involving cold pools and hot thermals. This memory appears strongly enhanced by convective organisation. Implications of these results for parameterizing convection are discussed.

2.2 Introduction

Understanding atmospheric moist convection is one of the main challenges to advance models used for climate projections, seasonal forecasts, and weather forecasts [Jakob, 2014]. These Atmospheric General Circulation Models (GCMs) have important shortcomings, and many of them are attributed to the convective parameterizations. GCMs rain too often and too little [Stephens *et al.*, 2010]. They tend to produce too much high cloud and too little shallow cloud [Chepfer *et al.*, 2008; Sherwood *et al.*, 2013]. They can even produce cloud and precipitation responses to warming that have opposite signs [Stevens and Bony, 2013]. They struggle to represent a realistic diurnal cycle [Rio *et al.*, 2009; Stratton and Stirling, 2012; Bechtold

et al., 2014; *Folkens et al.*, 2014], and to simulate the spatial organisation of convection [*Mapes and Neale*, 2011; *Rowe and Houze*, 2015; *Tan et al.*, 2015] and its temporal variability (e.g. Madden-Julian Oscillation (MJO)) [*Dai*, 2006; *CLIVAR Madden-Julian Oscillation Working Group: Waliser et al.*, 2009].

One prominent debate on convective parameterization concerned the “quasi-equilibrium” hypothesis, which formed the basis for pioneering convective parameterizations [*Arakawa and Schubert*, 1974; *Arakawa*, 2004]. Quasi-equilibrium in this context means that convection is in equilibrium with the large-scale forcing: convective effects act to keep modifications of a closure variable (e.g. Convective Available Potential Energy) close to zero, compensating for large-scale processes.

A similar but weaker and more fundamental assumption that has received much less scrutiny is the “diagnostic assumption”, made in most convective parameterizations. For convection, this assumption is that convective effects at a large scale (and at time t) can be diagnosed at all from the state variables at that scale (and at the same time). Convective schemes that involve a separate triggering of convection do not obey quasi-equilibrium [*Emanuel*, 1991; *Yano and Plant*, 2012b], since a triggering condition must be met before allowing convection to respond to the forcing. However, they usually do diagnose both the triggering and closure variables from the current grid-scale state: they still make the diagnostic assumption.

But it is far from clear that the diagnostic assumption is justifiable. Because of the finite resolution of models, many unresolved processes, which generally have their own internal time scales, bring inertia to the system. And a diagnostic relationship cannot represent this, because it effectively assumes that all such time scales are no longer than the model time step, which is typically of order 10 minutes in GCMs. Yet the time for a single updraft to penetrate the troposphere is longer than this. Moreover, the current trend is for models to have finer grid spacing and shorter time steps, so that this diagnostic assumption is increasingly problematic. This problem is already partly discussed in *Bougeault and Geleyn* [1989].

To go beyond the diagnostic assumption one would need to add one or more prognostic variables into the scheme, which would carry information (“memory”) on the previous behaviour of unresolved processes. If convection were to be diagnosed

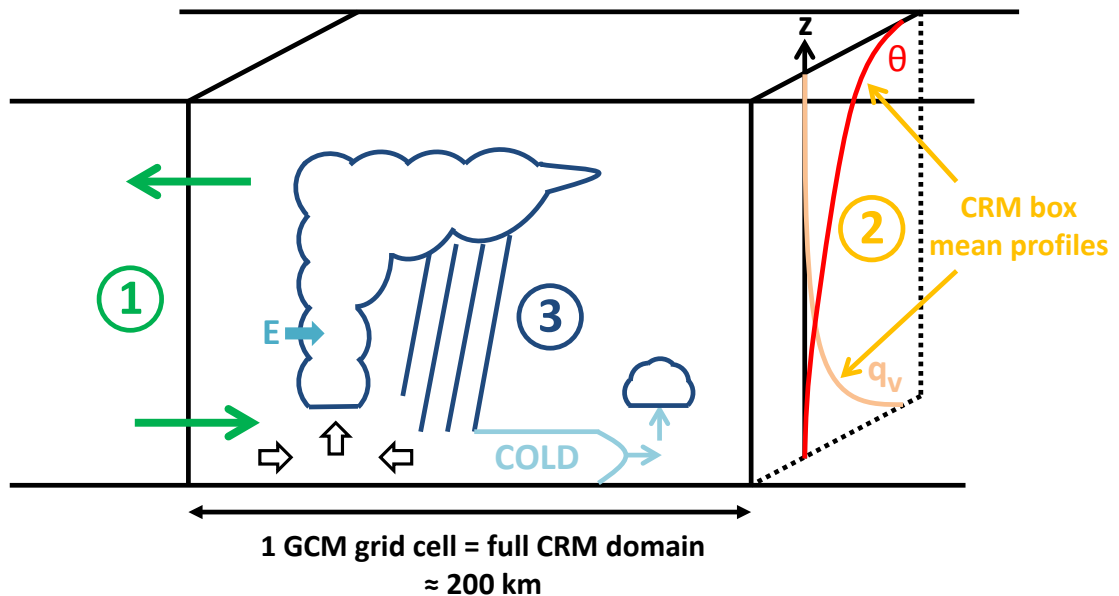
by an equilibrium with the large-scale forcing, it would only be sensitive to the recent history of the forcing. With a prognostic formulation, not only do we have non-equilibrium convection, but convection is also made sensitive to its own history.

A few examples of such schemes exist. To our knowledge, the first was the scheme by *Randall and Pan* [1993] or *Pan and Randall* [1998]. Their prognostic variable is the Cumulus Kinetic Energy (CKE), whose source is taken to be the product between the cloud work function and the cloud-base mass flux.

Another early work on prognostic closure is *Chen and Bougeault* [1993], whose memory resides in prognostic convective vertical velocity and convective area fraction. Later, in the parameterization with memory by *Pirou et al.* [2007], the prognostic memory variable is the probability of undiluted updraft, and its source is chosen to be precipitation evaporation, because downdraft-induced gust fronts are thought to be involved. The higher this variable, the lower the entrainment rate. Similarly, *Mapes and Neale* [2011] use a prognostic “ORG” variable to quantify the spatial organisation of convection. They assume that precipitation evaporation is the main source of ORG. *Guérémy* [2011] uses a prognostic convective vertical velocity, whose source is buoyancy. *Willett and Whitall* [2017] also introduce some memory in the UK MetOffice model, via a prognostic variable representing a recent surface precipitation bucket. Their source of memory is surface precipitation, and its effect is also on the entrainment rate. *Qian et al.* [1998], *Grandpeix and Lafore* [2010] and *Del Genio et al.* [2015] have some memory residing in prognostic cold pool thermodynamic (mostly temperature and/or water vapour) and geometric properties, although they do not necessarily remark on its role. Their sources are downdraft mass flux and associated cooling and moistening linked to precipitation evaporation. *Park* [2014] has memory residing in both cold pools and mesoscale organised flows, with similar sources: downdraft mass flux and associated cooling and moistening as well as other cold pool damping processes. Other potential memory sources are gust winds, and cloud spacing [*Cohen and Craig*, 2004].

While these efforts are important, they were arguably ad hoc and have not led to a consensus on whether memory needs to be explicitly included in models or how to do it. The current study is intended to be a step toward establishing more

generally whether memory is important and how it might best be represented.



- ① Synoptic-state memory (interaction between several GCM grid cells)
- ② Macro-state memory (one GCM grid cell, mean profiles in the CRM box)
- ③ Micro-state memory (sub-grid for a GCM, resolved for the CRM)

Figure 2.1 Schematic of the three different types of memory that can emerge with respect to a mesoscale λ (which may be a finite model resolution, but also more generally any length scale). Limited resolution stems from the GCM grid cell (equivalent to a full CRM domain). (1) refers to synoptic state memory: it arises from processes that involve several GCM grid cells, such as synoptic-scale convergence/divergence, the Hadley circulation or Convective Instability of the Second Kind. (2) refers to macrostate memory: it arises from processes that impact the local profiles of a single GCM grid cell, i.e. the mean profiles of the full CRM box (for example the mean profiles of specific humidity and potential temperature). And (3) refers to microstate memory: it arises from GCM sub-grid scale processes, i.e. resolved CRM processes (for example rain evaporation, cold pools, secondary triggering of convection by cold pools, cloud entrainment, convergence under cloud base). Current GCMs resolve the synoptic state memory through circulation, and the macrostate memory through convective parameterization. However, they are generally blind to microstate memory.

We define convective memory as the dependence of convective behaviour on its own history, for given current large-scale (i.e. external or “environmental”) conditions. This is broadly consistent with *Davies et al.* [2009] who define it via cloud life cycles. By analogy with statistical physics, one can define a microstate (description of all elementary units) and a macrostate (description of the collective behaviour) for convection. In accord with this analogy, let λ be a typical length scale of the system (e.g. typical GCM grid spacing ($O(100 \text{ km})$)). We refer to the state variable

fluctuations below the scale λ as the *microstate*. The mean state at the scale λ is referred to as the *macrostate*. Finally, the atmospheric state at a scale larger than λ is referred to as the *synoptic state*. System memory can reside at each of these three scales: we distinguish between microstate memory stored in microstate structures, macrostate memory stored in macrostate structures, and synoptic state memory stored in synoptic state structures (Figure 2.1). When λ becomes smaller, individual unit effects start to be seen at the macrostate, and we would expect a non-equilibrium description of the microstate to be increasingly necessary to explain the macrostate.

Microstate memory can be more precisely defined in terms of conditional probabilities. At each time t , let us define a measure of the convective state $C(\lambda, t)$ and a measure of the large-scale variables $\xi(\lambda, t)$. If convection had no microstate memory, the convective state $C(\lambda, t_0)$ would be conditionally independent from earlier convection $C(\lambda, t) \forall t < t_0$, given the large-scale state $\xi(\lambda, t)$. Microstate convective memory is the dependence of the PDF of $C(\lambda, t)$ on its own history, for given environmental conditions $\xi(\lambda, t)$.

Though convective memory as defined above will make convection more persistent, persistence alone does not establish memory: even if $C(\lambda, t_0)$ shows persistence, this could be due to persistence of $\xi(\lambda, t)$, itself arising for whatever reason.

Nonetheless, since memory should contribute to autocorrelation in time, convective memory may be viewed as strongly related to organisation of convection in time. Furthermore, spatial convective organisation is widely recognized as a key aspect of convective processes, more recently in simulations of self-aggregation [Bony *et al.*, 2015; Wing *et al.*, 2017] but for many years in studies motivated by observed organisation where background wind shear plays an important role [e.g. Moncrieff, 1981; Rotunno *et al.*, 1988]. Thus, we want to investigate the link between organisation in time (memory) and organisation in space [Davies, 2008; Mapes and Neale, 2011; Moseley *et al.*, 2016].

Most small-domain model studies examine unorganised (“popcorn”) convection [Parodi and Emanuel, 2009; Wang and Sobel, 2011; Singh and O’Gorman, 2014]. But the degree of convective organisation may be important in convective memory

[Mapes and Neale, 2011; Moseley et al., 2016]. Thus, we will examine convective memory for both organised and unorganised cases.

The approach for identifying convective memory proposed here is based on the response of convection simulated by a Cloud-Resolving Model (CRM) for a domain size λ comparable to a typical global-model grid cell. We first introduce the methods (Section 2.3). We then present results on the main variables and atmospheric layers where convective memory resides, and we examine the role of convective organisation (Section 2.6). Finally we summarize the results and discuss potential consequences for parameterization of convection (Section 2.9).

2.3 Methods

2.3.1 The simulations

For simplicity, this study uses control simulations in Radiative-Convective Equilibrium (RCE). RCE provides a testbed for assumptions about convection and memory: if the assumptions are good, they should hold in RCE.

To assess convective memory in a wide range of situations, we conduct simulations of several convection types:

- The “unorganised” case. It is run with fixed Sea Surface Temperature (SST), interactive surface fluxes, and no wind shear. The convection is non-organised.
- Unorganised case with fixed surface fluxes. Latent and sensible surface fluxes are held uniform in space and constant in time, to the average values in the RCE state of the “unorganised” control run.
- Wind shear organised case. A wind, linearly varying with height (uniform shear), is imposed between heights of 0 and 4 km, by a moderate relaxation applied only to the domain-mean horizontal wind value. The imposed wind profile is 0 m s^{-1} at the surface, and 20 m s^{-1} at 4 km and above. This is similar to what was used in some previous studies [Robe and Emanuel, 2001; Anber et al., 2014].

- Self-aggregated case. To get self-aggregation in the model, it was necessary to choose different turbulence and microphysics schemes (see Subsection 2.3.2).

In each case, simulations are spun up to an RCE state and then perturbed away from RCE to observe the response.

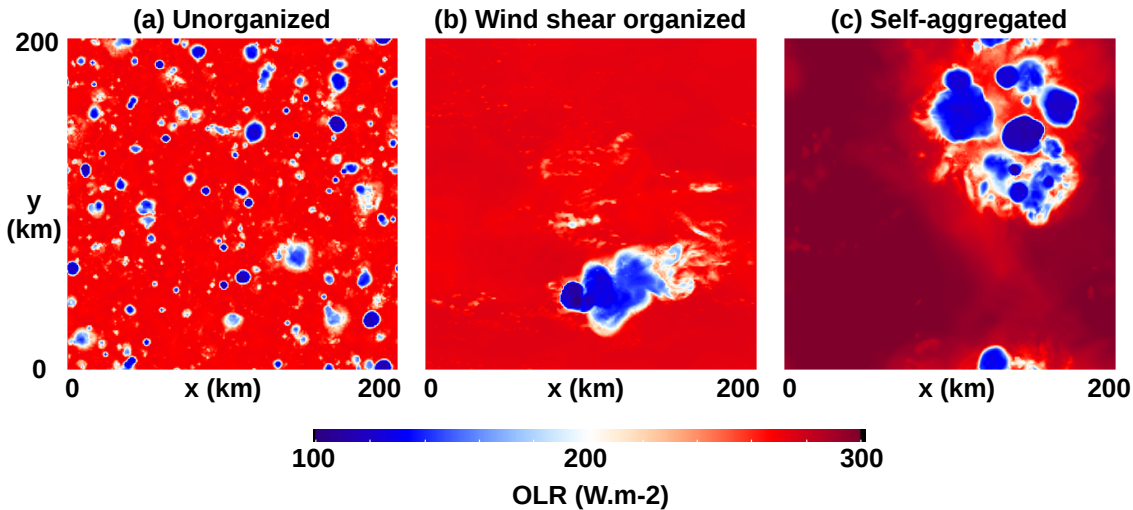


Figure 2.2 Snapshots of Outgoing Longwave Radiation (OLR) in the domain, in the Radiative-Convective Equilibrium state, towards day 80 or 81 of the control runs, for three convective types with different convective organisation: (a) unorganised case, (b) wind shear organised case, with the wind shear being positive and along the x-axis, (c) self-aggregated case.

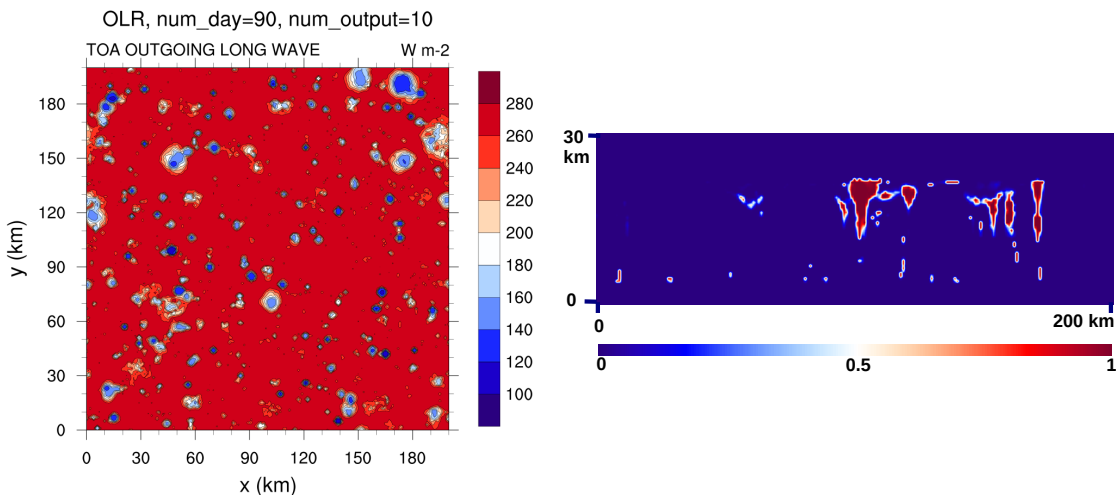


Figure 2.3 (left) Instantaneous snapshot of Outgoing Longwave Radiation (OLR) during the 90th day into the 3D control simulation, showing unorganised convection (right) Instantaneous vertical section of the 3D cloud fraction for the same simulation during the 90th day. Note that the y-axis is model levels, which are not linear with height nor pressure.

The unorganised case leads to scattered (“popcorn”) convective cells (Figure 2.2

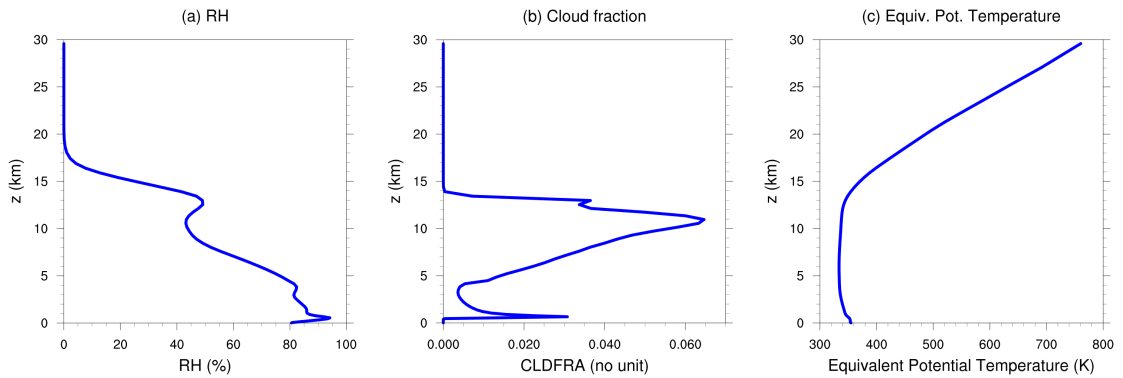


Figure 2.4 Horizontally-averaged equilibrium profiles for the 3D unorganised control simulation (3D-Ctrl) (see table D.1), computed on the last month of the simulation. (a) Relative Humidity. (b) Cloud fraction as defined on 3D grid cells. (c) Equivalent potential temperature.

and Figure 2.3). Overall, the mean RCE profiles (Figure 2.4) resemble those obtained in previous studies (e.g. *Romps* [2011]). They also compare well with the humidity profiles obtained from observations by radiosondes over the ocean, by *Liu et al.* [1991]. In the case with imposed wind shear, convection creates elongated anvils parallel to the shear, with only one or two large convective cores in the domain. This creates a single large cold area near the surface, fed by several downdrafts. In the self-aggregated case, convection self-aggregates into a humid region surrounded by extremely dry areas in about 20 days.

2.3.2 Model and setup

We use the Weather Research and Forecasting (WRF) model, Version 3.6, in its Advanced Research WRF (ARW) form [*Skamarock et al.*, 2008; *Wang et al.*, 2014] and in its “idealized test” framework. WRF-ARW dynamics solves the fully compressible, Euler non-hydrostatic equations. The horizontal grid staggering follows an Arakawa C-grid, and the vertical coordinate is the terrain-following hybrid σ -levels. Time integration is done by a sophisticated 3rd order Runge-Kutta scheme. Horizontal advection is a 5th-order scheme, and vertical advection a 3rd-order one. We hereby present 3D simulations.

We use doubly periodic boundary conditions, and a fixed Sea Surface Temperature (SST) of 302 K (except in the fixed-surface-flux case). The horizontal domain size is 202x202 points, and the horizontal grid spacing is 1km. The vertical grid

consists of 69 levels, going from the flat ocean surface up to the model top, which is about 30km. We use a stretched vertical grid spacing: the vertical distance between two consecutive levels starts from 30m near the surface, increases to 100m near the cloud base, stays at 400m in most of the free troposphere, reaches 500m near the tropopause, and further increases to 2km near the model top. The Coriolis parameter f is set to zero.

In terms of dynamical options, we choose an implicit gravity-wave damping layer (sponge layer) for vertical velocity in the top 5 km of the model. We also use full diffusion in physical space. A 3D prognostic equation for Turbulent Kinetic Energy (TKE) is used to calculate turbulent eddy fluxes via a K coefficient based on TKE, except for the self-aggregation case where the 3D Smagorinsky turbulence scheme is used instead. The influence of the turbulence scheme on self-aggregation has been investigated by *Tompkins and Semie* [2017].

The physical parameterizations include the Yonsei University Boundary Layer scheme, which is a non-local K scheme, and a revised MM5 (NCAR Mesoscale Model 5) surface layer scheme based on Monin-Obukhov theory for computation of surface heat and moisture fluxes. There is no need to impose a minimum wind for surface flux calculations in this scheme [*Jiménez et al.*, 2012], since the wind is automatically enhanced by a convective velocity (and for low-resolution runs by a subgrid velocity), and since our runs already show realistic values of surface fluxes. No cumulus parameterization is used. To be general, we choose a microphysical scheme with intermediate complexity and allowing for unorganised convection for most of our simulations: the WRF Single-Moment 6-class scheme (WSM6) [*Hong and Lim*, 2006], which includes water vapour, cloud water, rain, ice, snow, and graupel. We replace it by the Thompson microphysics scheme for the self-aggregated convection case, as tests showed that this scheme always produces strong self-aggregation. However, we could not use this latter scheme in all our cases, since it cannot lead to unorganised convection. Explaining the sensitivity of self-aggregation to the microphysical scheme would require further study. Sensitivity tests confirmed that choosing a different microphysical scheme does not change memory significantly, provided convective organisation can be kept similar (see Subsection 2.6.7).

We use interactive radiation, with the RRTMG schemes for both longwave (LW) and shortwave (SW) radiation. Solar absorption by the specified (default) ozone profile produces a stable stratosphere. For simplicity we remove the diurnal cycle by making the cosine of the solar zenith angle constant at 0.8 (following *Cronin* [2014]), and by decreasing the solar constant to 544 W m^{-2} , applying the usual mean insolation calculation to the Equator rather than to the whole Earth (see Subsection 2.4.2).

2.3.3 Other simulation settings

For the spin-up to RCE in the unorganised control run, the initial profiles for temperature and water vapour are chosen as the default initial sounding in the RCE test case available in WRF v3.7.1. There is no initial wind (even in the wind shear case). During initialisation, random temperature perturbations (white noise) of up to 3 K amplitude are added in the first 2.5 km. These initial profiles do not matter much since we only consider the RCE state in the rest of the study.

The runs are performed for 80 to 100 days, with about 30 days of spin-up time required to reach statistical RCE equilibrium as measured by the mean precipitable water [*Tompkins and Craig*, 1998]. To be conservative we skip the first two months of each control simulation before initiating any experiments.

Following *Held et al.* [1993] and *Wang and Sobel* [2011], a light nudging towards zero (or towards the imposed shear, in the shear case) is imposed on the domain-mean horizontal winds. We do not expect the light nudging towards zero to significantly affect results.

2.3.4 Design of perturbation experiments

To reveal convective memory, we impose instantaneous changes to the WRF microstate without changing the macrostate. Our experiments use a very simple kind of perturbation: horizontal averaging (hereby called “homogenisation”) of a given subset of prognostic state variables on model levels, at a selected time step. Then the model is restarted from these partly homogenised conditions with no other

changes. We compare the evolution of convection following perturbations of different prognostic variables (or sets of variables) to that with no perturbation applied (control). We perturb all prognostic variables in WRF, namely: potential temperature, water vapour mixing ratio, hydrometeor mixing ratios, 3D winds, geopotential, column-integrated dry air mass, and Turbulent Kinetic Energy (TKE) (see Table 2.1).

Table 2.1 List of variables averaged in the homogenisation experiments. The model is restarted from different horizontally homogenised conditions of combinations of these variables. q_c, q_r, q_i, q_s, q_g respectively refer to the mixing ratios of cloud liquid water, rain, ice, snow and graupel.

<i>Symbol</i>	<i>Variable</i>
q_v	water vapour mixing ratio
θ	potential temperature
\mathbf{u}	3D winds (u,v,w)
q_{cond}	all hydrometeors (q_c, q_r, q_i, q_s, q_g)
PH	geopotential
MU	dry air mass in the vertical column
TKE	Turbulent Kinetic Energy

Usually, Cloud-Resolving Model studies perturb the macrostate (the forcing), and observe the time scale of the response [*Kuang, 2010; Raymond and Herman, 2011*]. The recovery in this case involves feedbacks between convection and macrostate, so could be slow due to long macrostate memory, even in absence of microstate memory (i.e. even if convection adjusts instantly to the macrostate). To minimize this issue and reveal microstate memory instead, our homogenisation perturbations do not affect the macrostate, only the microstate.

The RCE state varies in time due to chaotic internal variability. Consequently, as in previous studies [*Cohen and Craig, 2004*], we ensure statistically significant results by constructing ensembles, repeating each experiment at 5-20 different restart times taken from the RCE state reached by each convective case. A measure of uncertainty is presented in Figure 2.13.

2.4 Supplementary information on the methods

2.4.1 Methods for the preliminary 2D tests

Model set-up and physical parameterizations for the preliminary 2D tests

The 2D tests performed in this study almost have the same set-up as the 3D experiments, except for the following points. The 2D tests are run with a 202x3 domain (the actual 2D set-up necessary in WRF). The boundary layer scheme (Yonsei University) was not activated in the 2D runs. And the diurnal cycle was kept in 2D.

Other simulation settings for the 2D tests

Some of the simulations are performed in a 2-Dimensional (2D) set-up. Since the earliest 2D Radiative-Convective Equilibrium studies [*Held et al.*, 1993; *Tompkins*, 2000; *Wang and Sobel*, 2011], it has been noticed that an instability develops in the 2D framework: horizontal wind jets become increasingly powerful and eventually make the model unstable. Our simulations have shown this unstable behaviour. As in previous studies [*Held et al.*, 1993; *Wang and Sobel*, 2011], to solve this problem, light nudging is imposed on horizontal winds: we add a term in the equation so that horizontal winds are slightly relaxed back towards zero at each time step, with a time scale $\tau_{nudg} = 6\text{h}$:

$$\frac{\partial u}{\partial t} = -\frac{u_{avg} - u_{target}}{\tau_{nudg}} \quad (2.1)$$

Here u is the wind along the x-axis, u_{avg} its horizontal average along x and y, and $u_{target} = 0$ is the nudging target that we chose for u , except for the simulation with shear where the target wind is non-zero.

This ensures stability in 2D. To ensure consistency and rigorous comparison with the 2D runs, this light nudging on winds has also been kept active in the 3D simulations.

2.4.2 Methods for the 3D simulations

Imposing fixed Short-Wave (SW) radiation in the 3D runs: solar zenith angle and solar constant choices

For an Equatorial situation, *Cronin* [2014] showed that a proper absorption-weighted zenith angle, reflecting best the diurnal mean reflection of Short Waves (SW) by the atmosphere, should have a cosine of 0.8 (see their figure 4). So we took the cosine of the solar zenith angle as a pure constant of the model

$$\mu^* = \cos(\zeta^*) = 0.8 \quad (2.2)$$

(where μ^* is the cosine of zenith angle to impose in the idealised simulation without diurnal cycle, and ζ^* the corresponding zenith angle). This choice implies $\zeta^* \simeq 37$ deg. The insolation given by our idealised case must be equal to the time-averaged insolation of the real Equatorial situation, which means [*Cronin*, 2014]

$$S_0^* \mu^* = \langle I \rangle \quad (2.3)$$

(where S_0^* is the solar constant to impose in the idealised case, I the insolation of the real world, and $\langle . \rangle$ denotes time and space average in the real world). The usual reasoning for a planetary mean insolation, is that an area section of πR^2 incoming solar beam is spread over the full area of the Earth $4\pi R^2$ (with R the Earth radius), so that

$$\langle I \rangle = S_0 \frac{\pi R^2}{4\pi R^2} = \frac{S_0}{4} \quad (2.4)$$

(with S_0 the solar constant of the real world). However, here, we only consider an Equatorial situation, so that the incoming 1D solar beam segment of length $2R$ coming towards the Equator is spread over a circle located at the Equator, of length $2\pi R$. This is where our approach differs from *Cronin* [2014]. Hence, we instead have

for the Equatorial case

$$\langle I \rangle = S_0 \frac{2R}{2\pi R} = \frac{S_0}{\pi} \quad (2.5)$$

Thus in the RRTMG short-wave radiation scheme used in WRF, we modified the value of the solar constant to be

$$S_0^* = \frac{\langle I \rangle}{\mu^*} = \frac{S_0}{0.8\pi} \simeq 544 \quad W.m^{-2} \quad (2.6)$$

This indeed gives us an insolation (downward SW flux at the top of the atmosphere) of

$$I^* = \langle I \rangle = \frac{S_0}{\pi} \simeq 436 \quad W.m^{-2} \quad (2.7)$$

Spin-up time before equilibrium in the 3D runs

The equilibrium state is reached after about 30 days in the main 3D control simulation (see Figure 2.5).

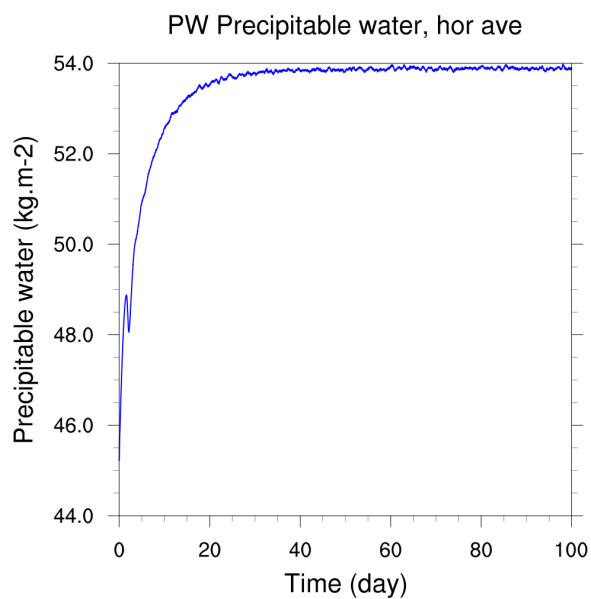


Figure 2.5 Time series of horizontally-averaged precipitable water (PW), for the 3D "normal" control simulation. Statistical equilibrium seems to be reached after 30-40 days, so that afterwards, the atmosphere is in Radiative-Convective Equilibrium (RCE) state.

2.5 Exploration by 2D test simulations

We performed preliminary tests in a more economical 2-D setup to refine the experiments to be done in 3-D. Results from these 2-D tests are shown here. All experiments reported in the rest of the chapter are performed in 3-D. The homogenisation method is schematically represented by Figure 2.6.

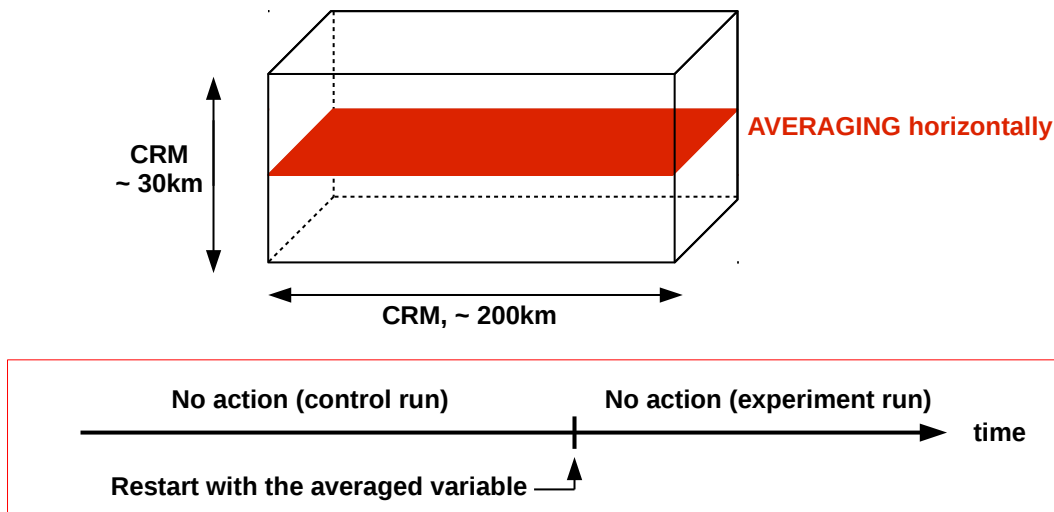


Figure 2.6 Schematic of the perturbations added in the model during restart: horizontal homogenisation of some variables at an instantaneous (pseudo-initial) time.

First we ran the most extreme experiment: homogenising all prognostic variables. In this particular case, the time required for convection to recover (12 hours) was determined by model numerics (e.g., related to float rounding errors) and so it was not physically meaningful; but this ensured our method had been implemented properly and we had not missed any prognostic variables. However, in experiments where only some variables are homogenised, the remaining inhomogeneities should relatively quickly be able to re-generate microscale motions and convection on a time scale physically meaningful for memory, since non-homogenised variables will keep their structures so numerical errors will be negligible.

Second, 2-D tests were used to qualitatively explore the role of different CRM variables on memory. These tests showed that geopotential, column dry air mass, and subgrid TKE did not contribute to convective memory, but that other variables may have a significant effect. Thanks to this result (which was confirmed in 3-D) we do not investigate further the role of these three variables.

Third, to test the sensitivity to the microphysical scheme in 2-D, we replaced the WSM6 microphysical scheme by the simple warm-rain Kessler scheme. Qualitatively the results were similar, including the relative importance of different variables for memory, even if the response amplitudes for some variables (temperature and hydrometeors mostly) were slightly different. We thus conclude that the results should not be qualitatively sensitive to the microphysical scheme.

2.5.1 Convective memory attributed to microstate structures

First, to test the role of structures in memory, we run the most extreme experiment: homogenising *absolutely all* the variables that are prognostic in WRF (Figure 2.7). Thus we get rid of all microstate structures that could impact subsequent convection. In this 2D experiment with diurnal cycle, convection is suppressed for the longest time: all precipitation is suppressed for up to 12 hours. This precipitation recovery time is longer than when we homogenise any smaller number of prognostic variables. Moreover, the system is able to go further away from the RCE state, and so the impact on convection is the strongest: precipitation drops considerably, and we detect the maximum amount of memory.

In this particular case, the time required for convection to recover (12 hours) is determined by model numerics and may not be physically meaningful: all we are doing is checking to make sure it is long. This ensures our method has been implemented properly. However, in other experiments when only some variables are homogenised, the remaining inhomogeneities should relatively quickly be able to re-generate convection on a time scale that will be physically meaningful.

The extreme experiment also confirms convective memory comes from the structures of the microstate. No microstate structures means no memory. As a contraposition statement, we can rephrase: microstate structures are a necessary condition for memory.

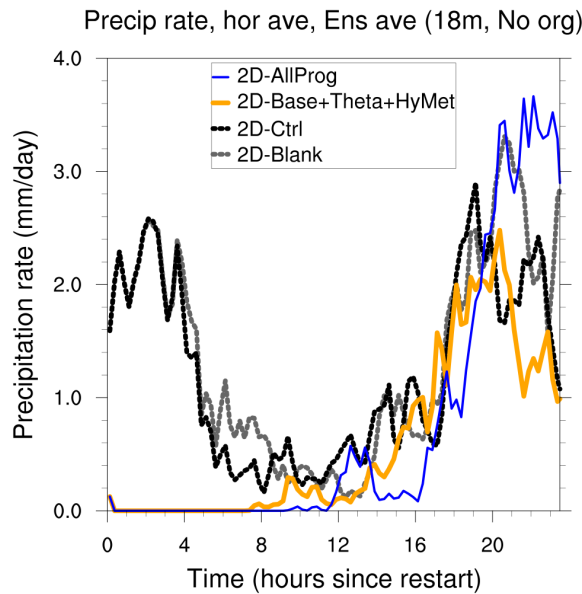


Figure 2.7 Time series of horizontally-averaged precipitation rate for different 2D Control and "Maximum effects" experiments (see table D.4), for the first 24h after restart. These results have been averaged over an 18-member ensemble of 2D simulations with warm rain microphysics (Kessler scheme), with members selected only when convection was considered clearly disorganised.

2.5.2 Which variables are the main sources of convective memory?

Second, the 2D tests are used to qualitatively explore the role of different variables on memory in the unorganised case, as 3D exploration would be too expensive. Geopotential (PH), column dry air mass (MU), and Turbulent Kinetic Energy (TKE) strictly have no impact on convective memory, although they are prognostic in the WRF model. Thanks to this result, which is confirmed in 3D too, we will not need to investigate further the role of these three variables on memory in the rest of the paper.

The 2D experiments also confirm that the only prognostic variables in WRF that may have an impact on memory are potential temperature, water vapour, winds, and the hydrometeors. All other prognostic variables have almost no impact on memory (see Figure 2.8 (right) and table D.4). It shows the additional impact of any prognostic variable on the top of a reference experiment where both water vapour and 3D winds were homogenised. Geopotential (PH), column dry air mass (MU), and Turbulent Kinetic Energy (TKE) strictly have no impact on convective memory,

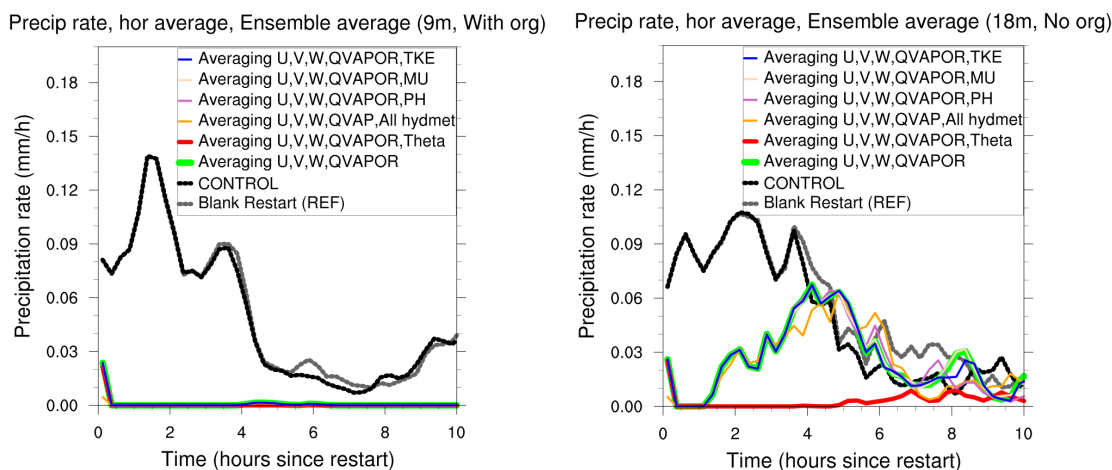


Figure 2.8 Response of horizontally-averaged precipitation rate after homogenisation and model restart, for the "Additional impact to base" 2D experiments (see table D.4). (left) and (right) respectively show ensemble averages over 9 and 18 members. (left) With the warm rain (Kessler) microphysics scheme, where there was clear convective organisation. (right) With the warm rain (Kessler) microphysics scheme, where there was no convective organisation.

although they are prognostic. Consistently with the 3D results, the hydrometeors only appear as a slight source of memory. Conversely, temperature enhances memory a lot, since precipitation recovery time scale increases at least by a factor 2, and the amplitude of the jump out of the RCE state is larger: precipitation remains zero for at least 6 hours. So water vapour, temperature and winds appear as the main variables to consider. All other WRF prognostic variables are a negligible source of convective memory.

So the thermodynamic variables are the dominant source of memory in comparison with dynamical and microphysical sources.

2.5.3 Role of convective self-aggregation in 2D

In 2D simulations with the Kessler (warm rain) microphysics scheme, some basic forms of organisation appeared (Figure 2.9).

As a proxy for convective organisation, we use the horizontal standard deviation of precipitable water. The simulation increasingly organises until day 30 (see Figure 2.10). Then the horizontal wind shear becomes too strong and progress-

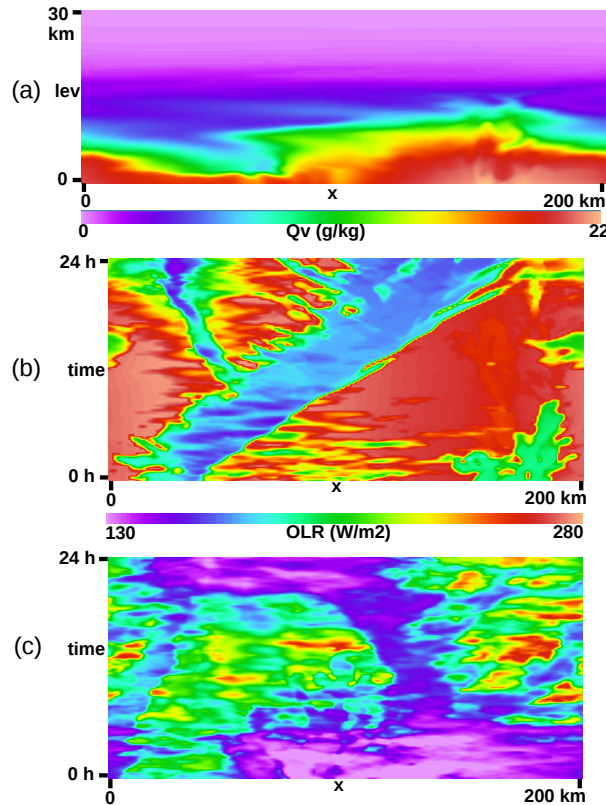


Figure 2.9 Organised and disorganised convection in the 2D control simulation with warm rain microphysics (Kessler scheme). (a) Instantaneous vertical section of water vapour mixing ratio at the 31st day, showing a dry and a humid region. (b) Hovmuller plot of Outgoing Longwave Radiation (OLR) during the organised phase (35th day). (c) Hovmuller plot of OLR during the disorganised phase (60th day).

ively breaks convective organisation. This allows us to separate days which were considered organised and days which were considered disorganised.

In 2D, there is a dramatic increase in memory in the case with organised convection, mostly for the thermodynamic variables: water vapour and temperature. Comparing precipitation response between the organised case (Figure 2.11 (middle)) and the non-organised case (Figure 2.11 (right)) clearly shows how memory increases with organisation. The precipitation response amplitude when homogenising temperature is 5 times as large with organisation, compared to without organisation. And the response time scale when homogenising water vapour is roughly 20 times as large: in the organised case, precipitation remains zero for as much as 21 hours after homogenising water vapour, whereas in the disorganised case, it remains zero for only an hour. This highlights convective organisation strongly enhances memory, at least for thermodynamic variables.

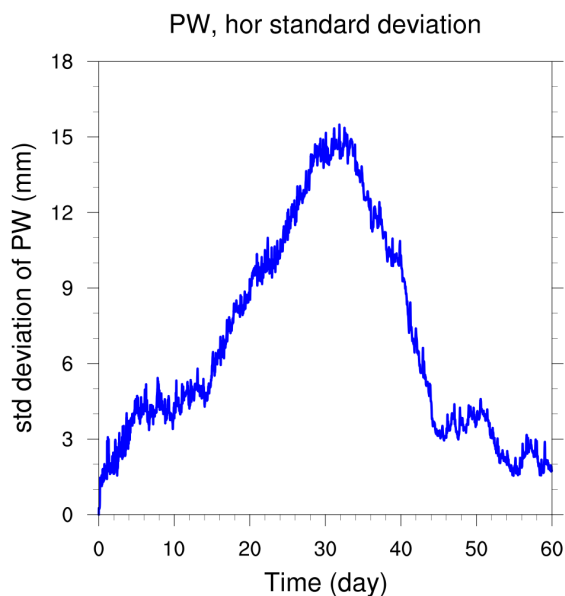


Figure 2.10 Time series of the horizontal standard deviation of precipitable water (PW), for the 2D control simulation with warm rain microphysics (Kessler scheme). The standard deviation of PW is a measure of convective organisation. There is an increase in convective organisation up to day 30, followed by a decrease. So we can split the simulation between the most organised days and the least organised days.

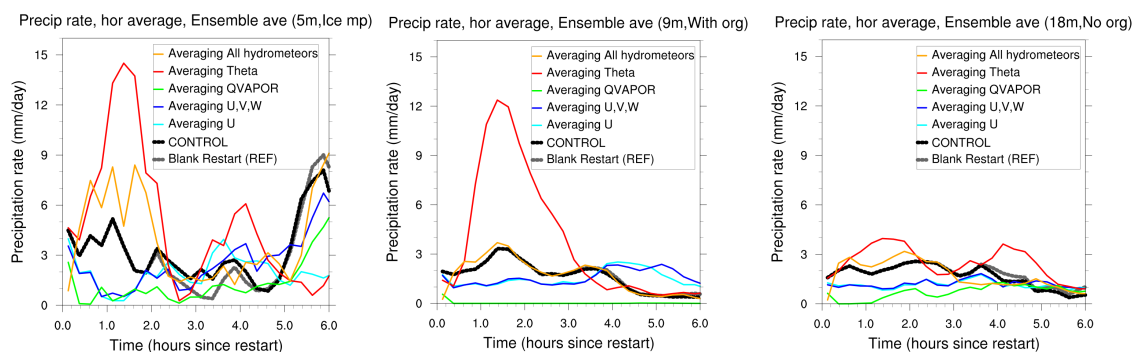


Figure 2.11 Response of horizontally-averaged precipitation rate after homogenisation and model restart, for the "Single set" 2D experiments (see table D.4). (left), (middle) and (right) respectively show ensemble averages over 5, 9 and 18 members. (left) With the normal (WSM6) microphysics scheme used in this study, in which there was no particular convective organisation. (middle) With the warm rain (Kessler) microphysics scheme, when there was clear convective organisation. (right) With the warm rain (Kessler) microphysics scheme, when there was no convective organisation.

2.5.4 Uncertainty estimate for the 2D results

Uncertainty has been estimated in the 2D "Single set" experiments by computing the standard error of the mean over the ensemble members. Each ensemble, corresponding to each experiment, is used to create a single line (Figure 2.11 without error bars, and Figure 2.12 with the error bars). And each member of an ensemble

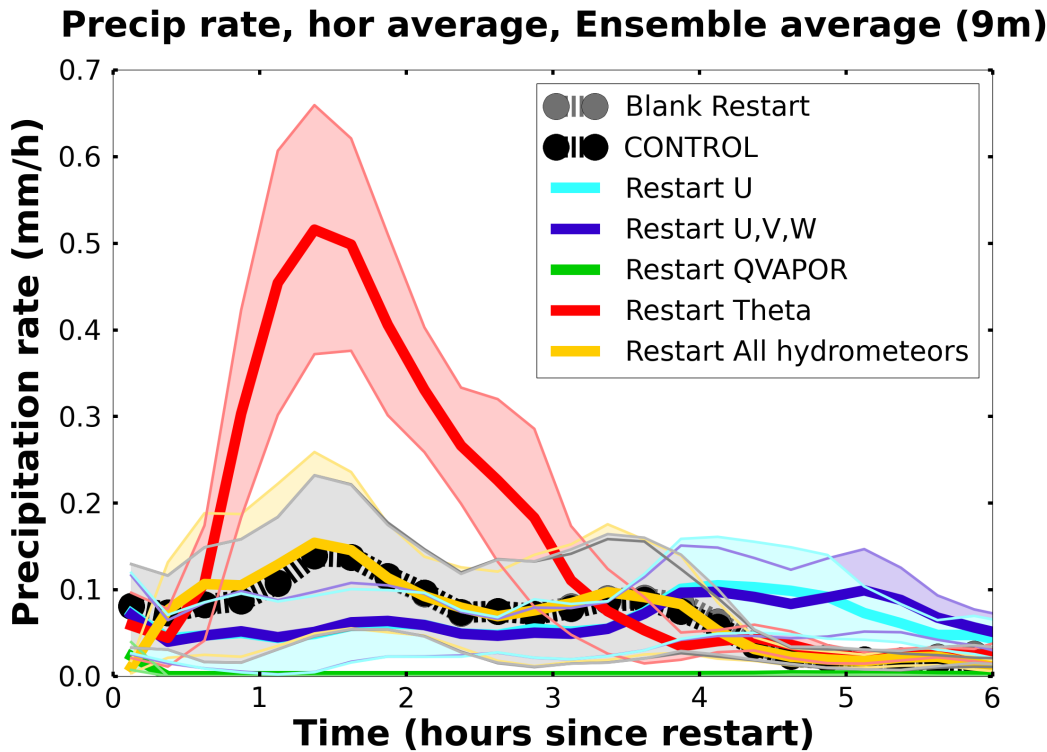


Figure 2.12 Same as Figure 2.11 (middle), but with error bars. The error bars were computed as the standard error of the mean, based on the ensemble of several members we have for each plotted line.

is a realization of the homogenisation experiment for a different restart time.

The shaded areas confirm that the results are statistically significant, in particular for temperature and water vapour in the 2D self-aggregated case: the ensembles are generally large enough.

2.5.5 Sensitivity to the microphysical scheme

Third, to test the sensitivity to the microphysical scheme in 2D, we replace the WSM6 microphysical scheme by the simple warm rain Kessler scheme. Qualitatively, the results are not found to be sensitive to the microphysical scheme, and the relative importance of different variables in memory is not altered, even though the actual amount of memory due to some variables (temperature and condensates mostly) can change slightly, when measured by response amplitude.

The previous experiments have shown the relative importance of different variables in micro-state convective memory: water vapour and temperature seem to be

the key to memory. But to test the robustness of this result, a simple sensitivity test to the microphysical scheme is performed in the 2D set-up.

In 2D, the hydrometeors contribute slightly more to memory than in 3D in terms of recovery time scale (Figure 2.11 (left)). Even though water vapour and temperature are still the main contributors to memory, winds and the hydrometeors are in this case equivalent secondary sources of memory.

Changing the single-moment 6-species WSM6 microphysical scheme for the very simple warm rain Kessler scheme, while focusing only on disorganised convection, led to a reduction in the importance of temperature and hydrometeors for memory (comparing Figure 2.11 (left) and (right)). In this 2D set-up, the choice of microphysical scheme does not matter for the memory time scale, but matters a bit for the amplitude of the responses. In particular, the impact is seen for the responses to homogenisation of temperature or hydrometeors: the importance of temperature and hydrometeors in carrying some memory is reduced with the very simple Kessler microphysical scheme. Although being speculative, it suggests the sources of memory could be slightly modified if we were to use a very refined microphysical scheme too. However, the qualitative responses were not modified as much, since the order of recovery to homogenising different variables was not swapped.

The microphysical scheme seems to play a slight role in the memory. In particular, 2D tests point out the role of temperature and hydrometeors themselves on memory becomes more important when the microphysical scheme represents more processes. It suggests that the development of microphysical schemes may help increase the memory of convection in models. This could support convective development attempts such as *Piriou et al.* [2007].

Despite this sensitivity to the microphysical scheme, shifting from a realistic single-moment scheme to a scheme without ice was a dramatic change in the physical processes being included in the computation, but only a slight change in the properties of memory, so that our results are unlikely to change with other reasonable changes to the microphysical scheme.

2.6 Results from 3D simulations

If convection were purely related to the macrostate via a diagnostic relationship, it would resume as before very rapidly. Here we therefore take the time required for recovery as a measure of microstate memory. Also, by eliminating particular microstate structures, homogenisation should erase any corresponding microstate memory, thus moving the system further away from RCE. We therefore take the magnitude of this departure as a second measure of microstate memory. Here, convection intensity is quantified via domain-averaged precipitation.

Independently, homogenising usually suppresses convection as well, because convection is inherently associated with these microstate structures. Thus, discarding structures should usually give responses with the same sign (a decrease in precipitation). As explained in Subsection 2.6.2, this turns out to be true for most experiments, and even exceptions can actually be explained by the same concept, but slightly generalized.

2.6.1 In which variables is convective memory stored?

We homogenise selected variables (see Table 2.1) at all vertical levels, for a single variable (“single set” experiments), and for multiple variables together (“double set” experiments). Preliminary experiments showed that geopotential, column dry air mass, and subgrid TKE did not contribute to convective memory. Therefore, we focus our analysis on the role of the other prognostic variables that could be important for memory: winds, hydrometeors, water vapour, and temperature.

The “single set” experiments (Figure 2.14) show that the amplitude of the precipitation response is larger when temperature or water vapour are homogenised than when winds or hydrometeors are homogenised, indicating that thermodynamic heterogeneities are more important than wind and hydrometeor heterogeneities. In the unorganised case (Figure 2.14(a) and Figure 2.16), temperature homogenisation leads to a recovery time scale of about 1.5 hours, water vapour 1 hour, and winds 1.5 hours, while for the hydrometeors the recovery time scale is about 20 min. The

response to homogenising the hydrometeors has a large amplitude but rapid time scale, indicating that while homogenising the hydrometeors impacts the precipitation initially, they are not important for memory. These results are statistically robust (Figure 2.13).

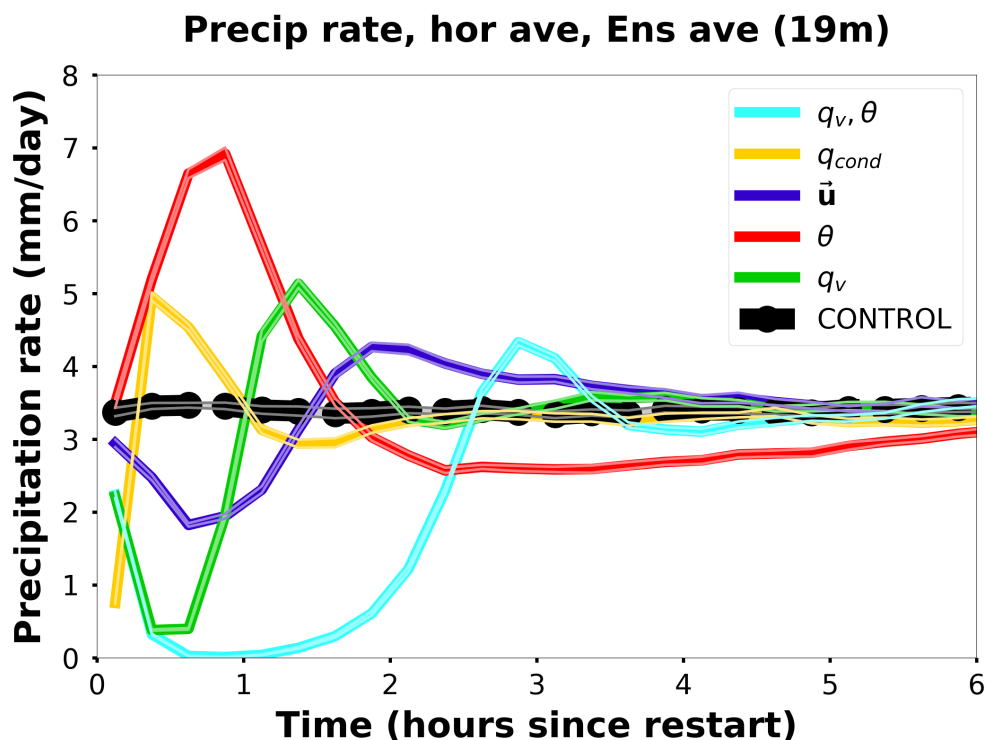


Figure 2.13 Same as Figure 2.14(a) but with a measure of the uncertainty. The standard error of the mean, for each type of homogenisation, is represented by lighter colors as the width of the lines representing the ensemble mean by darker colors. In practice, the standard error of the mean is smaller than the thickness of the lines, so that it is subtle to distinguish. This shows high statistical significance.

In the shear-organised case (Figure 2.14(b) and Figure 2.17), water vapour still carries most memory and hydrometeors still play a negligible role. But the winds become a more important source of memory than temperature, probably because the winds are what organises the convection.

In the self-aggregated case (Figure 2.14(c) and Figure 2.18), there is a dramatic increase in memory residing in the thermodynamic variables: mostly water vapour, but also temperature. The impact of the winds is just slightly enhanced relative to the unorganised case. It remains much weaker than in the wind shear organised case. The hydrometeors still do not store any memory. With self-aggregation, water vapour and temperature prevail by more than an order of magnitude over dynamics

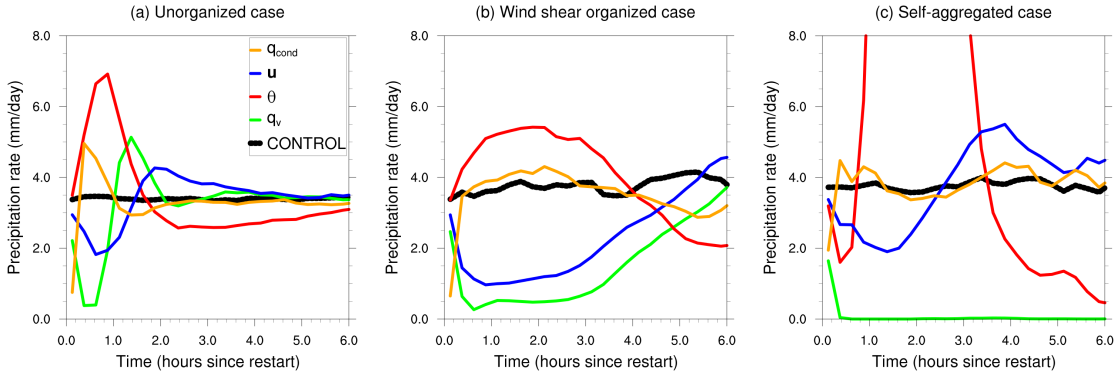


Figure 2.14 Response of horizontally-averaged precipitation rate after homogenisation and model restart, for the control run and for experiments on a single variable; colors indicate different experiments, and the legend indicates the variable homogenised in each experiment (see table 2.1). These are ensemble averages over 19 or 20 members. The panels represent experiments conducted on different convective types: (a) unorganised convection, (b) convection organised by wind shear, (c) self-aggregated convection. The peak precipitation rate following homogenisation of temperature in the self-aggregated case (off scale) is 32 mm/day.

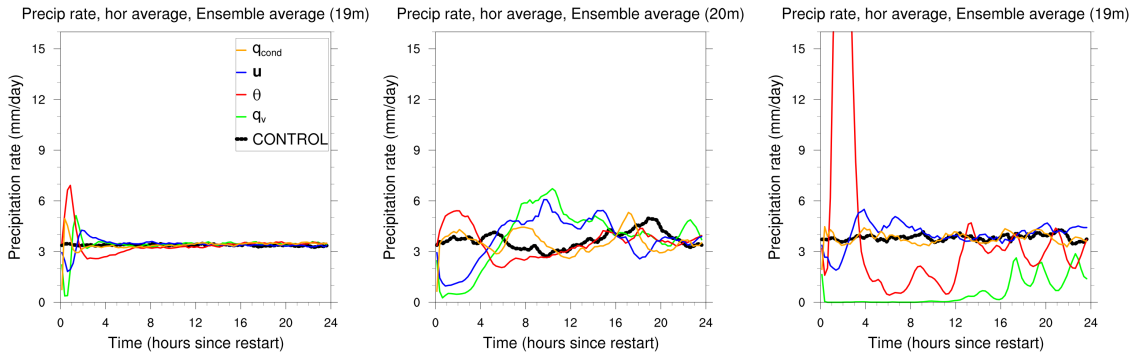


Figure 2.15 Same as Figure 2.14 but for the first 24 h after homogenisation instead of 6 h.

and microphysics for memory storage. This is consistent with the fact that, in the self-aggregated case, a strong contrast in humidity develops between wet and dry subdomains, which does not develop nearly as strongly with disorganised convection or wind shear organised convection.

The smaller memory storage of the dynamical variables (3-D winds) compared to the thermodynamic variables is confirmed by the “double set” experiments (Figure 2.19). In the unorganised case, homogenising winds and water vapour together has a similar impact as homogenising water vapour only. Likewise for winds and temperature together. However, homogenising both water vapour and potential temperature together leads to a recovery time scale twice as long (2.5 h) as when

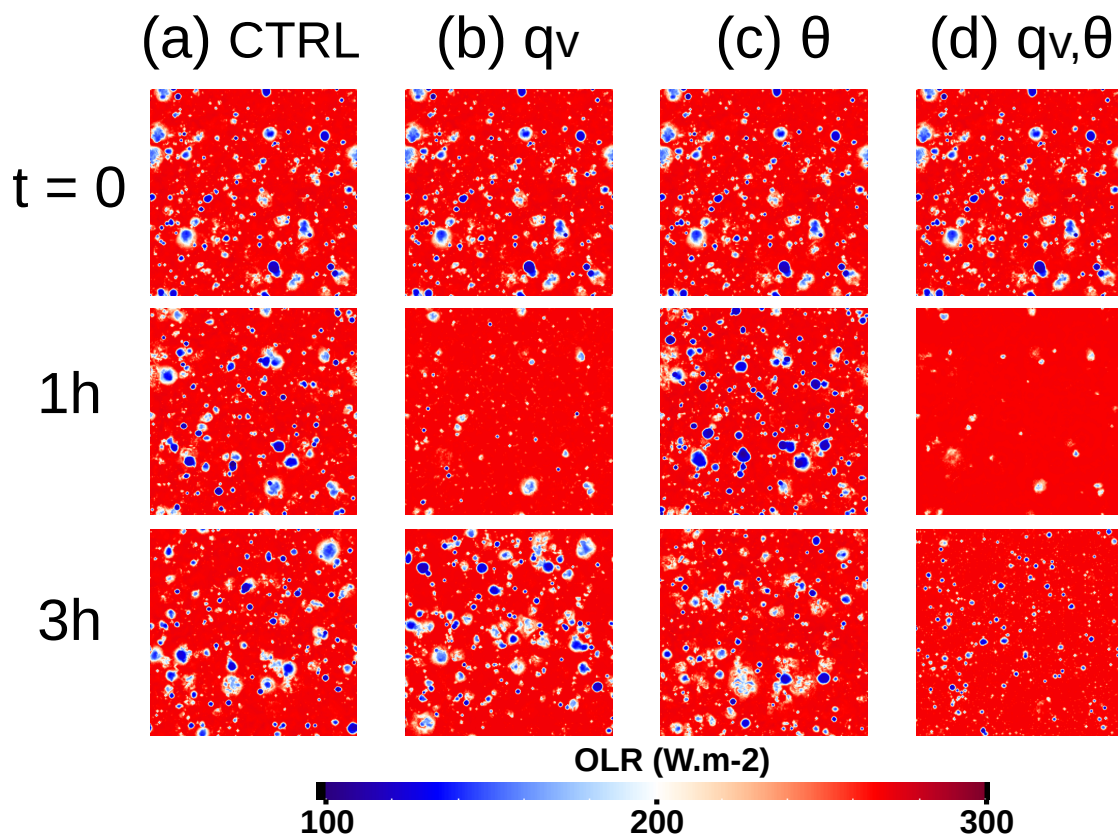


Figure 2.16 Snapshots of the OLR response to various homogenisation in the unorganised case. (a) Control run. (b) Water vapour homogenisation. (c) Potential temperature homogenisation. (d) Water vapour and potential temperature homogenisation. Time flows from top to bottom: at $t = 0$, 1 h, 3 h after homogenisation.

only one thermodynamic variable is homogenised (~ 1 or 1.5 h).

In the wind shear organised case, the combination of water vapour and temperature still carries more memory than the combination between winds and either of the thermodynamic variables. Homogenising water vapour and winds together leads to the same response as homogenising water vapour only, while homogenising both temperature and winds leads to an intermediate response more similar to wind-only. These results show that winds and temperature are important, but winds are now the secondary storage of convective memory after water vapour.

The self-aggregated case shows similar results in terms of the relative importance of variables, but with much greater memory overall. When both water vapour and temperature are homogenised, the combined effect is the largest of all experiments: precipitation remains zero for about 18 hours.

It is not straightforward to know whether recovery after homogenisation leads

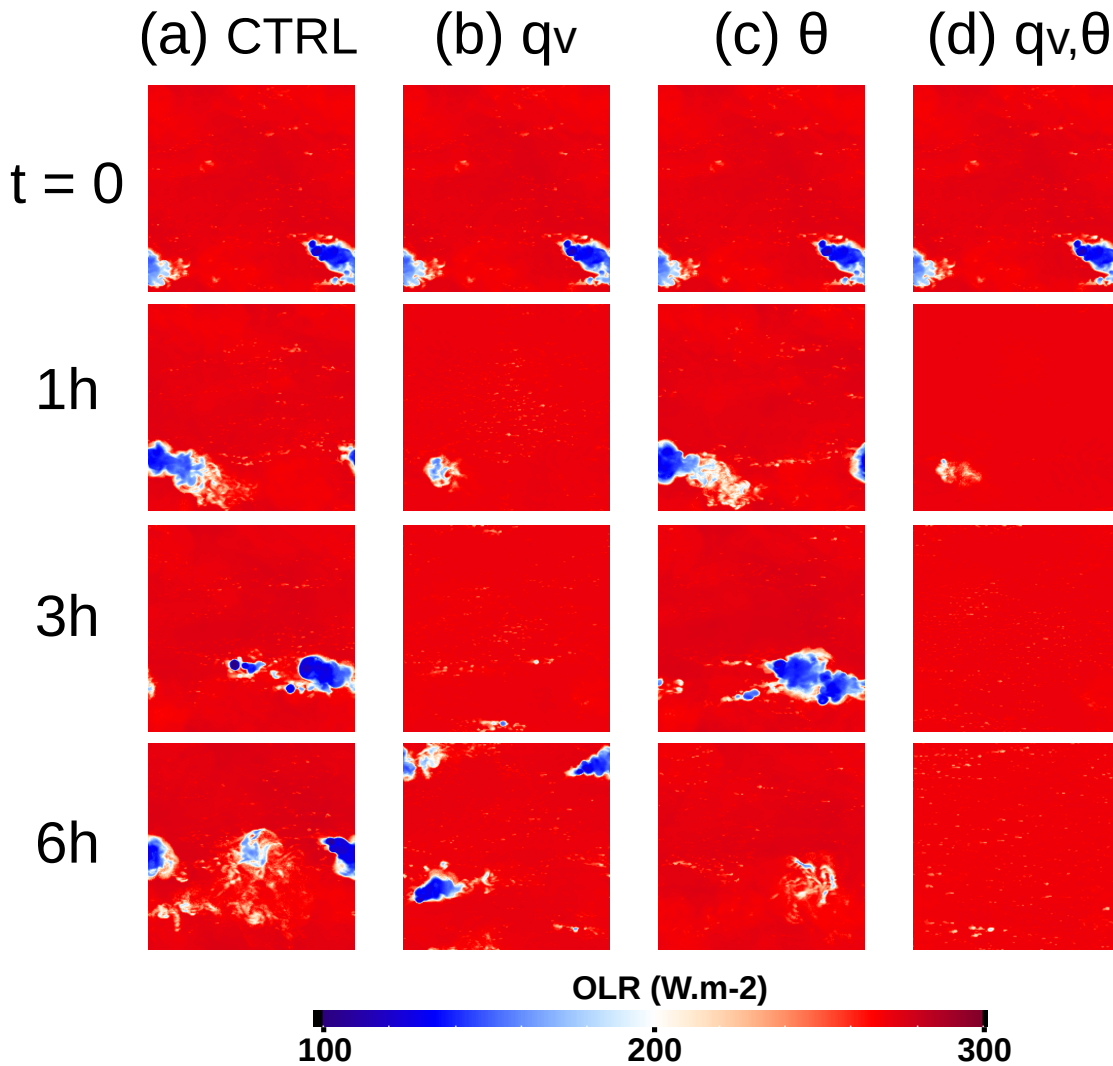


Figure 2.17 Same as Figure 2.16 but for the wind shear organised case. Time flows from top to bottom: at $t = 0, 1 \text{ h}, 3 \text{ h}, 6 \text{ h}$ after homogenisation.

to another self-aggregated state or not. Generally, convection remains aggregated after homogenisation (Figure 2.18). If only water vapour or temperature is homogenised, convection clearly recovers to an aggregated state. However, if both are homogenised, it recovers in a practically unorganised state, although slightly aggregated, probably due to the persistence of wind (and perhaps hydrometeors) structures. It is important to note where aggregation recovers: at the original location when temperature is homogenised, but in the opposite part of the domain when water vapour is homogenised. This is consistent with the modifications of sub-cloud layer MSE between the convective and the dry regions by homogenisation.

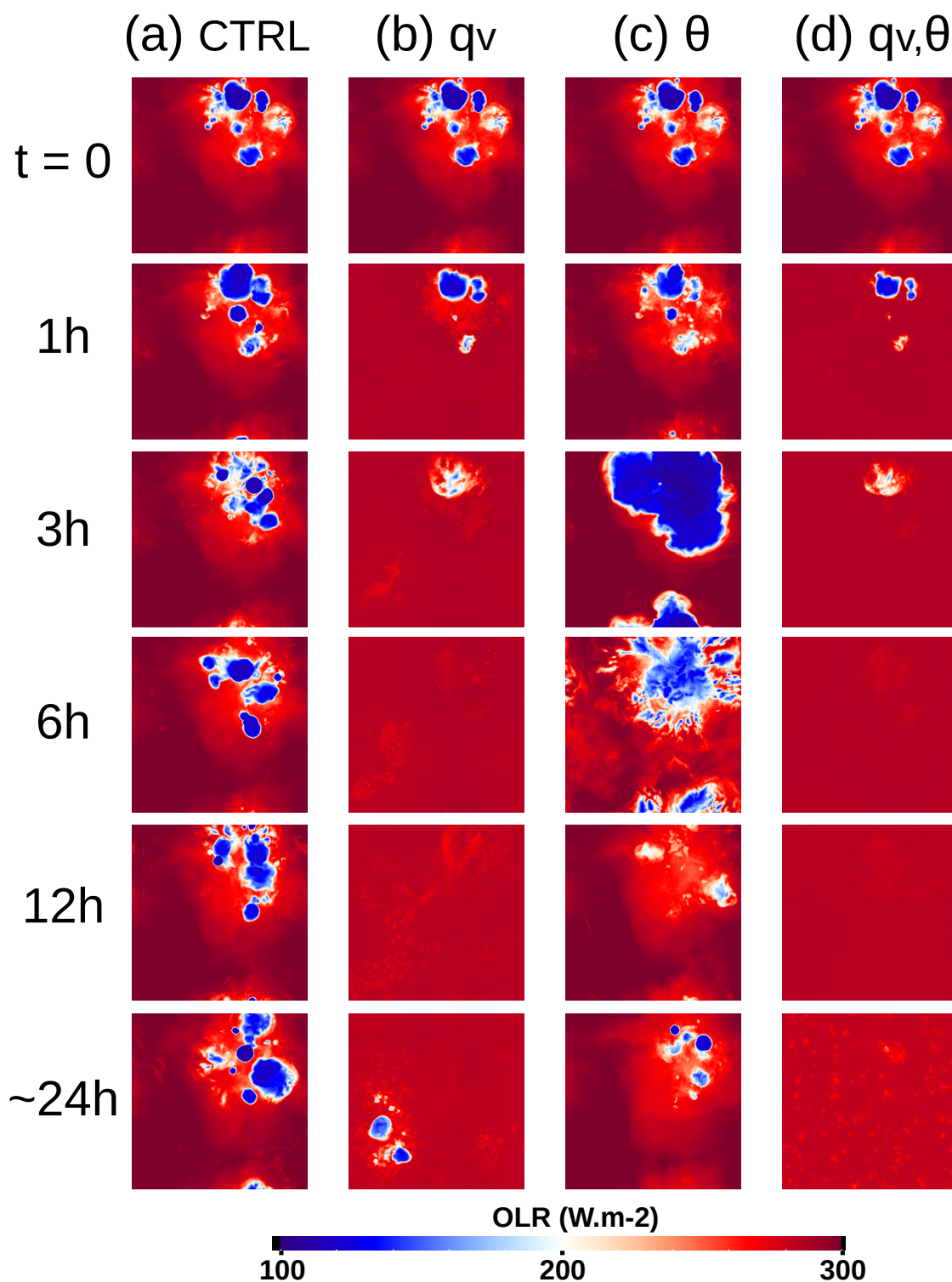


Figure 2.18 Same as Figure 2.16 but for the self-aggregated case. Time flows from top to bottom: at $t = 0$, 1 h, 3 h, 6 h, 12 h, and about 24 h after homogenisation.

2.6.2 Interpreting the response to homogenisation of temperature

We would usually expect precipitation to be reduced when homogenising any convective structures. Indeed, this happens in most experiments. However, when

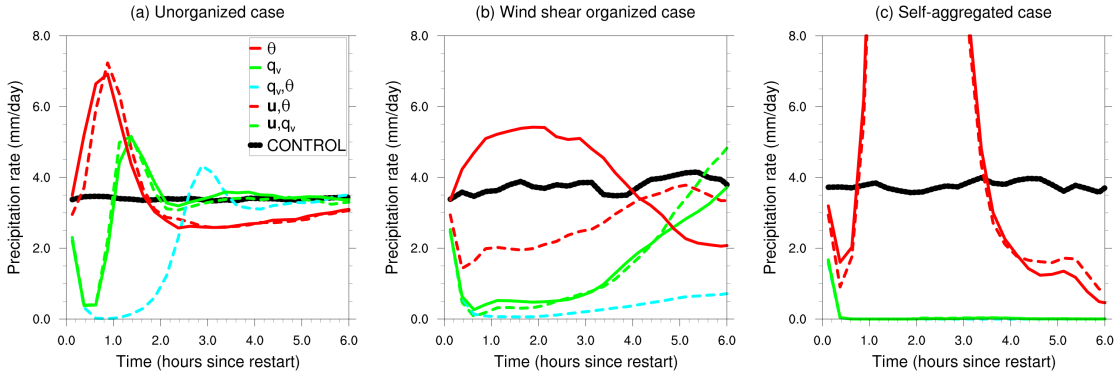


Figure 2.19 Response of horizontally-averaged precipitation rate after homogenisation and model restart, for the control run and for experiments on a double set of variables (dashed), compared to the single-variable temperature and humidity results (solid). Different experiments are indicated by different colors (see legend and Table 2.1). These are ensemble averages over 19 or 20 members. The panels represent experiments conducted on different convective types: (a) unorganised convection, (b) convection organised by wind shear, (c) self-aggregated convection.

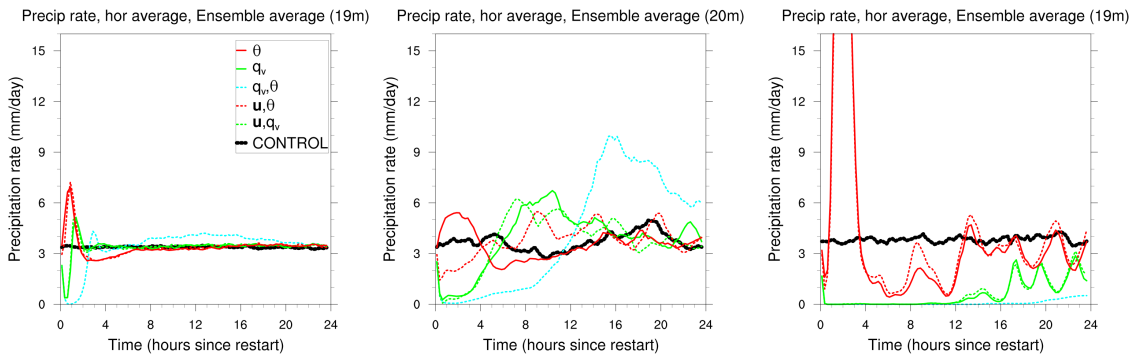


Figure 2.20 Same as Figure 2.19 but for the first 24 h after homogenisation instead of 6 h.

temperature is homogenised, precipitation is enhanced.

To explain this result, we note that raining locations are associated with cold pools, which means they are usually colder in the boundary layer than the non-convective locations. When homogenising temperature, these cold pool areas become warmer and more buoyant. Thus the humid areas of cold pools, now also warmer, can generate increased convection.

This effect can be verified by examining Moist Static Energy (MSE) changes. In most experiments the standard deviation of MSE near the surface (and to a lesser extent at 500 hPa) is reduced in the first few hours after homogenising (Figure 2.21), which is intuitive for homogenisation experiments on thermodynamic variables. Also, the standard deviation of MSE in the sub-cloud layer reacts earlier

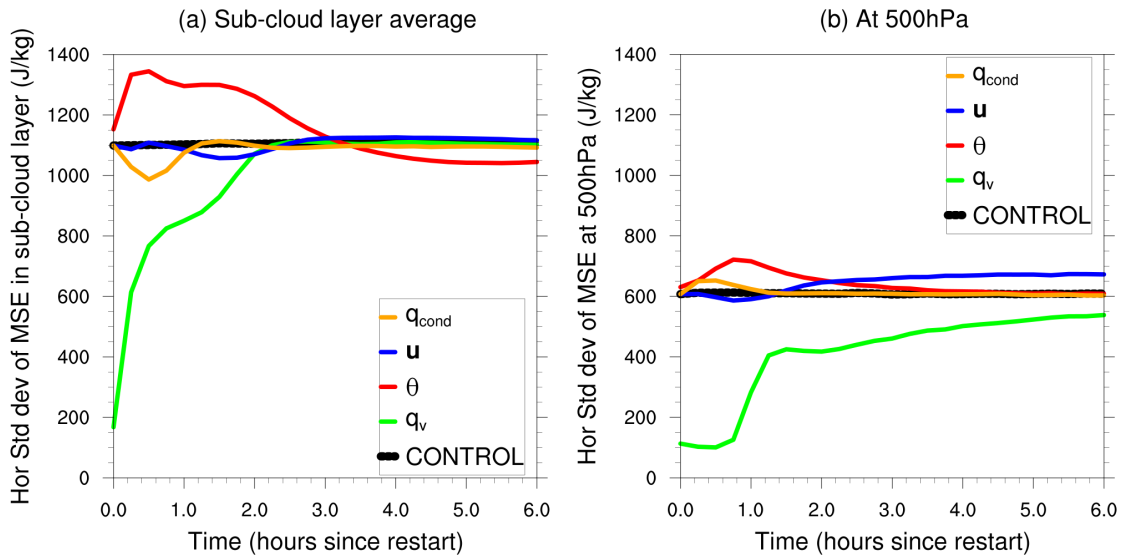


Figure 2.21 Response of micro-scale structures, for different 3-D experiments in the unorganised convection case. Different experiments are indicated by different colors (see legend and Table 2.1). Both panels show ensemble averages for 19 members. (a) Sub-cloud layer average of the horizontal standard deviation of Moist Static Energy (MSE). (b) Horizontal standard deviation of Moist Static Energy (MSE) at 500hPa.

than precipitation (see also Figure 2.14(a)), which suggests causality. The standard deviation of MSE is the most strongly reduced by homogenising water vapour, and it is precisely the experiment in which convection is the most strongly reduced. Conversely, and against the first intuition, homogenising temperature leads to an increase in the standard deviation of MSE instead of a decrease. In moist convective areas, even though near-surface MSE is high, the temperature is lower than in the environment because of cold pools. This effect is removed by temperature homogenisation, which makes MSE even higher there. So micro-scale MSE structures in the boundary layer are in fact strengthened by temperature homogenisation. Therefore we get more favourable areas for convection and an increase in precipitation.

2.6.3 Which layer of the atmosphere carries most memory?

The results from Subsection 2.6.2 suggest an important role for the boundary layer. To go one step further, we carry out experiments where we homogenise variables only in one specific layer at a time: the sub-cloud layer (surface to 940 hPa \simeq 600 m), shallow-cloud layer / mid-troposphere (940 hPa-700 hPa), or free troposphere (700 hPa to tropopause). Following the previous results, for these ex-

periments we only average the thermodynamic variables: water vapour and temperature.

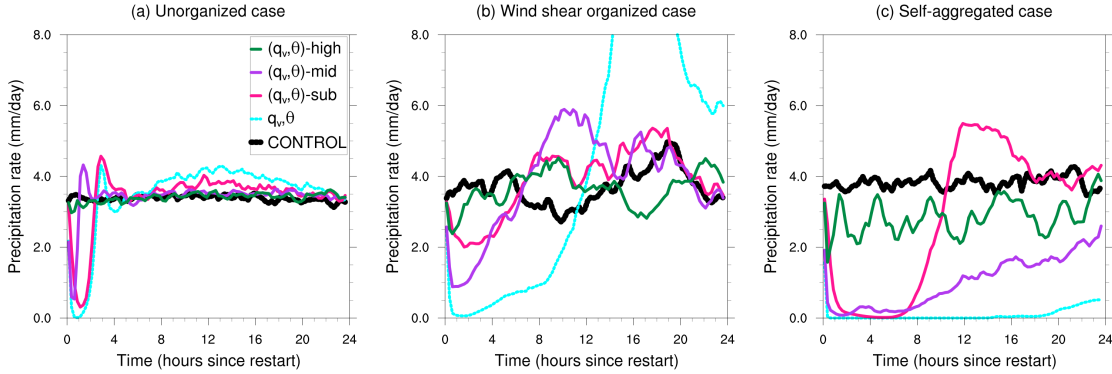


Figure 2.22 Response of horizontally-averaged precipitation rate after homogenisation and model restart, for the control run and for experiments on specific layers only: homogenisation before the restart is conducted over different atmospheric layers: sub-cloud layer (surface-940hPa), mid layer (940hPa-700hPa), high layer (700hPa-tropopause). Different experiments are indicated by different colors (see legend and Table 2.1). These are ensemble averages over 19 or 20 members. Different panels represent experiments conducted on different convective types: (a) unorganised convection, (b) convection organised by wind shear, (c) self-aggregated convection.

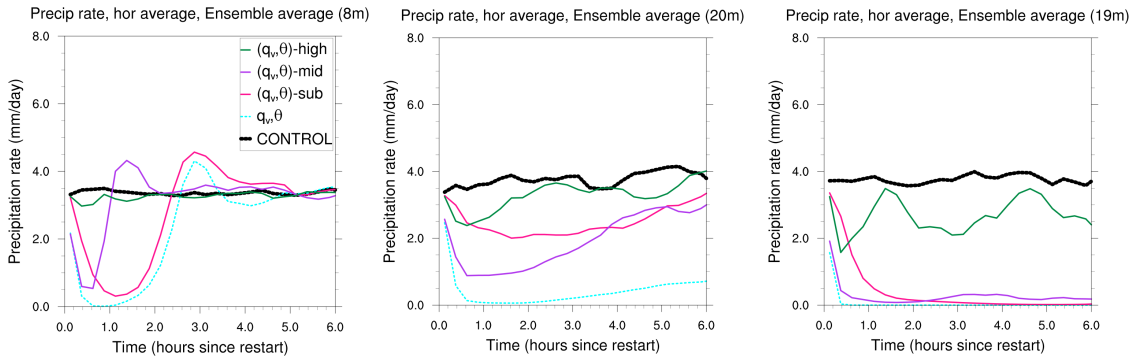


Figure 2.23 Same as Figure 2.22 but for the first 6 h after homogenisation instead of 24 h.

In the unorganised case, the precipitation recovery time scale is largest when the sub-cloud layer is homogenised (Figure 2.22(a)). In contrast, the amplitude of the response is almost zero when homogenising the free troposphere. Thus memory mostly resides in the sub-cloud layer.

The shallow cloud layer appears to contribute as a secondary storage of convective memory compared to the sub-cloud layer. The response time scale for homogenisation of this layer is only an hour, compared to the 2.5 h time scale for the sub-cloud layer.

It makes sense for the shallow cloud layer to have a very quick impact, since homogenising this layer will directly impact clouds and soon after precipitation. It also makes sense for the sub-cloud layer to have a slightly delayed impact since it takes more time for the air in the sub-cloud layer to generate updrafts, clouds and then only precipitation. This may explain the different precipitation recoveries observed for these two experiments.

In the case with wind shear, the relative role of the shallow cloud layer is stronger than the unorganised case, but not as strong as in the self-aggregated case (Figure 2.22).

In the self-aggregated case (Figure 2.22), as in the two other cases, most memory still comes from the lowest two layers: the sub-cloud and shallow cloud layers. The free troposphere (700 hPa to tropopause) still plays a much weaker role, although a little stronger than for the other cases, since there are slightly stronger structures in the free troposphere in the self-aggregated case (stronger differences between the convective and the dry regions). The main difference is that the memory coming from the sub-cloud layer is dominant in the unorganised case (by a factor of two in recovery time scale), but it is the memory coming from the shallow cloud layer that is dominant with self-aggregation (also by a factor of about two). In comparison, the memory coming from these two low layers is almost equivalent in the wind shear organised case (the recovery time scales are the same).

2.6.4 Role of convective organisation

Convective organisation leads to a dramatic increase in convective memory, particularly acute with self-aggregation. The recovery time scale for water vapour experiments are one hour for unorganised convection, six hours for convection organised by wind shear, and more than 24 hours for self-aggregated convection (Figure 2.14): convective organisation enhances memory by a factor of up to 25. Also, in the self-aggregated case, precipitation remains zero for 12 hours after homogenising, whereas in the unorganised case, it does not even reach zero. With self-aggregation, the precipitation response amplitude when homogenising temperature (32 mm/day) is about five times as large as in the unorganised case (7 mm/day). Sensitivity tests

confirmed that these memory changes are due to organisation, not to the choice of microphysical scheme (see Subsection 2.6.7).

To explain why organised convection shows so much more memory, we can assess the domain-mean value of CAPE in the equilibrium state of the different organisation cases. CAPE is highest in the unorganised state (3200 J kg^{-1}), intermediate in the case organised by wind shear (2350 J kg^{-1}) and lowest in the self-aggregated case (750 J kg^{-1}). With more organised convection, the CAPE is smaller, so the atmosphere is more stable, so it is harder to regenerate convective instability from a homogenised state, therefore it takes longer to recover from homogenisation. This is consistent with the fact that self-aggregation warms and stabilizes the domain.

Another explanation is that self-aggregation generates very large contrasts in humidity across the domain, and therefore a large variance of atmospheric fields. Likewise, wind shear organised convection has larger conversion of horizontal momentum to vertical momentum, and thus larger turbulence and associated variance. Since memory is related to microstate variances, it must be larger in the organised cases.

2.6.5 Negligible role of surface fluxes

In Subsection 2.6.3 we found that the sub-cloud layer thermodynamical variables are the main source of convective memory. Since this layer is in contact with the surface, it raises the question of whether part of the long recovery might be due to the surface fluxes (either to their average or to their microscale fluctuations). Here we investigate this using the fixed surface flux experiments (Subsection 2.3.1).

The results (Figure 2.24) are almost identical to those with fixed SST. With fixed surface fluxes the amplitude of the response is very slightly smaller, but otherwise the same. The slight decrease in response amplitude simply points at a slight enhancement of the memory with interactive surface fluxes. We draw two conclusions. First, surface flux heterogeneity is not a source of microstate convective memory. Second, the macrostate surface-flux feedback does not play a significant role in helping the system regain its RCE state. The overall result is that surface

fluxes do not matter much for convective memory.

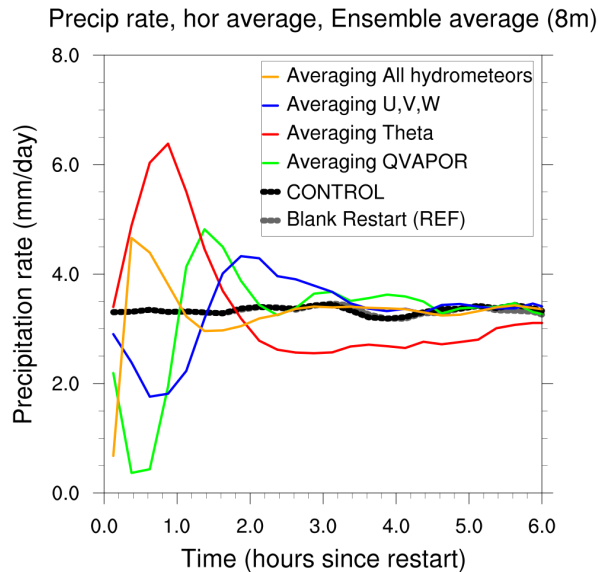


Figure 2.24 With fixed surface fluxes. Response of horizontally-averaged precipitation rate after homogenisation and model restart, for different 3D experiments (see table D.1). These are ensemble averages over 8 members, for control, blank, and single set experiments.

2.6.6 Secondary response: a microstate-macrostate feedback

In some of our experiments, there is a longer-term secondary response, which usually has the opposite sign compared to the initial response. For example for unorganised convection, see the experiment on θ and q_v together in Figure 2.22(a) (where there is a 24 h secondary response time scale), or experiment on θ (7 h time scale) or winds (5 h time scale) in Figure 2.14(a). While we cannot prove what this is due to, it appears that there is a feedback between the microstate response and the macrostate response.

Systems in RCE have many modes of variability, since they exhibit various natural oscillations [Randall *et al.*, 1994; Hu and Randall, 1995; Yano and Plant, 2012a]. The homogenisation experiments seem to excite some particular modes of this dynamical system. There are at least two modes: a rapid mode related to microstate memory, and a slow mode (secondary response) related to feedbacks between the microstate and the macrostate. We discuss this slow mode in this section only, and refer to it as the secondary response. Having such a dynamical

system in mind, it is not so surprising to see some variables responding in phase with precipitation, some others responding in quadrature, and some others with a different phase difference.

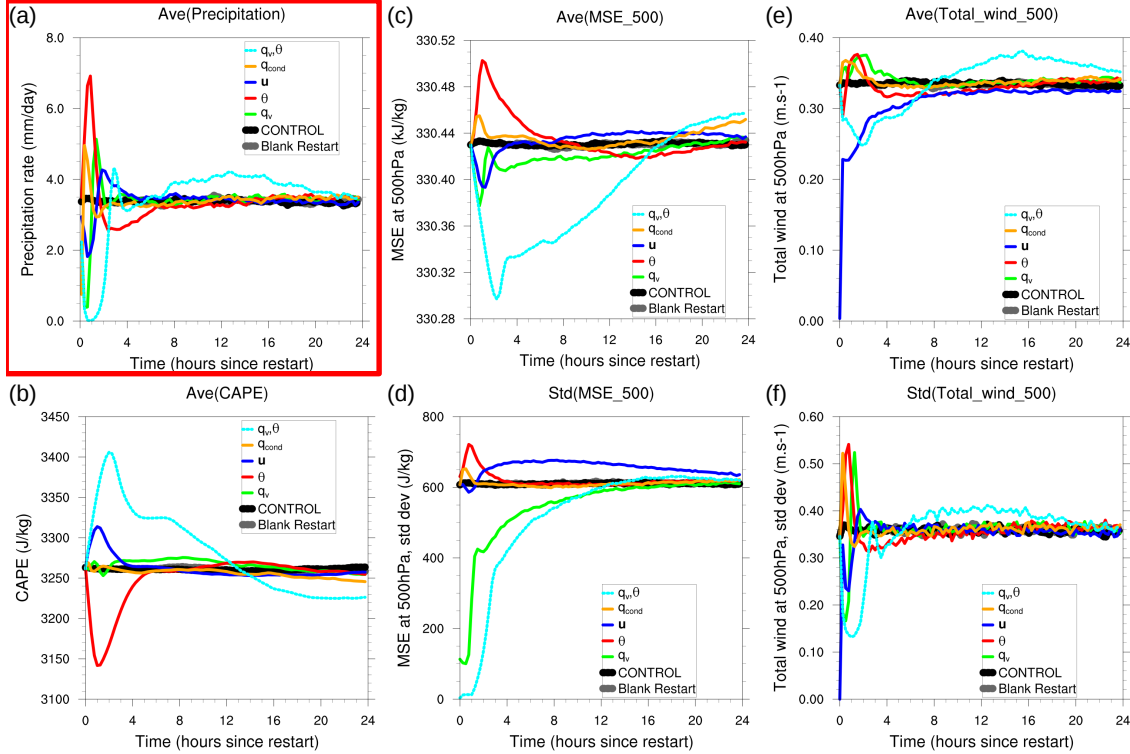


Figure 2.25 Response after homogenisation of variables given by the legend (colors, see Table 2.1) and model restart, on longer time scale (24 h), for unorganised convection. These are ensemble averages over 19 members. The response of different variables is presented: (a) Horizontal average of precipitation rate, (b) Horizontal average of CAPE, (c) Horizontal average of MSE at 500 hPa, (d) Standard deviation of MSE at 500 hPa, (e) Horizontal average of the total wind at 500 hPa, (f) Standard deviation of the total wind at 500 hPa. As shown by the legend, the lines show the control run (black), single set homogenisation experiments on water vapour, potential temperature, winds, hydrometeors (respectively green, red, dark blue, orange), and a double set homogenisation experiment on water vapour and potential temperature together (dashed cyan). The total wind is computed as the amplitude of the 3D wind vector. The standard deviation of the total wind is very similar to the Convective Kinetic Energy (CKE). CAPE and MSE respectively stand for Convective Available Potential Energy and Moist Static Energy. Note that here CKE refers to the CKE defined at each point by the velocities resolved by the CRM, which is different from the parameterized sub-grid TKE used by the CRM.

Usually, in the unorganised case, most variables recover to their RCE value after about 6 hours. This is true for most experiments, except for the one where both water vapour and temperature are homogenised (Figure 2.25). In the latter experiment, the precipitation response starts a longer-period oscillation away from equilibrium at 7 h, which peaks at 13 h. To explain this, note that after 6 h,

even though precipitation has recovered to its RCE value, CAPE has not, showing that the macrostate after 6 h is different from the macrostate in RCE. Therefore, even though the precipitation has temporarily recovered, the full equilibrium has not been reached yet. This may allow the secondary response to be triggered, with a new increase in precipitation away from equilibrium. Note that precipitation and CAPE are almost in quadrature during the secondary response, since the precipitation anomaly seems to be related to the time derivative of CAPE.

During the secondary response, the peak of precipitation (after 13 h) seems to be in phase with a peak in high cloud cover (since deep convection produces both high clouds and precipitation) and with the standard deviation of MSE in the sub-cloud layer (a microstate variable probably driving convective intensity), whereas the standard deviation of MSE at 500 hPa returns to equilibrium precisely at that time. The standard deviation of the total wind (microstate), similar to the Convective Kinetic Energy (CKE), peaks in phase with precipitation, But it already differs from the RCE value after 6 h, slightly before the precipitation (7 h), perhaps because of preconditioning of the deep convective anomaly. Overall, this suggests a non-trivial interaction between the macrostate and the microstate during the secondary response.

This secondary response should not influence our results on microstate memory too much since it is of smaller amplitude, and we are focusing on the first part of the response. We discuss a potential way to prevent interactions between the microstate and macrostate in Subsection 2.6.7.

2.6.7 General caveats

In this study, feedbacks from the macrostate onto convection are not forbidden during convective recovery to RCE. Domain-mean temperature, humidity, and CAPE are allowed to vary with time, so the macrostate is not held fixed (Figure 2.25). Thus, recovery of the microstate to homogenisation involves interaction with the macrostate (for example, increase of CAPE). So the responses measured here partly include macrostate memory. However, we conjecture the macrostate feedbacks to affect all perturbations more or less similarly, and on longer time scales,

so that comparing the recoveries to one another should still be valid. This conjecture is consistent with results by *Davies et al.* [2013a]. Significant work would be required to completely get rid of the macrostate feedbacks, which calls for further study. A method to achieve this would be to impose the macrostate by nudging the domain-mean temperature, humidity and horizontal winds towards their RCE value at each time step, and to repeat the homogenisation experiments on this new setup.

By changing the microphysical scheme, we strongly modified the convective organisation in space. We confirmed that the dramatic change in memory is due to the change in organisation, not just to the change in microphysical scheme, by evaluating the memory with the Thompson microphysics scheme but a very small domain which forces a relatively unorganised state. The results show that memory is similar to the unorganised case with WSM6 microphysics (see Figure 2.26). Despite this test, we acknowledge that the sensitivity to the microphysical scheme could be tested further.

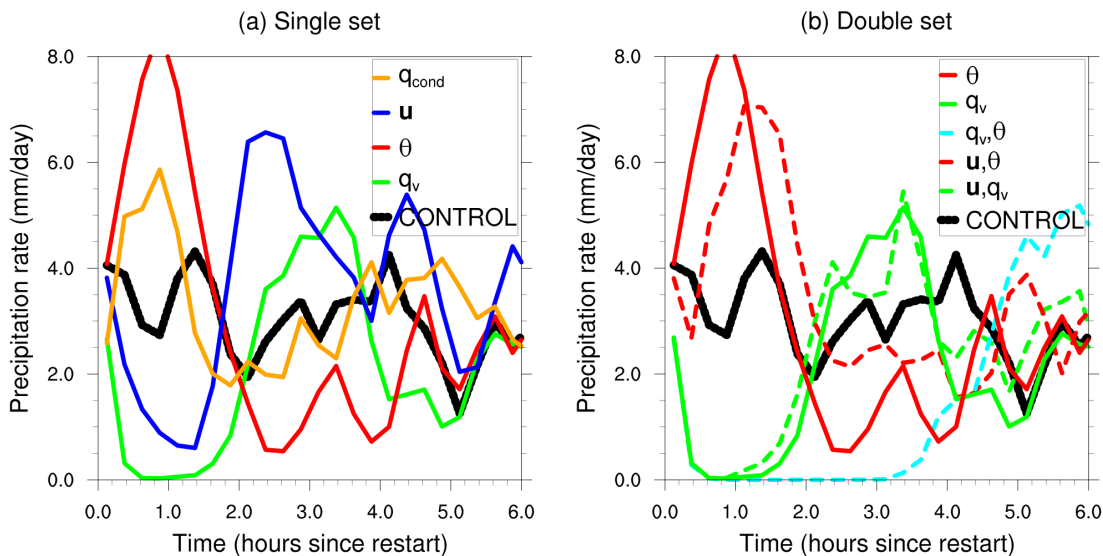


Figure 2.26 With Thompson microphysics, but a very small domain (31 km * 31 km), so that convection is not very organised (almost unorganised). Response of horizontally-averaged precipitation rate after homogenisation and model restart, for different 3D experiments (see table D.1). These are ensemble averages over 22 members. For homogenisation of control, and (a) single set experiments, (b) double set experiments.

Homogenisation is a very strong perturbation to the microstate. So one could argue that our experiments may over-estimate recovery times compared to, for example, replacing the convective microstate with a non-convective one. Nevertheless, we still expect that the relative importance of the different sources of memory found

in this simple approach, under different degrees of organisation, would hold in more realistic approaches. In the future, more realistic perturbations could be considered to test this.

This study is performed in the RCE set-up, so there is no externally-imposed large-scale forcing. This may limit the generality of our results. It would be interesting to check whether the results hold in an idealized atmosphere that undergoes a large-scale upward vertical velocity, representing the trough of a large-scale wave, and leading to higher precipitation rate. But even if RCE may neglect part of the complexity of the real atmosphere, it is still an excellent framework to look at convection-circulation feedbacks.

We have analysed the memory of tropical convection only. In the extra-tropics, the role of winds could increase. In a parameterization, one could add an efficacy term to the microstate memory as a function of the departure from tropical behaviour (e.g., latitude-based). Potentially, the wind shear experiments may partly capture behaviours of synoptic weather systems in the extra-tropics.

Convective memory as considered in this study includes convection but also the resolved turbulence, since the homogenisation technique acts on the whole microstate, independently from whether the microstate structures are more on convective length scales or on turbulent length scales.

2.6.8 Implications for parameterizations

Our results show that in all three convective organisation types, water vapour is the primary storage of memory, followed by temperature (especially in the unorganised case) and then wind (especially in the case organised by wind shear). There is thus a dominant “water vapour memory”. Our results also show that memory is mostly stored at low levels. These results resonate with *Stirling and Petch* [2004], who showed in a 2D set-up that the diurnal cycle of unorganised convection is most strongly affected by micro-scale variability of relative humidity in the boundary layer. They are also consistent with *Davies* [2008]. The importance of water vapour for convective memory is also consistent with its importance in self-aggregation

[*Tompkins*, 2001b].

Overall, our results suggest that some of the previous studies have chosen reasonable memory storage through thermodynamic variables (e.g., precipitation evaporation, cold pools), even though some other studies may have given too much memory role to the dynamical variables (e.g., convective vertical velocity, subgrid-scale TKE or CKE) or to the microphysics. Even though these dynamical variables are likely to be ultimately controlled by the thermodynamic structures, they do not appear to be the main storage of memory themselves. Choosing precipitation as the storage of memory is probably not ideal, as there is no memory in the hydrometeors, even though precipitation is also controlled by many thermodynamic conditions. The use of precipitation evaporation might be relevant, as it is perhaps more a thermodynamical variable than a dynamical or microphysical variable. Still, few studies have directly chosen water vapour and temperature as a memory storage, apart from studies using cold pool thermodynamic profiles. Hopefully this study will trigger more parameterization development based on these direct thermodynamic variables, for example by a prognostic representation of the unresolved boundary layer thermodynamic structures (e.g., via spatial variance of water vapour and temperature, or of Moist Static Energy). Finally, our results may help choose the prognostic variable in order to build a convective parameterization with memory in an implicit way such as *Mapes and Neale* [2011].

2.6.9 Why does memory come from near the surface?

In all three organisation cases, we found that microstate memory comes from the lowest layers. This is consistent with *Stirling and Petch* [2004], who showed that for unorganised convection, the most important atmospheric levels for diurnal cycle development were in the boundary layer.

We conclude that convective memory mostly resides in low-level thermodynamics (water vapour and temperature), which provides hints about the processes involved in convective memory. Cold pools and thermals are very strong intrinsic thermodynamical microstate structures at low levels, so they could be good candidates for processes leading to microstate convective memory. The apparent im-

portance of cold pools (and low-level thermodynamics in general) for memory is also consistent with the key role of cold pools in convective organisation [Tompkins, 2001a]. This inference tends to support the development of prognostic cold pool schemes, which have been shown to bring memory to the system [Qian *et al.*, 1998; Grandpeix and Lafore, 2010; Park, 2014; Del Genio *et al.*, 2015]. This also suggests that using precipitation (which occurs at the surface, though not clearly thermodynamic), or better, using precipitation evaporation (which occurs in the sub-cloud layer and generates cold pools), may be good quantities to spur future convective growth.

2.7 Supplementary results

All these results are produced from the unorganised case.

2.7.1 Which layer of the atmosphere carries most memory?

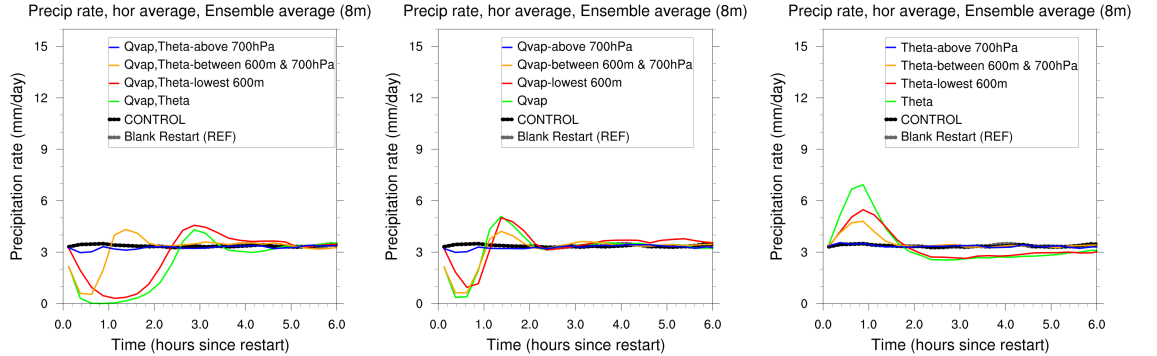


Figure 2.27 Response of horizontally-averaged precipitation rate after homogenisation and model restart, for different 3D experiments performed by layers (see table D.2) in the unorganised case. Homogenisation before the restart is conducted over different atmospheric layers: sub-cloud layer (surface-940hPa), mid layer (940hPa-700hPa), high layer (700hPa-tropopause). All panels show ensemble averages over 8 members. For homogenisation of (left) q_v and θ (middle) q_v (right) θ

When looking at the memory coming from water vapour, the sub-cloud layer and the shallow cloud layer have similar contributions, as shown by figure 2.27 (middle), even though after an hour the memory coming from the shallow cloud layer still drops. The dominance of the sub-cloud layer over the shallow cloud layer

in terms of memory is not as prominent when homogenising water vapour only, but it remains clear that the higher free troposphere is a negligible source of memory.

When looking at the memory coming from temperature, the sub-cloud layer contributes slightly more, but the difference with the shallow cloud layer is not as strong as when we averaged both thermodynamic variables (figure 2.27 (right)). So there seems to be a non-linear effect so that the memory is really increased in the sub-cloud layer when taking both water vapour and temperature into account.

Overall (figure 2.27 (left)), the sub-cloud layer is the main source of memory, in particular in terms of thermodynamic memory. The role of the shallow cloud layer is still important, but on time scales shorter than an hour. The higher free troposphere has clearly no memory in these experiments.

Note that when the thermodynamic variables are homogenised at all levels and when they are homogenised only in the sub-cloud layer, the responses are very similar, except for the first 45 min.

2.7.2 Existence of structures vs detailed description of them

The next step in understanding where convective memory comes from is to determine the scale of the micro-scale structures responsible for memory, via the perturbation scale. We do not accurately tackle the scale here, but we can estimate it in a simple way. We extend the homogenisation method in order to average a variable only in parts of the domain where it is above its mean, or only in parts of the domain where it is below the mean. The experiments consist in homogenising only the warm areas (warmer than the mean temperature), only the cold areas (colder than the mean temperature), only the humid areas (more humid than the mean humidity), and only the dry areas (drier than the mean humidity). This allows to compare the importance of hot spots versus cold pools for example.

This way, we can estimate whether the memory comes from the existence of both areas above and below the mean, or whether it depends more on the smaller-scale description of areas above the mean, or below the mean. For temperature for example, this method can allow us to assess the role of cold pools versus hot spots.

And it can tell us about the role of the existence of cold pools or hot spots versus the role of their internal variances/inhomogeneities.

In this subsection, we focus on the unorganised case, and we intend to compare the storage of memory either in the upper half or in the lower half of the thermodynamic variable distributions. This is a first step towards expanding the homogenisation method to estimate the horizontal scales mostly involved in micro-state memory, although other methods such as *Stirling and Petch* [2004] and *Davies et al.* [2013a] are probably more direct.

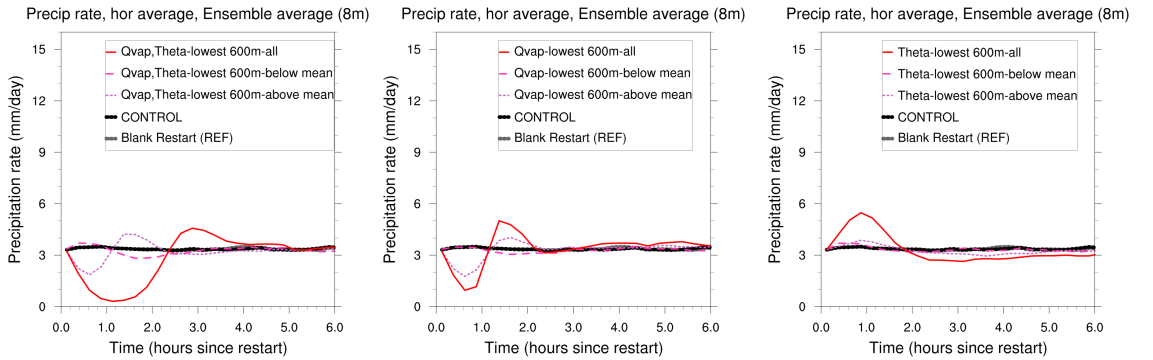


Figure 2.28 Response of horizontally-averaged precipitation rate after homogenisation and model restart, for different 3D experiments performed by layers and on specific points only (see table D.3) in the unorganised case. Homogenisation before the restart is conducted over the sub-cloud layer (surface-940hPa), and over specific areas only: where values are above the horizontal mean (without touching values below the mean), or when values are below the horizontal mean (without touching values above the mean). All panels show ensemble averages over 8 members. For homogenisation of (left) q_v and θ (middle) q_v (right) θ

In the case of sub-cloud layer temperature, homogenising only the areas warmer than the mean temperature, or homogenising only the areas cooler than the mean temperature does not lead to any response away from the RCE state (figure 2.28 (right)). However, homogenising the whole temperature field in the sub-cloud layer has an impact on precipitation. Thus, it suggests the microstate variance of cold areas (the description of cold pools) does not matter, and the microstate variance of hot areas (the description of hot spots or thermals) does not matter either. Rather, these results show that it is just the existence of cold and hot structures that matters: having a disparity between hot and cold areas. In that sense, we can say that the coarsest scales of the micro-state temperature variance seem to be responsible for the memory.

In the case of sub-cloud layer water vapour, results are similar in the sense that the variance of dry areas does not matter much. However, homogenising the areas that are more humid than the mean humidity has a more significant importance than what was shown for temperature (figure 2.28 (middle)). So the variance of humid areas matters significantly. This means that a description of the inhomogeneities of humid areas are more important for convective memory. Also, the existence of a contrast between dry and humid areas may have some importance too.

When averaging both hot areas and humid areas only, we do capture a small fraction of convective memory (figure 2.28 (left)). When we average both cold areas and dry areas only, we do not capture much memory. Still, averaging all allows us to detect much more memory. Consequently, memory seems to be strongly related to the basic existence of cold/hot areas and dry/humid areas, rather than details of cold/hot areas themselves. We speculate this could be due to the variance of MSE structures, an argument presented earlier. This points towards a micro-state memory mostly coming from the coarsest-scale structures.

2.8 Supplementary discussion

2.8.1 RCE state and method validation

This study is performed in the idealized Radiative-Convective Equilibrium (RCE) framework. At the spatial scales studied here, RCE is not a perfect representation of reality: there is no large-scale forcing, no diurnal cycle. However, our goal is not to have a perfect image of reality, but rather to have a simple case in which we can almost isolate the behaviour of convection from numerous feedbacks with other mechanisms such as circulation. Although RCE has some limits, many process studies have used it, and it is a good framework to work with for our purposes. Our idealized experiments can be used to underline processes that are less altered by the numerous interactions of the real atmosphere and its forcings.

Moreover, the equilibrium state reached here is satisfying enough, compared with other RCE states in previous studies.

2.8.2 Role of perturbation scale

Our experiments have shown that having a coarse description of the microstate was generally enough to capture most memory: there is no crucial need to describe the details of these structures. For example, having cold pools and warm thermals would be more important than having a detailed description of either of them. This can be interpreted as evidence showing that the larger-scale description of the microstate is the most important part in capturing convective memory. In other words, convective memory essentially arises from the coarsest scales of the micro-state.

This suggests that just parameterizing the existence of basic micro-state features should be enough to capture most of the memory. It is less important for a parameterization to have a description of the micro-state inhomogeneities inside these basic micro-state features.

These results are consistent with *Stirling and Petch* [2004] who showed that larger-scale sub-grid variances have the strongest influence of the development of convection. They even gave a threshold scale by arguing that structures larger than 10km were the most important for this memory-related effect. *Davies et al.* [2013a] found that structures of 5 to 20km spatial scale are carrying most of the memory. This is potentially smaller than what is suggested by our results and those by *Stirling and Petch* [2004], but it is still the same order of magnitude. Indeed, our results suggest that having simple descriptions of cold pools and warm thermals is enough to carry most memory. Besides, in our unorganised case, cold pools and warm thermals are roughly 20km in size, which is consistent.

2.9 Conclusion

This study introduces a framework for distinguishing several types of convective memory, based on whether or not the memory can already be represented by the large-scale processes resolved by GCMs. Convection can remember its previous states through the impact the earlier convection has on the current synoptic state (involving multiple GCM grid cells) or on the current macrostate (the local GCM

grid column state), and this large-scale influence of past convection will then feed back onto the current convection. This type of memory can in principle be captured by a GCM with an accurate diagnostic convection scheme (one that predicts convective effects based on the current macrostate). However, convection can also remember its previous state via persistence of the microstate itself (inside a single grid cell), which is not resolved. Such *microstate memory* will not be captured by a convective scheme unless the parent model carries additional prognostic variables representing the microstate (such as sub-grid scale Convective Kinetic Energy, cold pool variables, some measure of precipitation evaporation, or others).

We show that microstate memory is indeed present, and is highly enhanced by convective organisation. Self-aggregated convection has the most memory, wind shear organised convection has intermediate memory, and unorganised convection has the least. Yet, even in the unorganised case, recovery of the RCE state after a microstate perturbation can require several hours, which is much longer than a GCM time step ($\sim 10 - 20$ min). When convection is organised, such recovery can take longer than the diurnal time scale (24 h) in some cases. This is a new and significant finding which strongly supports efforts to add prognostic variables (i.e. memory) into parameterizations. It also indicates that the degree of memory is very sensitive to the degree of spatial organisation, so that a scheme capturing one should also capture the other. It appears that indeed, the amount of microstate memory is related to the magnitude of spatial inhomogeneities.

The main sources of microstate memory are found to be water vapour, then temperature, and then winds. But the importance of winds increases with wind shear. The memory mostly comes from the lowest part of the atmosphere: the sub-cloud layer and the shallow cloud layer (up to 700 hPa). For unorganised convection the sub-cloud layer is the most important, while the shallow cloud layer dominates for wind shear organisation and even more clearly for self-aggregation.

This suggests memory comes from processes which contribute to the spatial variance of low-level MSE and/or make convection sensitive to it. This includes cold pools, or hot thermals, or other rain-associated thermodynamic processes, and supports parameterizations in these directions. This supports choices made in some

previous attempts to include memory: e.g. precipitation evaporation, cold pool thermodynamic variables.

Some physical interpretation of memory can help explain why the persistence of micro-scale structures matters for convection. For example, convection will tend to localize on the maxima of the sub-cloud layer Moist Static Energy (MSE), and associated cold pools and local moistening by detrainment will favour nearby subsequent convection, creating some microstate memory. These maximum values of MSE also control the moist adiabat and thus the temperature profile of the whole domain, creating some macrostate memory.

To further understand the origins of microstate convective memory, subsequent investigations could experiment with less drastic perturbations, define perturbations of diagnostic variables such as rain evaporation, assess the sensitivity to wind shear strength and height, assess the sensitivity to a large-scale vertical velocity forcing, and repeat the experiments at higher resolution. To narrow down the number of low-level thermodynamic-based processes involved in memory, we could also use perturbations with spatial filtering to determine the scale of the processes or structures leading to memory.

The study focuses on microstate memory: at this stage, we have not provided insight on sources of macrostate and synoptic state memory. Presumably, free-tropospheric water vapour could play an important role in the macrostate memory [Tompkins, 2001b], as well as higher-tropospheric temperature [Raymond and Herman, 2011], and this could be further clarified by expanding methods such as Kuang [2010] via introducing time lag. An overall target for GCMs could be to better represent these three types of memory.

Finally, this study revealed the link between memory and organisation, which suggests that with improved representation of convective memory, a scheme should have a better representation of convective organisation [Tobin *et al.*, 2013]. So memory could be potentially helpful to improve the representation of organised phenomena in GCMs, such as the Madden-Julian Oscillation, or monsoons. Examples of this already exist, as seen in the improved representation of MJO by Del Genio *et al.* [2015] after adding memory which resides in prognostic cold pools. Their best

CHAPTER 2. IDENTIFYING THE SOURCES OF CONVECTIVE MEMORY

MJO is simulated where memory exists in the scheme, but too much memory also degrades the MJO: what is needed is the right amount of memory.

Chapter 3

Isolating microstate memory from macrostate feedbacks: comparison between a CRM (WRF) and a simple stochastic toy model of convection with memory (the predator-prey model)

3.1 Introduction

In the previous chapter, our goal was (1) to detect the existence of microstate memory in Cloud-Resolving Simulations in Radiative-Convective Equilibrium (RCE), and (2) to determine its sources from perturbation experiments. However, we could not completely isolate the microstate memory apart from macrostate memory. There are two types of evidence for this.

First, the time series of domain-mean CAPE, MSE, T500, and other macrostate variables show an oscillatory behaviour (Figure 3.1). Note that, except for precipitation, the variations are of relatively small amplitude compared to the RCE

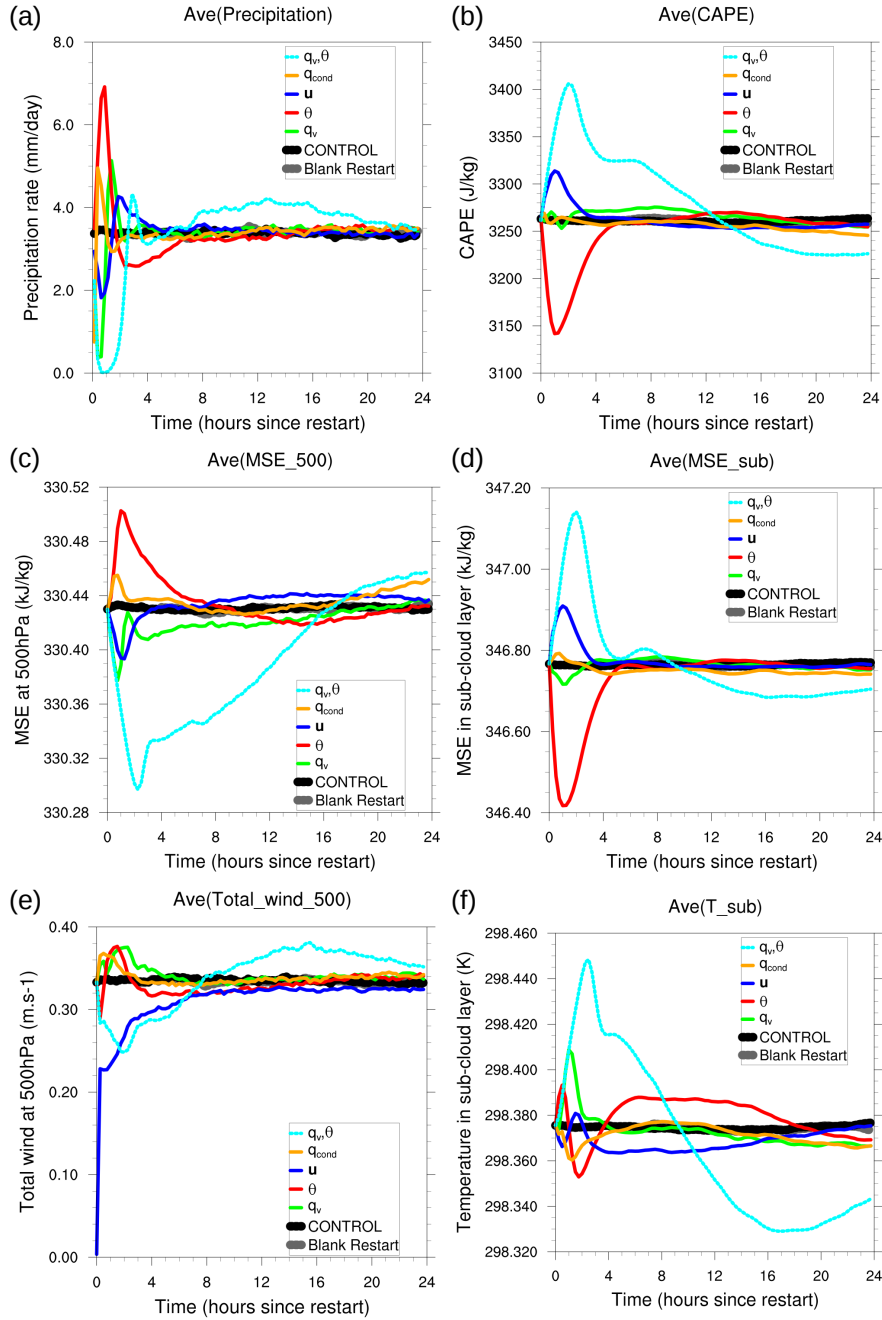


Figure 3.1 Response after homogenisation and model restart on a time scale of 24 h, for different experiments where different variables have been homogenised, for unorganized convection. The variables homogenised are given by the legend (colors, see table 2.1). These are ensemble averages over 19 members. The response of different variables is presented: (a) Horizontal average of precipitation rate, (b) Horizontal average of CAPE, (c) Horizontal average of MSE at 500 hPa, (d) Horizontal average of MSE in the sub-cloud layer, (e) Horizontal average of the total wind at 500 hPa, (f) Horizontal average of temperature in the subcloud layer. As shown by the legend, the lines show the control run (black), single set homogenization experiments on water vapor, potential temperature, winds, hydrometeors (respectively green, red, dark blue, orange), and a double set homogenization experiment on water vapor and potential temperature together (dashed cyan). The total wind is computed as the amplitude of the 3D wind vector. CAPE and MSE respectively stand for Convective Available Potential Energy and Moist Static Energy.

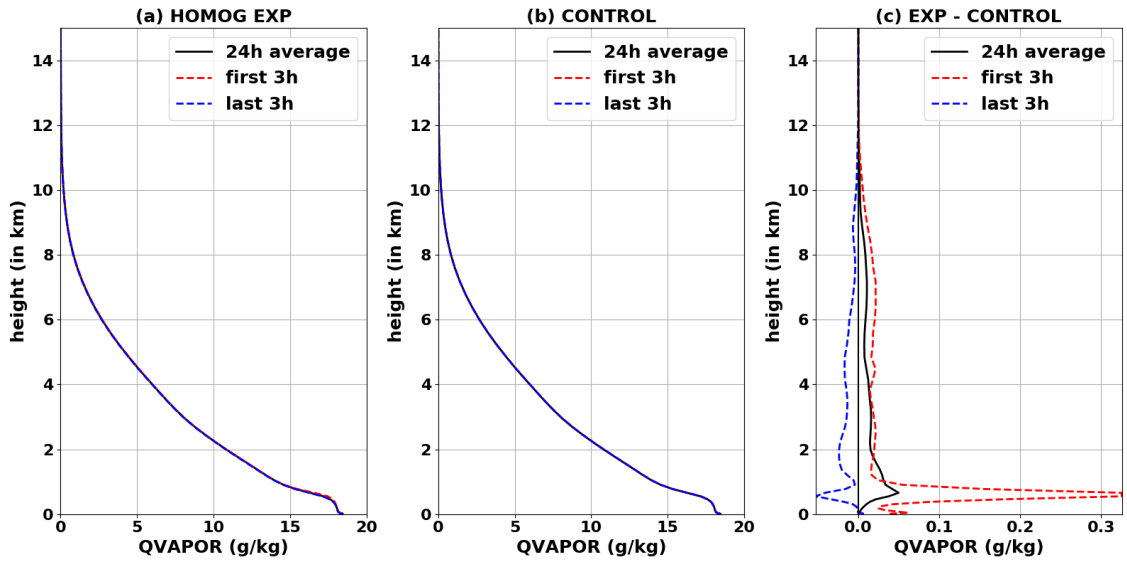


Figure 3.2 Vertical profiles of water vapour mixing ratio, for different simulations: (a) With homogenisation of water vapour and temperature (HOMOG EXP) (b) Control (c) For the difference HOMOG EXP minus CONTROL. The black lines correspond to the average for the first 24 h after homogenisation and restart. The red lines correspond to the average over the first 3 h after homogenisation and restart, while the blue lines correspond to the last 3 h of the first 24 h after homogenisation.

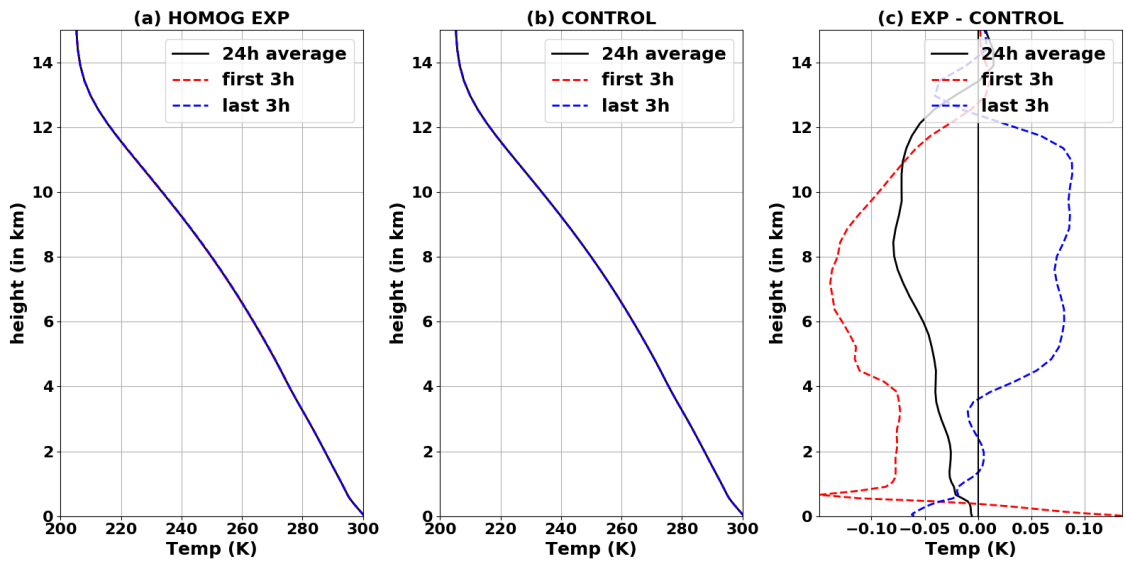


Figure 3.3 Same as 3.2 but for temperature instead of water vapour mixing ratio

value (see the control case, by the black line). Also, not all experiments show a strong long-lived response of the macrostate out of RCE: most experiments lead to macrostate recovery after 4 to 5 hours. But the experiment where both water vapour and temperature are averaged has a special behaviour since even after 24 hours, the macrostate has not recovered to its RCE value. This shows the macrostate does respond to homogenisation.

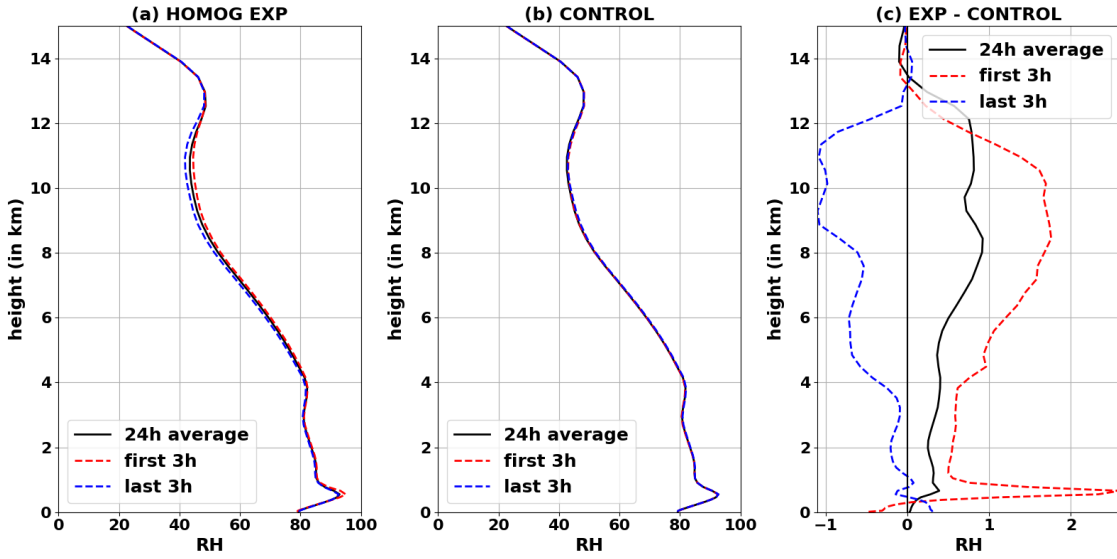


Figure 3.4 Same as 3.2 but for relative humidity instead of water vapour mixing ratio

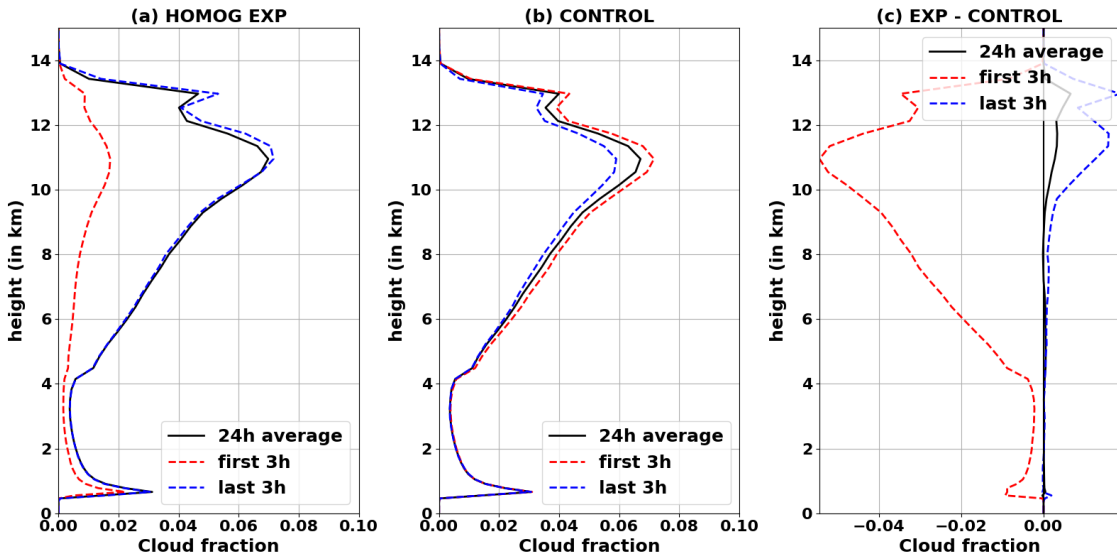


Figure 3.5 Same as 3.2 but for cloud fraction instead of water vapour mixing ratio

Second, the vertical structure of the macrostate response can be read from the domain-mean profiles of water vapour mixing ratio (q), temperature (T), relative humidity (RH), and cloud fraction (Figures 3.2, 3.3, 3.4, 3.5). If there is a difference between the macrostate response to homogenisation and the control simulation, this appears on panels (c), and it reveals that the macrostate was affected by homogenisation. The water vapour macrostate shows a strong response out of RCE in the first 3 hours near cloud base (≈ 600 m). Since the value of the difference in water vapour between homogenisation experiment and control simulation is much larger in the first 3 hours after restart compared to the last 3 hours of the first day

after restart, it reinforces that the macrostate responded away from its natural RCE fluctuations, which may be expected to feed back on the microstate. Cloud fraction macrostate response is also interesting as homogenisation led to a decrease in high clouds, which can have radiative feedbacks on future convection developments.

Because macrostate feedbacks are allowed, the macrostate memory and microstate memory are coupled: although the previous chapter intended to measure mostly microstate memory, we might have actually measured the microstate memory as coupled with the macrostate memory. Can we measure the microstate memory alone, instead of the coupled memory? To achieve this, we have to isolate the microstate memory from macrostate feedbacks.

Another major reason to isolate microstate memory from macrostate feedback is that the macrostate is already represented by any GCM. By isolating the microstate from the macrostate, we can mimic a GCM that would see no change in the macrostate and reveal what GCMs actually miss by not representing microstate memory. So it is a proper testbed for what GCM parameterizations are missing.

3.2 Isolating the microstate memory from the macrostate feedbacks in WRF: fixed-macrostate experiments and instability

3.2.1 Method for the fixed-macrostate experiments: strong nudging of domain-mean profiles

In order to isolate the microstate memory from macrostate feedbacks in WRF, one way is to prevent the macrostate from evolving with time. We do this by nudging. The general strong nudging method is to add an additional tendency term in WRF to the typical macrostate variables used by convective parameterizations: potential temperature (T), water vapour mixing ratio (q), and horizontal winds (u,v). This term is a first-order relaxation term proportional to the difference

between the domain-mean value at time t and a target value, as follows:

$$\frac{\partial a}{\partial t} = -\frac{\bar{a} - \bar{a}_{target}}{\tau_{nudg}} \quad (3.1)$$

where a is either of (T,q,u,v) ; t is time, τ_{nudg} is the nudging time scale, \bar{a} denotes the horizontal domain-mean average, and \bar{a}_{target} is the target value to be imposed by the user.

The target value is chosen to be the mean RCE macrostate profile when there is no homogenisation, that is, in the control run. To ensure the macrostate can really be considered fixed, the nudging time scale has to be quite short. So we will refer to this method as “strong nudging”. The corresponding experiments will be coined “fixed-macrostate” experiments since the macrostate is not allowed to vary.

To ensure a strong nudging, we set $\tau_{nudg} = 40$ s, while the model time step is 6 s. We impose this term at each grid point, but the value of $\frac{\partial q}{\partial t}$ only depends on (z,t) .

There are a few subtleties in the numerical implementation of this method in WRF, in particular due to the indices to use and to the parallelisation of the code for a supercomputer (see an example of a strong nudging code in Figure 3.6). It should also be pointed out that the way the target profiles of T,q,u,v are defined could be important. To ensure the target profiles are a relatively good approximation of the RCE state, we decided to define the target profiles by a 20-day average of the domain-mean fields, with the 20-day period being centred around the day to be run with strong nudging. Each simulated day would then have a slightly different target profile, due to the RCE fluctuations in time.

For reproducibility of the results, the following describes the technical details of the implementation into WRF of the strong nudging method, which is non trivial. This required a lot of time and many trials and errors before achieving a satisfactory implementation. The main WRF setup used for these experiments is to apply the strong nudging from the surface up to the tropopause. The nudging tendency terms are added not to the prognostic variables directly, but rather to their tendencies. The actual nudging computations require to call a new subroutine from a new module,

just before the tendencies are added up to the prognostic variables, at the end of the time step. Since the model is run on multiple processors, each only having information on the grid points they are in charge, computation of the domain-mean value for strong nudging purposes has to be done from a special function which gathers data from all processors. The loops over which the computations are done must be coded in tile indices (not in patch indices, memory indices or domain indices). More details can be found in Figure 3.6.

Applying this method on a test day chosen to be 2007-08-01 (the 62nd day of the RCE control run, starting from the end of the 61st day) led to a very strong instability with a huge amount of rain, extremely high local winds, and a highly cloudy situation (described in detail in subsection 3.2.2). To check whether this instability was a real physical phenomenon or a numerical mistake, we tried four modifications to the nudging method:

1. Changing some characteristics of the method used and its numerical implementation: using tile indices instead of patch indices, forbidding negative values for water vapour mixing ratio, multiplicative nudging instead of additive nudging, applying the nudging on tendencies instead of on prognostic variables, applying nudging in the troposphere only, nudging only in points away from clouds or humidity maximum.
2. Changing some options in the way to run the simulation: e.g., nudging time scale value, model time step value, radiation time step value, cold start instead of restart, damping of maximum vertical velocity option, 6th-order diffusion option, model configuration option, versions of the libraries used.
3. Applying the nudging on different subsets of the four variables it is supposed to be applied to: (T,q,u,v).
4. Modifying the initial conditions and the target conditions, by applying the strong nudging method from a different initial day. Following the way target conditions are computed, when initial conditions are changed, target conditions are changed as well.

The runs with the different modifications are summarised in the table presented

```

DO k = kts, min(kte,kde-1)
  dT_2_strong_nudging(k) = 0.0
END DO

DO k = kts, min(kte,kde-1, 54) ! We only nudge up to the tropopause (level 54)
  sum_var_hor = 0.
  count_hor = 0.
  DO j = jts, min(jte,jde-1) !jts , jte ! jts, min(jte,jde-1)
  DO i = its, min(ite,ide-1) !its , ite ! its, min(ite,ide-1)
    sum_var_hor = sum_var_hor + T_2(i,k,j)
    count_hor = count_hor + 1.
  END DO
  END DO
  ! ----- compute global sum now. Maxime Colin 2016-10-19 -----
  sum_var_hor = wrf_dm_sum_real ( sum_var_hor )
  count_hor = wrf_dm_sum_real ( count_hor )
  ! -----
  var_hor_average(k) = sum_var_hor / count_hor
  dT_2_strong_nudging(k) = - ( var_hor_average(k) - T_target_prof(k) ) / tau_nudging
  threshold_cldfra = 0.
  DO j = jts, min(jte,jde-1) !jts , jte
  DO i = its, min(ite,ide-1) !its , ite
    dT_2_strong_nudging_3D(i,k,j) = 0.
    !--- TO IMPOSE NUDGING ONLY OUT OF CLOUDS OR OTHER GIVEN CONDITIONS ---
    !if ( cldfra(i,k,j) .le. threshold_cldfra ) then
      dT_2_strong_nudging_3D(i,k,j) = dT_2_strong_nudging(k)
      T_tend (i,k,j) = T_tend (i,k,j) + dT_2_strong_nudging(k) * mut(i,j)
    !endif
  !-----
  END DO
  END DO
END DO

```

Figure 3.6 Extract of the implementation of the strong nudging method in WRF code

in the next two pages. Changing the details of the method (see 1) did not particularly help alleviate the instability problem, it only in some cases made it worse, which shows that the instability is a robust behaviour of the system under the conditions which we imposed. The only change that allowed the instability to appear 1.5 times later than originally was when the nudging was only imposed when humidity was less than 80% the humidity maximum at each level. So it seems humidity is involved in the instability, but this change is not enough to solve the instability problem.

Changing the options (see 2) allowed to slightly modify the instability. Most importantly, using a longer nudging time scale makes the instability appear later. But it required to have a nudging time scale 22.5 times larger to delay the instability by only a factor of 2. The problem is we do need a strong nudging if we really want to achieve fixed-macrostate experiments. These tests also showed that the 6th-order diffusion option is not appropriate in this setup since it completely gets rid of convection, which is not desired either. These changes reinforce our confidence that the instability is a real phenomenon, and not an artefact.

Applying the nudging on different subsets of of the four variables T, q, u, v (see 3) is very instructive. Our methods work totally fine in most cases: convection is reasonable and stable, and the strong nudging is successful in controlling the mean profiles. The only cases which develop an instability are when we try to nudge both temperature and humidity at the same time: the instability only appears when nudging (T, q) , or (T, q, u, v) , but nudging (T, u, v) or (q, u, v) for example works totally fine. This is important to show that our method is valid and that the implementation has been done successfully: there is no coding mistake. Further, it shows that the instability mechanism must involve both temperature and water vapour: it seems to be a thermodynamic instability. Can it be due to phase changes?

Finally, modifying the initial conditions (see 4) brings a new perspective. In some cases, convection becomes extremely active, the instability grows, and the system becomes unstable, but in other cases, convection slowly decays to zero. This shows that there is a diverse range of behaviour: the system presents either a rapidly growing instability or a decay of convection. In any case, the RCE state is unstable and the system moves to a new state, which is either unphysical or totally quiet.

CHAPTER 3. ISOLATING MICROSTATE MEMORY: CRM & TOY MODEL

Sheet1

MAIN CODE CHANGES	CODE AND OPTIONS	CLONE	T only	Qvap only	U only	T and Qvap	T,U,V	Qvap,U,V	All 4 var (T,Qvap,U,V)
Old nudging on patch indices. Global averaging with wrf_dm_sum_real.	With the old nudging on patch indices. Namelist: 6s time step, 40s nudging. Cold start. Old default modules.	v6.2	Good simulation (but takes more time to reach eq + too much cirrus at beginning) (at least 2 days) (part1_init_v21)	Good simulation (at least 9 days) (part1_init_v22)	Good simulation (about 47h) (part1_init_v23)	Unstable, then crashes after 8h (part1_init_v20)	Good simulation!! (about 29h) (part1_init_v25)	Unstable, then crashes after 11h (part1_init_v19)	Unstable, then crashes after 11h (part1_init_v19)
Title indices instead of patch indices. Stopping at "-1" when unsaggregated.	With the old nudging on patch indices. Namelist: 3s time step, 40s nudging. With restart. Old default modules.	v6.2.1				Unstable after 10h, but can run for at least 29h (part1_init_v27)	Good simulation (for at least 29h) (part1_init_v33)	Unstable for 10h, but can run for at least 28h (part1_init_v35)	Unstable for 10h, but can run for at least 28h (part1_init_v35)
	With the code with tile indices and min(je,jde-1). Namelist: 6s time step, 40s nudging time scale. Cold start. Old default modules.	v6.6.1						Unstable then crashes after 19h (part1_init_v26)	Unstable then crashes after 19h (part1_init_v26)
	With the code with tile indices and min(je,jde-1). Namelist: 6s time step, 80s nudging time scale. With restart. Old default modules.	V6.6.1					Good simulation (at least 47h) (part1_init_v36)	Unstable after 11h, but can run for at least 43h. Winds less strong than with 40s time scale. (part1_init_v34)	Unstable after 11h, but can run for at least 43h. Winds less strong than with 40s time scale. (part1_init_v34)
	With the code with tile indices and min(je,jde-1). Namelist: 6s time step, 40s nudging time scale. With restart. Old default modules. Configure -d	V6.6.1						Unstable after 10h, and crashes after 23h (part1_init_v41)	Unstable after 10h, and crashes after 23h (part1_init_v41)
No negative values allowed for Qvap	With the code with tile indices and min(je,jde-1) and no neg Qvap. Namelist: 6s time step, 40s nudging. With restart. Up-to-date modules.	v6.6.2					Good simulation (for at least 46h) (part1_init_v37)	Unstable after 10h, but can run for at least 43h (part1_init_v30)	Unstable after 10h, but can run for at least 43h (part1_init_v30)
	With the code with tile indices and min(je,jde-1) and no neg Qvap. Namelist: 6s time step, 40s nudging. With restart. Old default modules.							Unstable after 10h, but can run for at least 43h (part1_init_v28)	Unstable after 10h, but can run for at least 43h (part1_init_v28)
Multiplicative nudging on Qvap	With the code with tile indices and min(je,jde-1) and multiplicative nudging on Qvap (form 1). Namelist: 6s time step, 40s nudging. With restart. Old default modules.	v6.6.3						Seems stable but crashes after less than 1h (NaN values) (part1_init_v31, v38)	Seems stable but crashes after less than 1h (NaN values) (part1_init_v31, v38)
	With the code with tile indices and min(je,jde-1) and multiplicative nudging on Qvap (form 2 ok). Namelist: 6s time step, 40s nudging. With restart. Old default modules.	v6.6.5						Unstable after 10h, and crashes after 16h (part1_init_v32)	Unstable after 10h, and crashes after 16h (part1_init_v32)
Nudging done on tendencies (see DIJK) Instead of state variables	Nudging tendencies, strictly following DIJK. Namelist: 6s time step, 40s nudging. With restart. Old default modules.	v6.6.6					Good simulation (for at least 47h). But higher max OLR! (part1_init_v40)	Unstable after 9-10h, but can run for at least 43h (part1_init_v39)	Unstable after 9-10h, but can run for at least 43h (part1_init_v39)
	Nudging tendencies, strictly following DIJK. Namelist: 6s time step, 40s nudging, 0.33min radt. With restart. Old default modules.	v6.6.6						Unstable after 10h, but can run for at least 30h (part1_init_v42)	Unstable after 10h, but can run for at least 30h (part1_init_v42)
	Nudging tendencies (DIJK), using muu and muv. Namelist: 6s time step, 40s nudging. With restart. Old default modules.	v6.6.6						Unstable after 10h, but can run for at least 43h (part1_init_v43)	Unstable after 10h, but can run for at least 43h (part1_init_v43)

Page 1

3.2. ISOLATING THE MICROSTATE MEMORY IN WRF

Sheet1

		V6.6.7	Nudging tendencies (DIJ), using muu and muv, all 3 RK steps. Namelist: 6s time step, 40s nudging. With restart. Old default modules.							Unstable after 10h, and crashes after 22h (partl_init_v45)
		v6.6.6	Nudging tendencies (DIJ), using muu and muv, "rendf". Namelist: 6s time step, 40s nudging. With restart. Old default modules.							Unstable after 10h, and crashes after 30h (partl_init_v44_ALL4_var)
Nudging applied only in the troposphere (up to level 54)		v6.6.8	Nudging tendencies, strictly following DIJ, up to lev54. Namelist: 6s time step, 40s nudging. With restart. Old default modules.							Unstable after 10h, and crashed after 27h (partl_init_v46)
		v6.6.8	Nudging tendencies, strictly following DIJ, up to lev54. Namelist: 6s time step, 40s nudging, diff_6th_opt, w_damping. With restart. Old default modules.							No convection anymore! But can run for at least 49h (partl_init_v47)
		v6.6.8	Nudging tendencies, strictly following DIJ, up to lev54. Namelist: 6s time step, 40s nudging, diff_6th_opt. With restart. Old default modules.							No convection anymore! But can run for at least 48h (partl_init_v48)
		v6.6.8	Nudging tendencies, strictly following DIJ, up to lev54. Namelist: 6s time step, 40s nudging, w_damping. With restart. Old default modules.							Unstable after 10h, and crashes after 19h (partl_init_v49)
		v6.6.8	Nudging tendencies, strictly following DIJ, up to lev54. Namelist: 6s time step, 900s nudging, w_damping. With restart. Old default modules.							Unstable after 20h, but can run for at least 45h, NaN values appearing at the end (partl_init_v50)
Nudging only in points away from clouds or humidity maximum		v6.6.8	Only if T,q where 0.8 from qmax. Nudging tendencies, strictly following DIJ, up to lev54. Namelist: 6s time step, 40s nudging. With restart. Old default modules.							Unstable after 15h, but can run for at least 44h (partl_init_v51)
		v6.6.8	Only if cldfra < 0.01. Nudging tendencies, strictly following DIJ, up to lev54. Namelist: 6s time step, 40s nudging. With restart. Old default modules.							Unstable after 8.5h and crashes after 11h (partl_init_v52)
		v6.6.8	Only if cldfra <= 0. Nudging tendencies, strictly following DIJ, up to lev54. Namelist: 6s time step, 40s nudging. With restart. Old default modules.							Unstable after 9h, and crashes after 11h (partl_init_v53)

Page 2

3.2.2 Description of the instability that appears in the fixed-macrostate experiments in WRF: growth and decay

With strong nudging of the macrostate, aimed at holding the macrostate fixed, some of our simulations undergo a decay of convection, and some other simulations develop a growing instability with gigantic convection, depending on the initial and target conditions. The initial conditions we tested were all extracted from a natural RCE control simulation without strong nudging, at different days, so with different RCE state fluctuations (see Section 2.3). With different initial conditions, it does not take exactly the same time for the instability to appear, develop or decay. However, there is a consistent order of magnitude of about 10 hours before the instability becomes visible (Figure 3.7). Among 9 different initial conditions, about half led to a decay, and the other half to an instability growth.

Simulation	Instability?	Beginning of instability in OLR movie	Beginning of instability in Cloud fraction movie
wrfout_d01_2007-08-01_05:00:00	Yes, with growth	6.5 h – 8 h	7.5 h
wrfout_d01_2007-08-02_05:00:00	Yes, with growth	6.85 h	6.25 h – 8 h
wrfout_d01_2007-08-03_05:00:00	Yes, with growth	11 h – 13 h	14.5 h
wrfout_d01_2007-08-04_05:00:00	Yes, with growth	6.85 h – 8 h	6.5 h – 8 h
wrfout_d01_2007-08-05_05:00:00	Convection slowly decays to zero	8.25 h – 9.25 h	5.55 h
wrfout_d01_2007-08-06_05:00:00	Convection slowly decays to zero	13.5 h	10 h
wrfout_d01_2007-08-07_05:00:00	Convection slowly decays to zero	7.5 h	6 h
wrfout_d01_2007-08-08_05:00:00	Convection slowly decays to zero	8 h	5 h
wrfout_d01_2007-08-09_05:00:00	Convection slowly decays to zero	10 h	6 h – 11 h

Figure 3.7 Two major behaviours of simulations with strong nudging for different initial conditions: (1) instability growth up to an unphysical and highly convective state, and (2) a slow decay of convection up to a quiet state with no convection.

To provide more understanding of the growing instability, we chose the beginning of the 62nd day (2007-08-01, time = 61 day) as the initial condition, and analysed the first day of the simulation after strong nudging method activation. Note that strong nudging is activated at every time step, right from the initial condition. This particular simulation will be the one analysed in this subsection and the next subsection.

3.2. ISOLATING THE MICROSTATE MEMORY IN WRF

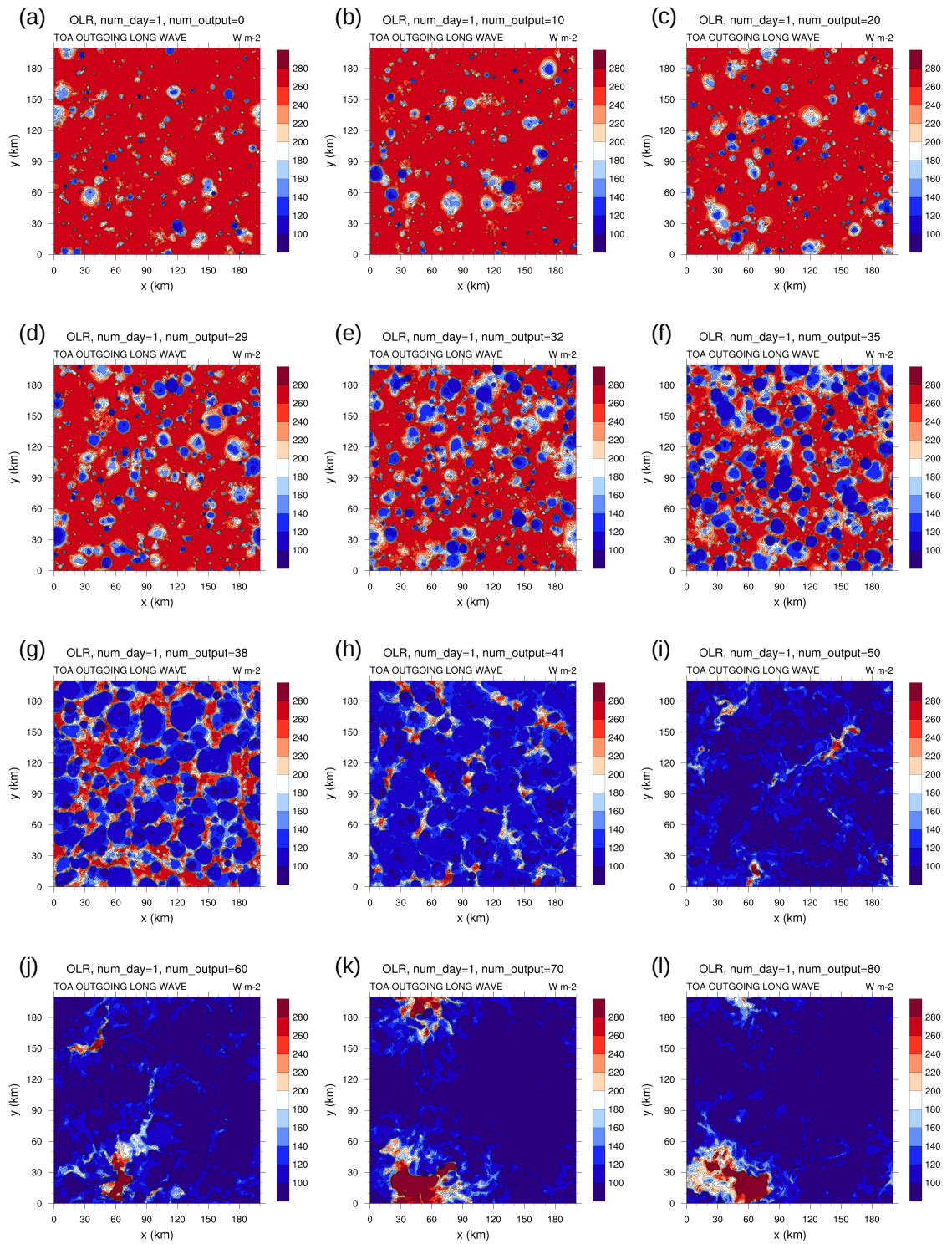


Figure 3.8 Snapshots of Outgoing Long-wave Radiation (OLR) in a simulation with strong nudging which developed an instability. Each panel corresponds to a different time into the simulation after we started to apply the strong nudging method: (a) 0 h, output=0 (b) 2.5 h, output=10 (c) 5 h, output=20 (d) 7.25 h, output=29 (e) 8 h, output=32 (f) 8.75 h, output=35 (g) 9.5 h, output=38 (h) 10.25 h, output=41 (i) 12.5 h, output=50 (j) 15 h, output=60 (k) 17.5 h, output=70 (l) 20 h, output=80. Blue corresponds to high clouds (low OLR) and red to the surface (high OLR).

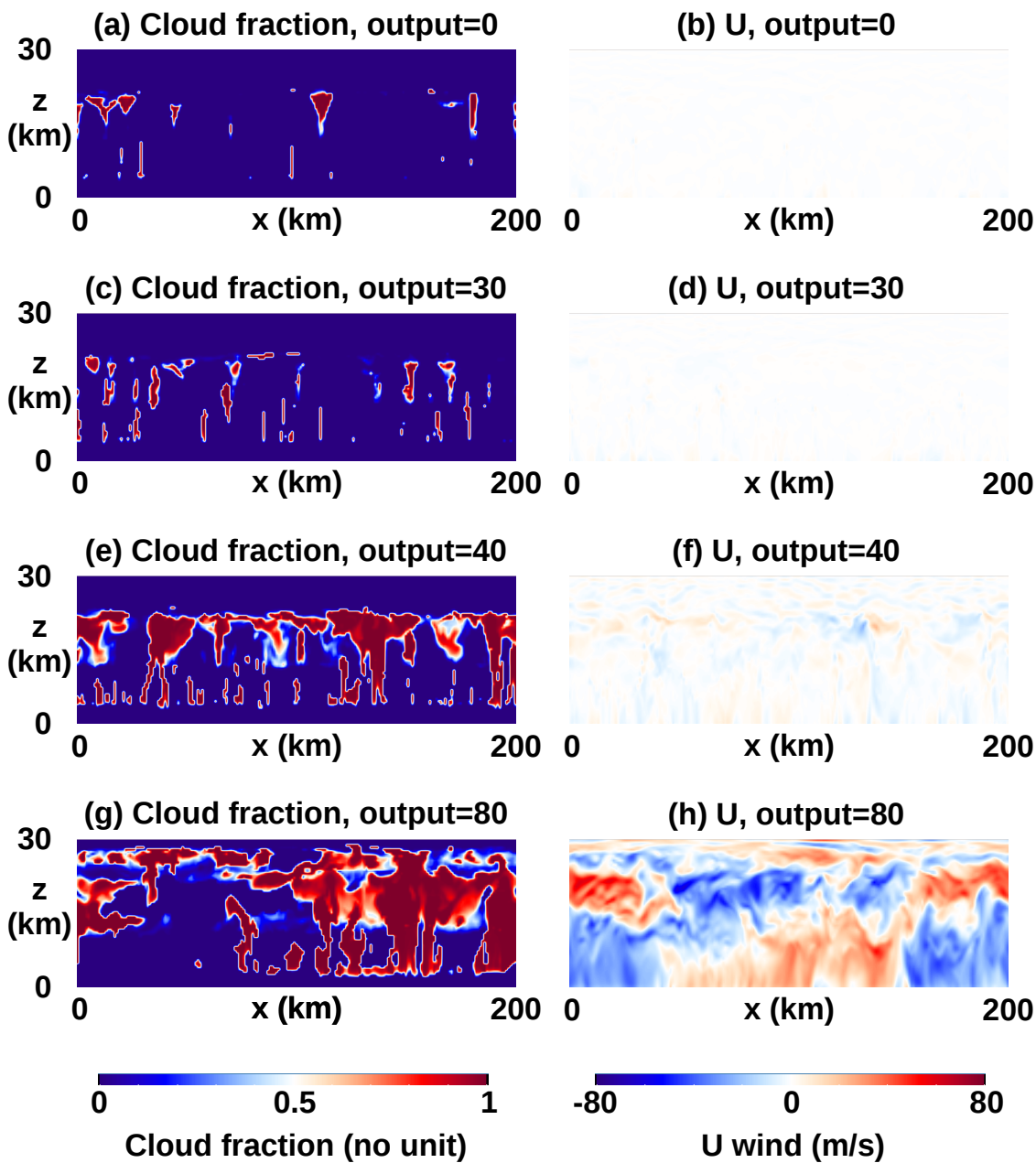


Figure 3.9 Vertical cross-section snapshots of cloud fraction (a,c,e,g) and U wind (b,d,f,h) in the same unstable simulation as figure 3.8. Note that this shows the 3-D cloud fraction, and that U wind is the wind along the horizontal x-axis. Each panel corresponds to a different time into the simulation after we started to apply the strong nudging method: (a,b) 0 h, output=0 (c,d) 7.5 h, output=30 (e,f) 10 h, output=40 (g,h) 20 h, output=80.

In this particular case, the instability develops after about 7 hours, and it reaches a saturation and thus a new form of equilibrium, after about 18 hours, as seen in Figure 3.8. While the RCE state has unorganised convection with well separated clouds, the instability creates an increasing number of clouds, with anvils that persist increasingly longer, so that in the end the system reaches a state almost

completely overcast. In this final state, Outgoing Long-wave Radiation (OLR) is low almost everywhere, except in one small area which manages to remain cloud-free.

The characteristics of the instability can be further understood with vertical cross-section snapshots (Figure 3.9). In the RCE state, the cloud fraction is small, there are a few shallow and congestus clouds, and a few larger deep convective clouds, but with moderate anvils. The horizontal winds are then of the order of 2-3 m/s, as expected for a 1-km resolution. Then the instability develops by creating a larger number of congestus clouds (7.5 h, output=30), which then quickly lead to a very large upper cloud fraction (10 h, output=40). At this stage, the winds start to increase, in the upper troposphere mostly. After the instability has saturated, the cloud fraction is very large in the whole domain, being almost fully overcast due to large thick high clouds. The winds then reach values of order of up to 80 m/s throughout the whole domain. This resembles Rayleigh-Benard convection, but at high Reynolds number, and with moist convection, so that it could be called turbulent moist Rayleigh-Benard convection. This is nothing similar to atmospheric convection.

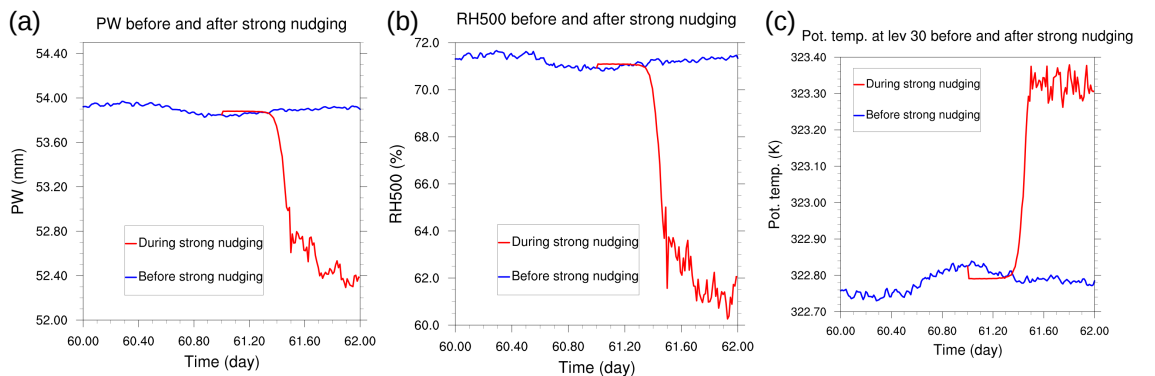


Figure 3.10 Time series comparing the control simulation without strong nudging (blue) and with strong nudging, i.e., the same unstable control simulation as figure 3.8 (red). (a) Domain-mean Precipitable Water (b) Domain-mean relative humidity at 500 hPa (c) Domain-mean potential temperature at model level number 30 (about 500 hPa). The red curves only start from day 61, when strong nudging is activated. The blue curves show RCE fluctuations.

To understand how this can happen even though strong nudging is activated precisely to maintain the RCE macrostate, we compare the evolution in time of a few key variables in the simulation with strong nudging, and in the equivalent simulation but without strong nudging (Figure 3.10). The simulation in RCE, without strong nudging, shows statistical fluctuations of the domain-mean variables around

its equilibrium (in blue). The strong nudging is activated from time = 61 day, and we can see the quick adjustment of the domain-mean values immediately after (in red). The values then remain successfully fixed for approximately 7 hours: the strong nudging method is effective, and the macrostate is held constant. This is true on either pressure levels (panels (a,b)) or model levels (panel c), for both water vapour (panels (a,b)) and temperature variables (panel c). Suddenly, after about 9 hours, the domain-mean values diverge out of the target values, and after 11.5 to 12 hours they have reached a completely new value (in red), out of the usual RCE fluctuation range (in blue). The instability takes time to appear, but it then develops very quickly. The new state reached after the instability has saturated has larger high-frequency fluctuations, and it seems to be a new stable equilibrium state, though unrealistic for an atmosphere. Since the macrostate was successfully held fixed for 7 hours even in a simulation which becomes unstable, it confirms that the strong nudging method in itself works. But at some point an instability manages to become stronger than the nudging terms, so that we lose control of the macrostate.

Even though the instability induces a drop of domain-mean precipitable water (PW) of less than 2 mm between the original RCE state and the new final equilibrium state, the increase in precipitation is tremendous: from 3 mm/day to 3000 mm/day (Figure 3.11). The new state is clearly unrealistic. Interestingly, in less than a day, the instability has pushed the tropopause significantly upwards, which also means that the tropopause is now much colder. The OLR has reduced to less than 100 W/m^2 on average. The troposphere, which is usually cooled by radiation, is now radiatively cooled only up to 5 km. Above 5 km, the troposphere is inversely warmed by radiation. There is a clear transfer of water vapour from the lower troposphere to the higher troposphere, as seen in the relative humidity profiles, which could be partly responsible for the change in radiative heating profiles. The standard deviation of PW, which is a simple proxy for convective organisation in general, has significantly increased after the instability develops, since the scale of the new state's "clouds" is now much larger. The mid-troposphere has warmed by 0.5 K, and the cloud fraction has sky-rocketed. Figure 3.11 shows that the instability affects all variables, and brings the simulation into a new state that does not represent a realistic Earth-like atmosphere. Still, this new state is a valid state as regards

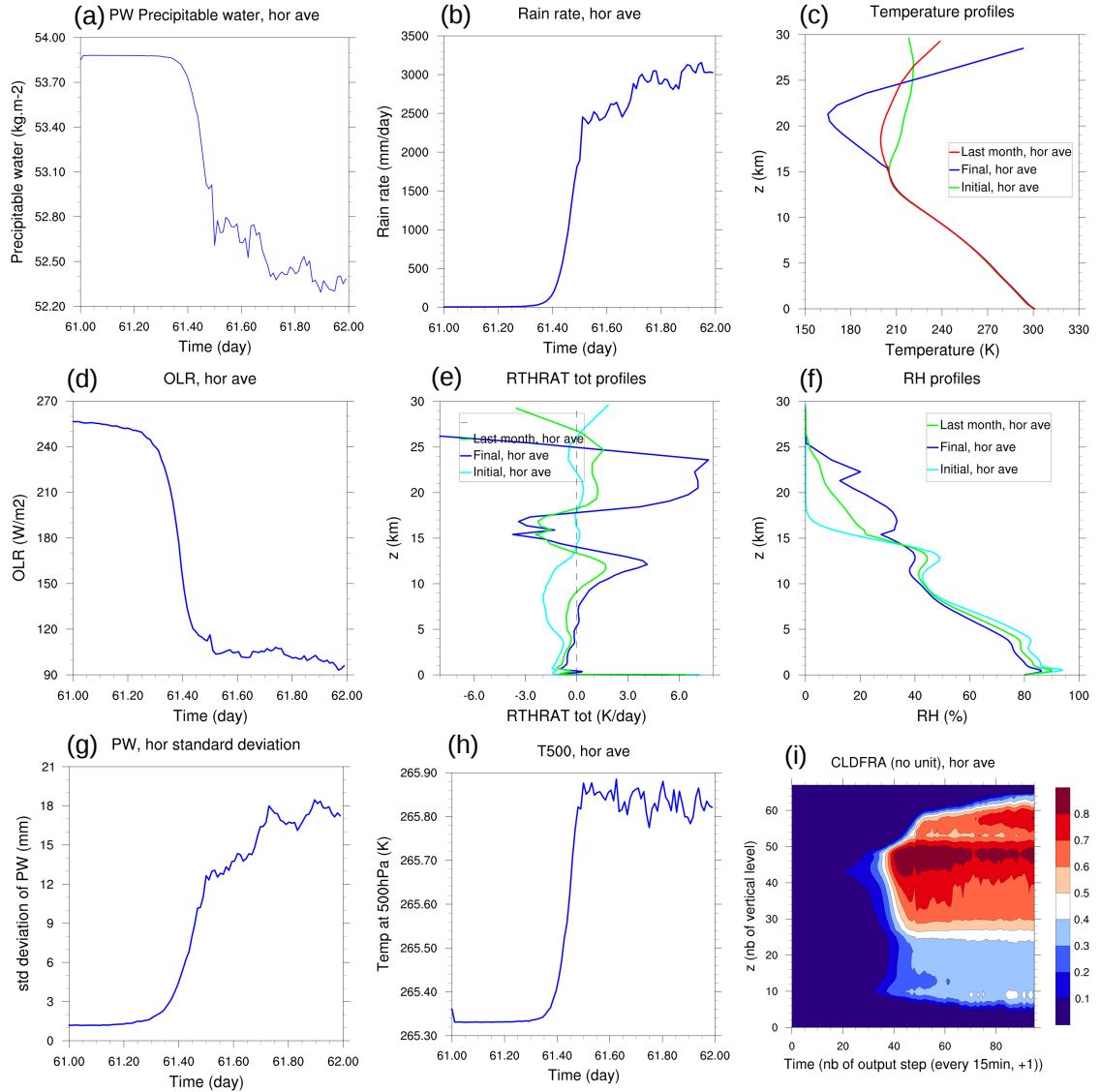


Figure 3.11 Time series and vertical profiles of the control simulation with strong nudging which developed an instability (same unstable simulation as figure 3.8), during the first day of simulation after we started to apply the strong nudging method. (a) Time series of the domain-mean Precipitable Water (b) Time series of the domain-mean rain rate (c) Domain-mean temperature profiles (d) Time series of domain-mean OLR (e) Domain-mean total (short-wave + long-wave) radiative heating profiles (f) Domain-mean relative humidity profiles (g) Time series of the horizontal standard deviation of Precipitable Water (h) Time series of domain-mean 500 hPa temperature (i) Domain-mean 3-D cloud fraction as a function of time and model level.

fluid mechanics and thermodynamics, so it is important to understand how a cloud-resolving model in a simple fixed-macrostate situation can lead to such a behaviour.

The next step is to compare the variables in the unstable situation with what they should look like if instability had not happened, level by level. In the first 3 hours of the unstable simulation, since strong nudging is effective in controlling the macrostate, there is virtually no difference between the domain-mean variables

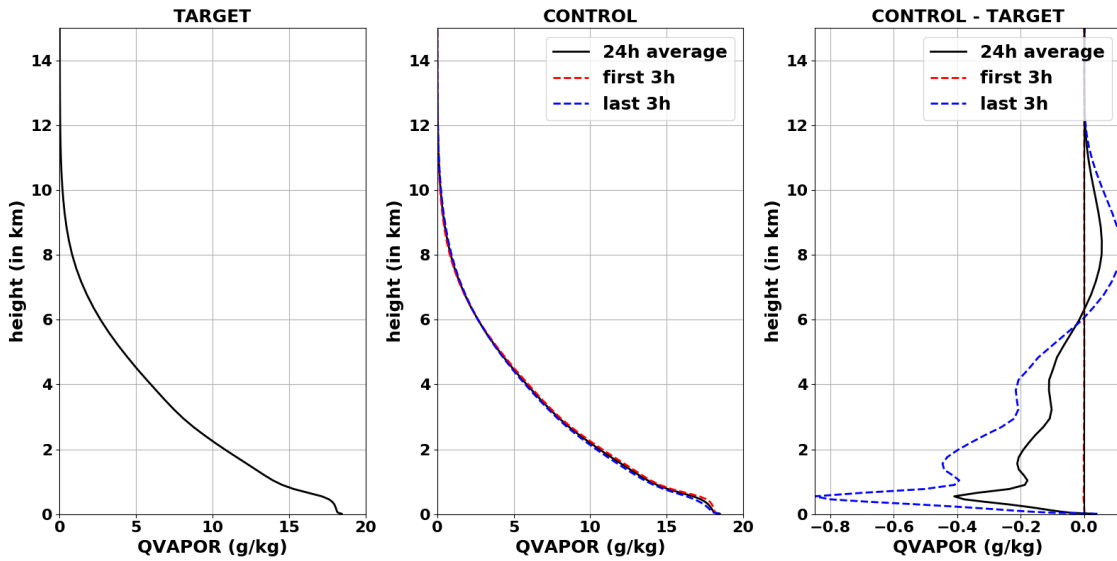


Figure 3.12 Vertical profiles of water vapour mixing ratio, for different cases: (a) The target to be imposed by the strong nudging method (b) The control simulation with strong nudging (same unstable simulation as figure 3.8) (c) For the difference (b)-(a). The black lines correspond to the average for the first 24 h after strong nudging activation. The red lines correspond to the average over the first 3 h after strong nudging activation, while the blue lines correspond to the last 3 h of the first 24 h after activation.

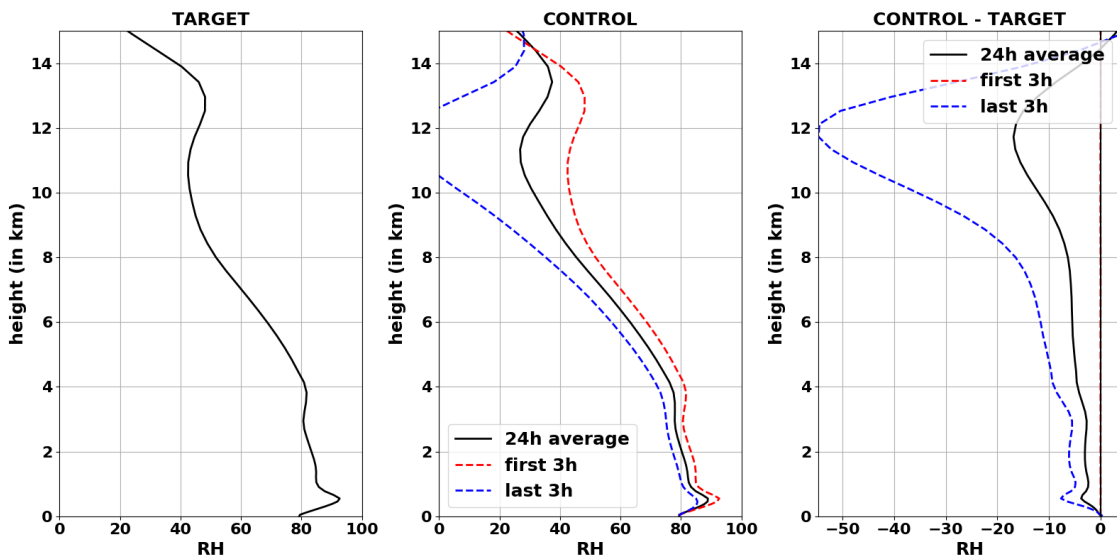


Figure 3.13 Same as figure 3.12 but for relative humidity

and their targets (red dashed lines in Figures 3.12,3.13,3.14,3.15). But in the last 3 hours of the first day after strong nudging is activated, that is, in the new state reached after instability saturates, there are large differences with the targets (blue dashed lines). Up to 6 km, the water vapour mixing ratio is lower than imposed by the target, while it is larger above 6 km. This makes sense since convection in the new final state is very violent, thus transporting a lot of water vapour from the

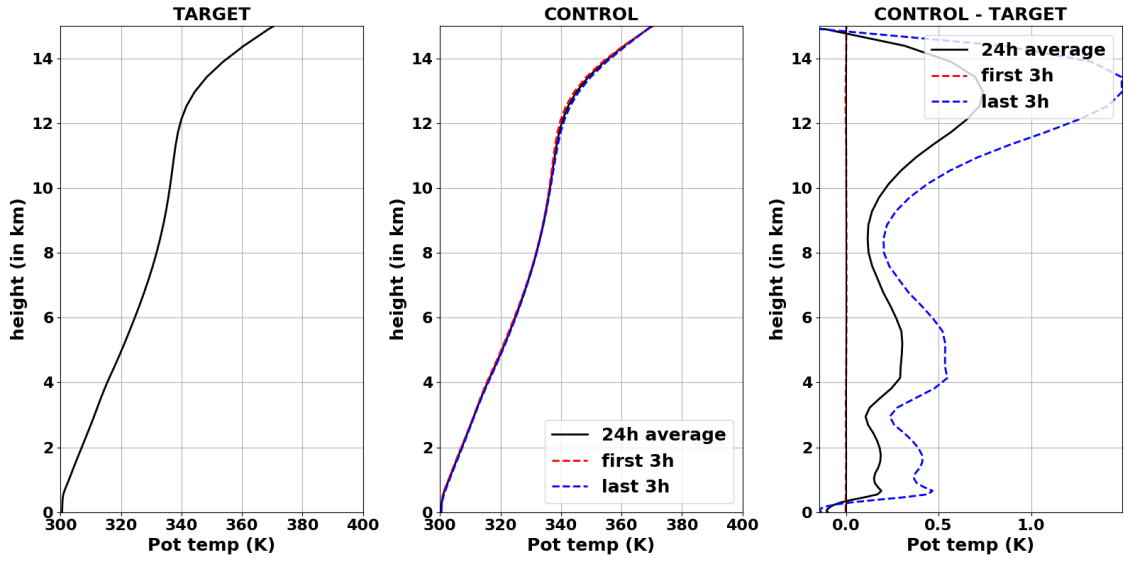


Figure 3.14 Same as figure 3.12 but for potential temperature

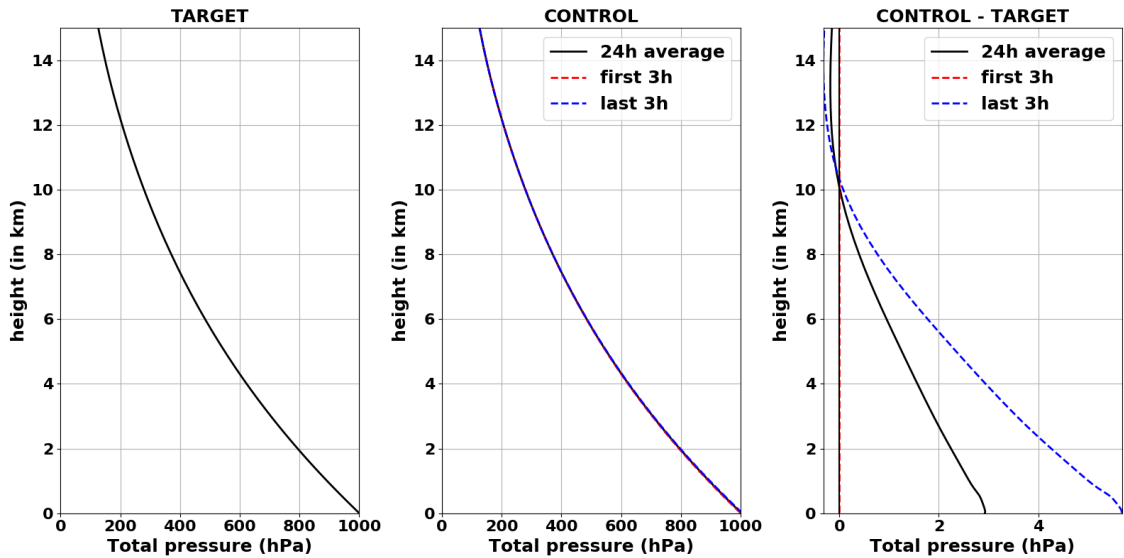


Figure 3.15 Same as figure 3.12 but for total pressure

lower troposphere to the larger troposphere. Throughout the whole troposphere, the relative humidity is much lower than the target profiles would require. This is due to the vertical water vapour transport mentioned previously, but also to the potential temperature which is larger than the target by roughly 1 K. Except in the lowest 300 m where it is lower than the target, the potential temperature in the new final state is indeed larger than the target. In terms of temperature, the values are greater than the target throughout the troposphere, even close to the ground. This is probably because of the pressure change: the pressure in the new final state is larger than the target value, so that even though temperature near the ground is

larger than its target, the potential temperature near the ground is lower than its target. Overall, the troposphere in the new final state is warmer than the target, so it has dilated, the lower troposphere is drier, and the higher troposphere more humid.

Now the question is: what is the mechanism that leads to this instability growth and eventually to this unrealistic but stable new final state?

3.2.3 Mechanisms explaining the instability development

To provide further understanding on the instability growth and propose a mechanism, it is useful to analyse how the variables can drift away from their target values imposed by strong nudging, and to do so level by level. We will first focus on the very beginning of the instability (soon after 7 hours after strong nudging activation).

In the early stages of instability development (Figures 3.16 and 3.17), the water vapour mixing ratio near cloud base (about 500 m) becomes lower than the target. Potential temperature and temperature throughout the troposphere become higher than their target, except very close to the surface where it is lower. Simultaneously, the pressure near the surface also starts to increase compared to its target. To understand the instability mechanism, it would have been easier if some variable anomalies grew before others, to detect causality. Unfortunately, it is not the case.

The evolution in time of the domain-mean anomaly profiles may also be useful to understand the anomaly growth (Figure 3.18). The lowest 6-7 km of the atmosphere become increasingly dry, while the troposphere between 6-7 km and 12 km becomes increasingly humid. The upward transfer of humidity can be attributed to the large increase in convection strength. The whole troposphere is increasingly warm (in terms of temperature), and it stays warmer than the target. In terms of potential temperature, the troposphere is also warmer than the target, except in the surface layer (lower than 300 m) where it is colder. This difference between the temperature anomaly and the potential temperature anomaly near the surface is likely to be related to the increase in pressure anomaly with time, which is greater as altitude decreases from 10 km to the surface. This causes the discrepancy between temperature and potential temperature to be the largest near the surface. And because

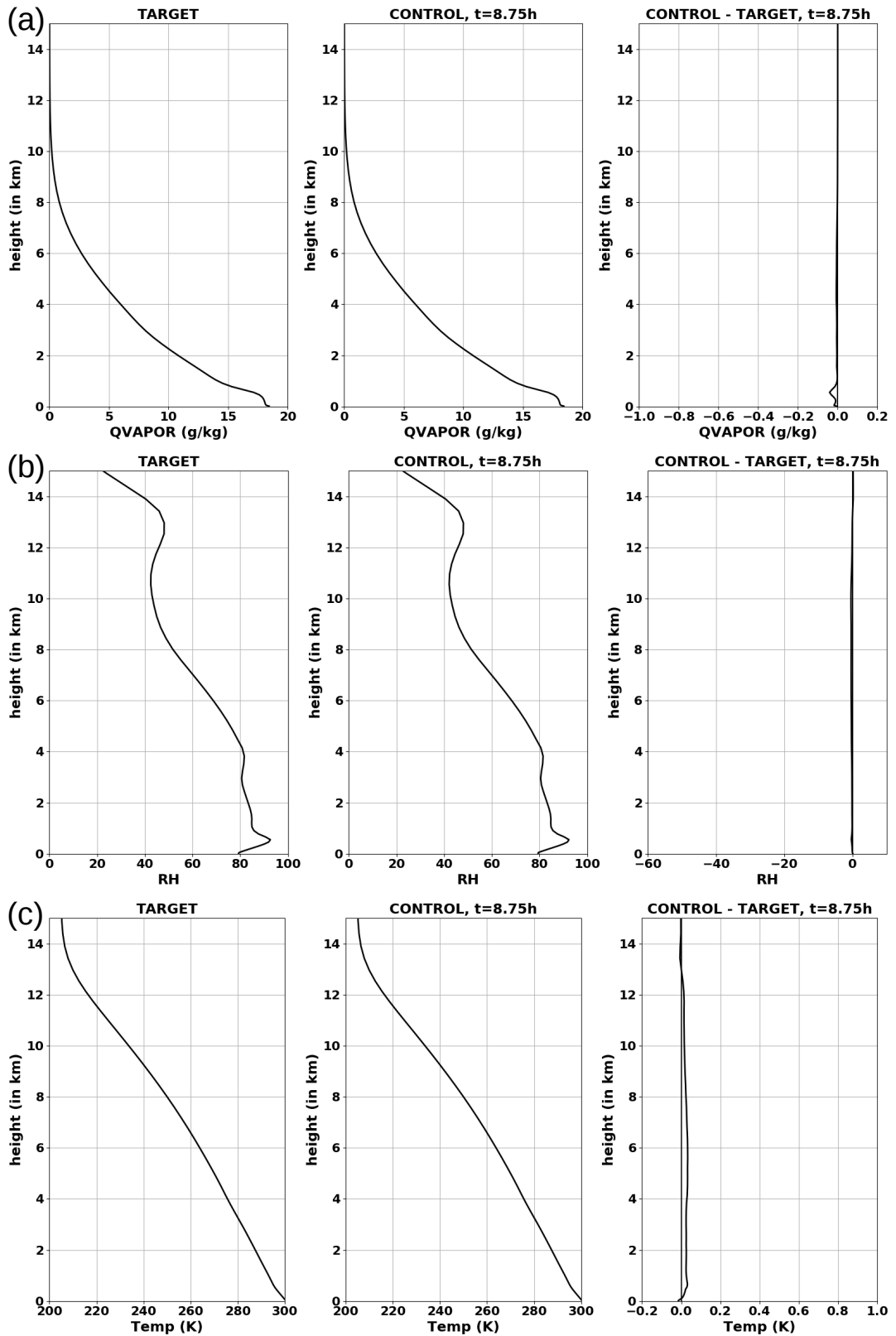


Figure 3.16 Vertical profiles of (a) water vapour mixing ratio (b) relative humidity (c) temperature, for: (left) The target to be imposed by the strong nudging method (middle) The control simulation with strong nudging (same unstable simulation as Figure 3.8), at time $t=8.75$ h after strong nudging activation (right) The difference (middle)-(left) between the control simulation at $t=8.75$ h and the target.

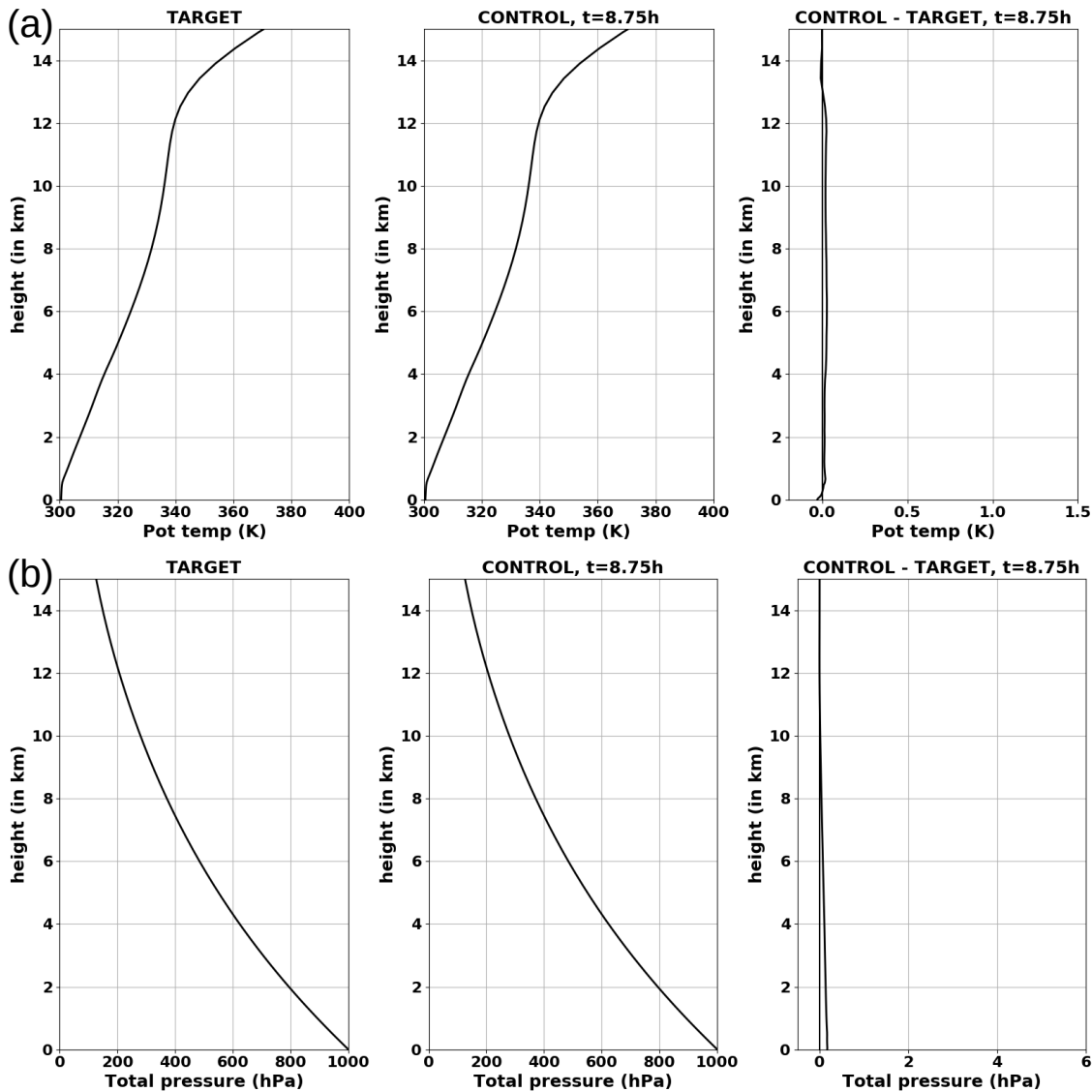


Figure 3.17 Same as Figure 3.16, but for (a) potential temperature (b) total pressure.

the strong nudging tendencies are imposed in terms of potential temperature (the actual prognostic variable in WRF), not in terms of temperature, this difference between temperature anomaly and potential temperature anomaly in the sub-cloud layer as soon the instability develops may be important. The temperature increase throughout the troposphere also translates into a slight increase in domain-mean vertical velocity up to 12 km. Since the system has periodic boundary conditions, we would expect the domain-mean vertical velocity to be zero if the system was in equilibrium. But the domain-mean temperature increase, symptomatic of the non-equilibrium state, causes a dilatation of the atmosphere, and thus a small non-zero domain-mean vertical velocity. Overall, it seems that all important variables move away from their target rather at the same time, in a coupled way. We will have to

3.2. ISOLATING THE MICROSTATE MEMORY IN WRF

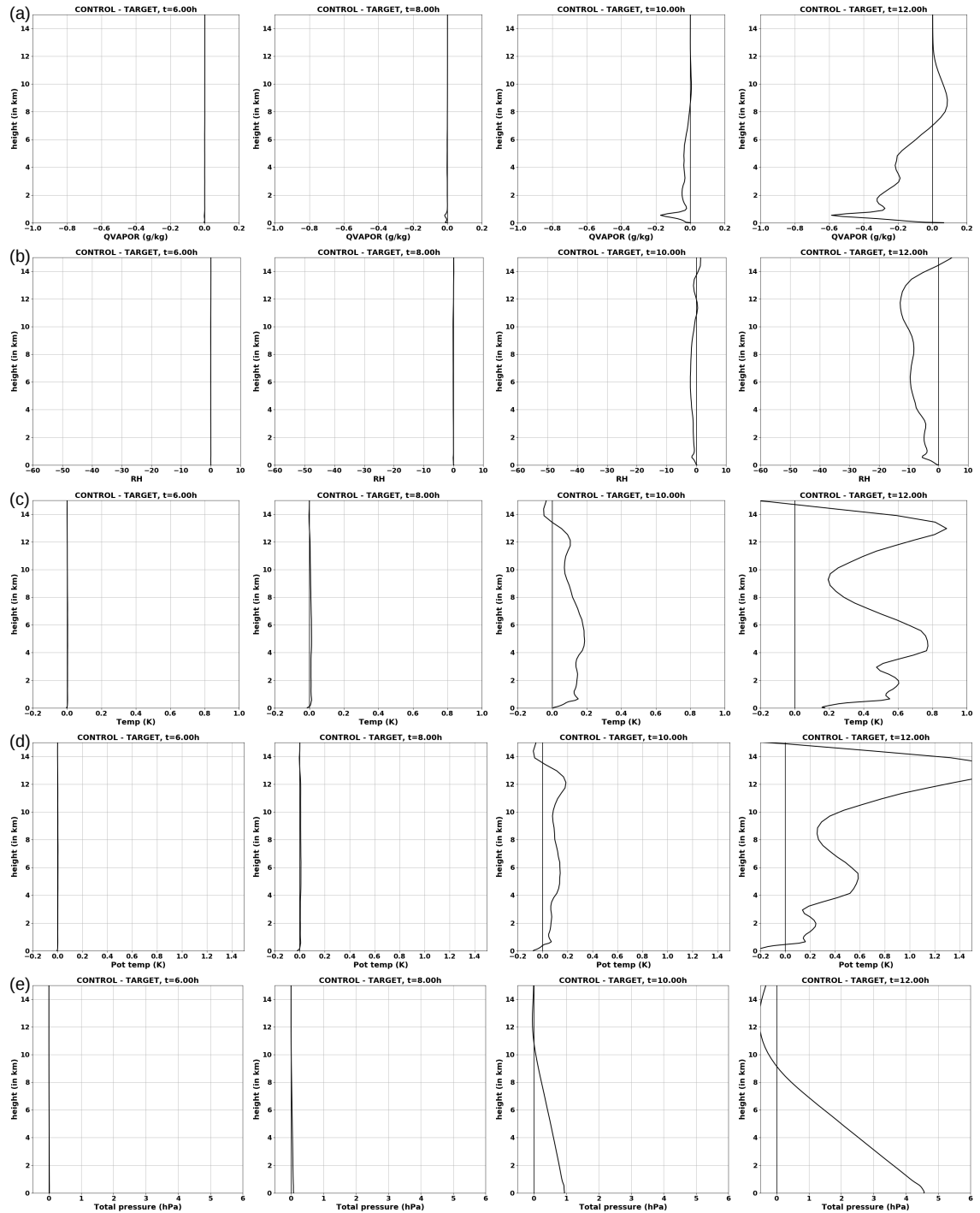


Figure 3.18 Vertical profiles of the difference between a variable and its strong nudging target, at different times of the control simulation with strong nudging (same unstable simulation as Figure 3.8). Time evolves in each panel from left to right: 6 h, 8 h, 10h, 12 h after strong nudging activation. The variable anomaly presented are (a) water vapour mixing ratio (b) relative humidity (c) temperature (d) potential temperature (e) total pressure.

find other types of analysis to determine a potential mechanism.

Because of these general differences between the actual domain-mean state during instability growth and the targets for potential temperature and water vapour,

the strong nudging tendencies are at each time step: (1) injecting dry static energy near the surface, (2) reducing temperature in the free troposphere, (3) injecting water vapour in the lowest 6 km of the atmosphere, and (4) reducing the water vapour above 6 km. The combination of (1) and (2) results in an increase in CAPE, thus partly explaining the steep increase in convection activity. The combination of (1) and (3) results in an increase in sub-cloud layer MSE, thus also explaining the increase in convection activity because of updraft strengthening and Lifting Condensation Level lowering. The strong nudging method is unfortunately in a situation where it always brings energy and moisture to the lower troposphere, and the system is efficient enough in exporting this to the higher troposphere via extreme convection to bring the lower troposphere back to a status where it is deficient in both energy and moisture. This feeds a continuous cycle of energy absorption by the system, and therefore help explain the instability growth up to a tremendously and unrealistically convective state.

To determine a mechanism for this instability growth despite the apparent coupling of all key variables to drift together, we chose to represent all time series of such key variables together. Because all have different units and different values, we rescaled the variables so that they are worth 0 on average over the first few hours of the simulation, and 1 on average over the last few hours of the simulation, to be able to precisely compare the variable evolutions together. If a variable v decreases during the instability, we instead plot $1-v$ so that it can be plotted alongside increasing variables. The first part of this analysis is presented on Figure 3.19. It is clear that for all variables, the fluctuations in the new final state are much larger than in the normal RCE state. The impact of strong nudging to control not only the nudged variables, but also their dependants, is visible by the small jump or drop near time=0.

To better understand the beginning of the instability growth and potentially detect what is causing the instability in the fixed-macrostate simulation, Figure 3.20 presents the same as Figure 3.19 but zoomed between hours 4 and 10. It seems the first variable to leave its expected value is the standard deviation of the temperature at 2 m (T_2), which is a microstate variable. Then the standard deviation of MSE in the sub-cloud layer as well as the standard deviation of CAPE start to

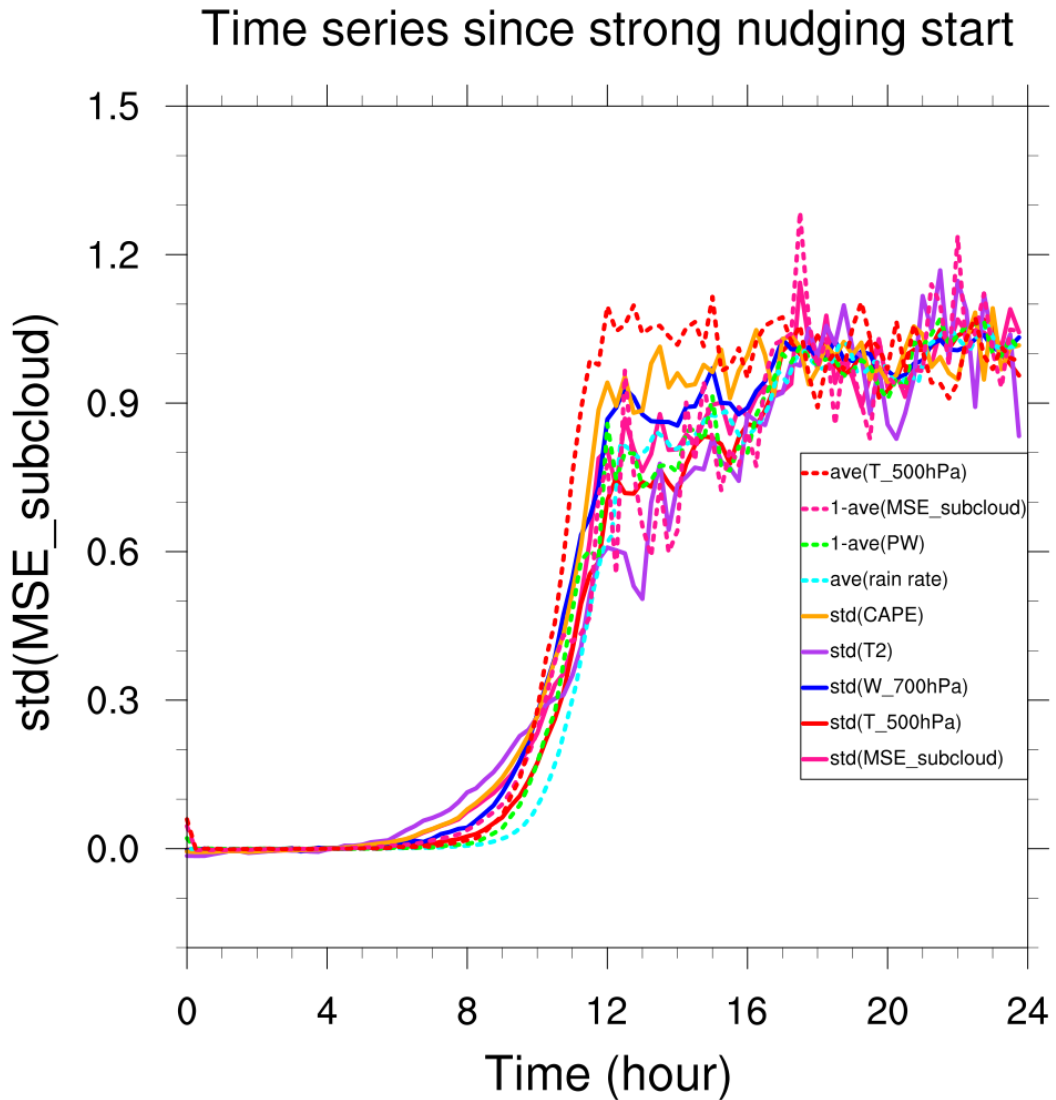


Figure 3.19 Time series of different variables (as indicated by legend), rescaled to evolve from 0 to 1 throughout 1 day of the control simulation with strong nudging (same unstable simulation as Figure 3.8). If a variable v was originally decreasing with time, we plot $1-v$ so that it can be compared with the other variables. The solid lines refer to standard deviations (microstate, std) and the dotted lines refer to domain averages (macrostate, ave). Different colours stand for different variables. $T_{500\text{hPa}}$ is the temperature at 500 hPa, $\text{MSE}_{\text{subcloud}}$ is the Moist Static Energy in the sub-cloud layer, PW is the Precipitable Water, CAPE is the Convective Available Potential Energy, T_2 is the 2-metre temperature, $W_{700\text{hPa}}$ is the vertical velocity at 700 hPa.

grow, which makes sense since the 2-m temperature will affect MSE and CAPE. Then the standard deviation of vertical wind at 700 hPa starts to grow. Later, the mean MSE in the sub-cloud layer decreases away from its target value, then the standard deviation of temperature at 500 hPa increases, then the mean temperature at 500 hPa increases, then the mean precipitable water decreases, then the rain rate increases. This indicates the instability grows from the surface up to the

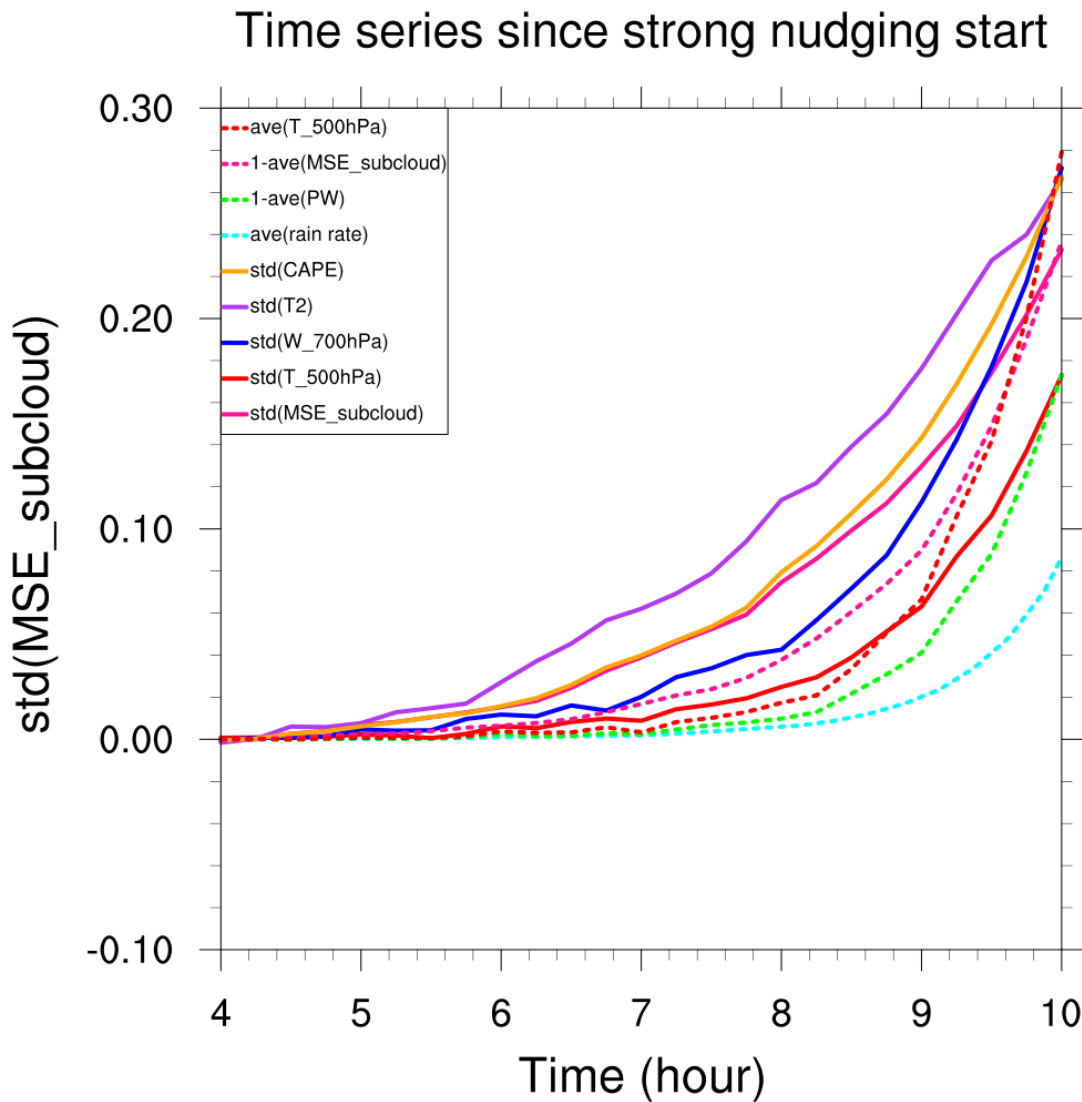


Figure 3.20 Same as Figure 3.19 but zoomed between 4 h and 10 h after strong nudging activation.

high troposphere, starting from thermodynamic surface properties, then affecting the sub-cloud layer thermodynamics, then affecting winds in the lower free troposphere, then affecting thermodynamic properties in the mid-troposphere, then only affecting the rain significantly. Another important feature is that the instability starts from the microstate variables, and then only affects the macrostate. After affecting the surface microstate, then the sub-cloud layer microstate, then the lower free tropospheric microstate, the sub-cloud layer macrostate is finally affected, perhaps as a response to downdrafts generated by the anomaly in standard deviation of winds at 700 hPa. Then only is the mid-tropospheric microstate responding. So this instability seems to be growing from the surface to the top, and seems rooted

in the microstate before affecting the macrostate. This raises the question of the role of microstate surface fluxes in generating the first anomaly in microstate 2-m temperature, or other surface and radiative variables.

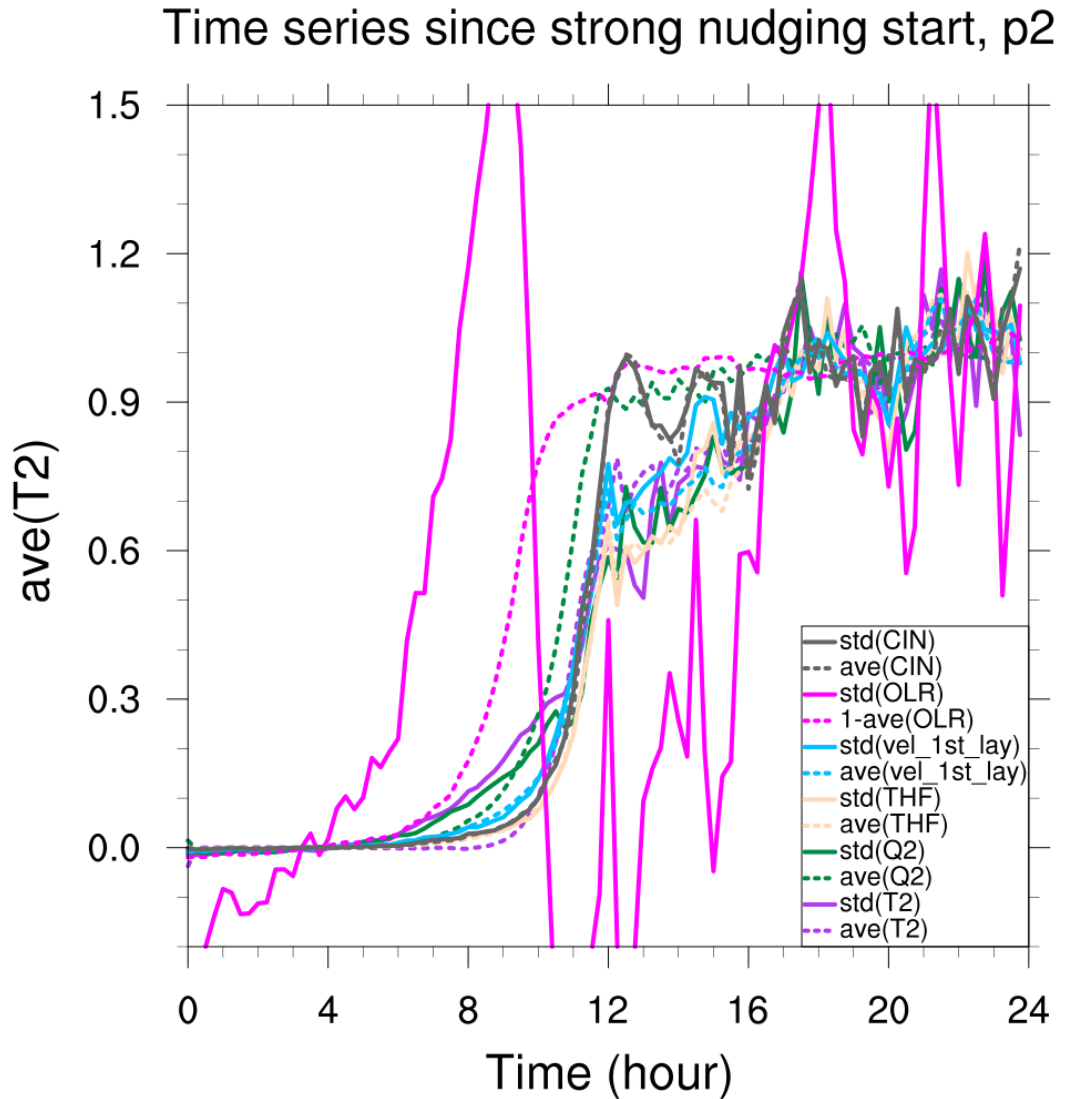


Figure 3.21 Same as Figure 3.19 but for different variables (as indicated by legend). CIN is Convective Inhibition, OLR is Outgoing Longwave Radiation, `vel_1st_layer` is the velocity in the lowest model layer, THF is the total surface heat flux (latent + sensible), Q2 is the 2-metre humidity, and T2 is the 2-metre temperature.

It turns out surface fluxes only grow well after 2-m temperature standard deviation, either via their microstate or via their macrostate (Figure 3.21). So they are not responsible for this instability. Analysing the timing of other variable growth shows that 2-m temperature standard deviation is definitely one of the first variable to diverge. Only the OLR microstate and macrostate appear to drift beforehand. The first point is that all variables in Figures 3.19 and 3.21 behave smoothly,

by a monotonic increase in their value during the instability, except the standard deviation of OLR (microstate OLR). And at this stage, we are unable to explain confidently why. It could perhaps be related to the bounded character of OLR to respect energy balance. Apart from the standard deviation of OLR, which drifts away first, it is possible to sort out variables by the time they start to diverge, starting with the quickest one after OLR standard deviation: OLR average, 2-m temperature standard deviation, 2-m humidity standard deviation, 2-m humidity average, first-level wind average and standard deviation, CIN average and standard deviation, surface fluxes average and standard deviation, and then only 2-m temperature average. This confirms the instability starts from surface temperature microstate, then affects surface water vapour, then surface winds, then surface fluxes and other variables, then 2-m temperature average. The only variable which may help trigger the anomaly in 2-m temperature standard deviation is OLR, but it is unclear by which mechanism it could do so.

Possible explanations for the role of OLR would require more careful analysis. We can speculate in two ways on how a system with fixed macrostate (domain-mean) temperature (T) and water vapour (q) may regulate itself in response to any infinitesimal perturbation. The regulation can be achieved either via a change in clear-sky OLR, or via a change in clouds. Since the microstate is allowed to vary, and since OLR is non-linear in both temperature and humidity, it is possible that the T and q microstates become more or less prominent (while still keeping the macrostate fixed), concentrating more or less of the heat or humidity in a small part of the domain, thus varying clear-sky OLR to maintain an equilibrium. If the clear-sky OLR does not vary enough, the only other factor which may regulate the system is the cloud cover. To create a large cloud cover, strong winds may be plausible, such as in our experiment.

To summarise, we are facing a rich intertwined instability, which grows in OLR first, then in surface temperature microstate, to then affect increasingly higher tropospheric variables (bottom-top development). The instability affects the microstate first, then only the macrostate. The energy and moisture provided by the strong nudging tendencies to the lower atmosphere is undoubtedly paramount to provide fuel to convection and an eternal source of energy to the system instability, hence

the dramatic precipitation rate and winds reached in the new final state. Overall, this instability only develops in half the cases, depending on initial conditions. The other final state that the system may choose if initial and target conditions are appropriate is a completely quiet state with no convection and no clouds. This is an instability of the formerly stable RCE state (local minimum of potential energy in phase space) which has probably become a local maximum of potential energy due to the macrostate being fixed. This twofold instability can evolve in either of the two directions of the local maximum of potential energy, each direction having its own “potential well”: exponential growth until a tremendous convective state, or exponential decay until a quiet state with no convection. The overall behaviour seems to be an unsuspected convective instability of the RCE state under fixed macrostate conditions, which has never been reported before. This adds to the radiative-convective instability of the RCE state to an SST increase reported by *Emanuel et al.* [2014].

To simplify, explain, and tentatively understand this twofold convective instability under fixed-macrostate conditions, we propose the study of a stochastic toy model of convection with memory, to reproduce the results obtained with the cloud-resolving model.

3.3 A stochastic toy model of convection with memory to understand microstate memory and WRF instability: the predator-prey model

3.3.1 Description of the toy model

We propose a stochastic toy model of convection with memory with 3 variables and 3 equations. The goal is to better understand convective memory, and its consequences in WRF simulations. In particular, it would be important (1) to assess the role of memory in the instability of fixed-macrostate WRF simulations reported in Section 3.2, and (2) to help interpret the results from the previous chapter

(Chapter 2) which did not isolate microstate memory from macrostate memory.

To represent microstate memory, one needs to have a prognostic variable capturing the microstate. We call this variable V and consider it to represent the small-scale heterogeneities. The most important here is to make sure that V is prognostic: this is what builds the microstate memory. Since we intend to work on convection, one also needs a variable acting as a proxy for convection. One could choose the convective vertical mass flux, but for simplicity we choose an easily observable variable, precipitation (P). Note that P is a consequence of convection, not a direct measure of it. But since the time scale for deep convection to produce precipitation is relatively short, P is probably a good proxy for convection. Finally, an essential effect to predict convection is the large-scale environment. So we choose r to be a representation of the large-scale environment, for example the mean precipitable water. As with a GCM, the large-scale state must be predicted from its previous value, so we also choose a prognostic equation for r . This gives macrostate memory to the system.

The physical foundations of the toy model are simple relationships described here. Precipitable water is decreased by precipitation and increased by evaporation. The microstate heterogeneities (V) are formed by convection, so that they increase when precipitation occurs. They are dissipated by turbulence and friction, and we capture the natural decay of the microstate heterogeneities by a sink term proportional to V . To produce precipitation, one requires both a moist environment (high r) and some small-scale turbulence or heterogeneities (V), so that P is given by a non-linear relationship involving r and V .

The toy model equation system is as follows:

$$\begin{cases} \frac{\partial r}{\partial t} &= E_0 - P \\ \frac{\partial V}{\partial t} &= -\alpha_{damp} V + \alpha_{Vp} P + \varepsilon_V \\ P &= \alpha_P r V \varepsilon_P \end{cases} \quad (3.2)$$

The three model variables are r , the atmospheric humidity (it could also be understood as the CAPE), P the precipitation rate, and V the small-scale variability

or variance or turbulence. r and P are macrostate variables, but V is by definition a microstate variable. These three variables are only dependent on time t : it is a 0-D toy model. The model constants are E_0 the evaporation rate, α_{damp} the damping coefficient, α_{VP} the sensitivity coefficient of V to P , α_P the sensitivity coefficient of P . Note that if r is understood as CAPE instead of humidity, then E_0 is the effective radiative cooling rate instead of the evaporation rate. Finally, there are two stochastic variables: ε_V is an additive stochastic term to the V equation, and ε_P is a multiplicative stochastic term to the P equation. The Probability Distribution Function (PDF) of ε_V approximately amounts to a normal distribution of mean 0.1 and standard deviation 0.1, whose negative values have then been replaced by 0. The PDF of ε_P is approximately a normal distribution of mean 1.5 and standard deviation 0.5, whose negative values have then been replaced by 0 (see the PDFs on Figure 3.22). The model has been cast in terms of non-dimensional variables and constants, but the constants can a priori be of any order of magnitude to satisfy the physics behind each equation.

Note that even though α_{damp} is the damping coefficient for the prognostic V variable, and even though it has the dimension of the inverse of time, α_{damp} is not the microstate memory itself. Microstate memory lies in the fact that the microstate variable V obeys a prognostic equation, not in the value given to α_{damp} . To measure the microstate memory of the whole system, we still prefer to use the recovery time scale to initial perturbations of the system as a proxy. While α_{damp} can contribute to establishing the memory of the system, it may not be the only active factor in the memory process.

The physics of the model necessary to justify the three equations is summed up in Figure 3.23, and detailed below equation by equation, based on physical intuition.

Equation 3.2 for r

One can justify associating r with either Humidity (e.g. Precipitable Water (PW)) or Convective Available Potential Energy (CAPE). If we interpret r as PW, then this equation is just water conservation: the water vapour in the

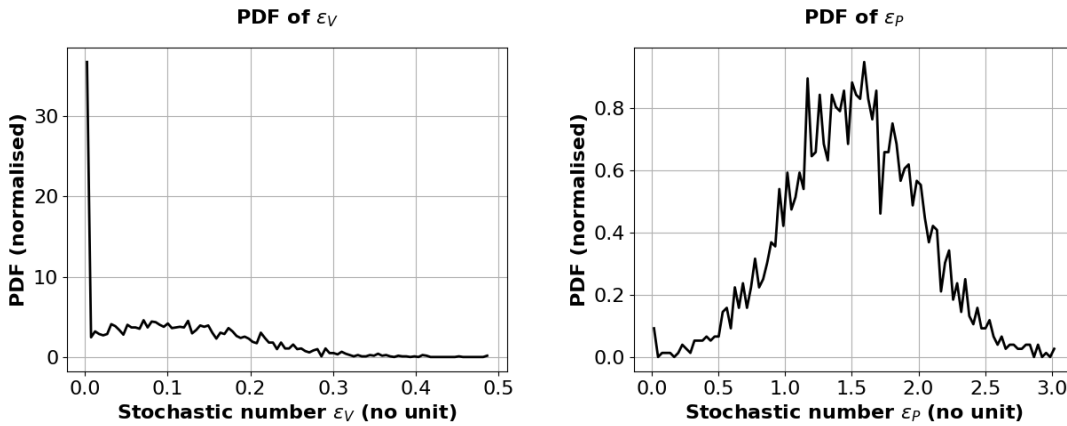


Figure 3.22 (left) Normalised PDF of the additive stochastic term in the V equation (right) Normalised PDF of the multiplicative stochastic term in the P equation.

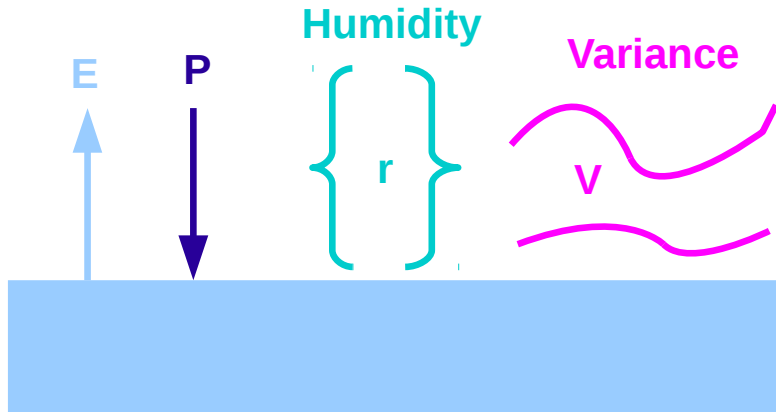


Figure 3.23 Schematic of the physics behind the toy model: the atmospheric humidity represented by a single variable r has a source term, evaporation E_0 (denoted by E here), and a sink term, precipitation P . The key variable in this model is the variance V , representing the microstate turbulence or microstate variability/heterogeneity.

atmosphere is a balance between surface evaporation and precipitation. If we interpret r as CAPE, there is a balance between free-tropospheric radiative cooling which steadily increases CAPE (E_0), and free-tropospheric heating due to convection/condensation/precipitation, which reduces CAPE (P). In both interpretations, E_0 is a source term, P a sink term, and this leads to a budget equation.

Equation 3.2 for V

V is abstract, but it can be interpreted as the turbulent kinetic energy. Since precipitation involves localised heating, P should generate V : when creating precipitation, convection introduces some turbulence and creates coherent microstate

structures increasing the variability. Surface heating should also generate V , hence the positive stochastic term ε_V . Otherwise, V should decay with time due to friction, therefore the first term on the right-hand side is simply expressed as an exponential decay. If we instead interpret V as boundary-layer heterogeneity (or microstate variability), convective drafts create cold pools and other types of heterogeneity, so precipitation generates variability. Many other phenomena can create some heterogeneity, such as surface fluxes (through dry convection) or radiation, hence the positive stochastic term. On the other hand, mixing and friction eventually eliminate heterogeneity, which justifies the exponential damping term.

Equation 3.2 for P

The more humid the atmosphere, the more likely it is to rain, the higher the precipitation. For example a more humid environment will favour precipitation by entrainment of more humid air, and reduced evaporation of falling rain. More variability V implies more areas with higher sub-cloud MSE and stronger wind convergence so enhanced convection and increased rain. This somehow reminds of the “natural selection” of updrafts by convection [Mapes and Neale, 2011]. Therefore, P should be increased by RH or CAPE, and by V . But the exact form of this equation is somewhat arbitrary. So this equation is a form of diagnostic parameterization for P . Here we chose to make P depend on the product of R and V , since this obeys the “ingredients” idea of convection which states that several ingredients are jointly needed (usually thermodynamic instability + lifting, perhaps other factors) so that convection can actually happen. In particular, a large CAPE alone or a large lifting alone will not be sufficient: the other also has to be present. This justifies that the product of r and V , rather than the sum, is generating P , assuming that r is analogous to instability and V to lifting. Precipitation is also modulated by a stochastic number usually greater than 1.

Summary

We have now postulated a system of stochastic non-linear ordinary differential equations with memory. The microstate memory comes from prognostic equation for the microstate variability V , while the macrostate memory is the water conservation formulated as a prognostic equation for r .

Derivation attempts

While we set our equation system by intuition and induction, it may be possible to derive it based on basic physical equations. Equation 3.2 for r can easily be derived from water conservation, since the atmospheric humidity variable has a source term (evaporation) and a sink term (precipitation). From the water vapour equation, written in terms of water vapour mixing ratio q and wind \vec{u} , one simply has to neglect the advection term:

$$\frac{\partial q}{\partial t} + \vec{u} \cdot \vec{\nabla} q = E_0 - P \quad (3.3)$$

Despite being less direct and not as compelling, it may be possible to establish Equation 3.2 for V from the dry static energy budget:

$$\frac{\partial s}{\partial t} + \vec{u} \cdot \vec{\nabla} s = P + R + Sens \quad (3.4)$$

where s is the dry static energy, P the precipitation (directly related to convective latent heat release), R the radiative warming (which we expect to be negative on average), and $Sens$ the surface sensible heat flux. We can introduce a Reynolds' decomposition to extract an equation for the local departures (microstates, denoted by $'$) to the macrostate averages (denoted by $\bar{}$). We thus write:

$$\left\{ \begin{array}{l} s = \bar{s} + s' \\ \vec{u} = \bar{\vec{u}} + \vec{u}' \\ P = \bar{P} + P' \\ R = \bar{R} + R' \end{array} \right. \quad (3.5)$$

By subtracting the average equation from the full equation, we get an equation for the microstate:

$$\frac{\partial s'}{\partial t} + \bar{\vec{u}} \cdot \vec{\nabla} s' + \vec{u}' \cdot \vec{\nabla} \bar{s} + \vec{u}' \cdot \vec{\nabla} s' - \overline{\vec{u}' \cdot \vec{\nabla} s'} = P' + R' + Sens' \quad (3.6)$$

If we now (1) parameterize the numerous non-linear advection terms into a simple exponential decaying term, advocating that the dynamical terms have a damping effect on any gradient, effectively acting to ensure stability:

$$\bar{\vec{u}} \cdot \vec{\nabla} s' + \vec{u}' \cdot \vec{\nabla} \bar{s} + \vec{u}' \cdot \vec{\nabla} s' - \overline{\vec{u}' \cdot \vec{\nabla} s'} = \alpha_{damp} s' \quad (3.7)$$

and (2) approximate part of the right-hand term as a small stochastic forcing: $R' + Sens' = \varepsilon_{s'}$, advocating that the radiative and sensible heat flux time scales are much slower than the precipitation time scales, R' and $Sens'$ thus varying spatially at a much slower pace, which makes them small compared to the precipitation forcing, we obtain:

$$\frac{\partial s'}{\partial t} = -\alpha_{damp} s' + P' + \varepsilon_{s'} \quad (3.8)$$

Naturally interpreting s' as the microstate variability V , we obtain an equation particularly similar to the Equation 3.2 for V in our model, which could complete the derivation.

Nevertheless, one objection could be coming from the positivity of the right-hand side terms, which is assumed in Equation 3.2 for V , but not guaranteed by Equation 3.8. A second attempt to prove our Equation 3.2 for V would be to multiply Equation 3.8 by s' , thus obtaining on equation on s'^2 :

$$\frac{\partial s'^2}{\partial t} = -\alpha_{damp}' s'^2 + 2 s' P' + \varepsilon_{s'''} \quad (3.9)$$

where the constants have been renamed to absorb various factors: $\alpha_{damp}' = 2\alpha_{damp}$ and $\varepsilon_{s'''} = 2 s' \varepsilon_{s'}$.

Since s'^2 is a positive term, it can be even more satisfyingly interpreted as V . In the rest of the derivation, we therefore set $V = s'^2$. As P' should have the same sign as s' most of the time, $s' P'$ should be a positive term too, as expected by the

$\alpha_{Vp} P$ term. This guarantees all expected positivity. The equation becomes:

$$\frac{\partial V}{\partial t} = -\alpha_{damp}' V + 2 \sqrt{V} P' + \varepsilon_s''' \quad (3.10)$$

We can now modify the exact formulation of the parameterization for P by altering the exponent used for V to 0.5, since our first choice of an exponent of 1 was arbitrary. It leads to the following system:

$$\begin{cases} \frac{\partial r}{\partial t} &= E_0 - P \\ \frac{\partial V}{\partial t} &= -\alpha_{damp}' V + 2 \sqrt{V} P' + \varepsilon_s''' \\ P &= \alpha_P r \sqrt{V} \varepsilon_P \end{cases} \quad (3.11)$$

To complete the second derivation, we now have to assume $P = P'$, and there is admittedly no good reason for that. Because of the fundamental difference made here between macrostate and microstate, it is even most likely wrong. This is unsatisfying and would require additional work. However, if we were to assume this, the system would become close enough to our postulated model:

$$\begin{cases} \frac{\partial r}{\partial t} &= E_0 - P' \\ \frac{\partial V}{\partial t} &= -\alpha_{damp} V + \alpha_{Vp} \sqrt{V} P' + \varepsilon_V \\ P' &= \alpha_P r \sqrt{V} \varepsilon_P \end{cases} \quad (3.12)$$

renaming all the constants as required. Even though we have modified the exponent of V in the parameterization for P, it still gives the same non-linear product of r and V as the source term for the equation for V. The prognostic equation for V is therefore functionally unchanged.

None of the two derivations of the Equation 3.2 for V proposed here is a complete derivation. But they still show that this equation is vaguely grounded in basic principles.

Comparison with other toy models

Finally, even though this is unintentional, our equation system resembles *Yano and Plant* [2012a]. Although our context is different, and our justification non-related to theirs, there is a parallel between these systems. Recall their equations:

$$\begin{cases} \frac{dA}{dt} &= F - \gamma M_B \\ \frac{dK}{dt} &= -D + A M_B \\ K &= \beta M_B^p \end{cases} \quad (3.13)$$

where A is the cloud work function (similar to CAPE), K the convective kinetic energy, M_B the cloud-base mass flux, F the large-scale forcing, γ a convective damping coefficient, D the dissipation, β a proportionality constant, and p a positive exponent, Then they assume $p = 1$ and $D = \frac{K}{\tau_D}$ where τ_D is a dissipation time scale. Their equation system becomes:

$$\begin{cases} \frac{dA}{dt} &= F - \gamma M_B \\ \frac{dK}{dt} &= -\frac{1}{\tau_D} K + A M_B \\ M_B &= \frac{1}{\beta} K \end{cases} \quad (3.14)$$

This system is quite similar to our system, except that (1) there is no stochastic term and (2) the formulation of the non-linearity is slightly different. Indeed, our r can be interpreted as CAPE, similar to their cloud work function A , our evaporation E is similar to their external large-scale forcing F , our precipitation P must behaves closely to their cloud-base mass flux M_B , our α_{damp} is the equivalent of the inverse of their τ_D , and our microstate variability reminds of their convective kinetic energy K . One important difference is that our non-linear term is in the diagnostic equation, which thus impacts both prognostic equations, while their non-linear term is directly a source term for K , which only impacts one of their prognostic equations. If we

substitute a new variable $X = \frac{K}{A}$, we can better compare the two systems:

$$\begin{cases} \frac{dA}{dt} &= F - \gamma M_B \\ \frac{dX}{dt} &= -\frac{1}{\tau_D} X + M_B - \frac{X}{A} \frac{dA}{dt} \\ M_B &= \frac{1}{\beta} A X \end{cases} \quad (3.15)$$

This new formulation of their system shows that the difference with our system of equations can be reduced to a single term: they have an additional term $-\frac{X}{A} \frac{dA}{dt}$. This confirms that our systems are similar but different, even without considering the stochastic terms. Since their system showed a periodic cycle based on the recharge-discharge mechanism, we are quite confident that our system captures the essence of a memory behaviour: a delay or phasing between variables due to a need to exceed some non-linear thresholds (the recharge and discharge processes).

Other toy models for memory have been proposed. The model by *Davies et al.* [2009] is a linear system of equation, in which non-linearity is introduced as an external condition to the system. And it shows a very interesting sensitivity of the qualitative nature of the convective diurnal cycle to the memory time scale.

Description as a predator-prey model

Our toy model (Equation 3.2) turns out to be a predator-prey model. Combining the equation for P, it can indeed be written as a system of two coupled non-linear equations, with the non-linearity being the product between the two variables, in both equations, but with a different sign.

$$\begin{cases} \frac{\partial r}{\partial t} &= E_0 - \alpha_P r V \varepsilon_P \\ \frac{\partial V}{\partial t} &= -\alpha_{damp} V + \alpha_{Vp} \alpha_P r V \varepsilon_P + \varepsilon_V \end{cases} \quad (3.16)$$

Neglecting the stochastic terms for simplicity, the system reads:

$$\begin{cases} \frac{\partial r}{\partial t} &= E_0 - \alpha_P r V \\ \frac{\partial V}{\partial t} &= -\alpha_{damp} V + \alpha_{Vp} \alpha_P r V \end{cases} \quad (3.17)$$

The canonical predator-prey system (also called Lotka-Volterra equations) is the following:

$$\begin{cases} \frac{\partial x}{\partial t} &= \alpha x - \beta xy \\ \frac{\partial y}{\partial t} &= -\gamma y + \delta xy \end{cases} \quad (3.18)$$

where x is the number of prey, y is the number of predator, and α , β , γ , δ are positive real parameters.

Our toy model system is a predator-prey model, except that unlike the typical predator-prey model which has an exponential growth of prey if no predator is present, our model only describes a linear growth of the prey if it is not consumed by the predator (through the constant E_0). In other words, the reproduction rate of r is linear with time instead of being exponential. However, this discrepancy with the canonical system is not key here.

By analogy, the prey is r (humidity, or CAPE), and the predator is V (boundary layer microstate heterogeneity). In other words, the rabbits are the macrostate r , and the foxes the microstate V . The microstate structures are thus “hungry” for convective instability.

Why isn’t P (or convection) the predator instead of V ? First of all, the predator is V and not P from the equation system shown above. It would not be very natural to have a prognostic equation for P since precipitation is rather a short-term and small-scale process compared to the microstate heterogeneities that we try to describe here. Second, the previous chapter showed that there is practically no memory stored in the hydrometeors whereas most memory is stored in boundary layer thermodynamic heterogeneities, which V is meant to capture. Third, P is different from convection. If one considers that a model where convection is the predator of CAPE or humidity makes more sense, then V can arguably be a

better description of convection than P. The low-level thermodynamic turbulence may indeed be well correlated with convection, while P is more clearly an effect of convection, with some lag relatively to the convective life cycle.

Predator-prey models are commonly used in biology and ecology [*Holmes et al.*, 1994]. They have also been studied by mathematicians and physicists [*Arneodo et al.*, 1980], sometimes in the context of fluid mechanics [*Garcia and Bian*, 2003]. But it has rarely been applied to convection in atmospheric science. There are three examples. *Koren and Feingold* [2011] used a predator-prey model to explain aerosol-cloud-precipitation feedbacks. *Feingold et al.* [2015] used a similar approach for the question of transition between open cloud cells and closed cloud cells. *Nober and Graf* [2005] built an interesting convective parameterization as a predator-prey model extended to a spectrum of prey, which may be a similar philosophy to the full spectrum of plumes in *Arakawa and Schubert* [1974]. We hereby present how to use a predator-prey model to understand convection and its memory.

3.3.2 Analytical analysis of the toy model

Non-dimensionalisation and canonical system

First, we will strive to learn as much as possible about the toy model by conducting an analytical analysis of the equation system. Throughout this analytical analysis, we neglect the stochastic terms for simplicity. As a first step, we non-dimensionalise the equations to absorb all constants and express the equations in a canonical way. Let the new non-dimensional variables be:

$$\left\{ \begin{array}{l} t' = \alpha_{damp} t \\ r' = \frac{\alpha_{Vp} \alpha_P}{\alpha_{damp}} r \\ V' = \frac{\alpha_P}{\alpha_{damp}} V \\ P' = \frac{\alpha_{Vp} \alpha_P}{\alpha_{damp}^2} P \\ E_0' = \frac{\alpha_{Vp} \alpha_P}{\alpha_{damp}^2} E_0 \end{array} \right. \quad (3.19)$$

Combining P' , we have the canonical system:

$$\begin{cases} \frac{\partial r'}{\partial t'} &= E_0' - r' V' \\ \frac{\partial V'}{\partial t'} &= V' (r' - 1) \\ P' &= r' V' \end{cases} \quad (3.20)$$

Stationary solutions

The stationary solutions of this system are such that:

$$\begin{cases} \frac{\partial r'}{\partial t'} &= 0 \\ \frac{\partial V'}{\partial t'} &= 0 \end{cases} \quad (3.21)$$

We conclude there are two stationary solutions. The first one verifies: $V' = 0$ and $E_0' = 0$. Since we do not intend to impose a null evaporation condition, and since having no homogeneity at all is not interesting, we disregard this case. The only other stationary solution is:

$$\begin{cases} r' &= 1 \\ V' &= E_0' \\ P' &= E_0' \end{cases} \quad (3.22)$$

Linearisation and consequences

Then, we can substitute the perturbations away from the stationary solution as new variables, following:

$$\begin{cases} r' &= 1 + x \\ V' &= E_0' + y \end{cases} \quad (3.23)$$

The full equation system becomes:

$$\begin{cases} \frac{\partial x}{\partial t'} = -y - (E_0' + y) x \\ \frac{\partial y}{\partial t'} = (E_0' + y) x \end{cases} \quad (3.24)$$

We can now easily linearise the system around the stationary solution (now formulated $x = 0$ and $y = 0$):

$$\begin{cases} \frac{\partial x}{\partial t'} = -y - E_0' x \\ \frac{\partial y}{\partial t'} = E_0' x \end{cases} \quad (3.25)$$

This is a system of coupled linear ordinary differential equations. A single equation can be expressed by differentiating the first equation in 3.25 and substituting the other one:

$$\frac{\partial^2 x}{\partial t'^2} + E_0' \frac{\partial x}{\partial t'} + E_0' x = 0 \quad (3.26)$$

This is the equation of the damped harmonic oscillator. Recall the typical formulations:

$$\frac{\partial^2 x}{\partial t'^2} + 2\zeta\omega_0 \frac{\partial x}{\partial t'} + \omega_0^2 x = \frac{\partial^2 x}{\partial t'^2} + \frac{\omega_0}{Q} \frac{\partial x}{\partial t'} + \omega_0^2 x = 0 \quad (3.27)$$

By analogy, we can extract the natural frequency ω_0 of the linearised system, the oscillator quality factor Q , and the damping ratio ζ :

$$\begin{cases} \omega_0 = \sqrt{E_0'} = \frac{\sqrt{\alpha_{Vp}\alpha_P E_0}}{\alpha_{damp}} \\ Q = \frac{1}{\zeta\omega_0} = \frac{1}{\zeta\sqrt{E_0'}} = \frac{\alpha_{damp}}{\sqrt{\alpha_{Vp}\alpha_P E_0}} \\ \zeta = \frac{\omega_0}{2} = \frac{\sqrt{E_0'}}{2} \end{cases} \quad (3.28)$$

Depending on the sign of $Q - \frac{1}{2}$, i.e., depending on the sign of $\zeta - 1$, the solution is either an overdamped, critically damped, or underdamped oscillator. But in any case, the solution converges back to zero after about Q pseudo-oscillations at the

frequency ω_0 .

To give orders of magnitude, let us estimate the oscillator parameters. We arbitrarily choose $\alpha_P = 0.1$, $\alpha_{Vp} = 0.5$, $E = 1$, and $\alpha_{damp} \in [0, 1]$. Let T' be the period associated with ω_0 . This leads to:

$$\left\{ \begin{array}{l} E_0' = \frac{1}{20 \alpha_{damp}^2} \\ \omega_0 = \frac{1}{4.47 \alpha_{damp}} \\ Q = 4.47 \alpha_{damp} \\ T' = 2\pi * 4.47 \alpha_{damp} \end{array} \right. \quad (3.29)$$

The natural frequency of the linearised system is thus approximately within $[0.2, +\infty]$ and the quality factor within $[0, 5]$, in the t' variable. Based on equation 3.19, there is a factor of $\frac{1}{\alpha_{damp}}$ to convert from the t' to the t variable. All the oscillator properties who have a time dimension must therefore be re-dimensionalised by this factor to convert them in actual time t unit. It means that in the actual time variable t , the linearised system has the following properties:

$$\left\{ \begin{array}{l} \omega_{0t} = \alpha_{damp} \omega_0 = \frac{1}{4.47} \\ Q_t = Q = 4.47 \alpha_{damp} \\ T_t = \frac{1}{\alpha_{damp}} T' = 2\pi * 4.47 \end{array} \right. \quad (3.30)$$

In the t variable, the period of the linearised system is $2\pi * 4.47$, which is approximately equal to 28 time units (independent from α_{damp}). And the quality factor, unitless, is still within $[0, 5]$. This is an important source of information to analyse the toy model.

Full non-linear system

However, the toy model is non-linear by nature. To resolve the full non-linear system, the usual method would require to use elliptic functions, which does not

give enough information (since elliptic functions do not have a direct expression) and is out of scope. *Yano and Plant* [2012a] manage to find a simple expression for the full non-linear orbit by separating the variables, but this does not work with our equation system. It is possible to express the full system as a simple unique equation:

$$\frac{\partial y}{\partial t'} + y = -\frac{\partial x}{\partial t'} \quad (3.31)$$

But this does not lead to a complete solution since it uses an integral of $\frac{\partial x}{\partial t'}$, which is unknown. Therefore, we will not go any further in attempting to solve the full problem.

Fixed-macrostate condition

In WRF, we wanted to hold the macrostate fixed to its RCE value by strong nudging (subsection 3.2.1). Mimicking what we did in WRF, we can also hold the macrostate fixed in the toy model. This amounts to imposing $r' = r'_{RCE} = 1$, that is $r = r_{RCE} = \frac{\alpha_{damp}}{\alpha_{Vp}\alpha_P}$. The equation system without stochastic terms then becomes:

$$\begin{cases} \frac{\partial r}{\partial t} = 0 \\ \frac{\partial V}{\partial t} = -\alpha_{damp} V + \alpha_{Vp} P \\ P = \alpha_P r V \end{cases} \quad (3.32)$$

This system can be reduced to:

$$\begin{cases} \frac{\partial V}{\partial t} = (\alpha_{Vp} \alpha_P r_{RCE} - \alpha_{damp}) V \\ P = \alpha_P r_{RCE} V \end{cases} \quad (3.33)$$

Re-injecting the condition that we fix the macrostate to its RCE value, we get the equation:

$$\frac{\partial V}{\partial t} = 0 \quad (3.34)$$

So the solutions to the fixed-macrostate problem are $V = \text{constant}$ and con-

sequently $P = \text{constant}$. All three toy model variables should be constant, in the case without stochastic terms. If we were to include the stochastic terms, the RCE state could be slightly modified, and under fixed-macrostate conditions, V should mainly be the integration of the stochastic term ε_V , i.e., a Markov chain (a random walk):

$$\begin{cases} R & = r_{RCE} \\ \frac{\partial V}{\partial t} & = (-\alpha_{damp} + \alpha_{Vp}\alpha_P r_{RCE}\varepsilon_P) V + \varepsilon_V \\ P & = \alpha_P r_{RCE} V \varepsilon_P \end{cases} \quad (3.35)$$

Experimentally, in a real or simulated system, it is impossible to perfectly fix the macrostate to its RCE value. There is always a small inaccuracy. We denote $\delta r = r_{target} - r_{RCE}$ this small inaccuracy, with r_{target} the target value actually imposed and r_{RCE} the ideal RCE value. The system becomes:

$$\begin{cases} \frac{\partial V}{\partial t} & = \left(\alpha_{Vp} \alpha_P [r_{RCE} + \delta r] - \alpha_{damp} \right) V \\ P & = \alpha_P r_{target} V \end{cases} \quad (3.36)$$

Re-injecting the value of r_{RCE} , we finally have:

$$\frac{\partial V}{\partial t} = \alpha_{Vp} \alpha_P \delta r V \quad (3.37)$$

This is an ordinary first-order differential equation, which leads to an exponential behaviour of V . The exponential time scale is:

$$\tau_{fixed-macrostate} = \frac{1}{\alpha_{Vp} \alpha_P |\delta r|} \quad (3.38)$$

The time scale $\tau_{fixed-macrostate}$ is very large if δr is very small. Depending on the sign of δr , V is an exponential growth to infinity, or an exponential decay to zero. Since P is proportional to V , it follows the behaviour of V : an exponential growth or decay of relatively long typical time scale.

A toy model without microstate memory

To assess how much of the toy model behaviour comes from microstate memory, we can also decide to solve for a model without microstate memory. One way to do this is to replace the prognostic equation for V (the one responsible for microstate memory) by a diagnostic equation, with a similar physical link that P increases V . For example, we could write:

$$\begin{cases} \frac{\partial r}{\partial t} &= E - P \\ V &= \alpha_{Vp} P + \varepsilon_V \\ P &= \alpha_P r V \varepsilon_P \end{cases} \quad (3.39)$$

If the macrostate is held fixed to its RCE value:

$$\begin{cases} r &= r_{RCE} \\ V &= \alpha_{Vp} P + \varepsilon_V \\ P &= \alpha_P r_{RCE} V \varepsilon_P \end{cases} \quad (3.40)$$

This leads to a direct analytical solution:

$$\begin{cases} r &= r_{RCE} \\ V &= \frac{\varepsilon_V}{1 - \alpha_{Vp} \alpha_P r_{RCE} \varepsilon_P} \\ P &= \alpha_P r_{RCE} V \varepsilon_P \end{cases} \quad (3.41)$$

For a toy model without microstate memory, the solution under fixed-macrostate conditions is a series of stochastic numbers following the formulations in Equation 3.41: at each time t , each variable value is independent from its past value. So each time step is similar to a new jump out of the origin of the domain. This is very different from the solution of the toy model with microstate memory, and under fixed-macrostate conditions, i.e. a Markov chain, since a Markov chain always remembers its past value to advance a time step. In this case, each time step is

similar to an additional jump, but starting from the previous position, not from the origin of the domain. So microstate memory does matter under fixed-macrostate conditions, even with stochastic numbers.

3.3.3 Numerical integration of the toy model: RCE runs

To fully exploit the toy model, we solve it numerically. The general method is the following. We choose a very simple explicit forward first-order numerical scheme in time. We first solve for r , then for V , then for P . The stochastic terms are built from a Gaussian PDF modified to follow the rules specified in subsection 3.3.1. A general stochastic time series is then defined for each stochastic number ε_V or ε_P . To increase the statistical significance, we need to use an ensemble made up of several members (typically 100 or 1000). Each member is a restart of the RCE Control run, starting from a different time. The RCE state is computed by averaging a numerical integration without any forcing nor perturbation over a long period (typically 200 or 1000 time units). Homogenisation experiments are carried out by setting all microstate heterogeneities to zero (i.e., $V = 0$) before restarting the toy model.

We use two different methods to define the stochastic terms. In the default method, the stochastic time series corresponding to a member is taken from the general stochastic time series defined for the control run, but starting from the member's restart time. As a result, two consecutive members, starting for two consecutive time units, have a stochastic time series shifted by one time unit. In other words, both members use a different stochastic time series, but with a 1-time unit lag-correlation. In the alternative method, each member uses a completely independent time series for their stochastic terms. So in this case, there is no lag-correlation among stochastic time series for different members.

Several variations of the toy model have been used to further understand its behaviour: different method for the stochastic terms, fixed random seed, varying ensemble size, varying the RCE computation duration, ability to have memory or not, etc... These have generally shown consistency with the previous results, so that we will not dwell on this any longer.

3.3.4 Oscillations in the free RCE experiments

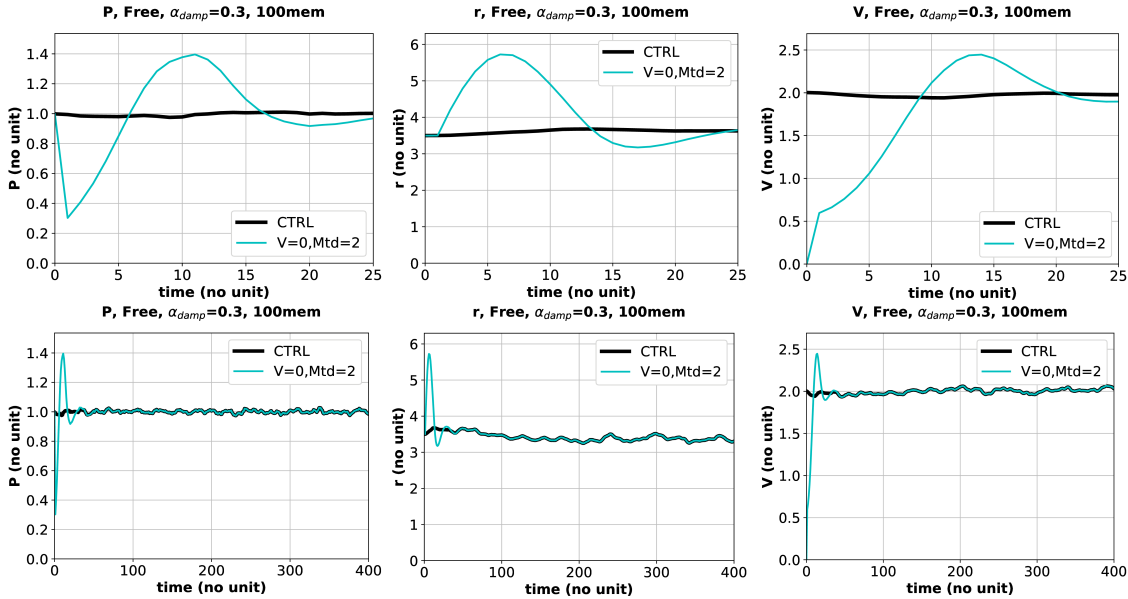


Figure 3.24 Responses of (left) P, (middle) r, and (right) V, for the toy model under usual RCE conditions, i.e. without strong nudging (“Free” runs). The top row presents the first 25 time units after homogenisation, and the bottom row the first 400 time units. The black line shows the RCE time series if no homogenisation is performed (Control), the blue line shows the time series after homogenisation ($V=0$). All simulations have been done with $\alpha_{damp} = 0.3$. Plots show the ensemble average over 100 members.

The results presented in Figure 3.24 show that homogenisation leads to damped oscillations back towards the RCE state, for all three model variables. After homogenisation, precipitation first decreases strongly, then increases to a value higher than the RCE state, starting an oscillation which is quickly damped. Because we solve for r and V before solving for P, it takes one time step for the whole model to feel the feedbacks from other terms, hence the non-differentiable (angular) point seen in all three variables at $t=1$ after homogenisation. On longer time scales, the toy model follows perfectly the fluctuations of the RCE state: it has perfectly recovered from homogenisation.

We can now compare numerical results and analytical results. The typical period of the oscillations is approximately 20 time units, in all three variables. Recall that we found in the analytical analysis of the linearised equation system that the period should be about 28 time units. So there is a relatively good agreement between the analytical result from the linearised model and the numerical result from the full model.

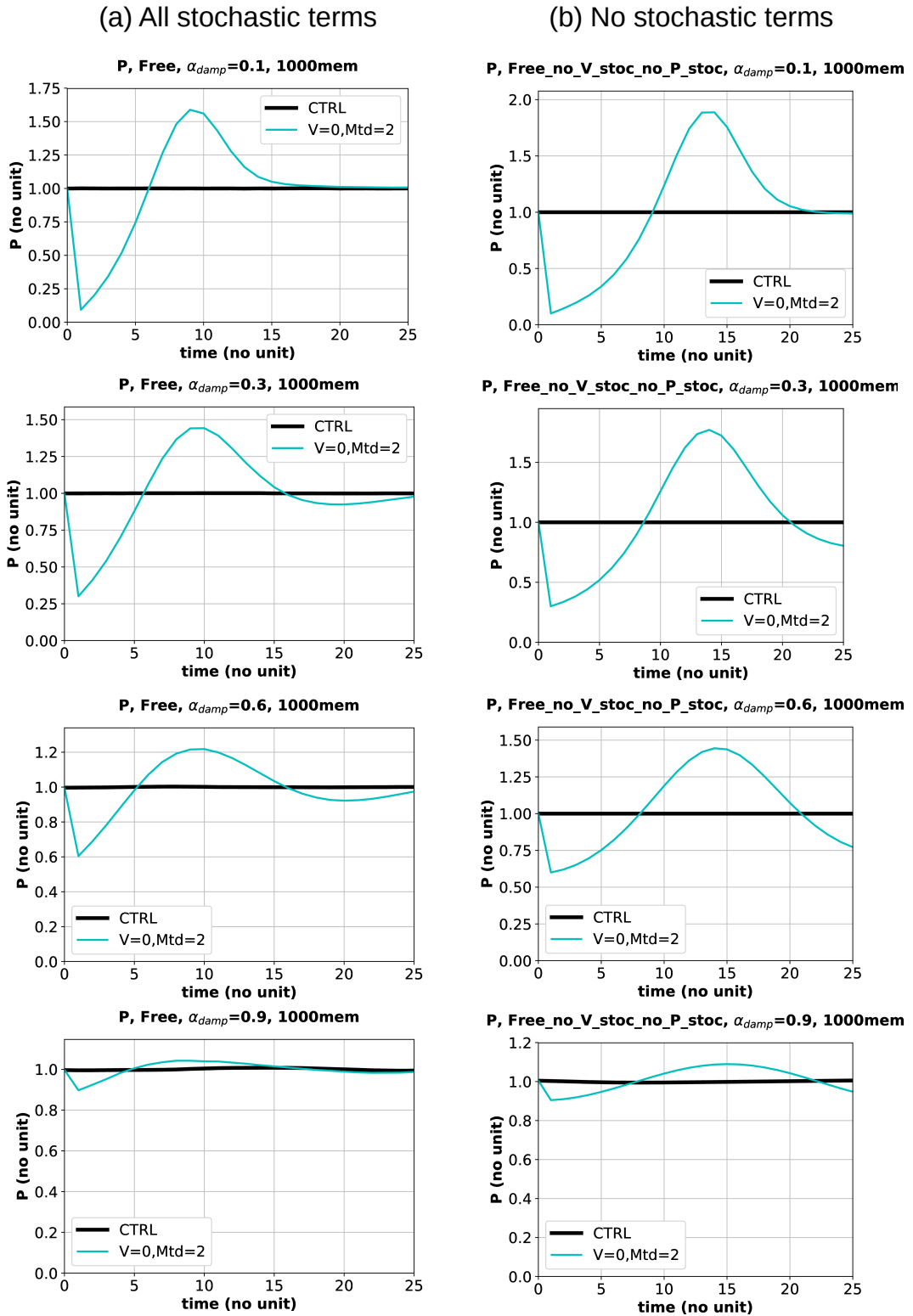


Figure 3.25 Responses of P to homogenisation in the toy model under RCE conditions, i.e, without strong nudging (“Free” runs). (a) For a toy model in the default configuration. (b) For a toy model where all stochastic terms have been turned off. Each row is for a different value of α_{damp} , from 0.1 at the top to 0.9 at the bottom. The black line shows the RCE time series if no homogenisation is performed (Control), the blue line shows the time series after homogenisation ($V=0$). Plots show the ensemble average over 1000 members.

We now analyse the sensitivity to α_{damp} . When writing the toy model equations, we introduced α_{damp} as a coefficient to damp the microstate heterogeneities. The hypothesis could be that the more damped V is, the less it is able to carry its value forward in time, the less memory we expect. To test this thinking, we can assess the influence of α_{damp} on the homogenisation recoveries (Figure 3.25). With a larger damping coefficient, the oscillations have a smaller amplitude, which is consistent with our intuition about the damping term. Nevertheless, oscillation frequency is almost unchanged (slightly reduced only) with a larger damping coefficient. This shows that the aforementioned hypothesis is not valid in terms of time scales. With the linearised analysis, we also showed that the oscillation period should be independent from α_{damp} . The slight reduction of frequency with increased α_{damp} can thus be attributed to non-linear effects. This confirms the validity of a linear approach in the RCE runs, even for homogenisation which is not a small perturbation of the system at all. It also demonstrates that, at first order, the memory time scale in RCE is not sensitive to α_{damp} : the damping effect may play some secondary role on memory, but at least it does not control the memory.

When stochastic terms are turned off, the ensemble-mean of all toy model runs behaves almost exactly as when they are turned on. This shows that the stochastic terms are not crucial to understand the response to homogenisation from the RCE state, at least in terms of ensemble mean.

The spread between ensemble members may be important to check (Figure 3.26). There is a significant spread between the 1000 members, although the general oscillatory tendency is confirmed by the overall shape of the spread boundaries. This result is consistent with both methods to set the stochastic terms.

3.3.5 The stochastic toy model reproduces well the key memory aspect of the CRM

To test how realistic our toy model is, we can compare the results we those obtained in similar homogenisation experiments in WRF, as detailed in chapter 2. It is clear that we can compare the toy model's P variable with WRF precipitation

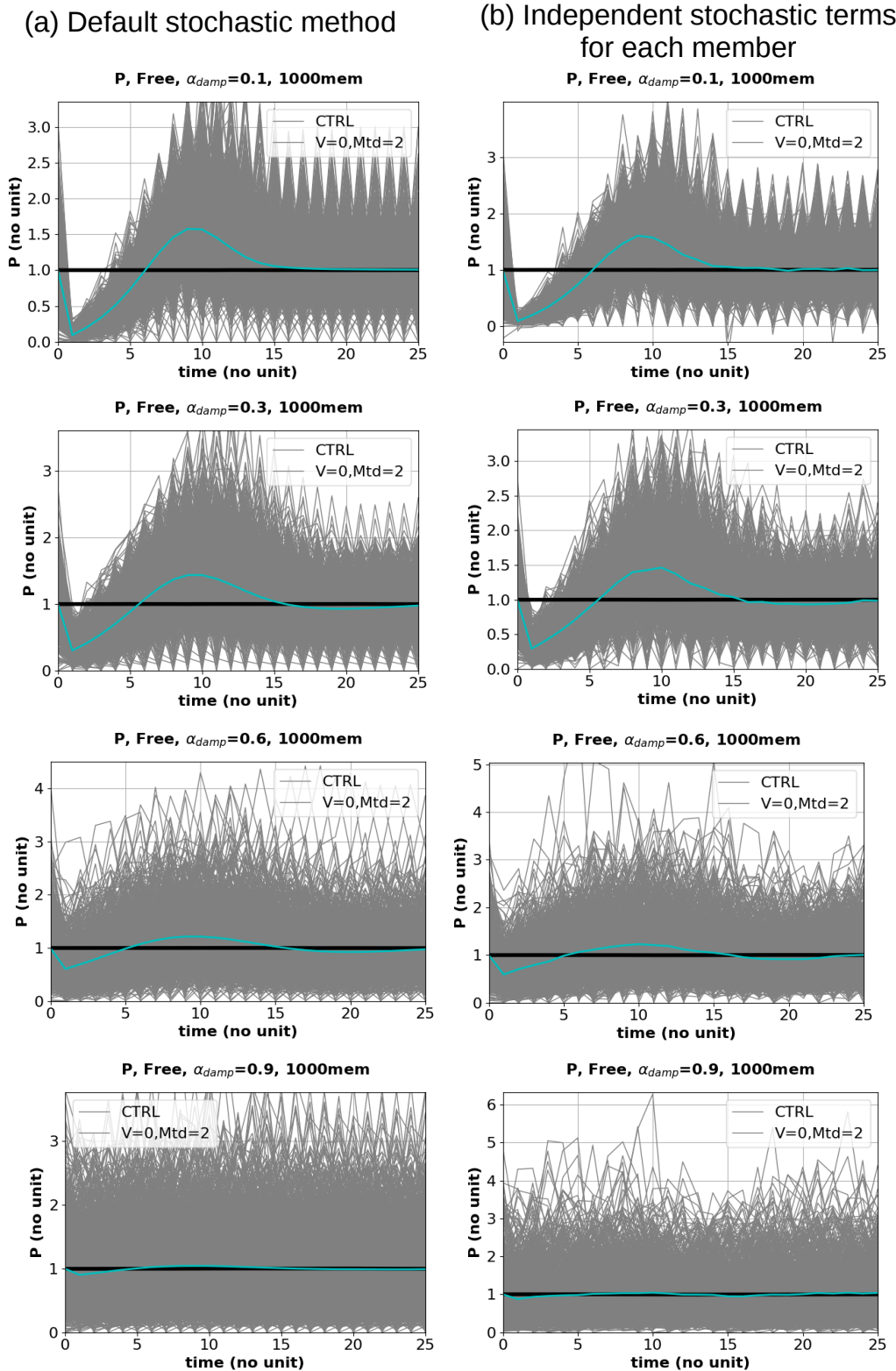


Figure 3.26 Same as Figure 3.25 but with the spread between ensemble members added in gray, relative to the ensemble average in blue. (a) For a toy model in the default configuration except that the RCE state was computed over 1000 time units instead of 200. (b) For a toy model in which the stochastic terms were calculated in an alternative way (each member having a different stochastic time series), and in which the RCE state was also computed over 1000 time units instead of 200.

rate. As for r and V , it is less clear which variables they should be compared to, but the significance of toy model variables presented in subsection 3.3.1 can guide us. We also heuristically determine that the best homogenisation that should be compared with the toy model is the one where both humidity and temperature are homogenised.

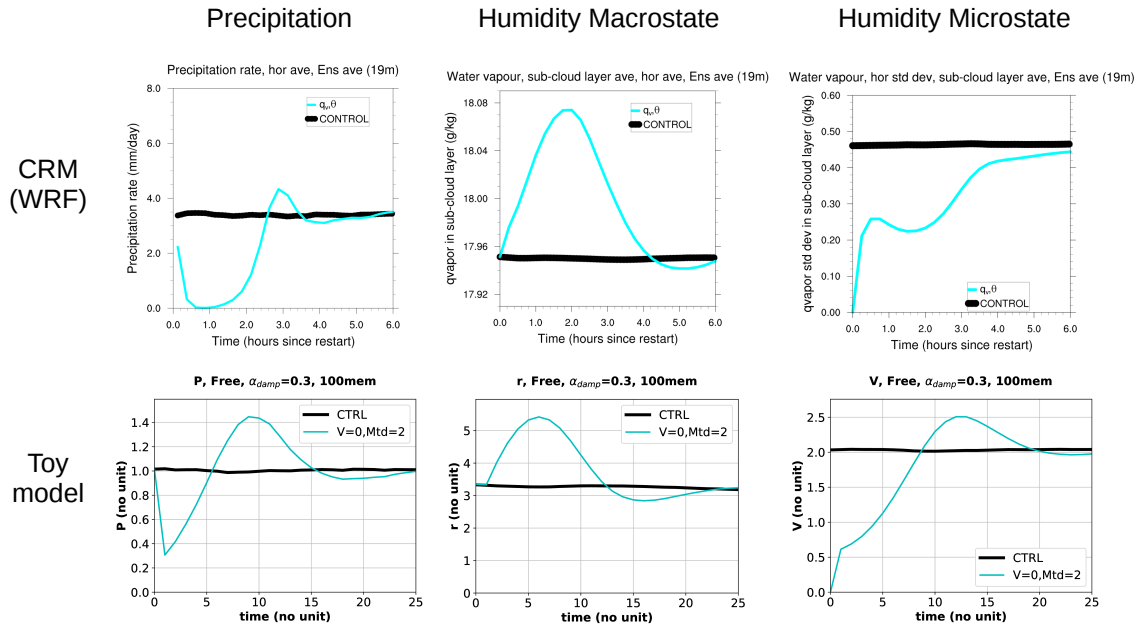


Figure 3.27 Comparisons of the responses to homogenisation of different variables in WRF (top row, see chapter 2) and in the toy model (bottom row). (left) Precipitation rate, (middle) Horizontally-averaged water vapour mixing ratio in the sub-cloud layer (humidity macrostate), (left) Standard deviation of water vapour mixing ratio in the sub-cloud layer (humidity microstate). The black line shows the response if no homogenisation is performed (Control, RCE state), the blue line shows the response after homogenisation ($V=0$ in the toy model, homogenisation of potential temperature and water vapour in WRF).

The best comparison is achieved with WRF sub-cloud layer humidity (Figure 3.27). This makes sense since r can be considered as the domain-mean humidity. The precipitation response is surprisingly very similar, though the oscillations do not resemble a damped harmonic oscillator as much in WRF, as they do in the toy model. The response of the macrostate (r in the toy model, horizontal average of sub-cloud layer humidity in WRF) match extremely well. The general shape of the microstate response (V in the toy model, horizontal standard deviation of sub-cloud layer humidity in WRF) is also well reproduced. In particular, the angular behaviour of the toy model after 1 time unit is almost visible in the WRF humidity microstate after 20 minutes. However the WRF response does not show any pseudo-periodic behaviour since the response never exceeds the RCE state value, contrary to the

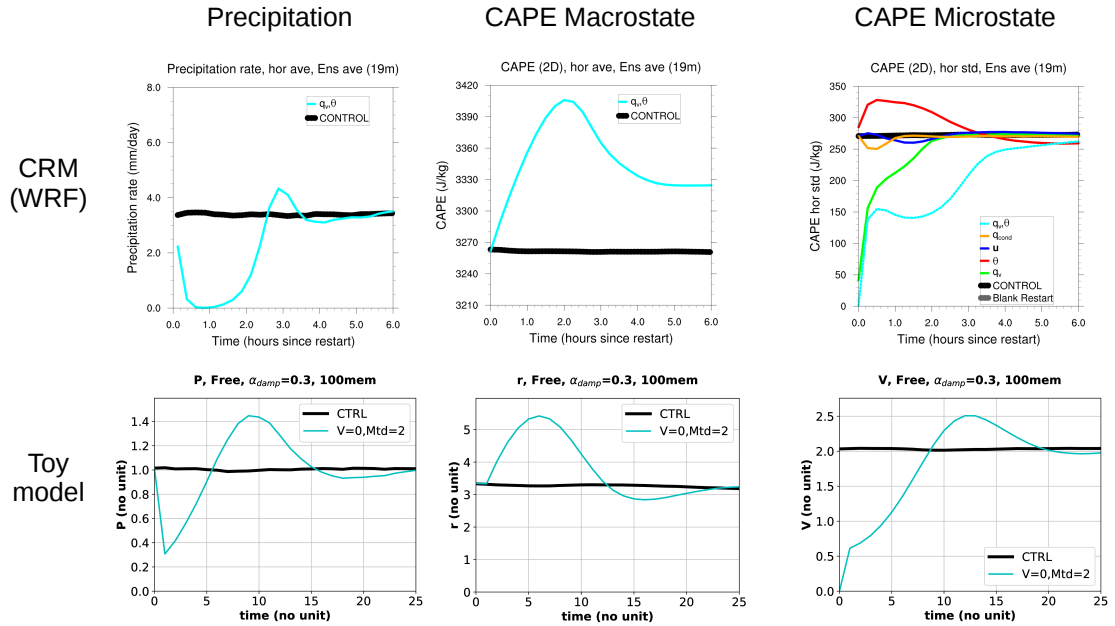


Figure 3.28 Same as Figure 3.27, but for different variables in WRF to be compared to the toy model’s r and V : (left) Precipitation rate, (middle) Horizontally-averaged CAPE (CAPE macrostate), and (right) Standard deviation of CAPE (CAPE microstate). In the WRF plots, additional lines have been left where different variable subsets are homogenised (see legend). It is still the homogenisation of both potential temperature and water vapour that compares best to the toy model.

toy model. Overall, it is satisfying that the toy model, built to capture convective memory, does reproduce the WRF response to homogenisation so closely.

Another comparison can be drawn with the other interpretation of r : CAPE. The toy model also seems to represent quite well the CAPE macrostate and microstate responses (Figure 3.28). The CAPE macrostate does not compare as well as the humidity macrostate, but the overall behaviour is still well explained by the toy model’s r variable. The microstate CAPE response and the microstate humidity response are very similar, so they compare as well with the toy model’s V variable. So the toy model does manage to capture both humidity and CAPE responses to homogenisation, in both a macrostate and a microstate sense.

Other WRF variables show some similarities with the behaviour to our toy model after homogenisation: 500 hPa water vapour, sub-cloud layer temperature, precipitable water. But these variables do not match as closely as the the sub-cloud layer humidity and CAPE. The precipitable water is an interesting case, since its macrostate only loosely matches r , but its microstate does match V in a nice way. Although it is elegant to compare a single WRF variable’s average and standard

deviation with the toy model's r and V , this is not a requirement of the toy model: V is the overall heterogeneity of the domain, not only the unresolved standard deviation of r , whatever r is. Actually, there is no reason for V and r to be based on the same state variable. V could plausibly be Turbulent Kinetic Energy (TKE), but r would clearly not be the mean kinetic energy. However, in the WRF responses, we find that TKE only partly matches with toy model's V . To conclude, it appears V would be the standard deviation of precipitable water, and r would be the mean sub-cloud layer humidity.

The close resemblance between the toy model responses and WRF responses gives us confidence that the toy model reproduces the key aspects of memory. Furthermore, the toy model is built on r , which represents humidity or CAPE, and it does match best with the experiment where both water vapour and temperature are homogenised in WRF. Therefore, the same quantity found to control memory in Chapter 2 also matches the behaviour of V , which makes a strong argument for V mainly being sub-cloud thermodynamic heterogeneity, and in particular sub-cloud moisture heterogeneity.

3.3.6 Interpretation of the CRM instability to fixed macrostate experiments by a Markov chain

One advantage of the toy model is that we can reproduce the fixed-macrostate experiments to try to isolate microstate memory, which showed an instability in the WRF model (Section 3.2). Do we manage to avoid the instability in the toy model? Or else if the instability appears, can we learn more about it?

When the macrostate is held fixed in the toy model (Figure 3.29), there are no more damped oscillations of period 20 time units as we saw in the “Free” RCE runs (Figure 3.24). Instead the responses are more similar to exponential approaches. On long time scales, the toy model state does not come back to the RCE state, but to a different value (for either P or V). [The time series of P and V on long time scales show a response which first exceeds the final value, then decreases towards the final value. This somehow resembles the responses under “Free” RCE conditions,

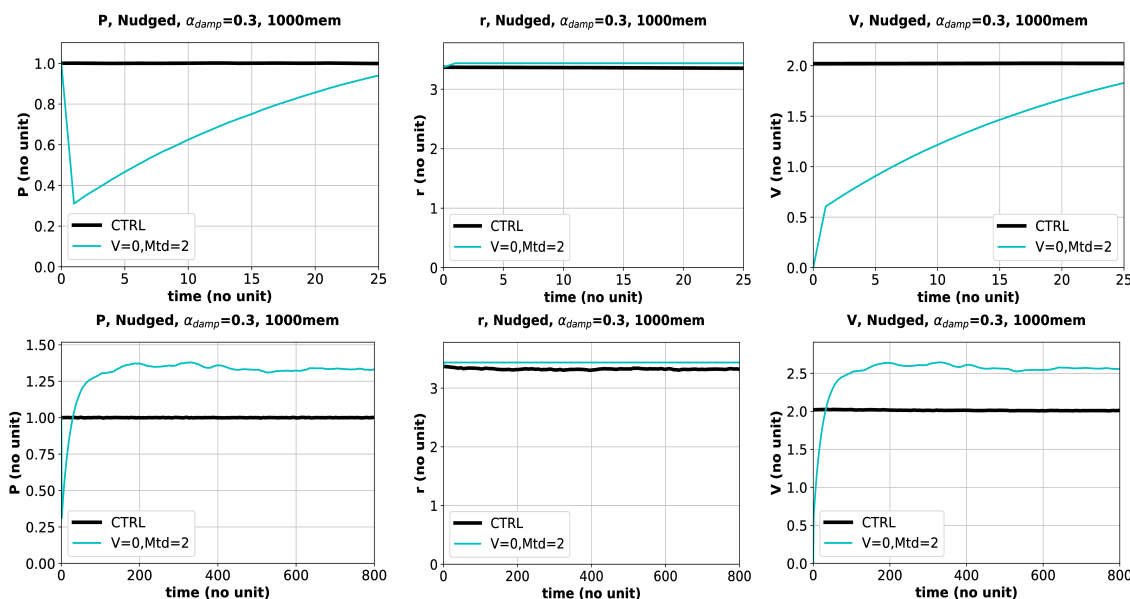


Figure 3.29 Same as Figure 3.24 but for a toy model under fixed-macrostate conditions (“strong nudging” runs). The top row presents the first 25 time units after homogenisation, and the bottom row the first 800 time units. The black line shows the RCE time series if no homogenisation is performed (Control) and with free macrostate; the blue line shows the time series after homogenisation ($V=0$) and under fixed-macrostate conditions. Stochastic terms are activated, and plots show the ensemble average over 1000 members.

but with a much smaller amplitude and a much larger time scale, so it may not be relevant.]

The final state reached by fixed-macrostate experiments takes a very long time to eventuate, and is very sensitive to tiny differences in the macrostate. Contrary to WRF, r is successfully nudged throughout the simulation, by construction of the fixed-macrostate experiments in the toy model. However, it is impossible to impose the exact RCE value to r . Consequently, r is sometimes nudged slightly too high, which makes P and V reach values higher than their RCE states (Figure 3.29). In other cases, r is nudged slightly too low, and to within positive stochastic terms, this leads to P and V reaching lower values than their RCE state.

We now analyse the sensitivity to α_{damp} (Figure 3.30). With higher damping coefficient, the response time scale seems to be much shorter, and the system approaches its final value earlier. In all cases, precipitation never recovers to exactly the RCE value: it reaches greater or smaller values, depending on the value of imposed r . Overall, the impact of stochasticity seems larger under fixed-macrostate conditions: with fewer degrees of freedom, the system cannot adjust as easily to its

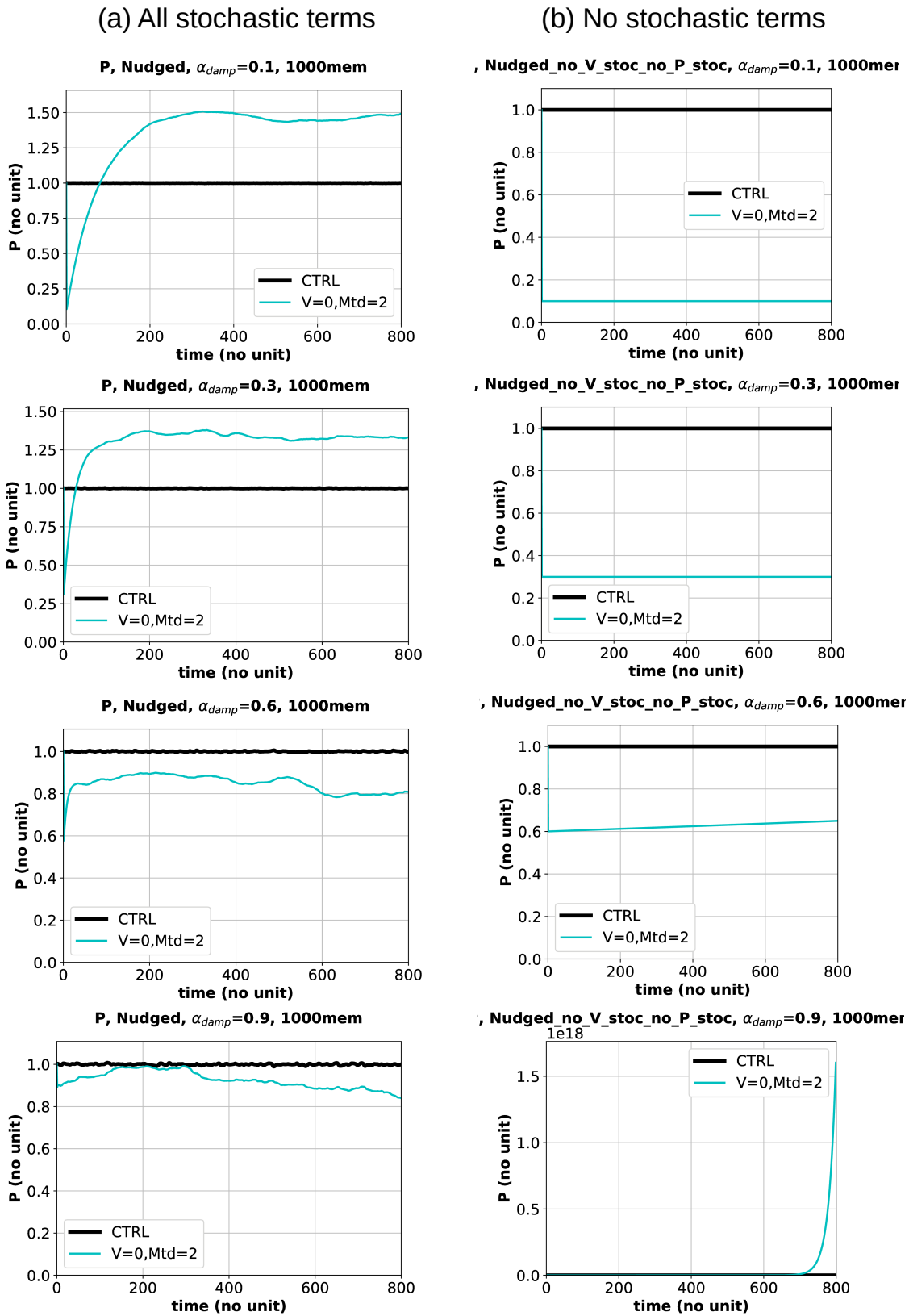


Figure 3.30 Same as Figure 3.25 but for a toy model under fixed-macrostate conditions (“strong nudging” runs). (left) For a toy model in the default configuration. (right) For a toy model where all stochastic terms have been turned off.

preferred equilibrium. These results also show that without macrostate feedbacks, the response time scale, related to microstate memory only, can become larger. So in this case, the evolution of the toy model variables is similar to a Markov chain which remembers its previous state and which jumps at each time step from its previous state to a new value depending on a stochastic term. However, this may not be called a random walk per se, since the spread between individual realisations does not grow monotonically with time (Figure 3.31), contrary to the typical random walk, in which the standard deviation σ of the distribution varies as $\sigma \sim \sqrt{t}$, where t is time.

When stochastic terms are turned off, the evolution of precipitation is either flat or an exponential. In the realisations shown on Figure 3.30, the response is apparently flat for $\alpha_{damp} = 0.1$ or 0.3 , shows a tendency upwards for $\alpha_{damp} = 0.6$, and is a clear exponential growth for $\alpha_{damp} = 0.9$. This is consistent with the analytical results, which showed that a perfect fixed-macrostate experiment where the macrostate is imposed to have its RCE value should lead to constant P and V (same as cases $\alpha_{damp} = 0.1$ or 0.3 here). However, if there is a discrepancy between the RCE value and the target value, the coefficient in Equation 3.33 is non zero. Depending on whether the target value is too high or too low compared to the RCE value, the coefficient sign changes, and we end up with an exponential growth or an exponential decay (same as cases $\alpha_{damp} = 0.6$ or 0.9 here). The larger the discrepancy, the smaller the time scale of exponential behaviour. This possibility for exponential growth or exponential decay depending on the realisation strongly reminds us of the WRF instability which led to exponential growth or decay depending on the initial conditions (which influence the discrepancy between target value and RCE value).

Given the random walk behaviour, the spread between ensemble members may be important (Figure 3.31). The spread is not small, but the ensemble spread shape follows the ensemble average line. The stochastic terms can definitely play a role in a given member, in particular for high-frequency variability, but overall it still resembles the ensemble mean. This result seems robust to both methods of choosing stochastic numbers.

(a) Default stochastic method

(b) Independent stochastic terms for each member

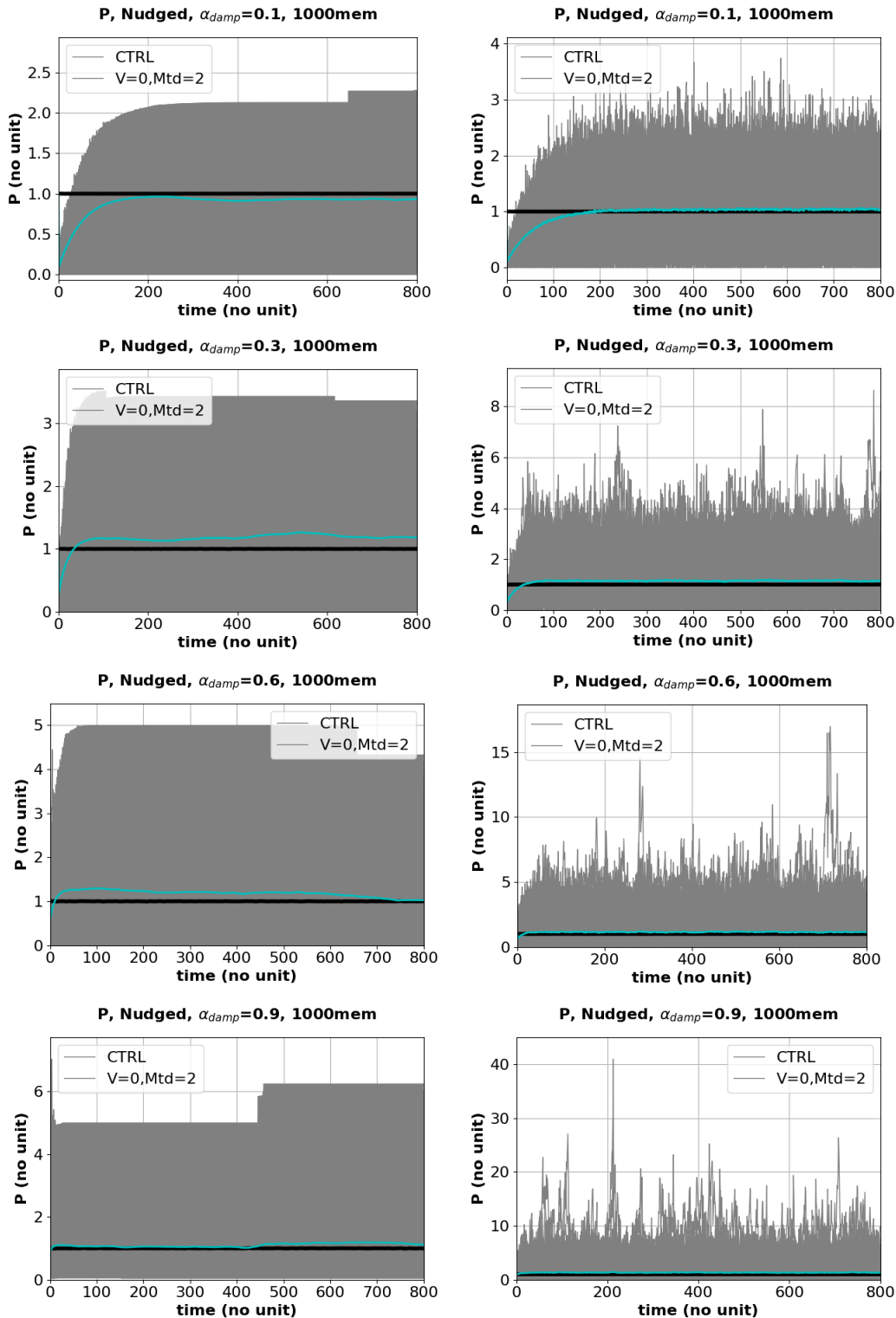
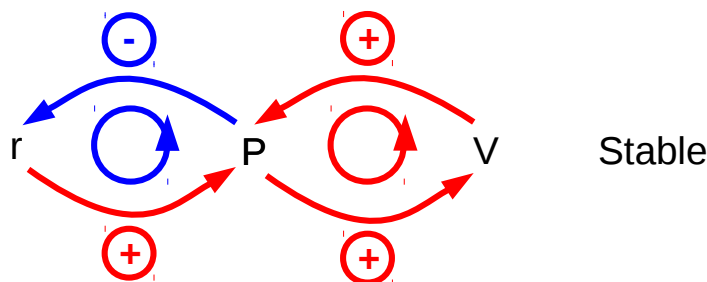


Figure 3.31 Same as Figure 3.26 but for a toy model under fixed-macrostate conditions (“strong nudging” runs). (left) For a toy model in the default configuration. (right) For a toy model in which the stochastic terms were calculated in an alternative way (each member having a different stochastic time series), and in which the RCE state was also computed over 1000 time units instead of 200.

- “Free” RCE runs



- Fixed-macrostate runs $\frac{\partial r}{\partial t} = 0$

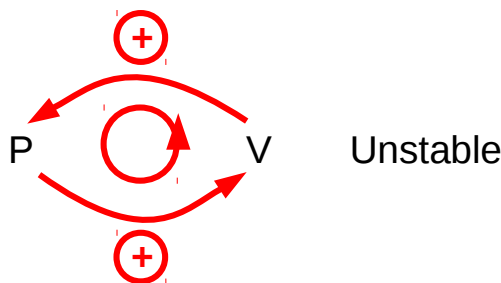


Figure 3.32 Schematic representation of the toy model equations as a combination of positive and negative feedbacks, depending on the term sign on the right-hand side of the equations. (top) For the “free” runs, i.e., without strong nudging. (bottom) For the “nudged” runs, i.e., with strong nudging. In a toy model with strong nudging, one negative feedback has been removed, allowing for instability to occur.

We can interpret the toy model equations by the association of a positive feedback (effect of P on V) and a negative feedback (effect of P on r), as shown by Figure 3.32. This association ensures the stability of the model under “Free” RCE conditions. For fixed macrostate, r is imposed so that the negative feedback loop is inactive. Only the positive feedback loop remains. This can intuitively explain why the toy model exhibits an instability with fixed macrostate.

With fixed macrostate (strong nudging), we expected the memory to be less large, since there is no macrostate memory involved. But our experiments with the toy model show that the response time scale to pseudo-homogenisation experiments can be much larger when there is strong nudging of r to its RCE value. Why is this happening? From the linearised solution, we showed that the “free” RCE oscillations have a relatively short time scale. However, in the fixed macrostate experiments, r is forced to be very close to its RCE value, so that the time scale on the right-hand

side of Equation 3.33 is very large. The more accurate the nudging of r to RCE, the longer the time scale of the exponential growth or decay. Physically, this behaviour is perhaps may stem from the fact that the degree of freedom in the nudged system is too small for it to adjust its own state quickly. To equilibrate quickly, a system may require many ways to convert one form of energy to another, which requires many degrees of freedom.

The exponential instability of the microstate also shows that macrostate feedbacks must have a stabilising effect. In the strong nudging experiment, where there is no macrostate feedback, the response time scale is much larger, and the system painfully (or even never) returns to equilibrium. But in the free RCE experiment, the system follows a stable oscillation in all cases.

3.4 Conclusion

Summary

The first main conclusion is that there is a kind of convective instability that has not been recognised before: the instability of the convective microstate. Indeed, convection becomes unstable when its large-scale state (macrostate) is held fixed, which can be attributed to the small-scale (microstate) memory. This instability can be explained by the combination of two aspects: (1) the fact that the interaction between convection and the macrostate is prevented (i.e., the fact that no asymptotic quasi-equilibrium between convection and the large-scale is possible on long time scales), and (2) the fact that the small-scale (microstate) memory is naturally unstable, thus unable to ensure any equilibrium on its own. This instability, which can either lead to an exponential growth or an exponential decay of convection, has been described in CRM simulations, and successfully reproduced by a toy model with three variables. The instability mechanism has been explained by an initiation from low-level temperature microstate, which reaches increasingly high levels.

The fact that the microstate is unstable may have implications on our current

understanding of convection, and it may contribute to modifying the way we approach the convective parameterization exercise. It suggests that convective schemes should allow enough departure from quasi-equilibrium to take into account the life cycles of the microstate structures. Even though GCMs naturally never assume a fixed macrostate, they may still benefit from incorporating the microstate memory, due to its potentially large influence.

The second main conclusion is that knowledge of the macrostate is not enough to predict convection. Indeed, our experiments show that the final convective state is highly sensitive to the target macrostate. Changing the target state by a very small amount leads to a dramatic change in convection, when close to the threshold value between exponential growth and exponential decay. This is in contrast to the usual understanding and modelling of convection. It is usually thought that rain can be predicted simply based on a good knowledge of the large-scale state [Arakawa, 2004; Davies *et al.*, 2013b]. Our study shows this is not sufficient, since the microstate also plays a role.

The microstate instability is an important phenomenon which may have implications for modelling because convective parameterisations specifically represent the effects of the unresolved structures (microstate), and generally assume the microstate can be diagnosed (therefore implying the microstate is stable). Our results imply not only that the diagnostic assumption is a problem in convective parameterizations, but also that the microstate processes deserve a significant place within parameterizations.

The toy model manages to reproduce the behaviour of the CRM in terms of memory in both the free RCE case, and the fixed-macrostate case. So it captures in a realistic way the key elements of convective memory, both in terms of macrostate and microstate memories, and can be studied to explore aspects of memory. It is fit for purpose.

In the free RCE case, the toy model confirms that the recovery of precipitation to homogenisation is due to memory, since the recoveries in both models are extremely similar. Memory is thus a key concept to understand the short-term behaviour of rainfall over a few hours.

In the fixed-macrostate case, both models show that isolating the microstate memory from macrostate feedbacks leads to instability. This instability is either an exponential growth or decay according to the sign of the discrepancy between the macrostate target value and the actual RCE state. In the toy model, stochastic terms act to saturate the instability until it reached a new state. In the CRM, the instability also saturates and brings the system either to a turbulent moist Rayleigh-Benard convective state, or to rest. This instability to externally-fixed macrostate explosively reveals the microstate memory in both models, hence emphasizing that microstate memory is important.

The macrostate feedbacks, which are turned off in the fixed-macrostate experiments, stabilise convection. There are thus critically important for stability.

The microstate memory in itself leads to a wide range of states/behaviours: there is no RCE equilibrium possible in practice. This shows the importance of properly coupling microstate memory to the macrostate, to avoid stability problems. Could it also show the weak potential for the microstate to predict the long-term behaviour (predictability issue)? On short time scales at least, the free RCE runs clearly show the high potential of microstate memory for rain predictability.

This has an implication for GCMs. Can GCMs capture the inherent absence of equilibrium related to microstate memory? Can they capture the wide range of possibilities related to microstates? The GCMs which have a diagnostic representation of convection implicitly assume an instantaneous recovery of the microstate to any perturbation, because they do not represent prognostically any microstate structures. But it seems that instead of being instantaneous, the microstate recovery is almost infinite when uncoupled to the macrostate. This is the case when the macrostate is not involved to stabilise the system. This reinforces the importance of the microstate for memory, which may act on the top of the macrostate control of convection. The results show that the macrostate has a negative feedback on memory, useful to ensure stability and long-term equilibrium.

Some convective schemes use the large-scale vertical velocity, ω , as a predictor for convection. In our memory framework, ω is a macrostate variable, it can only affect convection through macrostate temperature and water vapour, and

therefore it is irrelevant in microstate memory. But one may object that using ω as a predictor captures microstate memory indirectly. Although there is no obvious reason why this would work and although this seems to contradict our framework, knowing whether ω can indirectly capture microstate memory is still an open question. Additional work may thus be required on the coupling between macrostate vertical velocity and the microstate.

Discussion

Of course, it is not because we chose to perform fixed-macrostate experiments that the convective parameterizations assume that convection can be predicted without taking into account the interaction between convection and the macrostate. The fixed-macrostate condition is just another idealised setup useful to test ideas, alongside RCE for example.

An implication here relates to the separation between short time scales and large time scales. Microstate memory appears to be very important for short time scales of a few hours (and up to a few days in some organised cases). But its relevance for longer time scales may not be large. The reason is that, with fixed macrostate, microstate memory on long time scales does not allow the system to reach an equilibrium. Instead it follows an instability or a random walk. In reality, fortunately, there are some macrostate feedbacks to prevent this from happening. This shows the importance of the macrostate to stabilise the system and impose convection on long time scales. From this, we may speculate that the microstate memory is critical on short time scales, but not that important on time scales larger than a day.

However, the discussion on the role of microstate memory could be brought further. With fixed macrostate, there is no equilibrium found: the system follows an instability, or a random walk. This suggests knowing the value of the macrostate is not enough to make a good prediction of the rain rate. With fixed macrostate and when microstate is allowed to evolve, precipitation can also evolve, whatever the macrostate is. It leads us to think that knowing the microstate is important to

predict convection and precipitation. However, this does not mean that microstate becomes more important than an approach to quasi-equilibrium to predict convection in a real context: they are complementary. The importance of the microstate argues for a slightly modified idea of parameterizability. Recall that convection is considered to be parameterizable when it can be related to the past history of the large-scale forcing [Arakawa and Schubert, 1974], i.e, to the recent history of the forcing [Emanuel 2017, conference talk]. Our analysis of the microstate shows that knowing the large-scale state may actually not be enough to know the intensity of convection. What one also needs to know to predict convection is the microstate. The macrostate is always important, but both the microstate and the macrostate are relevant for direct prediction of convection. In other words, convection could be said to be parameterizable when it can be related to both the recent history of the large-scale forcing and the recent history of convection itself.

Conversely, one might argue that the instability that we noticed in the fixed-macrostate experiments supports the fact that microstate is irrelevant on long time scales. There are at least two ways to justify this statement. First, in the real world, the precipitation does not diverge to extremely high value out of an equilibrium. There is no exponential growth or exponential decay of convection with time, so that the microstate never seems to take over. Second, in practice, there are always some macrostate-microstate feedbacks which ensure that the system remains stable. In that case, no instability can be felt. The macrostate does impose its value to the long-term convection equilibrium, even though this macrostate undergoes slight fluctuations. As we showed, these fluctuations are paramount to ensure the system remains stable. With such feedbacks, the macrostate always keeps the microstate under relative control, so that the long-term value of convection does remain controlled by the macrostate.

While this chapter advocates for a more generalised use of microstate memory, it does not claim that it should replace the widely accepted use of the macrostate to predict convection. What seems to be needed to predict convection on a large range of time scales is a combination of (1) an approach to quasi-equilibrium based on the macrostate and (2) some elements of microstate convective memory.

Chapter 4

Comparing the memory of convection in a GCM and in a CRM: how to represent convective memory in GCMs?

4.1 Introduction

In Chapter 2, we used a Cloud-Resolving Model (CRM) to show how important microstate convective memory is, and to determine its main sources. In Chapter 3, we adopted another point of view to show that, due to the effects of memory in the CRM, knowledge of the large-scale conditions is not enough to determine the convective state: there is a microstate convective instability. We successfully built a simple predator-prey model for convection with memory, to explain these results.

Now that we understand better the origins and effects of microstate convective memory in a CRM, it is natural to assess how GCMs represent it. In this thesis, we choose the LMDZ GCM, since it already has some microstate memory through its cold pool scheme (see Chapter 1 and Chapter 5). We should first identify where the microstate memory could possibly come from, by identifying microstate prognostic variables. Since we previously investigated memory as the recovery to homogen-

isation, both in the CRM and in the predator-prey model, we will also compare the GCM memory to CRM memory via the same method. We will then test the potential memory improvements in the GCM when improving the cold pool scheme with slight modifications of the memory process.

In the hierarchy of models, the GCM is probably at an intermediate level of modelling between the CRM (which is more directly related to basic physical equations) and the predator-prey model (which is the most abstract and the one with the least basic dynamical processes). So a comparison of memory in the three models may reveal ways to improve memory.

In particular, we will extensively assess the memory of the GCM when the cold pool number density is modified. We choose this parameter rather than any other cold pool scheme parameter since we expect it to alter not only the memory but also the overall properties of the scheme thanks to its presence in many crucial equations of the scheme and in many tendencies due to the scheme. Moreover, the value of this parameter is likely to be inaccurate. Finally, it has the potential to improve model performance, as will be shown in Chapter 5. Therefore we develop a two-step strategy. First, in this chapter, we will explore the impact of the cold pool number density parameter on memory in idealised situations, and we will compare with the earlier results. Second, in Chapter 5, we will investigate its impact on more realistic simulations of climate and in particular precipitation.

4.2 Presentation of LMDZ

4.2.1 Overview of the cold pool scheme in the LMDZ model

The LMDZ (Laboratoire de Météorologie Dynamique Zoomed) GCM is the atmospheric component of the IPSL (Institut Pierre-Simon Laplace) coupled global climate model [Hourdin *et al.*, 2013]. It includes a buoyancy-sorting mass flux deep convection scheme based on Emanuel [1991] and Emanuel and Živković Rothman [1999] but with subsequent modifications, such as a new closure controlled by two sub-cloud processes: thermals and cold pools [Rio *et al.*, 2013]. The triggering is

also controlled by the competition between thermals and cold pools to overcome convective inhibition. There is a cumulus size threshold to exceed as well as a stochastic component in the triggering due to thermals [*Rochetin et al.*, 2014a,b]. Note that there is a competition between cold pools and moist saturated thermals to trigger deep convection, but both effects sum up in the closure.

The LMDZ cold pool scheme has been briefly presented in Subsection 1.5.5 in the context of the whole LMDZ deep convective parameterization, including its closure and its triggering. We hereby provide further details relevant to the current chapter.

The cold pool scheme has been developed by *Grandpeix and Lafore* [2010]. It was summarised and tested in a 1-D version by *Grandpeix et al.* [2010]. In summary, these sub-grid cold pools (1) spread at the surface as a density current, (2) have their own downward vertical movement, entraining environmental air downwards as well, and (3) have separate thermodynamic variables compared to their environment. Consequently, cold pools are described by three prognostic variables: the temperature anomaly profile with respect to their environment, the humidity anomaly profile, and the surface area fraction they occupy in the grid cell.

Cold pools and convection have a two-way interaction. Cold pools influence convection in 3 ways: (1) by the triggering via Available Lifting Energy (ALE), (2) by the closure via Available Lifting Power (ALP), (3) by creating a warmer environment outside the cold pools which is available to generate convection. In turn, convection influence the cold pools in 2 ways: (1) the sources of cold pools are the unsaturated downdrafts provided by the convection scheme, and (2) the saturated drafts remain only outside the cold pools.

Physically, ALP is a convective power at cloud base, which determines the convective mass flux since, in this scheme, the intensity of convection is given by the power provided at the base of deep clouds by sub-cloud processes. The convective mass flux at the Level of Free Convection (LFC) is the convective power that remains available after being consumed to overcome Convective Inhibition and after being lost by dissipation related to the friction onto vertical velocity [*Rio et al.*, 2013].

Convection also interacts with BL thermals so that only the maximum of the triggering energy (ALE) from thermals (ALE_bl) or from cold pools (ALE_wk) is compared to Convective Inhibition (CIN) to decide whether or not to trigger. But the intensity of convection (ALP) is the sum of the closure power from thermals (ALP_bl) and from cold pools (ALP_wk).

4.2.2 Potential sources of memory in LMDZ: key variables and parameters

In the LMDZ GCM, there are a few potential prognostic variables where convective memory may reside. Unfortunately, we cannot be exhaustive since there might be hidden prognostic variables in the convective scheme. Nevertheless, we know that the convective mass flux is prognostic, and there are three prognostic variables in the cold pool scheme. The convective mass flux, from Emanuel’s convection scheme [Emanuel, 1991], has a relaxation time scale $\tau_m = 2$ h, and to simplify follows the following relationship:

$$\left\{ \begin{array}{l} dm \\ dt \end{array} \right. = -\frac{1}{\tau_m} (m - m_0) \quad (4.1)$$

where m is the convective mass flux, m_0 is the target convective mass flux given by the CAPE closure in Emanuel’s scheme, and t is time. The relaxation time scale τ_m leads to a 2-hour inertia of precipitation.

Despite this prognostic convective mass flux, we choose to focus on the cold pool scheme, since we hope that the most important prognostic variables are there. Indeed, in Chapter 2, we showed that convective memory mostly resides in low-level thermodynamic variables, and cold pools are strong microstate thermodynamic structures at low levels. However, this is an hypothesis, since the repository in which the memory resides in the GCM depends on model construction, not necessarily on where it resides in reality. But even if the GCM memory is not only stored in the cold pool scheme, it is a component whose memory is worth improving based on the results of Chapter 2.

The cold pool scheme has three prognostic variables: the cold pool temperature

anomaly (difference between the temperature inside the cold pool and outside), the cold pool humidity anomaly (difference between the specific humidity inside the cold pool and outside), and the cold pool fractional surface area (fraction of the grid area occupied by cold pools). While the cold pool temperature and humidity anomalies are profiles, depending on z , the cold pool fractional area is a 2-D variable, independent from z . Note that in practice, for simulations in RCE over the ocean, the cold pool fractional area often saturates to its upper bound (i.e., 40% here), so that it almost behaves like a diagnostic variable.

4.3 Preliminary experiments: Influence of cold pool parameters on cold pool properties

The LMDZ cold pool scheme has six important parameters. We first study the sensitivity of the large-scale state to these parameters. Our sensitivity tests are all conducted in a 1-D Single-Column Radiative-Convective Equilibrium (RCE) setup, over an ocean at fixed Sea Surface Temperature (302 K). We only study the atmospheric and cold pool properties in the established RCE state. More details on this setup can be found in Chapter 5. A previous sensitivity analysis to these parameters was carried out by *Grandpeix et al.* [2010], but this was not in the RCE framework, since they instead had a diurnal cycle taken from real cases during two field campaigns: one over land and one over the ocean.

Gravity waves act to damp the cold pools, and they can thus affect the influence of cold pools on convection. The larger the gravity wave damping coefficient, the more gravity waves affect the cold pool temperature anomaly. At high values of this coefficient, cold pools are well damped and therefore do not have much power to provide for convection, causing a decrease in the Available Lifting Power (ALP) provided by cold pools (Figure 4.1). This decrease is associated with an increase in the ALP provided by thermals, so that the effect on the total ALP is attenuated. The default value of this coefficient has particularly properties, since it is for the default value that cold pools and thermals provide exactly the same power to convection. This is worth noting, even though this attribute may not have been chosen on

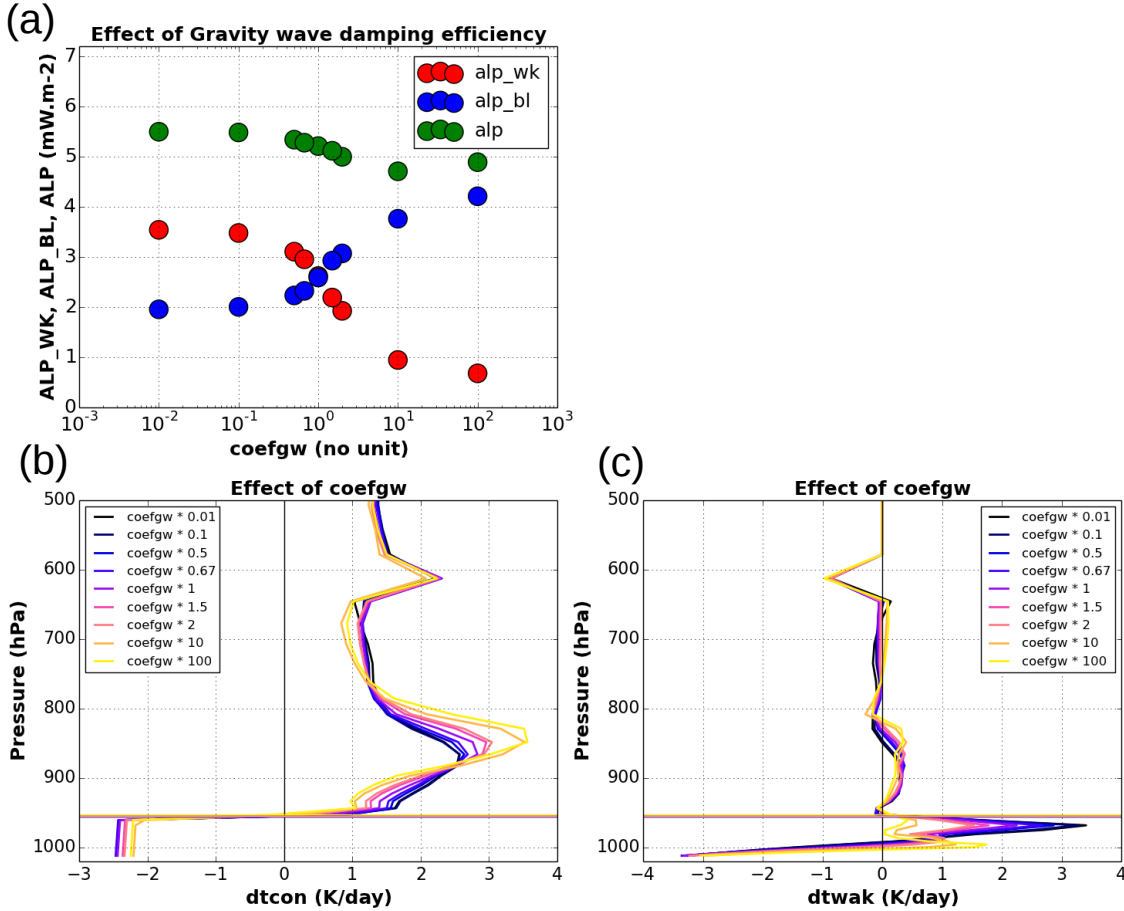


Figure 4.1 Impact of the gravity wave parameter (which acts to damp cold pools) on several variables. (a) Available Lifting Power (ALP, related to convective intensity) for different values of the multiplicative factor to the gravity wave parameter (1 means default, 100 means 100 times greater). Red is for ALP due to cold pools, blue is for ALP due to thermals, and green is the total ALP (sum of the ALP due to each). (b) Convective heating profiles (excluding cold pools) for different values of the multiplicative factor to the gravity wave parameter. Colours (see legend) indicate the value of the multiplicative factor (yellow means high value). The horizontal lines indicate the Lifting Condensation Level. (c) Same as (b) but for the cold pool heating profile.

purpose, and there is no evidence on whether or not this balance between the two processes is an advantage.

The gravity wave damping coefficient also affects the heating profiles related to the convection and cold pool schemes, which can be distinguished in this model. The heating profile related to the cold pool scheme is the heating rate due to the existence of a non-zero cold pool temperature anomaly. The convective heating related to the convection scheme is the rest of the “convective heating”. At higher values of the gravity wave damping coefficient, cold pools are weakened by gravity waves, so that there is less heating due to the cold pool scheme (Figure 4.1(c)). This

is associated with a convective heating (due to the convection scheme) which is less homogeneous on the vertical axis, especially in the critical region between the Lifting Condensation Level (LCL) and 800 hPa (Figure 4.1(b)). This essentially means a redistribution of the convective vertical mass flux. This parameter therefore has a potential to control a key aspect of convection: the heating profile just above the boundary layer.

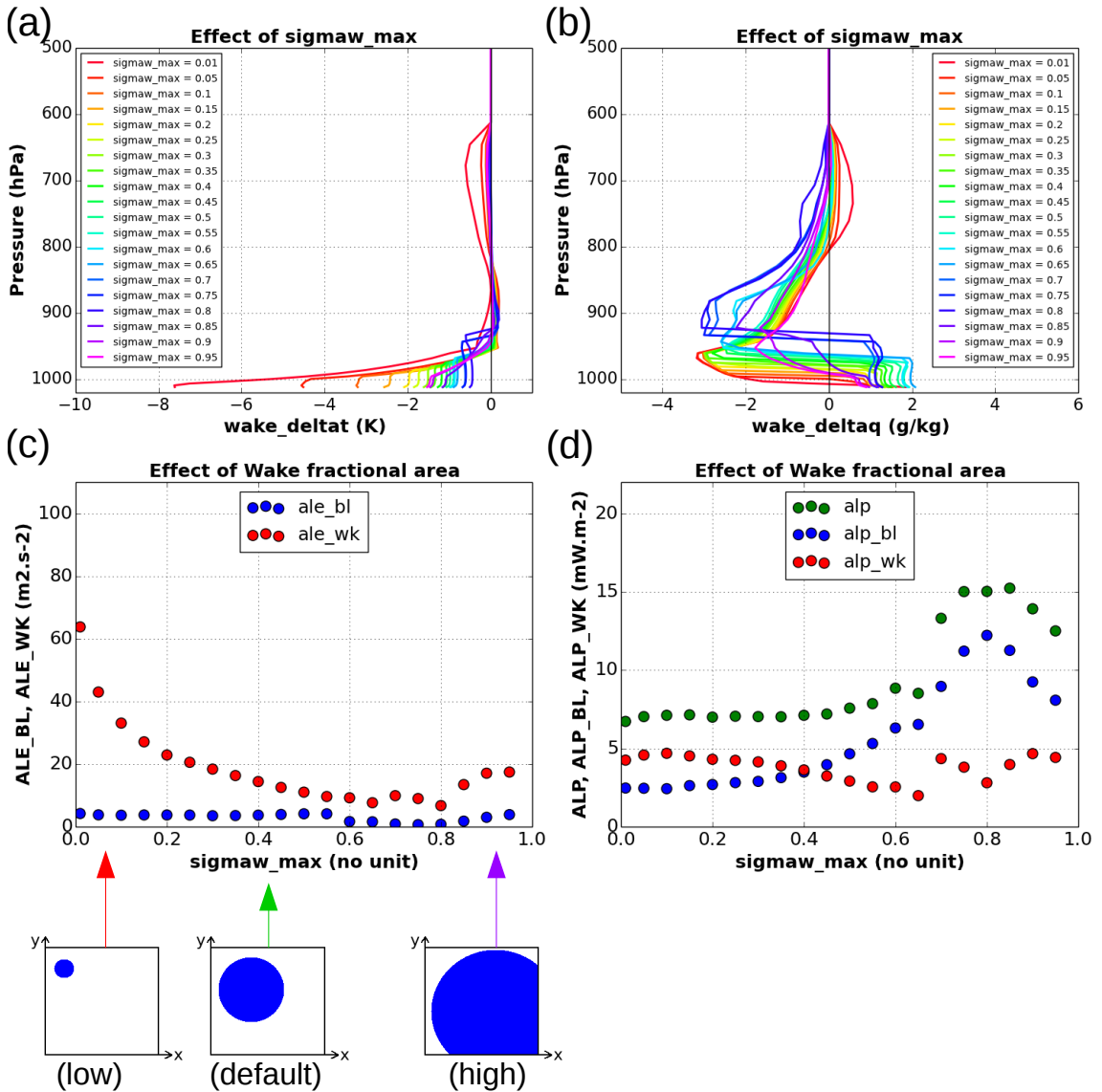


Figure 4.2 Impact of the upper bound parameter for cold pool fractional surface area on several variables. (a) Vertical profiles of cold pool temperature anomaly. Colours (see legend) indicate the value of the cold pool fractional area upper bound (red means small, purple means large) (b) Same as (a) but for the vertical profiles of cold pool humidity anomaly. (c) Available Lifting Energy (ALE, related to convective triggering) for different values of the cold pool fractional area upper bound. Red is for ALE due to cold pools, blue is for ALE due to thermals. (d) Same as (c) but for Available Lifting Power (ALP, related to convective intensity). Green is for the total ALP. At the bottom, cartoons show the meaning of low, default and high cold pool fractional area upper bound, viewed from the top and with cold pools being blue.

The cold pool fractional surface area is a prognostic variable in LMDZ. But in practice, it often saturates at its upper bound value. The parameter which sets the upper bound for cold pool fractional area, denoted $\sigma_{w,max}$, is thus an important parameter of the model. This parameter was set in the scheme to simply capture a termination of cold pools life cycle, and thus limit their growth, since this is not explicitly represented in the model at this point [Grandpeix *et al.*, 2010]. The cold pool temperature anomaly is highly sensitive to $\sigma_{w,max}$ (Figure 4.2). With a low $\sigma_{w,max}$, cold pools are very cold at the surface. A value of about 0.75 for $\sigma_{w,max}$ makes cold pools the least cold (local extremum). Any higher value increases again the cold pool temperature anomaly. The sensitivity of the cold pool humidity anomaly also shows an extremum at a value at around 0.7 for $\sigma_{w,max}$. With very low values for $\sigma_{w,max}$, cold pools are relatively dry below the LCL, not very dry aloft, thus somewhat shallower. Increasing $\sigma_{w,max}$ makes cold pools more humid up to the LCL, and drier aloft. When $\sigma_{w,max}$ exceeds the extremum, the behaviour is rather different, in particular cold pools are drier under the LCL, and usually drier aloft again.

As a result, the convective triggering and intensity both strongly depend on the upper bound parameter for cold pool fractional area, $\sigma_{w,max}$. At low $\sigma_{w,max}$, cold pools are particularly cold, so that their ALE (indicating triggering ability) is large. Around a value of 0.7, the cold pool ALE is minimum, consistent with variations in cold pool thermodynamic properties. The effect of $\sigma_{w,max}$ on ALP (indicating convective intensity) due to cold pools is similar, though more attenuated than the effect on the triggering. However, ALP due to boundary layer thermals is also sensitive to $\sigma_{w,max}$, contrary to thermal ALE. The total ALP is therefore almost constant for a value of $\sigma_{w,max}$ less than 0.65, but it is significantly higher at higher values of the parameter, with a maximum for a value of $\sigma_{w,max}$ of about 0.8. $\sigma_{w,max}$ thus plays an important role in the control of convection by cold pools and even by thermals. Moreover, since cold pools in the tropics almost always saturate to the upper bound, this disrupts the prognostic nature of the parameter, and it is not satisfying. This could be investigated in future studies.

The sensitivity to the cold pool number density (number of cold pools per unit area) is particularly promising, and will thus be described in more detail in

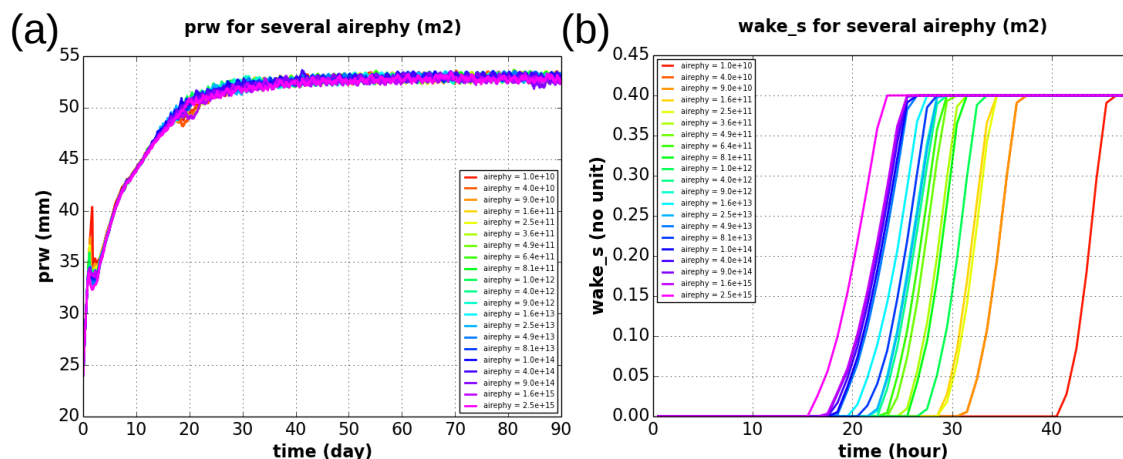


Figure 4.3 Impact of the 1D simulation grid area on several variables. (a) Time series of the precipitable water for the 90 days of simulation (spin-up then RCE). (b) Time series of the cold pool fractional surface area, for the first 50 hours of the simulation. Colours (see legend) indicate the value of the grid area (red means small, purple means large).

Chapter 5.

Another parameter of the SCM which could potentially play a role in convective memory is the grid cell area, since parameterization statistics can be different at different resolutions, and since memory could depend on resolution. This is not a parameter related to the cold pool scheme. The results show that this parameter has no influence on the equilibrium state and on the time series of most relevant variables (Figure 4.3). The only notable effect is that a larger grid cell area leads to more rapid saturation of the cold pool fractional area to its upper bound during spin-up of the RCE simulation.

These preliminary experiments allowed us to investigate the influence of cold pool parameters on cold pool properties in the RCE mean state, and therefore to better understand the cold pool scheme. Several of these parameters lead to useful sensitivities, which may be exploited in future studies. But the parameter which seems to have the highest potential for physical improvement of the model is the cold pool number density. Moreover, we will show in Chapter 5 that changing this parameter improves model performance. So the rest of this chapter will focus on the sensitivity to this parameter. In particular, since we are interested in improving the convective memory of the LMDZ GCM, we will assess the sensitivity of memory to the cold pool number density. To evaluate this sensitivity, we consider the CRM as “truth”, and we evaluate both the default version of LMDZ and a version with

modified cold pool number density.

4.4 Methods

The method to compare the memory in different models is based on initial homogenisation of a system originally in RCE, and on an analysis of the recovery to RCE. The homogenisation method in the CRM has been described in Chapter 2. The pseudo-homogenisation method in the predator-prey model consists in setting $V = 0$, as described in Chapter 3. All the figures referring to the CRM results are made from the experiments presented in Chapter 2, and many of them are simply taken from this chapter. All the figures referring to the predator-prey model results were presented in Chapter 3. All figures referring to the SCM are new.

Here, we set the 1D LMDZ GCM, i.e., its SCM version, in RCE over ocean. The setup will be described in more details in Chapter 5. From the RCE state, we conduct pseudo-homogenisation by setting either the cold pool temperature anomaly to zero, or the cold pool humidity anomaly to zero, or both. Indeed, cold pool temperature and humidity anomaly profiles describe the microstate and can therefore be subject to homogenisation. The method of selecting variables for pseudo-homogenisation in the GCM somehow resembles the way to select different subsets of variables to homogenise in the CRM.

We study the recovery of precipitation to pseudo-homogenisation at an initial time taken from the RCE state, in all three models.

Furthermore, in the LMDZ SCM (Single-Column Model, 1D GCM), we also focus on a modification of the cold pool number density (denoted by D_{CP}), a parameter in the cold pool scheme which controls the number of cold pools per unit area. We compare two versions of the SCM: one with the default D_{CP} (“default LMDZ”), and one with D_{CP} 100 times greater than the default value (“modified LMDZ”). In Chapter 5, we will show that the performance of the scheme is enhanced by changing D_{CP} , so here we investigate specifically the impact of this parameter on the memory behaviour of the model.

To enhance the statistical significance of the results, we repeat the pseudo-homogenisation experiments in the GCM on many members and only show the ensemble mean. We build each new member by modifying the timing of homogenisation, and calling this the new $t = 0$. We tested the sensitivity of the results to the ensemble size, with 1, 29 and 60 members. Since the results did not change between 29 members and 60 members, the 29-member ensemble could be considered a large enough sample. To be conservative, we use the 60-member ensemble throughout the rest of the study.

4.5 Does LMDZ have the same sources of memory as WRF?

Comparisons of the precipitation recoveries in the three models helps determine the strengths and weaknesses of the memory representation in the GCM (Figure 4.4). In general, we measure the recovery time scale by the time it takes until the first return to the RCE state, after the first peak response (i.e., after the first half-oscillation). Note however that there are multiple time scales in this problem, since there are oscillations or fluctuations that remain important for a long time in some cases.

One may wish to know which element of the CRM recovery to homogenisation is the most important for the GCM to reproduce: the recovery time scale, the sign of the response, or the amplitude of the response. We have no compelling reason to prefer one to another, since they are all part of the same recovery. Moreover, our method does not impose which part of the recovery one should look at in particular. Nonetheless, we have the intuition that if any choice was to be made, it could be in the following order: (1) the recovery time scale, (2) the response sign, (3) the response amplitude. If possible, a good representation of the whole response should still remain the only objective.

The precipitation response to pseudo-homogenisation in the predator-prey model was very similar to the precipitation response to homogenisation of temperature T and humidity q in the CRM (see also Subsection 3.3.5). Undoubtedly, the fact that

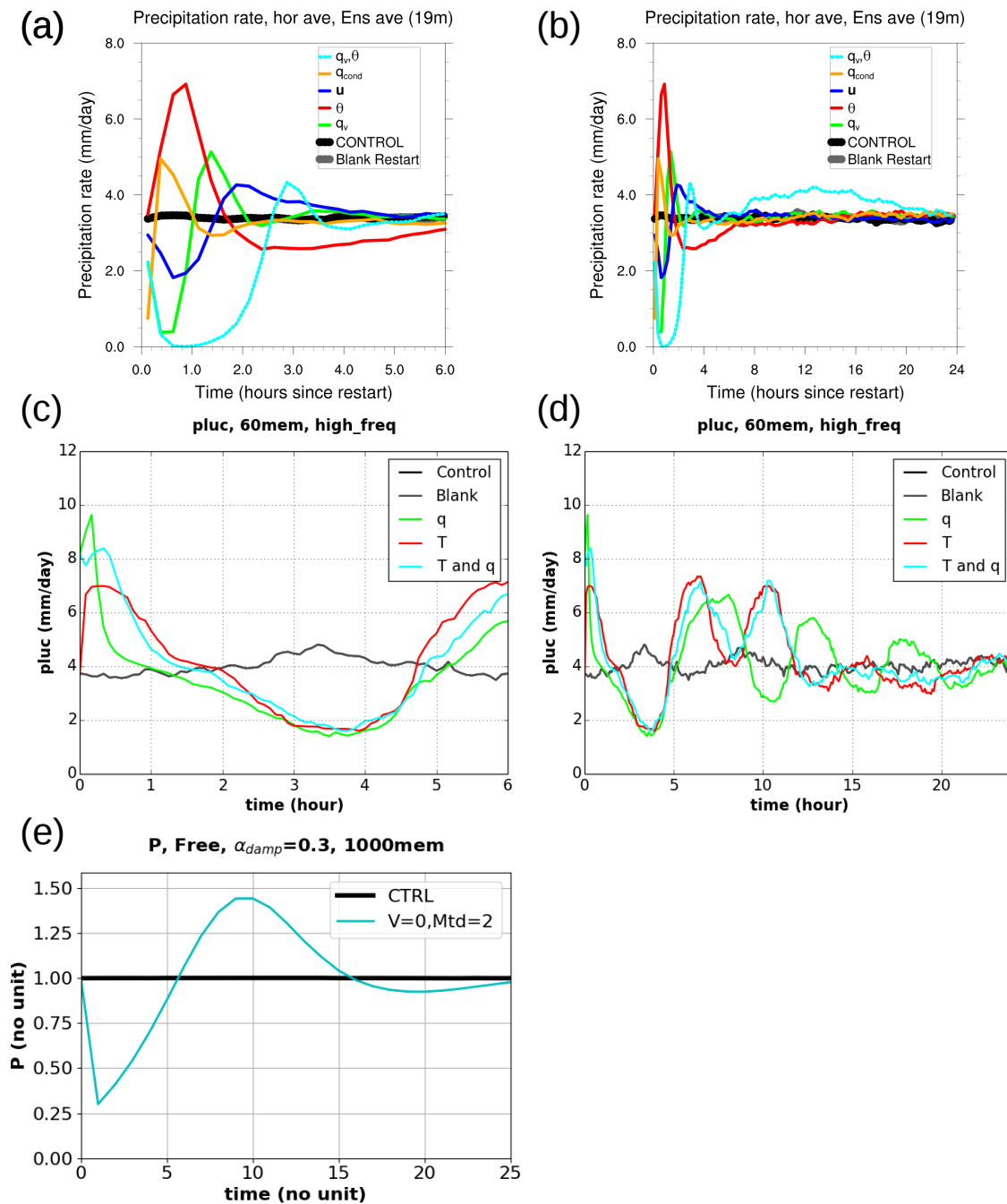


Figure 4.4 Responses of precipitation rate to different types of initial homogenisation (see colours and legend: control (black), no homogenisation (grey), temperature homogenisation (red), water vapour homogenisation (green), both water vapour and temperature homogenisation (light blue), wind homogenisation (dark blue), condensate homogenisation (orange)). (a) In the CRM, for the first 6 h after homogenisation (as in Figure 2.14(a) but modified to include the response to homogenisation of both temperature and humidity, and the response to a blank restart with no homogenisation at all). (b) In the CRM, for the first 24 h after homogenisation (as in Figure 2.25(a)). (c) In the SCM, for the first 6 h after homogenisation. (d) In the SCM, for the first 24 h after homogenisation. (e) In the predator-prey model, for what seems equivalent to the first 6 h after homogenisation (as in Figure 3.25(a)). The CRM responses are averaged over 19 members, the GCM ones over 60 members, and the predator-prey model ones over 1000 members.

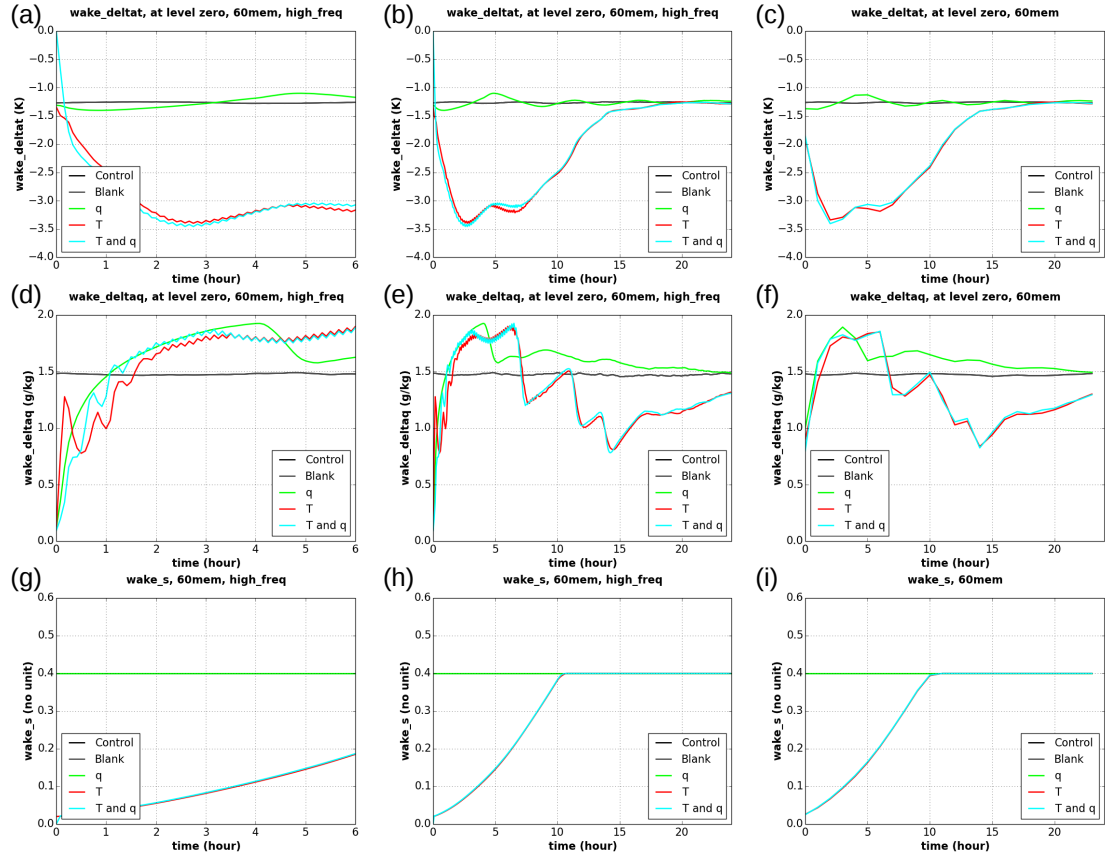


Figure 4.5 Responses of different cold pool properties (microstate) in the SCM to different types of initial homogenisation (colours and legend: see Figure 4.4). (a) Cold pool temperature anomaly, with high frequency output (every 5 min), for the first 6 h after homogenisation. (b) Same as (a) but for the first 24 h after homogenisation. (c) Same as (b) but with hourly output. (d) Cold pool humidity anomaly, with high frequency output, for the first 6 h after homogenisation. (e) Same as (d) but for the first 24 h after homogenisation. (f) Same as (e) but with hourly output. (g) Cold pool fractional surface area, with high frequency output, for the first 6 h after homogenisation. (h) Same as (g) but for the first 24 h after homogenisation. (i) Same as (h) but with hourly output. The responses are averaged over 60 members. For cold pool temperature and humidity anomalies, lines only show the time series at the first model level (near surface).

we chose the most adapted parameters helps. For example, we chose α_{damp} so that it reproduces the response amplitude best, and we chose the dimension of time to best reproduce the recovery time scale. But making such choices is not a surprise for a toy model. Nevertheless, the fact that the sign and shape of the responses are so close to the CRM is very encouraging.

However, the equivalent pseudo-homogenisation in the GCM (both cold pool T and q anomaly) leads to a very different recovery. Let us focus on the first 6 h of recovery. Although the recovery time scale seems to have an order of magnitude similar to the CRM (which we consider realistic), and the response amplitude in

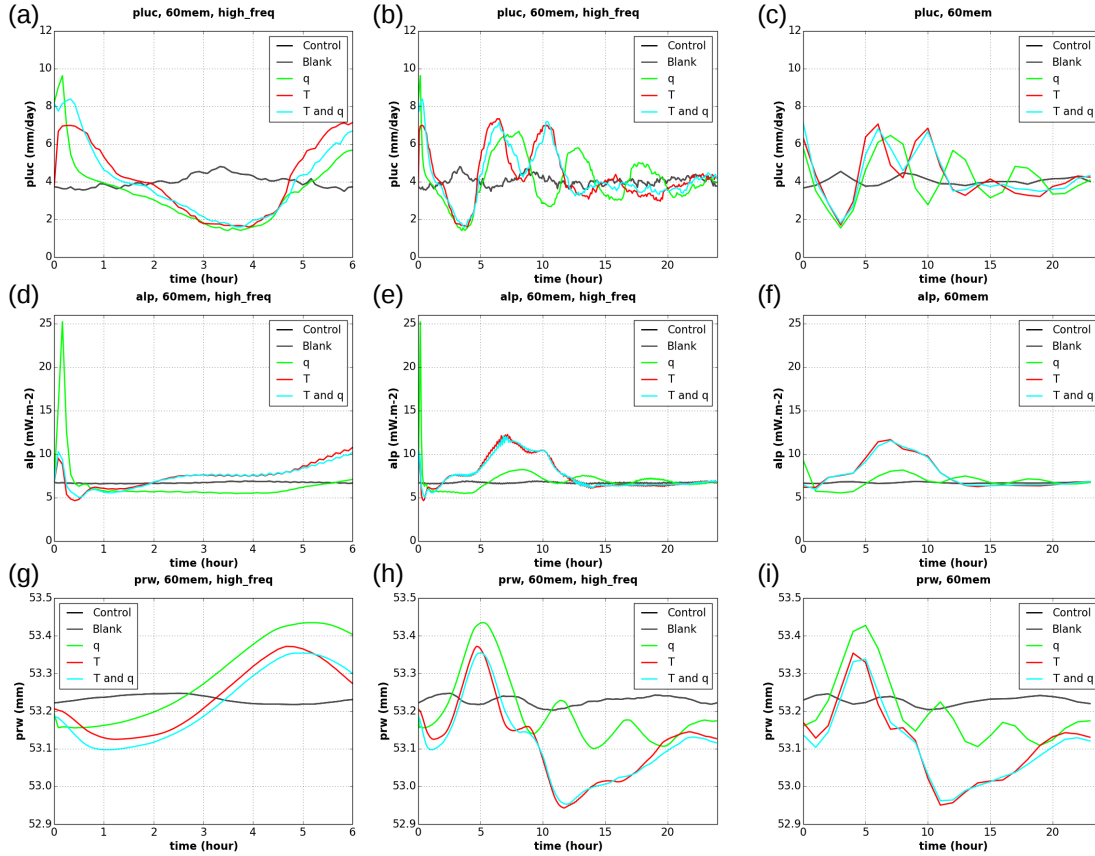


Figure 4.6 Responses of different macrostate variables in the SCM to different types of initial homogenisation (colours and legend: see Figure 4.4). (a) Precipitation rate, with high frequency output (every 5 min), for the first 6 h after homogenisation (as in Figure 4.4(c)). (b) Same as (a) but for the first 24 h after homogenisation (as in Figure 4.4(d)). (c) Same as (b) but with hourly output. (d) Available Lifting Power (convective intensity due to cold pools), with high frequency output, for the first 6 h after homogenisation. (e) Same as (d) but for the first 24 h after homogenisation. (f) Same as (e) but with hourly output. (g) Precipitable water, with high frequency output, for the first 6 h after homogenisation. (h) Same as (g) but for the first 24 h after homogenisation. (i) Same as (h) but with hourly output. The responses are averaged over 60 members.

absolute value is reasonable, the sign of the original response anomaly (which we may call “sign of the response” or “sign of the recovery”) is opposite to the two other models. Pseudo-homogenisation of cold pool q anomaly in the GCM also leads to the right recovery time scale but the wrong sign of the original response, when comparing with the CRM. Conversely, pseudo-homogenisation of cold pool T anomaly in the GCM gives not only the right time scale but also the right response sign and amplitude. While the recovery time scale is almost doubled when homogenising both T and q in the CRM, compared to homogenising only one, the recovery when homogenizing both variables in the GCM is almost the same as when only T is homogenised. Thus, the role of water vapour in the GCM memory is almost non-

4.5. DOES LMDZ HAVE THE SAME SOURCES OF MEMORY AS WRF?

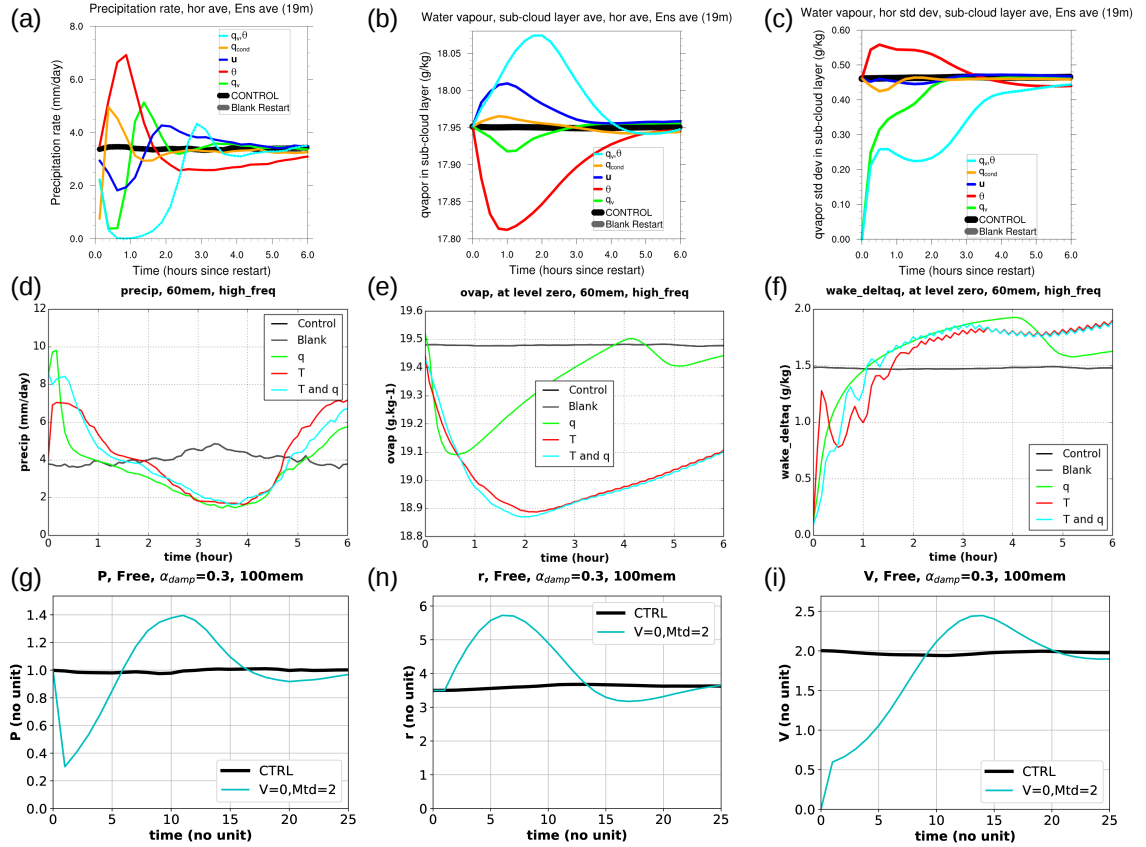


Figure 4.7 Responses of precipitation rate (a,d,g), a typical macrostate variable (b,e,h), and a typical microstate variable (c,f,i), to different types of initial homogenisation (colours and legend: see Figure 4.4), for the first 6 h after homogenisation, in different models. (a) Precipitation rate in the CRM (as in Figure 4.4(a)). (b) Average of water vapour mixing ratio in the sub-cloud layer (macrostate), in the CRM. (c) Standard deviation of water vapour mixing ratio in the sub-cloud layer (microstate), in the CRM. (d) Precipitation rate in the SCM (as in Figure 4.4(c)). (e) Mean humidity (macrostate), at first model level, in the SCM. (f) Cold pool humidity anomaly (microstate), at first model level, in the SCM (as in Figure 4.5(d)). (g) Precipitation rate P in the predator-prey model. (h) Average humidity r (macrostate) in the predator-prey model. (i) Boundary-layer heterogeneity V (microstate) in the predator-prey model. The CRM responses are averaged over 19 members, the GCM ones over 60 members, and the predator-prey model ones over 100 members. The predator-prey model panels are reproduced from Figure 3.24.

existent, in contrast with the role of humidity in the CRM memory. Overall, these results show that the memory time scale for precipitation is fine, but the response has the wrong sign (except for T homogenisation). The results on the reasonable memory time scale are valid as long as only the first half-oscillation is considered, not the subsequent fluctuations. Over 24 h of recovery, the responses show that in all cases, oscillations persist for a very long time in the GCM, whereas they are quickly damped in the CRM. The memory damping is too weak in the GCM compared to the CRM.

Therefore the GCM has a microstate convective memory of the right capacity (time scale), but this appears to be a very inaccurate memory (response sign, lack of damping, missing role of humidity). In other words, the persistence of convection in the GCM with prognostic cold pools appears to differ significantly from that in the CRM.

Some insights on the memory process can be gained by investigating the recovery of cold pool properties in the GCM, since they are the microstate variables in which memory resides (Figure 4.5). All the panels show that the recoveries from homogenisation of T only, or from homogenisation of T and q together, lead to the same behaviour. Moreover, there is almost no impact of q homogenisation on the cold pool T anomaly, whereas there is a clear impact of T homogenisation on the cold pool q anomaly. This could be due to the fact that homogenising q does not influence the cold pool fractional surface area, while homogenising T resets the cold pool fractional area to zero. Therefore, the memory is strongly concentrated in the cold pool T anomaly in the GCM.

Additional insight can be provided by the macrostate variables (Figure 4.6). During the first few minutes after homogenisation, there is an increase in Available Lifting Power (ALP, which amounts to convective intensity). This leads to an automatic increase in precipitation. Even though ALP quickly returns to its RCE value (~ 30 min), precipitation takes much more time (1-2 h), showing evidence of the memory effect. From 5 h to 12 h after homogenisation, there is a secondary increase in ALP. This appears just after the increase in precipitable water and just before the beginning of the secondary increase in precipitation (second oscillation). So precipitable water variations may provoke variations in ALP, which in turns lead to a precipitation response, but with delays due to memory in each step of the process.

We can now compare the three models in terms of the response of precipitation, microstate and macrostate variables (Figure 4.7). The macrostate is represented here by the domain-mean water vapour in the sub-cloud layer (as in Subsection 3.3.5) or its equivalent (r in the predator-prey model, grid cell mean water vapour at the first model level in the Single-Column GCM). The microstate is represented by the standard deviation of water vapour in the sub-cloud layer or its equivalent (V in

the predator-prey model, cold pool humidity anomaly at the first model level in the GCM). For these three variables, the predator-prey model is a good representation of the recovery to both water vapour and temperature homogenisation in the CRM. In the GCM, the recovery of microstate water vapour is similar in all three types of homogenisation: T only, q only, T and q together. And it is in reasonable agreement with the other two models, at least in terms of time scale and overall shape. It compares best with the homogenisation of q in the CRM, and does not really show the inflexion point observed in the CRM when homogenising both T and q together. The recovery of precipitation in the GCM is not as good as the recovery of microstate water vapour. The recovery time scale is of the right order of magnitude. However, the response generally has the wrong sign and the recoveries to the three types of homogenisation lead to a very similar response in the GCM, whereas they are significantly different in the CRM. The recovery time scale of cold pool q and T anomaly is longer than the precipitation recovery time scale. The recovery of cold pool T anomaly is well damped, whereas the recovery of cold pool q anomaly and precipitation is too weakly damped.

The reason why the GCM precipitation usually responds with the wrong sign could be related to the macrostate response having the wrong sign. In the CRM, there is no response of the macrostate to homogenisation at $t = 0$, for example in terms of macrostate water vapour (Figure 4.7). However, the GCM shows a non-zero response of the macrostate at $t = 0$ (Figures 4.6 and 4.7). After $t = 0$, when both water vapour and temperature are homogenised, the sign of the macrostate water vapour response in the GCM and in the CRM are opposite, which may explain why the precipitation responses also have opposite signs. When only temperature is homogenised, the signs of the macrostate water vapour response in the GCM and in the CRM are the same, and so are the signs of precipitation response. However, when water vapour is homogenised, this does not seem to be true, since the signs of the macrostate water vapour response in the GCM and in the CRM are the same, but the signs of precipitation response are opposite. We speculate that there may be a link between these signs, but it is not completely validated.

Note that in this chapter, we compare the GCM with the CRM, so we tend to consider the CRM as the response to reproduce. An evaluation of the WRF response

would be useful to confirm its realism, but we leave this for future work.

In a nutshell, this comparison shows some encouraging forms of memory in the SCM (Single-Column GCM), in particular in terms of time scale, and of temperature-stored memory. Nevertheless, the SCM misrepresents several paramount aspects of memory, such as the sign of the response anomaly, and most importantly the memory stored in the water vapour structures. This suggests that additional work on the cold pool scheme (and more generally on the whole convection scheme) is needed to better represent convective memory.

4.6 With modified cold pools, does modified LMDZ have the same sources of memory as WRF?

With more numerous cold pools in LMDZ (“modified LMDZ”), the precipitation recovery time scale to pseudo-homogenisation is about the same as in the default LMDZ (Figure 4.8). So in terms of memory time scale, both versions compare well with the CRM. With more numerous cold pools, precipitation recovery over 24 hours is much more damped than in the default LMDZ, making it more consistent with the CRM than the default LMDZ. However, the response amplitude is strongly reduced with modified LMDZ, compared to default LMDZ. The CRM shows a response amplitude somewhere in between the one from modified and from default LMDZ, but perhaps closer to the one from default LMDZ. Finally, both versions of the GCM show a relatively similar response whatever variables are homogenised, whereas the CRM shows recoveries of opposite signs for diverse homogenised variables. In conclusion for precipitation response, while the default LMDZ behaves more like the temperature-homogenised CRM, modified LMDZ may behave more like the CRM where both water vapour and temperature are homogenised. Even though modified LMDZ might be more similar to the CRM on some aspect of memory, it is unclear whether this change benefits to the overall memory behaviour, at least for precipitation.

To clarify the link between convective memory and the recovery time scale, recall that the proxy used to measure memory is precisely the recovery time scale

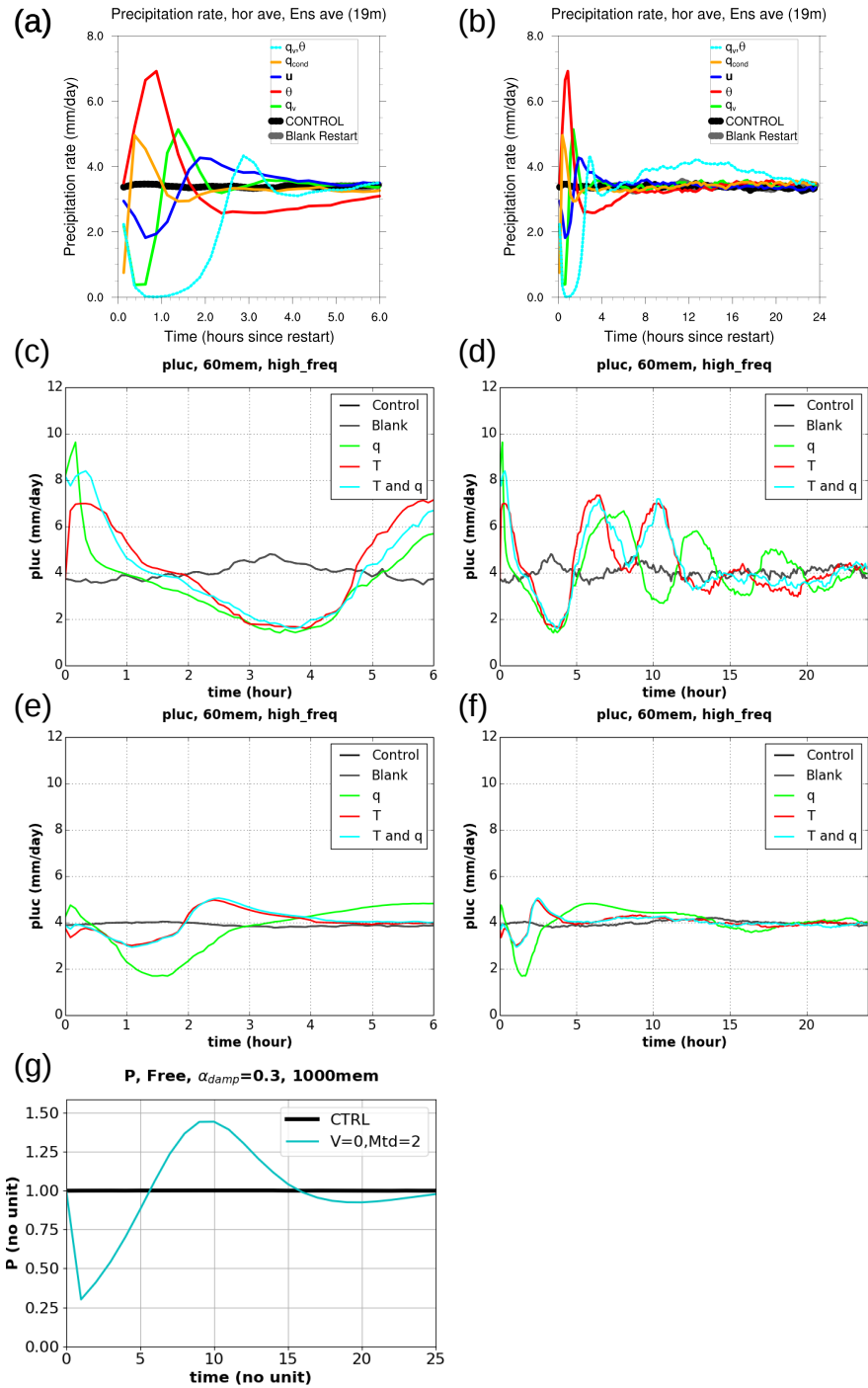


Figure 4.8 Responses of precipitation rate to different types of initial homogenisation (colours and legend: see Figure 4.4). (a) In the CRM, for the first 6 h after homogenisation (as in Figure 4.4(a)). (b) In the CRM, for the first 24 h after homogenisation (as in Figure 4.4(b)). (c) In the SCM with default cold pool number density (D_{CP}), for the first 6 h (as in Figure 4.4(c)). (d) In the SCM with default D_{CP} , for the first 24 h (as in Figure 4.4(d)). (e) Same as (c), but for a SCM with D_{CP} 100 times greater than the default (f) Same as (d), but for a SCM with D_{CP} 100 times greater than the default (g) In the predator-prey model, for what seems equivalent to the first 6 h after homogenisation (as in Figure 4.4(e)). The CRM responses are averaged over 19 members, the GCM ones over 60 members, and the predator-prey model ones over 1000 members.

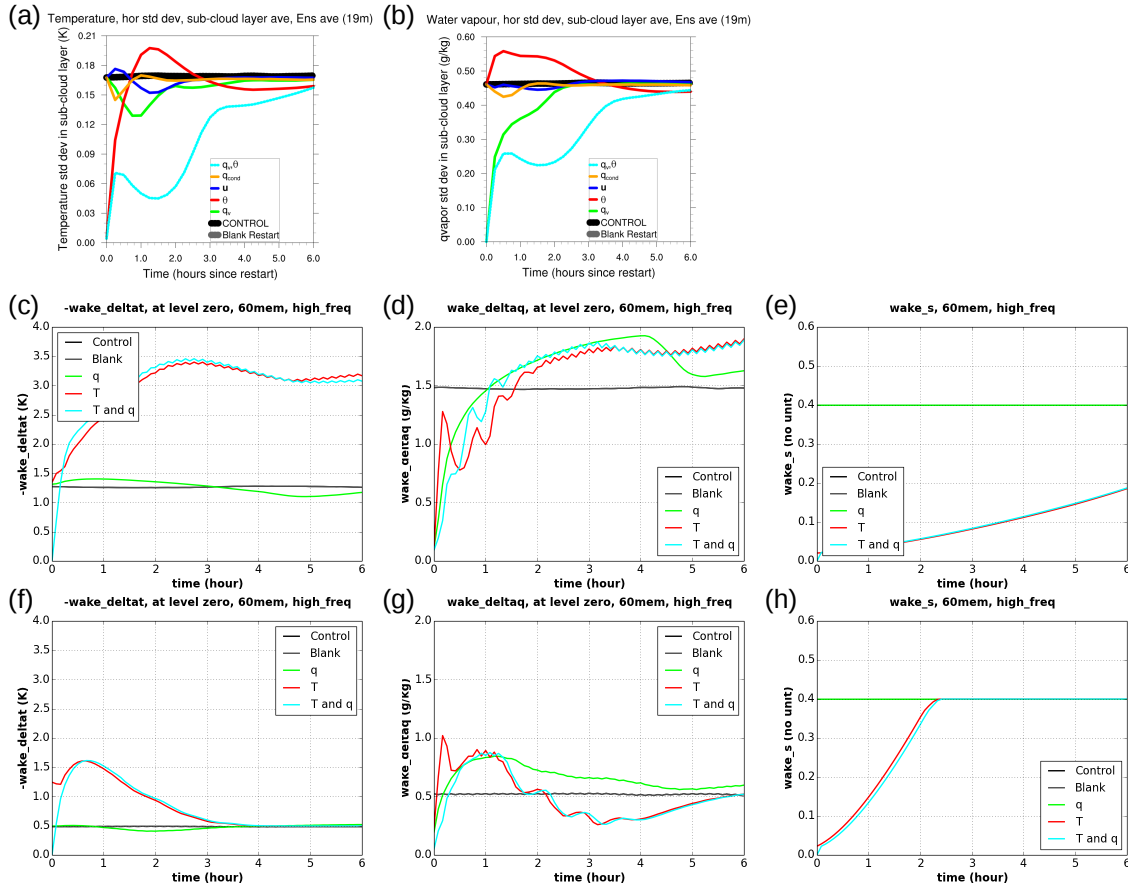


Figure 4.9 Responses of different microstate (or cold pool) properties to different types of initial homogenisation (colours and legend: see Figure 4.4), in the CRM (a,b), in the default SCM (c,d,e) and in the modified SCM (f,g,h), for the first 6 h after homogenisation. (a) Standard deviation of temperature in the sub-cloud layer in the CRM, to be compared to (c) and (f). (b) Standard deviation of water vapour in the sub-cloud layer in the CRM, to be compared to (d) and (g) (as in Figure 4.7(c)). (c) Cold pool temperature anomaly (in absolute value) in the default SCM (as in Figure 4.5(a) but in absolute value). (d) Cold pool humidity anomaly in the default SCM (as in Figure 4.5(d)). (e) Cold pool fractional surface area in the default SCM (as in Figure 4.5(g)). (f) Same as (c) but for the modified SCM. (g) Same as (d) but for the modified SCM. (h) Same as (e) but for the modified SCM. The responses are averaged over 19 members for the CRM, over 60 members for the SCM. We use high frequency output (every 5 min). For cold pool temperature and humidity anomalies, lines only show the time series at the first model level (near surface).

(Chapter 2). This means that the memory is not determined by any specific time constant a priori (e.g., $\frac{1}{\alpha_{damp}}$ in the toy model), because of the numerous interactions within each model. As a consequence, when the recovery time scale to homogenisation decreases, we can say that there is “less” memory.

For microstate variables, it is clear that the recovery time scale to pseudo-homogenisation in modified LMDZ is reduced by about a factor of 5 with respect to default LMDZ (Figure 4.9). For example, it takes 10 hours for the cold pool fractional area to recover to its RCE value in default LMDZ, but it takes only

4.6. DOES MODIFIED LMDZ HAVE THE SAME MEMORY SOURCES?

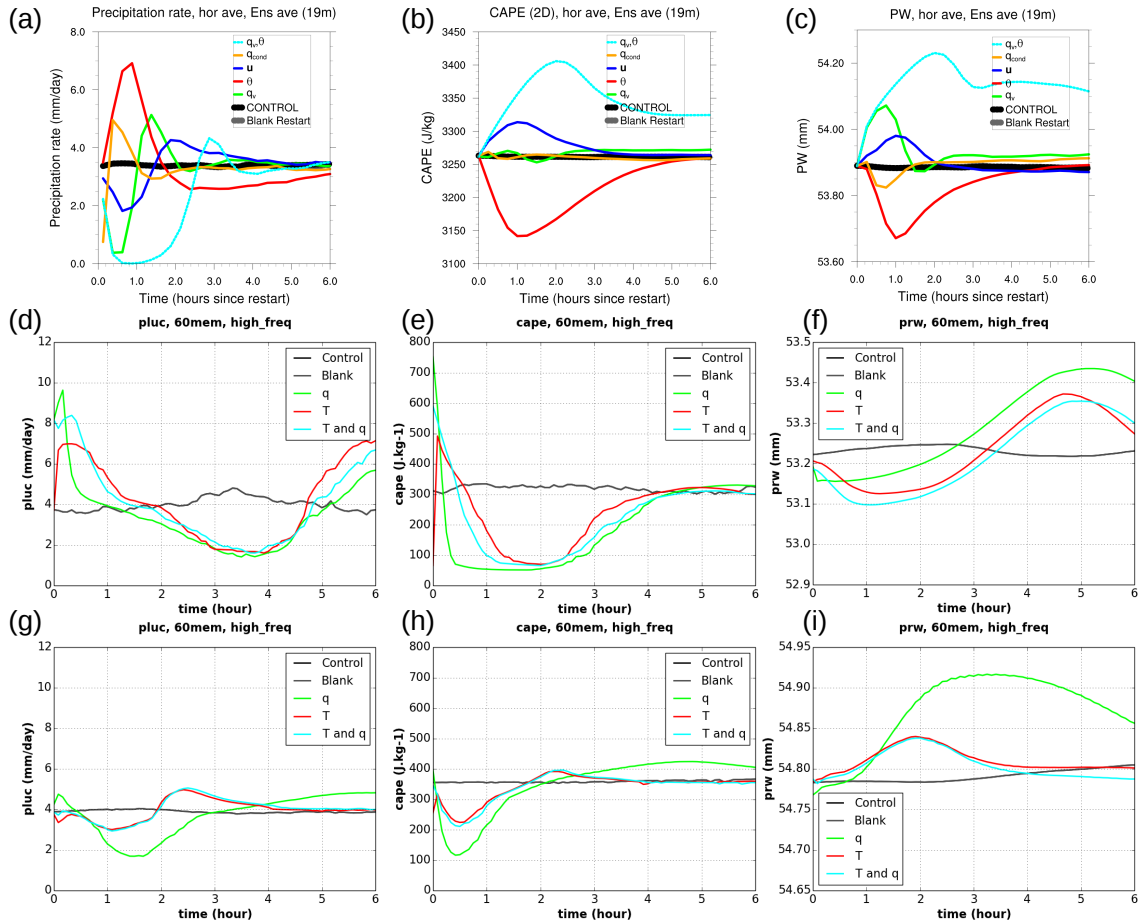


Figure 4.10 Responses of different macrostate variables to different types of initial homogenisation (colours and legend: see Figure 4.4), in the CRM (a,b,c), in the default SCM (d,e,f) and in the modified SCM (g,h,i), for the first 6 h after homogenisation. (a) Precipitation rate in the CRM, to be compared to (d) and (g) (as in Figure 4.4(a)). (b) Mean Convective Available Potential Energy (CAPE) in the CRM, to be compared to (e) and (h). (c) Mean Precipitable Water, in the CRM. (d) Convective precipitation in the default SCM (as in Figure 4.4(c)). (e) CAPE in the default SCM. (f) Precipitable Water in the default SCM (as in Figure 4.6(g)). (g) Same as (d) but for the modified SCM. (h) Same as (e) but for the modified SCM. (i) Same as (f) but for the modified SCM. The responses are averaged over 19 members for the CRM, over 60 members for the SCM. We use high frequency output (every 5 min).

2 hours in modified LMDZ. For the temperature microstate, it takes 15 hours in default LMDZ and only 3 hours in modified LMDZ, while it takes from 3 to 6 hours in the CRM. Modified LMDZ represents fairly well the recovery trajectory that the temperature-homogenised CRM exhibits, for both temperature and water vapour microstates. Conversely, the default LMDZ is not as similar to the CRM for any type of homogenisation. In terms of microstate, modified LMDZ has a reduced memory time scale, and shows an overall improvement of the recoveries. However, a major problem persists: all types of homogenisation in the GCM lead to a very similar response, contrary to the large diversity of responses in the CRM.

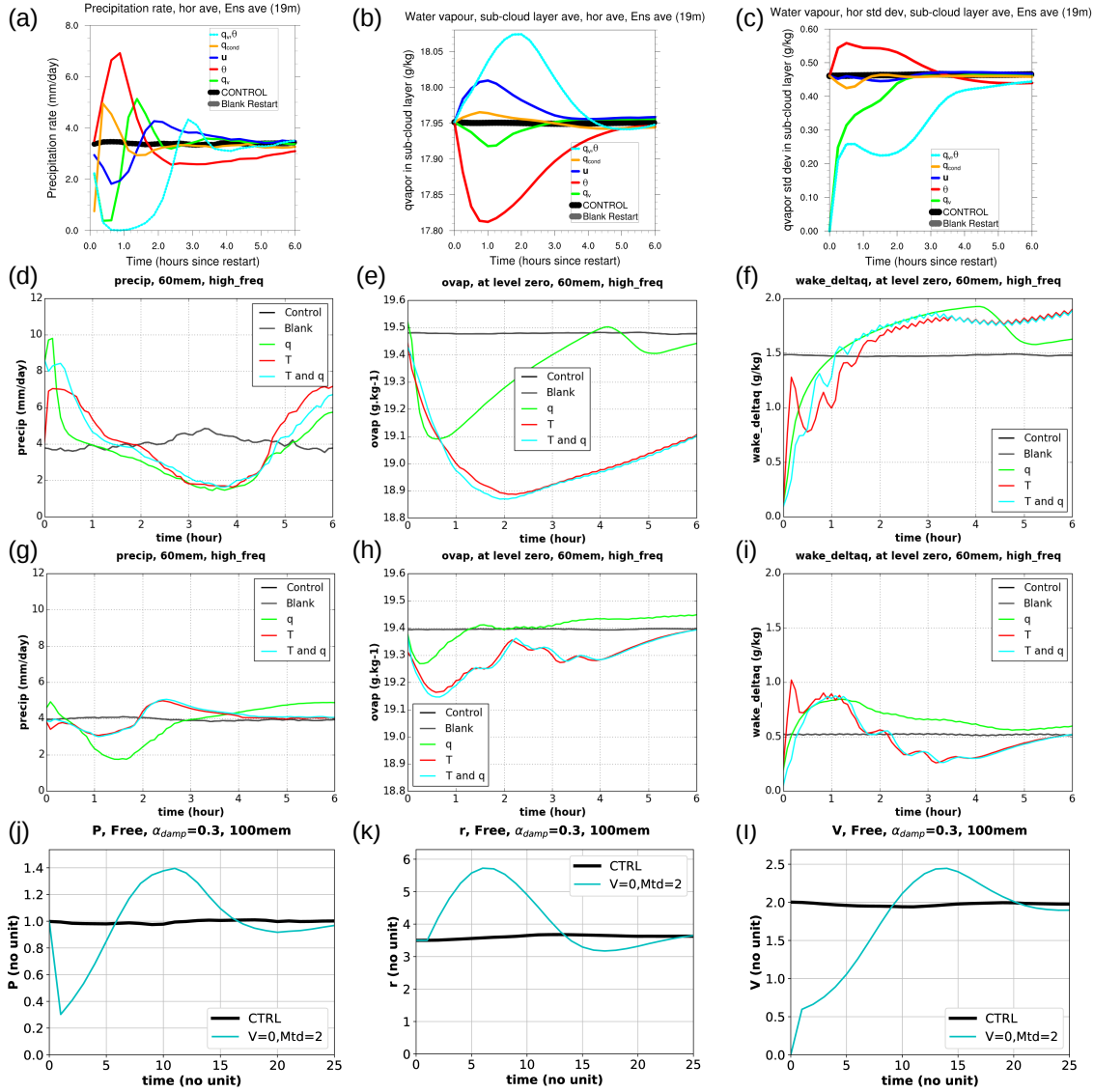


Figure 4.11 Responses of precipitation rate (a,d,g,j), a typical macrostate variable (b,e,h,k), and a typical microstate variable (c,f,i,l) to different types of initial homogenisation (colours and legend: see Figure 4.4), in the CRM (a,b,c), in the default SCM (d,e,f), in the modified SCM (g,h,i), and in the predator-prey model (j,k,l), for the first 6 h after homogenisation. (a) Precipitation rate in the CRM. (b) Mean water vapour mixing ratio in the sub-cloud layer (macrostate), in the CRM. (c) Standard deviation of water vapour mixing ratio in the sub-cloud layer (microstate), in the CRM. (d) Precipitation rate in the default SCM. (e) Mean humidity (macrostate) in the default SCM. (f) Cold pool humidity anomaly (microstate), at first model level, in the default SCM. (g) Same as (d) but for the modified SCM. (h) Same as (e) but for the modified SCM. (i) Same as (f) but for the modified SCM. (j) Precipitation rate P in the predator-prey model. (k) Mean humidity r (macrostate) in the predator-prey model. (l) Boundary-layer heterogeneity V (microstate) in the predator-prey model. The responses are averaged over 19 members for the CRM, over 60 members for the SCM, and over 100 members for the predator-prey model. We use high frequency output (every 5 min). Panels (a,b,c,d,e,f,j,k,l) are all taken from Figure 4.7.

In terms of macrostate variables, the recovery for default LMDZ is similar to the homogenisation of temperature in the CRM (Figure 4.10). Conversely, the recovery

4.6. DOES MODIFIED LMDZ HAVE THE SAME MEMORY SOURCES?

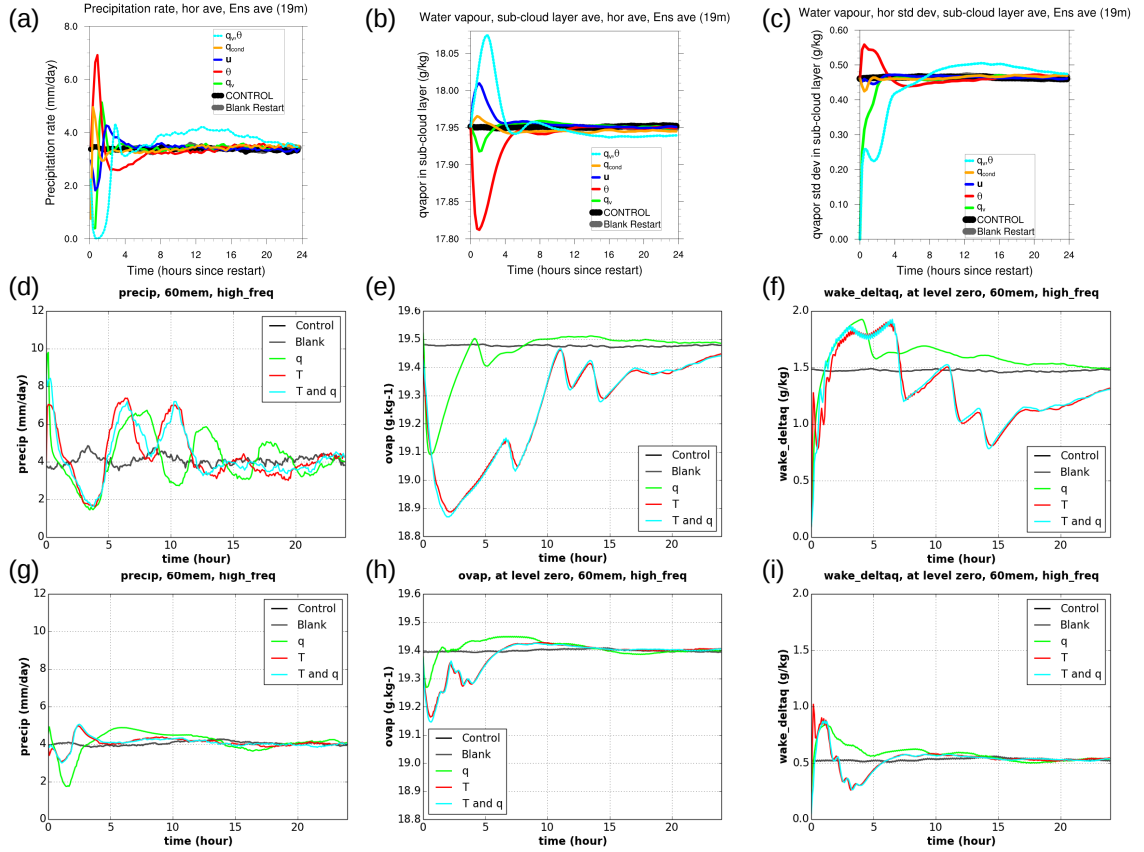


Figure 4.12 Same as Figure 4.11 but for the first 24 h after homogenisation, and without the last three plots on the predator-prey model.

for modified LMDZ is less comparable to the CRM, but to some extent similar to the homogenisation of both water vapour and temperature in the CRM (e.g., for Precipitable Water). Moreover, the recovery time scale is reduced in modified LMDZ compared to default LMDZ (e.g., for CAPE), even though it is less obvious than on the microstate variables. The sign of the original response is still unclear and depends on the type of homogenisation, and whether it is default or modified LMDZ.

To have an overall picture to assess potential improvement in the representation of memory in modified LMDZ, we can look at precipitation, a typical macrostate variable and a typical microstate variable, in four models: the CRM, the two versions of the SCM, and the predator-prey model (Figure 4.11). In terms of humidity macrostate, default LMDZ is relatively similar to the CRM: homogenising water vapour leads to a similar recovery of 3-hour time scale in both default LMDZ and the CRM, and homogenising temperature leads to a very similar shape except that the recovery time scale in default LMDZ is too long. Modified LMDZ shows a better

recovery time scale when homogenising temperature (6 hours) but the overall recovery shape is not as smooth. However, when homogenising water vapour, modified LMDZ does not perform as well as default LMDZ. Conversely, in terms of microstate, modified LMDZ generally performs better, which is an important result since we modified a microstate parameter in hope to improve the cold pools themselves. As for precipitation, it is unclear whether there is any improvement with modified LMDZ: the response sign is better, but the amplitude and recovery time scale are slightly worse. Default LMDZ also had the advantage of showing a very strong resemblance to homogenisation of temperature in the CRM. Overall, some aspects are more similar to the CRM (considered improved) and some are less similar to the CRM (considered deteriorated) with modified LMDZ.

On longer time scales, modified LMDZ performs better than default LMDZ, since it damps the oscillations relatively quickly, like in the CRM (Figure 4.12). This is valid whatever the variable is. The recovery time scale is confirmed to be decreased by a factor of about 5 with modified LMDZ, for both microstate and macrostate humidity, although this does not seem to apply to precipitation.

4.7 Conclusion

Thanks to its prognostic cold pools, LMDZ does have a representation of microstate memory. This is confirmed with the significant response away from RCE when cold pool variables are pseudo-homogenised in the SCM. The SCM memory has some encouraging features. First, the precipitation recovery time scale has an order of magnitude similar to the CRM. Second, the overall amplitude and shape of the recoveries is reasonable. The recovery of microstate variables is also a strength of this scheme.

However, memory in the SCM is not an accurate representation of the CRM memory. Most importantly, the recovery to homogenisation in the default SCM is practically the same whatever variable is homogenised, whereas homogenising different variables in the CRM leads to very different responses in terms of sign, time scale and amplitude. The most important recovery, the one to homogenisation of

both water vapour and temperature, even has the wrong sign. Memory through temperature is much better represented in LMDZ than memory through water vapour, since most LMDZ responses resemble recoveries to temperature homogenisation in the CRM. Therefore, the SCM completely misrepresents the impact of water vapour heterogeneity on subsequent convection as shown in the CRM, although it seems to capture the impact of temperature heterogeneity. Thus the memory is too highly concentrated in the temperature microstate. Physically, this suggests that the cold pool water vapour anomaly, despite being prognostic, does not have enough influence on the convective triggering or closure. Convection seems to be sensitive to the cold pool temperature anomaly but not to the humidity anomaly, making the added value of a prognostic representation of cold pool humidity anomaly too small. The coupling between cold pools and convection through cold pool humidity anomaly could therefore be changed. On longer time scales, homogenisation leads to a highly oscillatory response in SCM whereas it should be quickly damped, as shown in the CRM. In a nutshell, the SCM captures some microstate memory of the right capacity, but it is still an inaccurate memory: there is room for improvements.

We tested the memory behaviour for a modified LMDZ where cold pool number density (D_{CP}) is increased by a factor of 100. An increase in cold pool number density in LMDZ generally reduces its memory time scale, even though it depends on variables. A significant improvement in modified LMDZ is that the recovery oscillations are much more quickly damped, as in the CRM. Another improvement is that the microstate recovery is more similar to the CRM. However, some other aspects of memory are deteriorated in modified LMDZ, generally for macrostate variables. In terms of precipitation, some new improvements are noted on the response sign, but new deteriorations occur as well, for example on the recovery amplitude and time scale. Note that here, improvements and deteriorations are only relative to the CRM, not to observations or truth.

While the memory in default LMDZ was strongly focused in the temperature microstate, this imbalance is partly alleviated in the modified LMDZ. This is encouraging, therefore we will investigate other potential improvements of the model with more numerous cold pools in the next chapter.

Some aspects of memory might be more similar to the CRM in modified LMDZ (i.e with increase in cold pool number density), but overall the memory in the SCM would still need a lot of corrections. In particular, one should look for a diverse range of behaviour when homogenising different variables, like in the CRM. To start with, one should strive to improve the role of water vapour in memory, the damping time scale, and importantly the coupling between microstate and macrostate (i.e., the coupling between the cold pool scheme and convection and the large-scale).

One can also reflect on the usefulness of the homogenisation method. This chapter made a compelling demonstration of how one can use this homogenisation testbed in order to draw conclusions on the details of the operation of a physical scheme. This testbed promises to help reveal the realistic and unrealistic aspects of parameterizations. Therefore, it supports the use of the homogenisation testbed, in combination with other setups, to compare different convective parameterization schemes and to guide new scheme developments.

Chapter 5

Impact of cold pools on the intermittence/properties of precipitation in a General Circulation Model

5.1 Introduction

There are a number of long-standing systematic biases in General Circulation Models (GCMs). In terms of precipitation, GCMs rain too often and too little [Stephens *et al.*, 2010]. They produce too much convective rain compared to stratiform rain [Dai, 2006]. In terms of clouds, GCMs tend to produce too much high cloud and too little shallow cloud [Chepfer *et al.*, 2008; Sherwood *et al.*, 2013]. In terms of humidity, the correlation between precipitable water and precipitation is often flawed [Masunaga and Sumi, 2017]. This could be related to the lack of sensitivity of convective schemes to environmental humidity [Derbyshire *et al.*, 2004]. In terms of intraseasonal variability, most GCMs do not capture the Madden-Julian Oscillation (MJO) [CLIVAR Madden-Julian Oscillation Working Group: Waliser *et al.*, 2009; Jiang *et al.*, 2015]. As for storm representation and convective organisation, they do not capture the upscale growth towards Mesoscale Convective Systems

[*Rowe and Houze, 2015*].

The rain frequency bias in GCMs is particularly important because of the human perception of weather. Over oceans, GCMs rain roughly twice as often as they should, and this bias is larger in midlatitudes than in the tropics [*Stephens et al., 2010*]. Over land, it is essentially the light precipitation that occurs too often, while the heavy precipitation shows a reasonable frequency [*Sun et al., 2006*]. And for land and ocean altogether, the light precipitation occurs much too often, whereas the heavy precipitation may occur slightly too rarely in some GCMs [*Trenberth et al., 2017*]. Because the rain frequency seems better simulated over the Northern hemispheric land, the frequency bias might be even larger over ocean than over land. However, measuring precipitation frequency remains challenging, particularly over land [*Herold et al., 2016*]. One hurdle when comparing precipitation frequency in models and in observations is that the frequency is highly dependent on the spatial and temporal resolutions: for a larger grid cell, rain is likely to occur more often. For example, at 0.25° grid spacing and with hourly data, observations show that precipitation occurs 11% of the time between 60°N - 60°S , but only 8% of the time over land only [*Trenberth and Zhang, 2018*]. Because most GCMs rain too often but still have realistic accumulated precipitation, their simulated rain events are not heavy enough.

Different remedies have been proposed to improve the large-scale variability of convection in GCMs, which may indirectly help improve the intermittence of precipitation. Using a prognostic organisation variable designed to represent the effects of the microstate on subsequent convection was hoped to increase the variability [*Mapes and Neale, 2011*]. A similar objective was present in *Del Genio et al. [2015]*, since they tried to improve the variability captured by the MJO.

This study aims at testing the idea that convective memory may be involved in the rain frequency bias. Convective memory means that convection depends on its own history (see Chapter 1), and it relates to persistence of convection in time. Therefore the persistence of precipitation in time is expected to be modified by convective memory. If GCMs rain too often, it may be because they have an inaccurate representation of convective memory. This inaccuracy would point at

deficiencies in convective parameterizations, which is often invoked as the cause of the precipitation frequency bias.

One of the key components of convection which can create convective memory are the cold pools. Cold pools are formed by rain evaporation under mature convective clouds, and through both their dynamical impact and thermodynamical impact, they can generate new convection. By their dynamical impact, cold pools spread at the surface as density currents, which induces the warmer environmental air to move upwards, hence favouring convection. By their thermodynamical impact, cold pools collect humidity through enhanced surface fluxes when spreading at the surface. This forms moisture rings located around cold pool edges, i.e. at the boundary between cold pools and their environment. These moisture rings reduce Convective Inhibition (CIN) and make air parcels more buoyant, which enhances convection [Tompkins, 2001a; Schlemmer and Hohenegger, 2014; Langhans and Romps, 2015; Torri et al., 2015; Schlemmer and Hohenegger, 2016]. Therefore, cold pools have a double ability to create convective memory [Mapes and Neale, 2011]. Furthermore, Chapter 2 carried out a thorough analysis of convective memory and showed that convective memory mostly resides in low-level thermodynamic variables (below 700 hPa). Cold pools being a major thermodynamic feature at low levels, they are thus an appropriate candidate for convective memory.

Despite their important role in convective memory and convection in general, cold pools are usually not represented in GCMs. However, a few GCMs now have some representation of cold pools, either by a simple physical approach (e.g. Mapes and Neale [2011], or in the UK MetOffice UM model [MetOffice newsletter]) or by a full parameterization [Qian et al., 1998; Grandpeix and Lafore, 2010; Del Genio et al., 2015]. But these developments are still in their infancy. So by improving cold pool representation in GCMs, we can naturally aim at better convective parameterizations, in particular at better convective memory, and consequently at better precipitation frequency.

In this study, we use the LMDZ (Laboratoire de Météorologie Dynamique Zoomed) atmospheric model to test the hypothesis that the rain frequency bias is due to inaccurate convective memory, which can be improved by cold pools. We

choose this model for two reasons. First, this GCM is one of the few models to include a cold pool parameterization in its default version [*Grandpeix and Lafore*, 2010]. Second, unlike most GCMs, LMDZ has the advantage of already having some microstate convective memory (see Chapter 2), which makes it a perfect laboratory to test the accuracy and usefulness of memory. Moreover, LMDZ microstate memory precisely resides in the cold pool scheme: its prognostic variables are the cold pool thermodynamic and geometric properties (see Chapter 2 and Subsection 1.5.5).

However, the cold pool scheme parameter choices could be reviewed, such as the cold pool number density (number of cold pools per unit area, referred to as cold pool density in *Grandpeix and Lafore* [2010]). In LMDZ default version, the cold pool number density is a fixed parameter throughout the world, chosen to be representative of cold pools over land. But it is not a good representation of cold pool number density over ocean, where cold pools are expected to be weaker (i.e. smaller temperature drop), and probably more numerous (although this has not yet been proved). Cold pools over ocean also have a shorter life cycle, as reported by *Del Genio et al.* [2012] and used in *Del Genio et al.* [2015]. Consequently, we will explore the sensitivity of precipitation frequency to cold pool number density, especially over oceans.

The strategy to test our hypothesis is twofold. First, we will focus on improving the representation of cold pools over oceans in the LMDZ GCM, via the cold pool number density, in a simple 1-D framework. We will use equivalent Cloud-Resolving Simulations to guide our choices. And second, we will use this new value for cold pool number density over oceans in 3-D climate simulations, and assess how it affects precipitation frequency. Therefore, the goal of this work is to show that a better representation of cold pools in GCMs can help alleviate a long-standing bias of GCMs, the rain frequency bias, thanks to a better representation of convective memory.

5.2 Methods

5.2.1 Overview of the cold pool scheme in the LMDZ model

The LMDZ cold pool scheme [Grandpeix and Lafore, 2010; Grandpeix et al., 2010] has been presented in Subsection 1.5.5 as well as in Section 4.2. In summary, it represents a population of identical circular cold pools, whose geometry is described by the fractional surface area occupied by cold pools in the grid cell (a prognostic variable), and the cold pool number density, i.e., the number of cold pools per unit area (a parameter). The thermodynamic properties are described by a cold pool temperature anomaly profile and a cold pool water vapour anomaly profile with respect to their environment, which are two prognostic variables. Through their negative buoyancy, cold pools act as a density current spreading at the surface, and can therefore trigger deep convection. The ability of cold pools to trigger convection is measured by their Available Lifting Energy (ALE), calculated as their vertically-integrated negative buoyancy. Cold pools are in competition with boundary layer thermals to trigger convection. Triggering occurs when the ALE provided by either cold pools or thermals exceeds a threshold in Convective Inhibition (CIN). Likewise, cold pools provide a mass flux that can partly determine the convective intensity, so that cold pools intervene in the closure. The fuel for convective intensity, provided by both cold pools and thermals, is called Available Lifting Power (ALP). The two types of origins for ALP sum up in the closure.

One issue is that, in the original version of the scheme, the cold pool number density (denoted by D_{CP}) is a constant parameter. Its value was chosen to be close to the expectations for cold pools over land. So it is not a good approximation of its value over oceans, given the spatio-temporal variability of cold pools.

There is an important functionality in the cold pool scheme called the “splitting” of the Boundary Layer (BL). This is motivated by the difference between thermodynamic properties inside and outside cold pools. First, this difference leads to different surface fluxes: sensible heat fluxes should be larger in cold pools, and latent heat fluxes should also be different. Second, given the different thermody-

dynamic profiles, static stability is expected to be different in cold pools, so that the boundary layer turbulence should be different as well. We can decide to activate or not a different computation of surface fluxes and thermals in the cold pools, compared to their environment. When the BL “splitting” is activated, there are two different situations that the boundary layer and thermal schemes consider: inside the cold pools, and outside the cold pools.

5.2.2 Experimental approach with the LMDZ 1D and 3D simulations

For simplicity, we conducted the first step of this work in a 1-D set-up (Single-Column Model, SCM). We ran a series of Radiative-Convective Equilibrium (RCE) simulations over an ocean with a fixed Sea Surface Temperature, which means there was no external forcing. We chose this framework for two reasons. First, having a simple, atemporal, and easily reproducible testbed is useful for parameterization development, assessment, and inter-comparison. Second, this facilitates the comparison of cold pools between the SCM and Cloud-Resolving Model (CRM) simulations described below. The SCM has 79 vertical levels, represents a box of 500 km x 500 km, the time step is 5 min, and the SST is imposed at 302 K. The RCE is run for 90 days, and we discard the first 60 days due to spin-up.

We varied the D_{CP} parameter over a range of possibilities centred around the model default value. The default value was $8 \cdot 10^{-12} \text{ m}^{-2}$. This amounts to a cold pool every 350 km. We tested the sensitivity of cold pool properties and simulated precipitation for values of D_{CP} ranging from 100 times larger than the default to 100 times smaller than the default. That implies a spectrum ranging from a cold pool every 3500 km (low number density) to a cold pool every 35 km (large number density). And we studied the sensitivity of the RCE state and its cold pool properties to D_{CP} .

In this series of RCE simulations in 1-D mode, we analysed the mean properties of cold pools for different cold pool number densities. We are not interested in the atmospheric mean state in RCE (e.g., mean humidity, mean precipitation) but

rather in the mean properties of cold pools and cold pool-convection interactions, so that the RCE framework does not impede our ability to study the intermittence of precipitation.

We also tried to assess the sensitivity of the RCE state and its cold pools to other cold pool scheme parameters [*Grandpeix et al.*, 2010], but the results were not as interesting, so we will not present them here.

In the second step of this work, we performed 3-D runs which consisted in 10 years of global simulation, with climatological SSTs. These simulations also have 79 vertical levels, but unlike the 1-D setup, they have 2.5° zonal grid spacing, 1.25° meridional grid spacing, and the time step is 2 min.

5.3 Results

5.3.1 Insights on cold pool properties from a Cloud-Resolving Model simulation over ocean

We begin by further exploring the unorganised control run of the cloud-resolving model presented in Section 2.3 in order to gain insight on resolved cold pools. The CRM-simulated cold pools over the ocean are found to be almost uniformly cold at a given altitude: there is almost no horizontal gradient of temperature inside a cold pool (Figure 5.1). Vertically, the cold pools become increasingly cold as the air is closer to the surface, most likely because of continuing rain evaporation cooling the air moving downwards. The order of magnitude of the temperature drop is 0.5 K, which is roughly consistent with observations [*Feng et al.*, 2015].

However, cold pools are not uniformly dry horizontally. Instead there is a strong horizontal specific humidity gradient inside the cold pools, pointing from the dry centre of the cold pools, i.e., where the downdraft falls, towards the humid boundaries of the cold pool. Downdrafts are bringing dry air because the air comes from aloft where the saturated specific humidity is much lower. When moving towards the cold pool boundaries, cold pools collect water vapour through surface

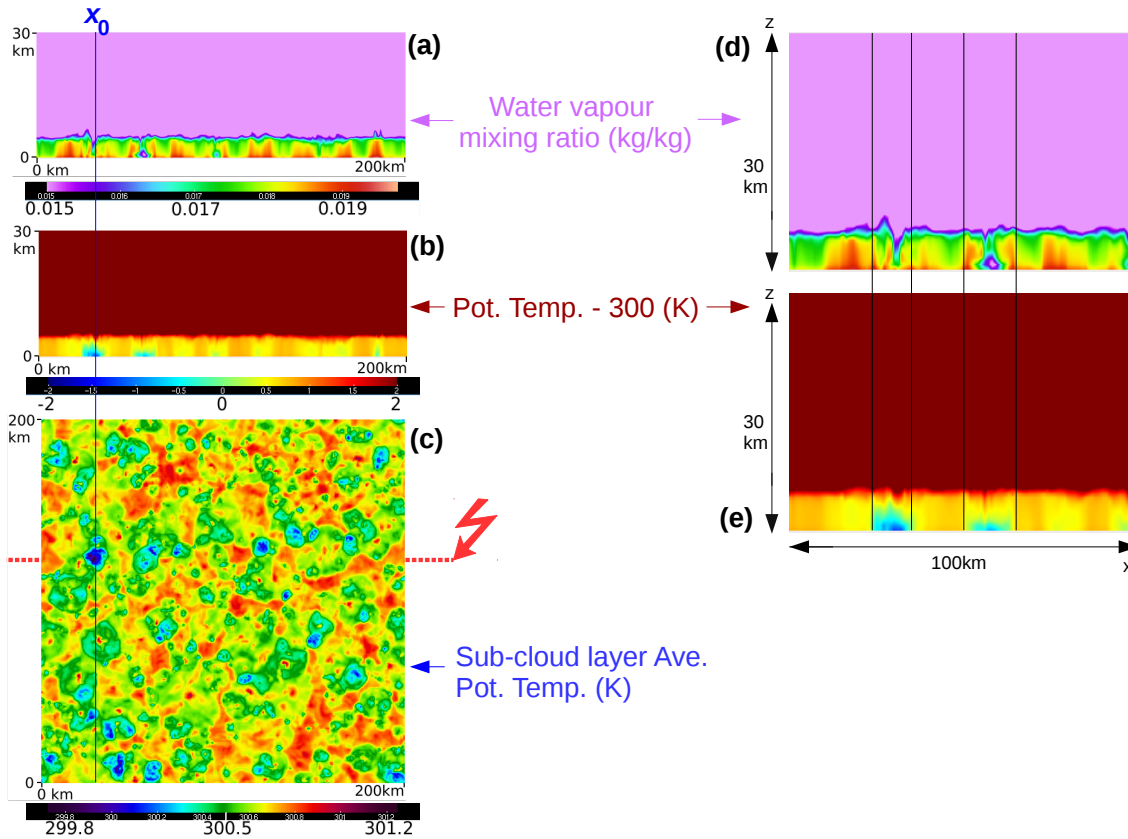


Figure 5.1 Snapshots of cold pools in a CRM simulation in Radiative-Convective Equilibrium. (a) Vertical cross-section of water vapour mixing ratio (kg/kg), in an (x,z) plane. (b) Vertical cross-section of potential temperature anomaly (K) compared to a fixed 300 K value, in an (x,z) plane. (c) View from the top of the potential temperature averaged in the sub-cloud layer, in an (x,y) plane, which allows to visualise the horizontal distribution of cold pools. (d) Same as (a) but zoomed over the region where cold pools are the strongest. (e) Same as (b) but zoomed over the region where cold pools are the strongest. x_0 denotes the x -axis location of a cold pool at its apex. The red zig-zag in (c) denotes the y -axis location of the vertical cross-sections showed in (a),(b),(d),(e). The vertical black lines in (d),(e) denote the x -axis boundaries of two particular strong cold pools in the cross-sections presented here.

fluxes, which gradually increases their water vapour mixing ratio, which is consistent with previous studies [Langhans and Romps, 2015; Schlemmer and Hohenegger, 2016; Torri and Kuang, 2016].

These CRM simulations over ocean also show that there is about 1 cold pool every 30 km in the equilibrium state. This order of magnitude was determined by basic visual counting of the cold pools found in the 200 km x 200 km CRM domain as in Figure 5.1 (c). To be counted as a cold pool, a cold area in the domain had to be roughly 0.4°C colder than the mean sub-cloud layer averaged potential temperature (i.e. less than 300.1 K or so in Figure 5.1 (c)). Note that this method is not intended to be precise, just to give an order of magnitude. The corresponding

D_{CP} is $10^{-9} m^{-2}$. The simulations also show that there are about 20 new cold pools every hour, which gives a cold pool birth rate of $5 \cdot 10^{-10} m^{-2}.h^{-1}$. And finally the cold pool life duration can be up to 1h45min.

The values we determined from the CRM can be compared with LMDZ cold pool scheme. The scheme assumes that cold pools are horizontally uniform since they have a single temperature and humidity profiles. While the CRM shows that this is a reasonable approximation for temperature, it is not a good approximation for humidity. Furthermore, although LMDZ default D_{CP} may be representative of cold pools over land (in particular over Sahel), the CRM shows that the expected D_{CP} over ocean should be approximately 100 times larger. Instead of modelling a cold pool every 350 km, the scheme should model a cold pool every 30 to 35 km over the ocean. As a comparison, *de Szoeke et al.* [2017] showed that D_{CP} is twice as large during active MJO (about 5 cold pools per day at their measurement station), compared to suppressed MJO (about 2.5 cold pools per day). The natural range of variability in D_{CP} over the ocean seems to be of a factor of 2, therefore the error of order 100 that LMDZ parameterization does over the ocean definitely needs a correction.

5.3.2 Comparison with the cold pools over land

In comparison, over land, cold pools can be much larger, deeper and colder. Observations show that cold pools are about 1 K to 2 K colder than their environment over ocean [*Feng et al.*, 2015; *de Szoeke et al.*, 2017] but 5 K to 10 K colder over land [*Marshall et al.*, 2013; *Provod et al.*, 2016]. Cold pools over ocean have a diameter of order 25 km [*Feng et al.*, 2015; *Rowe and Houze*, 2015], but cold pools over land have a diameter of at least 60km [*Lothon et al.*, 2011]. Cold pools over ocean are usually shallow (less than 800 m) [*de Szoeke et al.*, 2017], but over land they can be as deep as 2.5 km [*Lothon et al.*, 2011].

Physically, cold pools over land are deeper and colder than over ocean for two main reasons: (1) because Boundary Layer (BL) air is usually drier over land, and (2) because cloud base is usually higher over land. Rain evaporation being favoured by dry and thick air under cloud base, cold pools are deeper and colder and therefore

more intense over land. Moreover, wind shear helps convection self-sustain itself, thanks to the coupling with cold pools [Rotunno *et al.*, 1988; Robe and Emanuel, 2001]. Since wind shear is usually larger over land, this reinforces cold pool strength over land, making them deeper and colder.

As cold pools over ocean are weaker, they tend to dissipate more quickly, so that they do not have enough time to merge with other cold pools, contrary to cold pools over land. This tends to make cold pools more numerous over ocean. The BL height reinforces this tendency: since BL height is larger over land, and since BL thermals tend to scale over horizontal and vertical scales, BL thermals (or rolls) tend to be wider and stronger over land. After triggering, this makes convective systems occur further apart over land, which may later give birth to cold pools further apart from one another over land. As a result, cold pools are also thought to be much less numerous over land.

5.3.3 Sensitivity of cold pool thermodynamic and dynamic properties to cold pool number density in 1-D LMDZ

From now on, we focus on the sensitivity of cold pools to cold pool number density (D_{CP}) in the series of RCE simulations conducted with LMDZ in a 1-D mode.

With a higher D_{CP} , LMDZ cold pools become less cold and less deep (Figure 5.2 (a)). When D_{CP} is increased by a factor of 10^4 , the cold pools become about 10 times less cold near the surface. In RCE over ocean, the total cold pool surface fraction area in the grid cell is in practice fixed to its maximum value, 0.4. Therefore, having more numerous cold pools indirectly implies having smaller cold pools. In the scheme, since cold pools become smaller at high number density, they cannot spread for a long time before vanishing, and they are thus forced to be younger (although in reality, causality would impose that it is because a cold pool is young that it is smaller, relationships in the cold pool scheme imply the cold pool age). So it makes sense that at high number density, they are less cold than if they had undergone continuous rain evaporation.

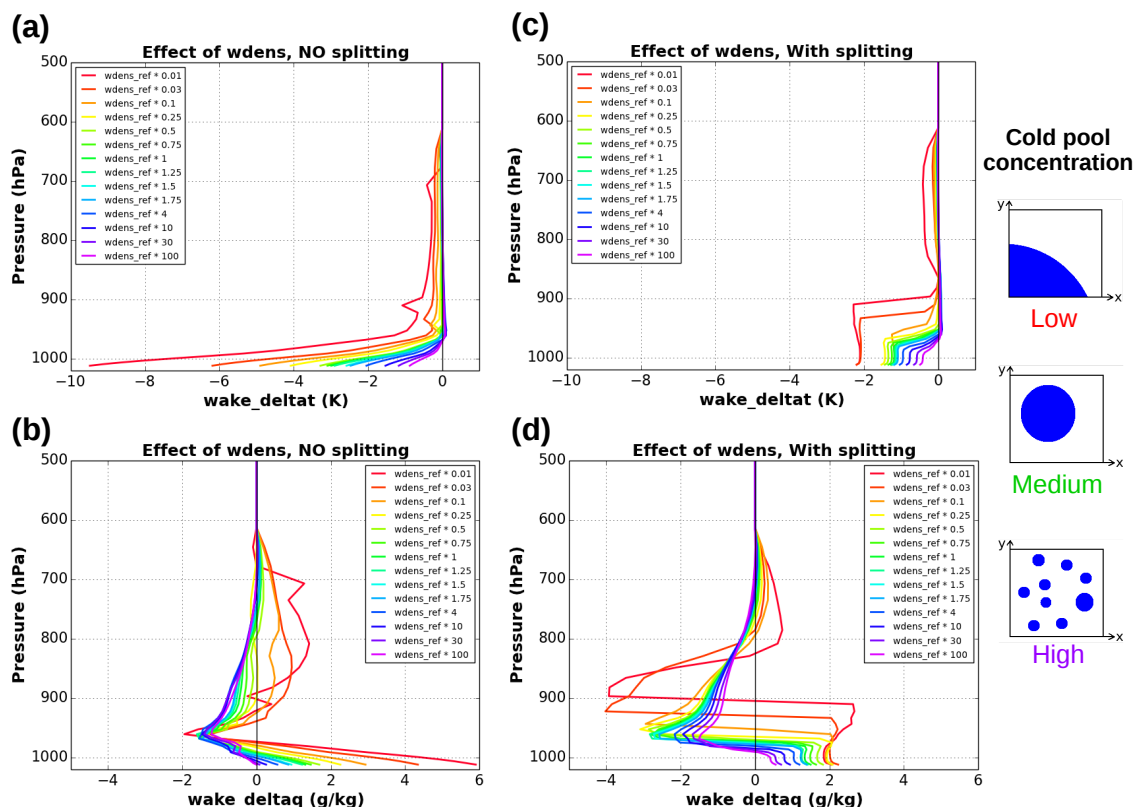


Figure 5.2 Sensitivity of cold pool properties to the cold pool number density. (a) Vertical profiles of cold pool temperature anomaly for simulations where the “splitting” option is deactivated. (b) Vertical profiles of cold pool humidity anomaly for simulations where the “splitting” option is deactivated. (c) Same as (a) but with the “splitting” option activated. (d) Same as (b) but with the “splitting” option activated. The cold pool number density is denoted by w_{dens} , shown by the colours, and values are given in the legend (red related to sparse cold pools, i.e. low cold pool number density, and purple to numerous cold pools, i.e. high cold pool number density), relatively to the default value which is written w_{dens_ref} . On the right-hand side, cartoons show the meaning of low, medium and high cold pool number density, viewed from the top and with cold pools being blue.

In terms of humidity, a higher D_{CP} makes LMDZ cold pools less humid near the surface, slightly less dry near 950 hPa, and again less dry aloft, in their downdraft region (Figure 5.2 (b)). Indeed, with more numerous cold pools, they are smaller, younger, and therefore they do not have much time to accumulate humidity through surface fluxes (near the surface), or through precipitation evaporation (aloft). Consequently they are less humid near the surface and also aloft. The reason why they are less dry near 950 hPa (near the Lifting Condensation Level) is less clear. But it could be related to enhanced entrainment of environmental air at lower altitudes, leading to air with higher temperature and thus higher humidity to enter the cold pools.

A higher D_{CP} also leads to an increase in downward vertical velocity inside the cold pools (not shown), which would explain the enhanced entrainment, at least in the scheme. The reason for this is that with higher D_{CP} , LDMZ cold pools would have the tendency to quickly occupy more surface area when growing as they are 2-D objects but grow in 1-D. And this must be compensated by a larger downward vertical velocity.

In summary, when BL “splitting” is not activated, we have the following sensitivities. When cold pools are more numerous (higher D_{CP}), they become less cold and the humidity anomalies are weaker, but the cold pool downward vertical velocity anomaly is larger.

With splitting of the boundary layer into 2 environments, very similar sensitivity of cold pool properties to D_{CP} is observed (Figure 5.2 (c) and (d)), so that the previous results prove to be robust. However, the absolute anomaly profiles of cold pools with respect to their environment are qualitatively different. In particular, the amplitude of the cold anomaly at the surface is reduced, and the cold pool temperature and humidity anomalies are much more uniform with height. Also, the cold pools are much drier than their environment around 950 hPa - 800 hPa than they were without splitting, and this behaviour occurs over a much deeper layer.

Comparing with the CRM, the LMDZ temperature anomaly profiles seem more similar to the CRM when the splitting is deactivated, though the processes that the splitting is trying to capture make physical sense (Figures 5.2 and 5.1(d,e)). In terms of humidity anomaly profile, it is harder to conclude which option is more similar to the CRM at this point, because the CRM analysis of vertical profiles remains to be done, and because the CRM argues for a representation of horizontal gradients of humidity which do not exist in the LMDZ scheme.

5.3.4 Sensitivity of the cold pool - convection interaction to cold pool number density in 1-D LMDZ

Sparse cold pools correspond to low cold pool number density (D_{CP}), and numerous cold pools to high cold pool number density.

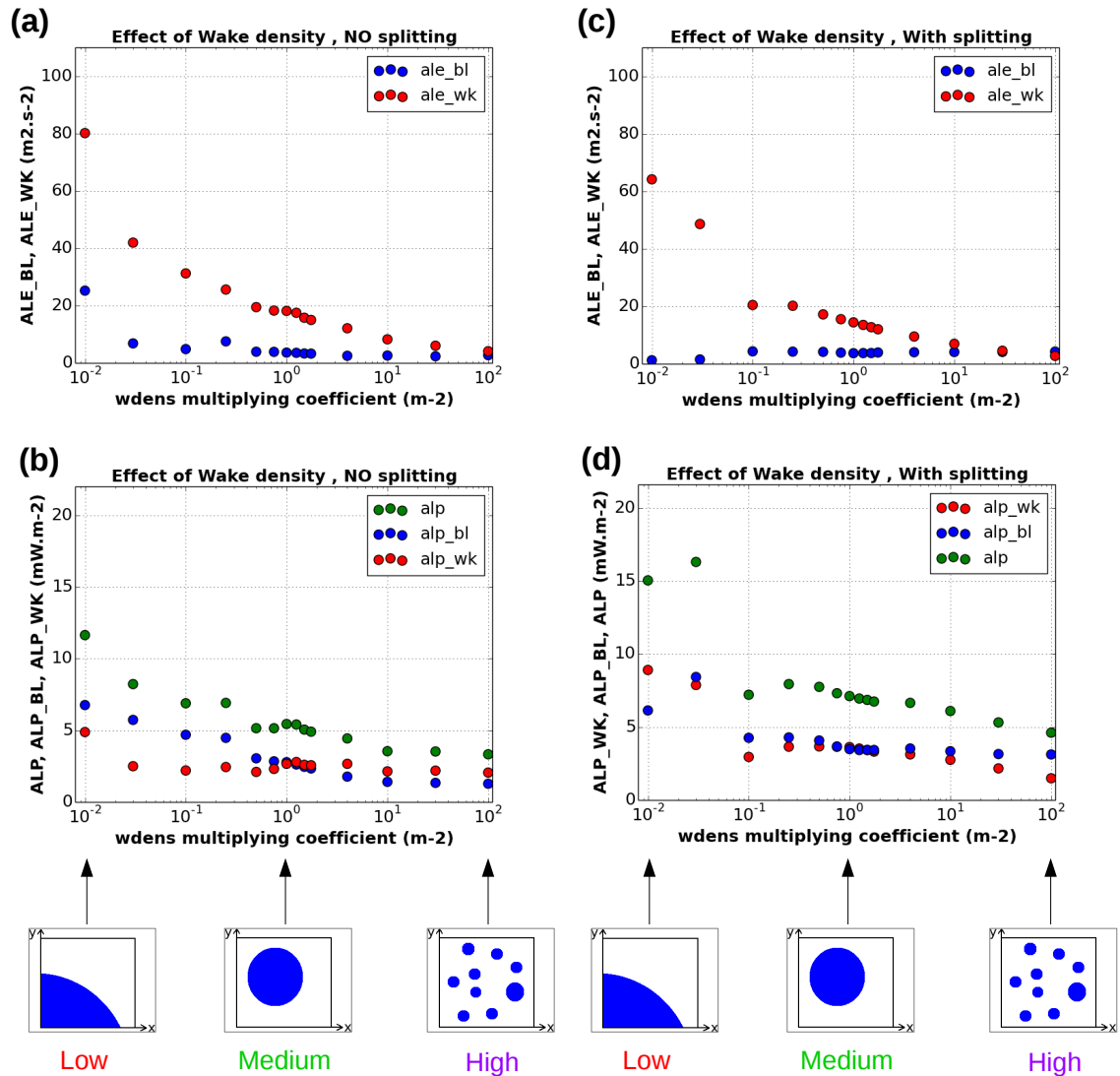


Figure 5.3 Sensitivity of the impact of cold pool on convection to the cold pool number density. (a) Available Lifting Energy (ALE, triggering) with respect to cold pool number density, with “splitting” option deactivated. (b) Available Lifting Power (ALP, closure) with respect to cold pool number density, with “splitting” option deactivated. (c) Same as (a) but with “splitting” option activated. (d) Same as (b) but with “splitting” option activated. Colours refer to ALE or ALP due to cold pools (red), to thermals (blue) and to the association of both cold pools and thermals eventually seen by the convection scheme (green), as per the legend. The cold pool number density, denoted by w_{dens} , is shown on the x-axis as a multiplying coefficient with respect to the default value (the multiplying value is 1 for the default cold pool number density, and 100 when the cold pool number density is 100 times larger than its default value). At the bottom, cartoons show the meaning of low, medium and high cold pool number density viewed from the top and with blue cold pools.

At higher D_{CP} , cold pools become much less powerful to trigger convection, whereas the ability of thermals to trigger convection is a small value which remains insensitive to D_{CP} at first order (Figure 5.3 (a)). Therefore, the likelihood of any of the two processes to exceed the Convective Inhibition and trigger convection is large at low D_{CP} (favouring endless persistence) and low at high D_{CP} (favouring breaks

in convection). Another consequence is that the competition between thermals and cold pools to trigger convection is increasingly less favouring cold pools at high D_{CP} . And there is a stochastic component in the triggering of the convection scheme by thermals. So with cold pools weaker than thermals, convection should become more sporadic.

This effect stems from the sensitivity of cold pool thermodynamic properties to D_{CP} (Figure 5.2). At higher D_{CP} , cold pools are smaller and less cold, so that they are less negatively buoyant. Therefore, they have a weaker thermodynamic potential energy and spread less fast, which gives them less energy to trigger convection.

When “splitting” is activated, these results hold well, and cold pools are even slightly less powerful in the triggering (Figure 5.3 (c)). A D_{CP} just 20 times the default is enough for cold pools to become weaker than thermals, while it has to be at least 100 times the default without splitting. Splitting should thus make convection even more sporadic at high D_{CP} .

When cold pools are more numerous, thermals generate less convection, whereas cold pools generate almost as much at first order: the intensity of convection, which is the sum of both effects in the closure, is reduced overall (Figure 5.3 (b)). This could lead to reduced heavy precipitation events. The fact that it is the thermals that lead to less intense convection can be explained by the indirect thermodynamic effect of cold pools in the scheme: when cold pools are less cold, the air outside cold pools is relatively less warm, less buoyant, and thus less active for convection by thermals.

When splitting is activated, the results are roughly similar, except that convective intensity from both thermals and from cold pools is reduced at higher D_{CP} (Figure 5.3 (d)). The intensity of convection due to cold pools even seems more sensitive to D_{CP} than the intensity due to thermals. This effect, opposite to the case without splitting, may be due to two factors. First, with splitting, thermals outside the cold pools are independent from those inside the cold pools, so that the thermals outside cold pools can remain more active for convective intensity, even at higher D_{CP} . Second, with splitting, cold pools are damped by enhanced surface fluxes, so that their ability to feed convection can be reduced. In any case, with

more numerous cold pools, convection is expected to be less intense once triggered.

Even though splitting leads to cold pool thermodynamic profiles which seem less similar to the CRM than without splitting, conversely it does seem to provide triggering and closure behaviours closer to our expectations.

This shows a sensitivity which can affect the precipitation persistence of the model. There are two reasons for that. First, with higher D_{CP} , cold pools have less energy to trigger or maintain convection, so more sporadic convection is expected. Second, the stochastic triggering due to thermals may then start to express itself, enhancing the intermittence.

This change in convective persistence may be interpreted as a change in the memory process, although this interpretation is not necessary to explain the results: reducing triggering by cold pools by making their ALE smaller than the CIN is enough to explain why convection becomes more sporadic. Note that the link between memory and persistence is not obvious (as pointed out in Subsections 1.4.2 and 2.2). Memory implies persistence, but the contraposition statement is wrong: persistence does not necessarily imply memory. However, the fact that this sensitivity can be interpreted in terms of memory is partly confirmed by the results presented in Chapter 4: with increasing D_{CP} , we noted almost no change in recovery time scale for precipitation, but a reduction in precipitation response amplitude and more response damping on longer time scales (Figure 4.8). We also noted that the recovery time scale of many other variables was reduced (e.g. all microstate variables, macrostate CAPE, macrostate humidity) (Figures 4.9,4.10,4.11). This suggests that with more numerous cold pools, LMDZ clearly has a weaker microstate memory, except for precipitation where it only has a slightly weaker memory. This could lead to less persistence of precipitation (i.e. more intermittence).

5.3.5 Higher precipitation frequency over oceans with a higher cold pool number density in 3-D LMDZ

We now analyse the effects of the cold pool number density on the climate in 3D global LMDZ simulations performed with climatological SSTs (Subsection 5.2.2).

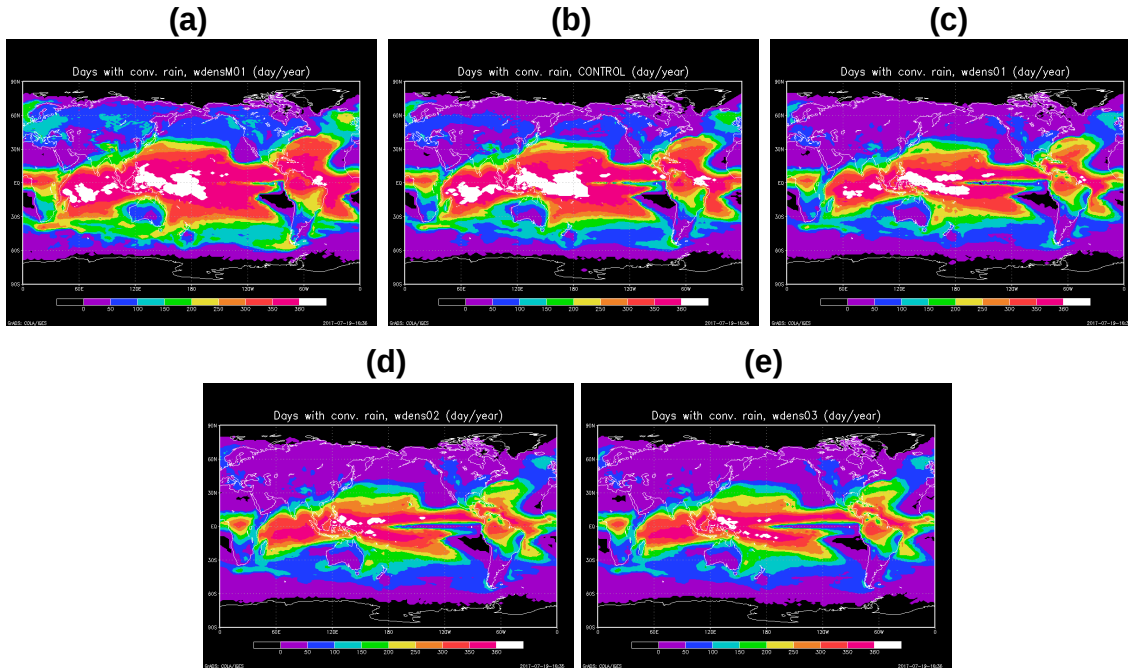


Figure 5.4 Global maps of the number of convectively rainy days in a year (number of days in a year for which convective rain exceeds a threshold of 10^{-6} mm.day $^{-1}$ $\approx 4.10^{-8}$ mm.h $^{-1}$). Each map corresponds to a different value of the cold pool number density: (a) 10 times less than default (b) default (c) 10 times more than default (d) 100 times more than default (e) 250 times more than default.

This allows to test the conclusions from the 1D runs in a fully interactive case where the large-scale circulation can respond to convection.

To study the precipitation intermittence, we come up with a simple proxy which is the number of convectively rainy days in a year. This is defined as the number of days in a year for which convective rain exceeds a threshold of 10^{-6} mm.day $^{-1}$, and this is computed from daily model output.

There is a significant increase in precipitation intermittence when increasing D_{CP} (Figure 5.4). At a given location, the number of days with convective precipitation is monotonically reduced when cold pools become more numerous. Also, for example, the area where convective rain happens more than 350 days per year (in red-pink) is strongly reduced when D_{CP} increases. Note that this sensitivity is very obvious over the oceans, but also exists over land, to a lesser extent. Results are insensitive to the choice of the threshold used to determine whether or not there is precipitation, for values ranging from 10^{-6} mm.day $^{-1}$ to 10^{-1} mm.day $^{-1}$.

The most sensitive areas to D_{CP} can be better determined by the differences in the amount of convectively rainy days between simulations with the modified value

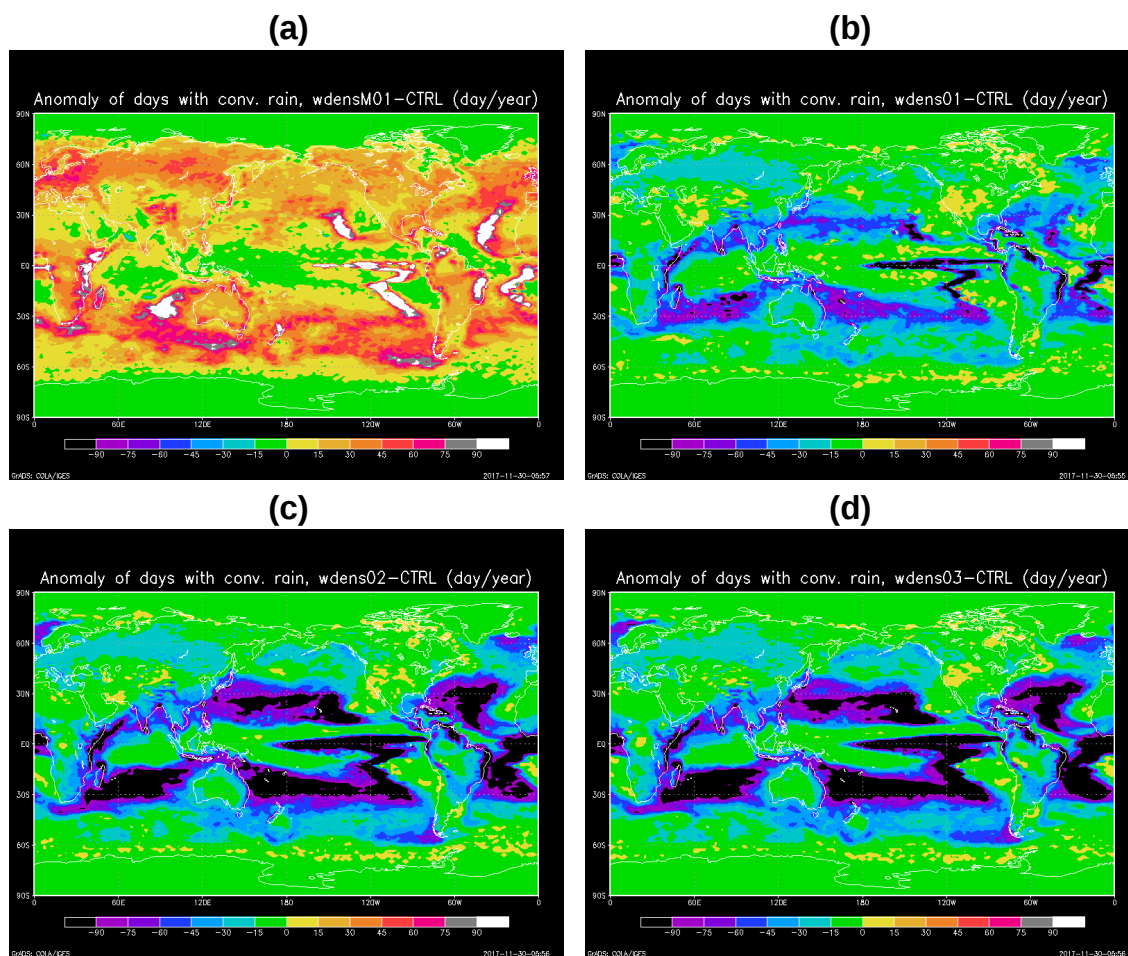


Figure 5.5 Similar maps as Figure 5.4 but expressed as a difference to the default. Maps show the difference between (1) the number of convectively rainy days in a year for the cold pool number density used in a given experiment, and (2) the number of convectively rainy days for the default cold pool number density. Cold pool number density in the experiment is (a) 10 times less than default (b) 10 times more than default (c) 100 times more than default (d) 250 times more than default.

of the parameter and the simulation with the default value (Figure 5.5). Overall, it is over the tropical oceans, except the Warm Pool, that precipitation intermittence is the most sensitive to D_{CP} . It even seems it is over the subsidence areas of the Hadley cell around 20-30°, and over the Pacific cold tongue that this sensitivity is the highest.

However, the mean convective precipitation remains generally unchanged when increasing D_{CP} (Figure 5.6). Therefore D_{CP} is a powerful parameter to modify convective precipitation frequency without modifying convective precipitation amount itself.

This sensitivity can be explained by the decrease in triggering energy due to cold pools at high D_{CP} , as well as the altered competition between cold pools and

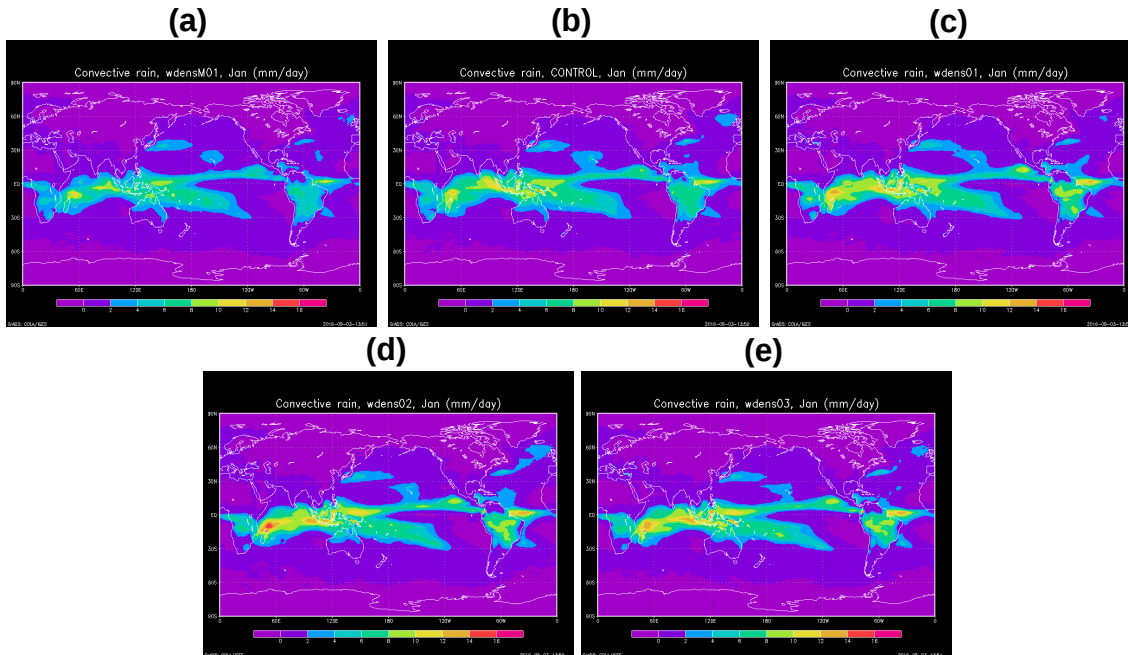


Figure 5.6 Same maps as Figure 5.4 but for the amount of convective precipitation.

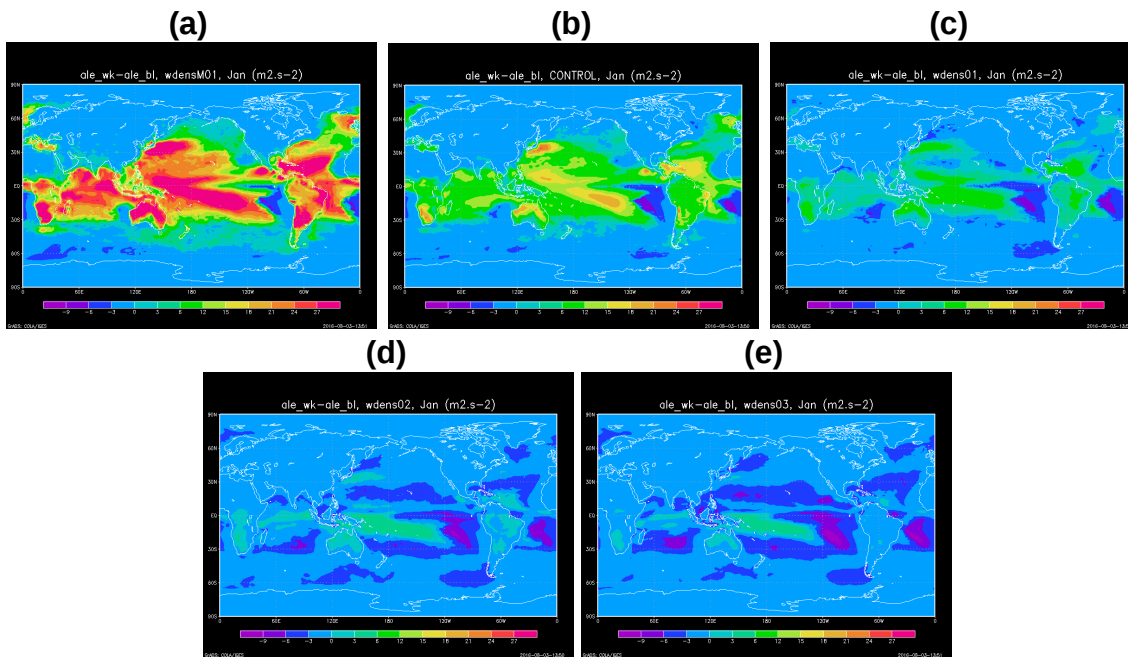


Figure 5.7 Same maps as Figure 5.4 but for the difference between the triggering energy of cold pools and the triggering energy of boundary layer thermals ($ALE_wk - ALE_bl$), showing which sub-cloud process dominates the triggering between cold pools and thermals.

thermals, as seen with the 1-D experiments. Cold pools are largely favoured to trigger convection with sparse cold pools, whereas the competition is more balanced with numerous cold pools, with thermals dominating the competition over the tropical oceans (except the Warm Pool) in areas with high sensitivity in terms of convective precipitation frequency (Figure 5.7).

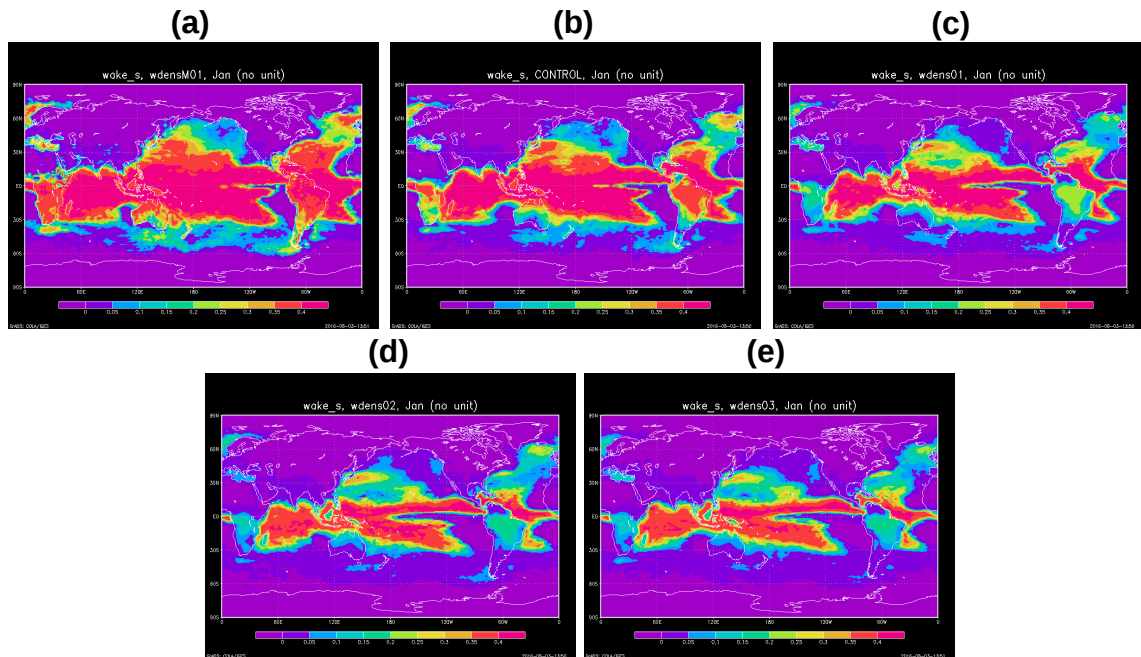


Figure 5.8 Same maps as Figure 5.4 but for the cold pool surface area fraction (surface occupied by cold pools in each grid cell, capped at a maximum of 0.4 by LMDZ scheme)

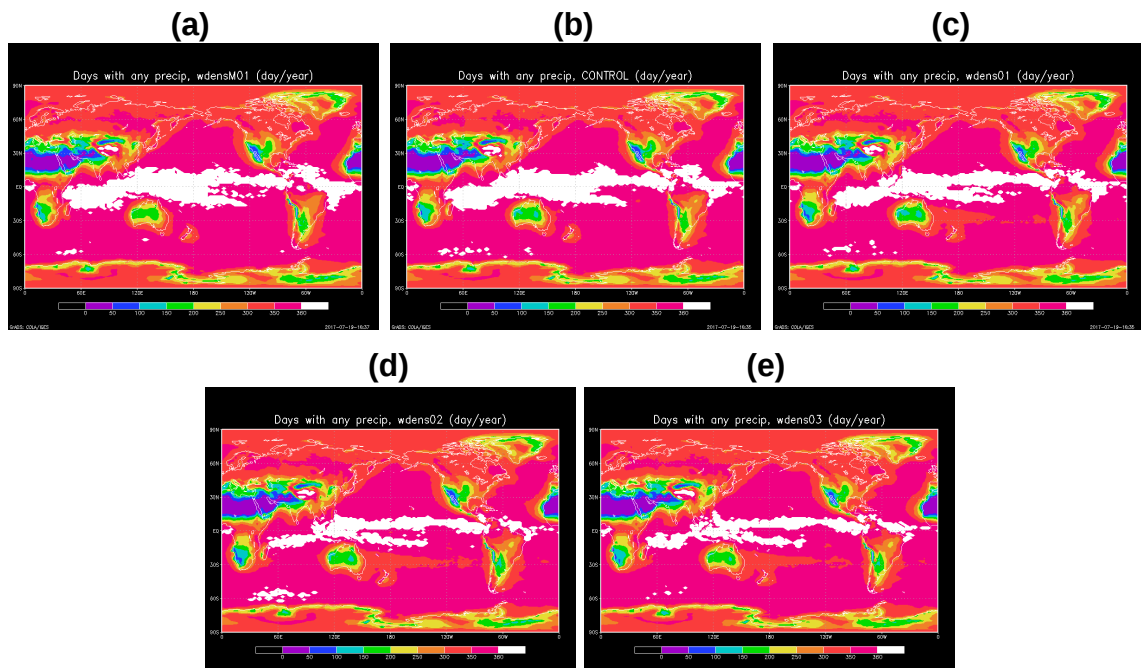


Figure 5.9 Same maps as Figure 5.4 but for the number of days with total precipitation (convective + stratiform)

The fractional area occupied by cold pools also reflects whether or not they have enough energy to continuously maintain convection, and thus whether or not they dominate thermals for the triggering (Figure 5.8). There is an overall reduction in the surface area occupied by cold pools when D_{CP} increases, and that seems well

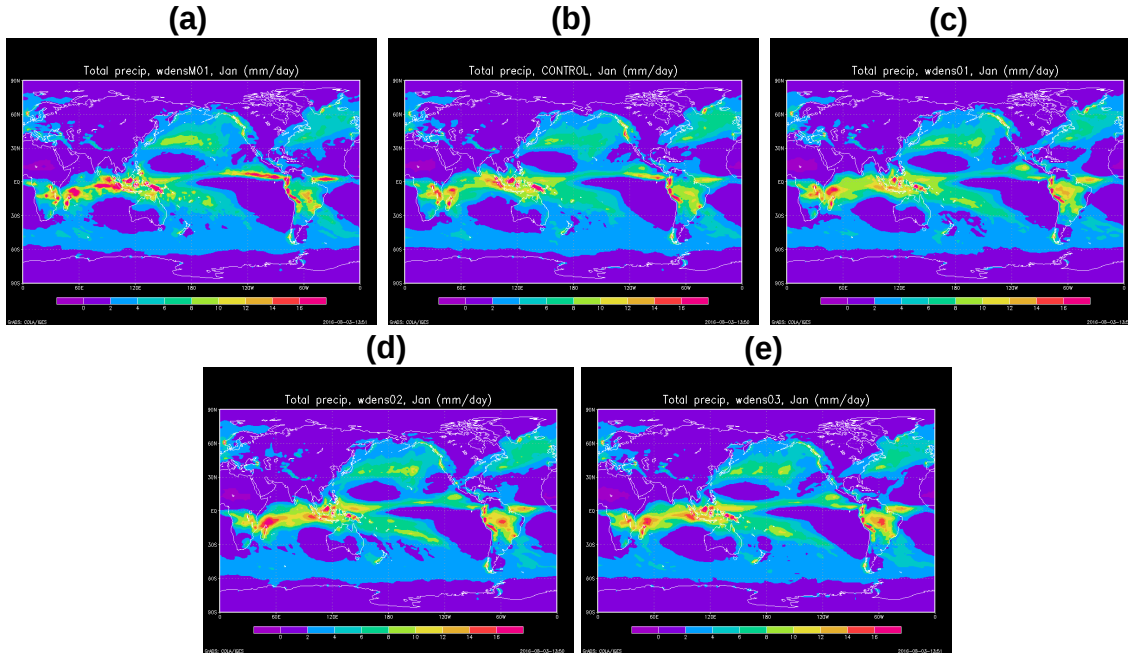


Figure 5.10 Same maps as Figure 5.4 but for the amount of total precipitation (convective + stratiform)

correlated with the increase in convective precipitation intermittence.

In terms of overall precipitation (convective + stratiform), there is still more intermittence at high D_{CP} , but the effect is strongly reduced compared to the effect on convective precipitation intermittence (Figure 5.9). This is probably due to partial compensation by the stratiform rain, which is out of direct control of the convective parameterization.

The total precipitation amount (convective + stratiform) still remains unchanged with modified D_{CP} (Figure 5.10). Even though the sensitivity of total precipitation frequency to D_{CP} is not as large as the convective one, it is still a sensitivity well isolated from the total precipitation amount. This is very encouraging to improve precipitation frequency without degrading precipitation amount, usually good enough in GCMs.

The maps on Figure 5.4 show that there may be a qualitative improvement of rain frequency in LMDZ in comparison with the observations (Figures 5.11, 5.12, 5.13, 5.14, 5.15 extracted from *Trenberth and Zhang [2018]* (Fig 4, Daily), *Stephens et al. [2010]* (Fig 6), *Sun et al. [2006]* (Fig 8)). In particular, it is the highest value of D_{CP} that gives the most similar map to the one made with daily data by *Trenberth and Zhang [2018]*, at least qualitatively in terms of patterns.

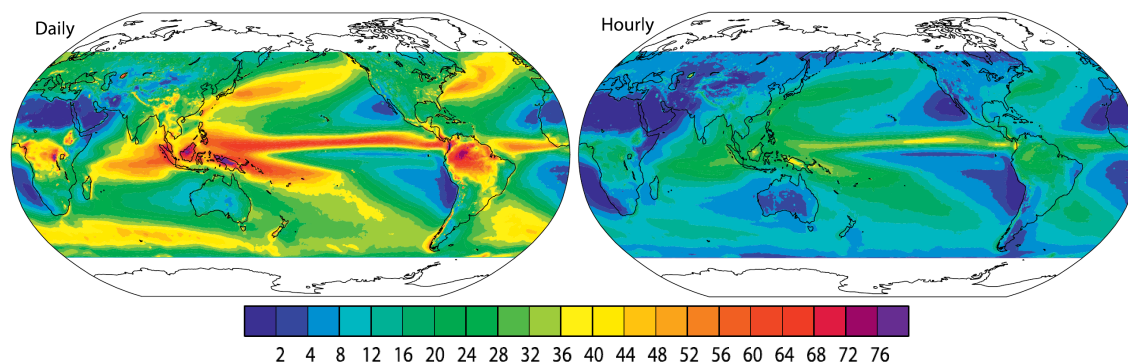


Figure 5.11 Annual mean of the percentage time precipitation occurs above a given threshold of 0.02 mm/h in observations at 0.25° spatial resolution for (left) daily data (right) hourly data. Adapted from Figure 4 in *Trenberth and Zhang* [2018].

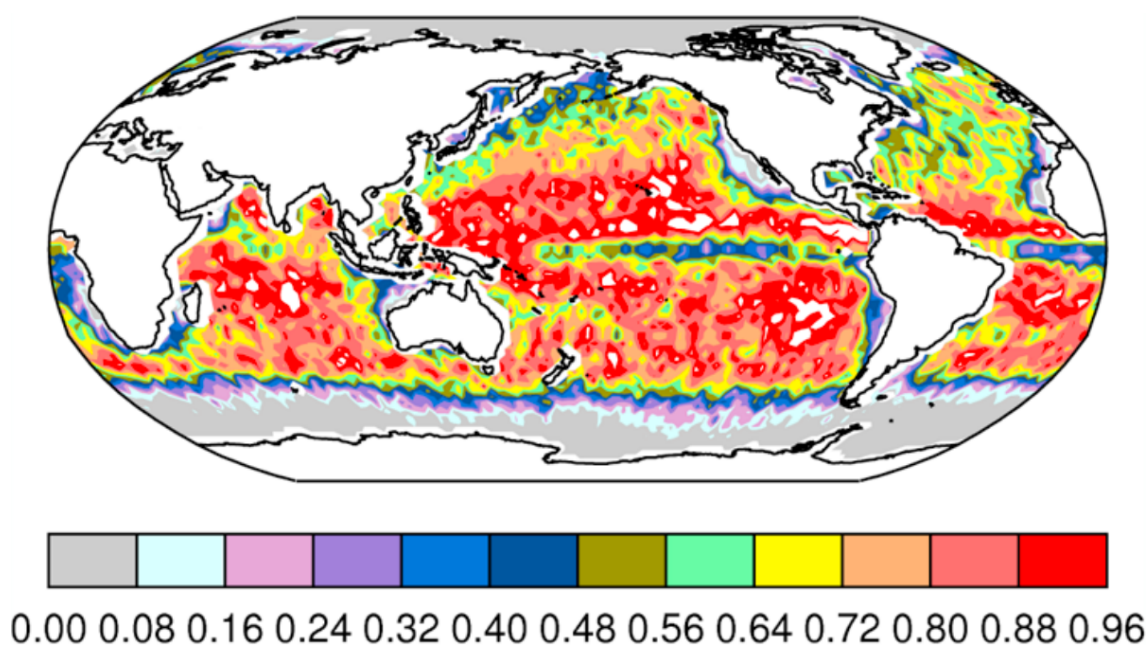


Figure 5.12 Observed global distribution of the frequency of occurrence of precipitation with an approximate 2° resolution. Adapted from Figure 6d in *Stephens et al.* [2010].

Comparisons in terms of precipitation frequencies come with caveats since precipitation frequency is by definition highly dependent on spatial and temporal resolutions. In particular *Trenberth and Zhang* [2018] show results at 0.25° spatial resolution while LMDZ grid spacing is much larger, and *Stephens et al.* [2010] do not mention what their temporal resolution is. Also, some observations are only available over land [*Sun et al.*, 2006]. Since we use daily data at 2.5° zonal resolution, 1.25° meridional resolution in LMDZ, the most relevant comparison is with *Stephens et al.* [2010]. Comparing with the daily data in the other studies is better than comparing with hourly data. To allow for a better comparison, it would be necessary for us to plot additional maps based on the same variables and the same

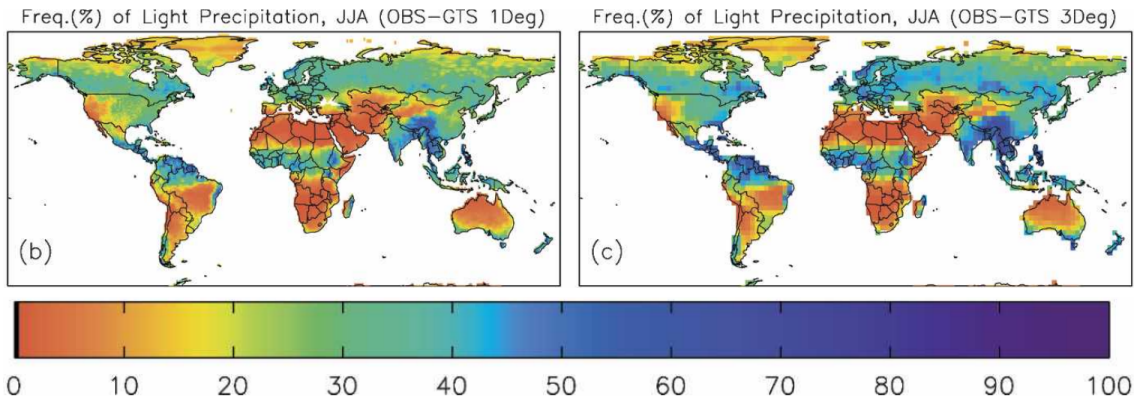


Figure 5.13 Mean JJA precipitation frequency (%) for light precipitation (1-10 mm/day), from daily data, from gridded GTS (Global Telecommunications System) observations (b) on a 1° grid (c) on a 3° grid. Adapted from Figure 3 in *Sun et al.* [2006].

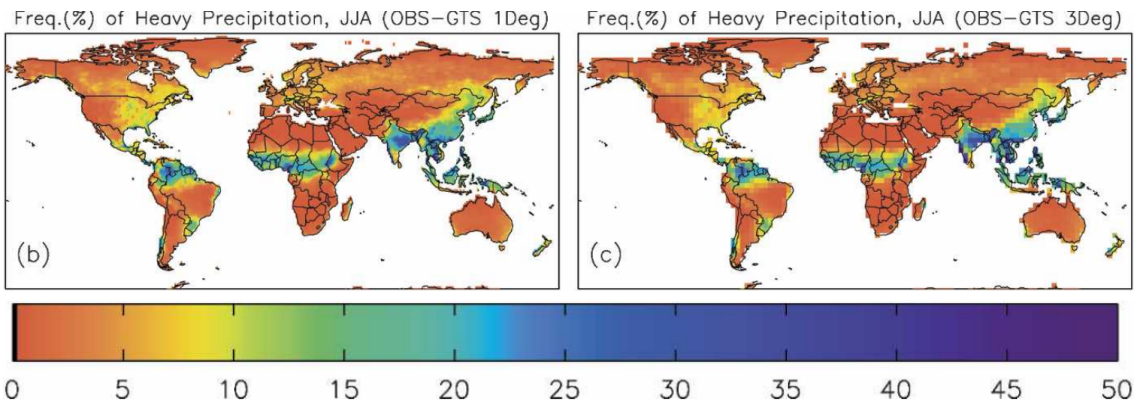


Figure 5.14 Same as in Figure 5.13 but for the frequency (%) of heavy precipitation (> 10 mm/day). Adapted from Figure 4 in *Sun et al.* [2006].

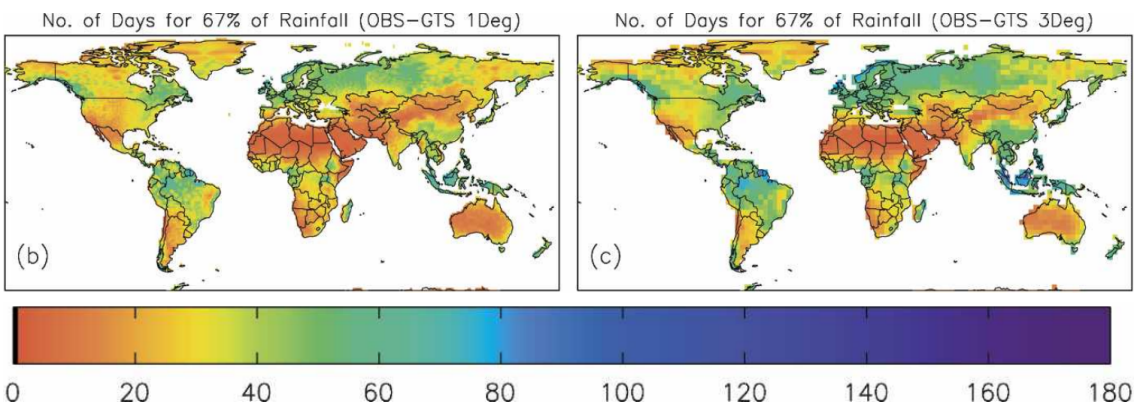


Figure 5.15 Same as in Figure 5.13 but for the number of rainy days contributing to 67% of the annual precipitation. Adapted from Figure 8 in *Sun et al.* [2006].

colourbar as the observations. This could be improved in future work.

This more sporadic behaviour with more numerous cold pools is somewhat confirmed by selected time series of convective precipitation (Figure 5.16). First,

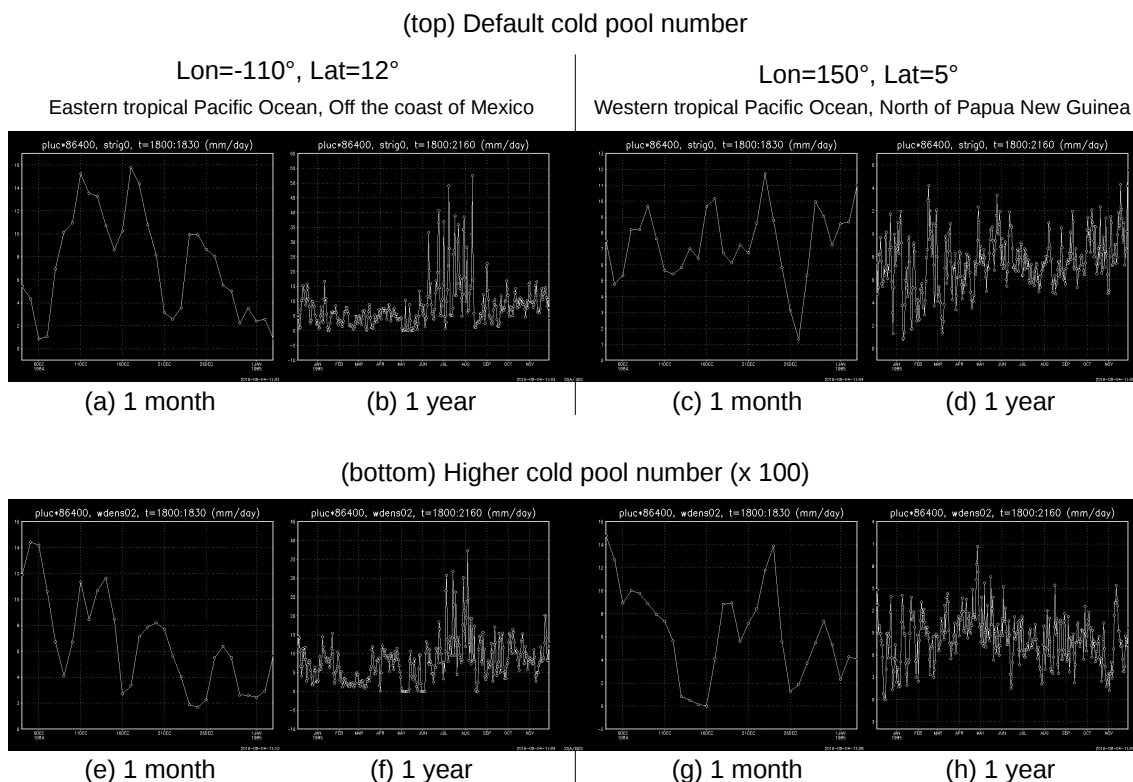


Figure 5.16 Time series of convective rain, for different values of cold pool number density: either the default (top, (a),(b),(c),(d)) or 100 times the default (bottom, (e),(f),(g),(h)). These plots are taken for either an Eastern tropical Pacific location, -110° longitude and 12° latitude (left, (a),(b),(e),(f)) or a Western tropical Pacific location, 150° longitude and 5° latitude (right, (c),(d),(g),(h)). There are two different time periods: either over a month, 4 Dec 1984 to 3 Jan 1985 ((a),(c),(e),(g)) or over a year, 4 Dec 1984 to 3 Dec 1985 ((b),(d),(f),(h)).

these time series being taken at local points, they cannot be considered as strong evidence. Second, they show the interplay between multiple time scales, and we cannot extract too much information. Still, with the default value, convective rain never reaches a null value in these time series. Conversely, with a value 100 times larger, convective precipitation does reach zero, and even for an extended period of time on Figure 5.16(f). This embodies the change in precipitation frequency with changing D_{CP} , even if it is not a compelling argument.

In order to compare the simulations with various D_{CP} with one another as well as with observations in terms of precipitation frequency, the next step is to plot in each case a PDF of (1) precipitation rate, (2) precipitation event duration, and (3) autocorrelation of precipitation in time. This will be done in future work.

As noted in the introduction, GCMs usually rain too often, which suggests their precipitation is too persistent. However, since persistence does not necessarily

imply memory, we cannot conclude whether or not GCMs have too much microstate memory. Most likely, they cannot have too much microstate memory, unless they already have a prognostic representation of the microstate. But it is possible that the persistence of large-scale conditions causes the persistence of precipitation. If the persistence of large-scale conditions is itself due to convection, then GCMs may have too much macrostate memory and too much synoptic state memory. Whatever the reason is, if the large-scale forcing is too persistent, convection will also be too persistent. That means microstate memory is not involved (and even the other types of memory may not be involved).

5.4 Conclusion

We first modified the cold pool parameterization in the LMDZ model over oceans, by changing the cold pool number density in a 1-D setup, following the orders of magnitude found in Cloud-Resolving simulations. In particular, having more numerous cold pools made cold pools less cold, less deep, and consequently less energetic to trigger convection. This weakening effect was even enhanced by increased competition with thermals to trigger convection.

This allowed for better precipitation intermittence in 3-D simulations, especially over tropical oceans. The results thus show a sensitivity which could make GCMs rain less often, and thus help alleviate the typical rainfall frequency bias in GCMs.

This effect can be partly interpreted by the convective memory which resides in LMDZ's prognostic cold pools (see Chapter 2). By changing the cold pool number density, we changed the memory process captured by the cold pool scheme, and therefore changed the ability for cold pools to maintain convection and make rainfall persist in time. Furthermore, this shows the interaction between spatial scales: improving the memory related to cold pools at small scales helped improve the behaviour of precipitation frequency at larger scales.

These results call for a two-step improvement of the GCM. First, although the default cold pool number density is a global parameter in this version of the model, this study shows it is necessary to have a different value over ocean and over land.

There are two reasons: (1) to have a value of the cold pool number density over ocean closer to our expectations, and (2) to improve the rainfall frequency bias over oceans. In a second step, it should be useful to turn the cold pool number density parameter into a prognostic variable (see Chapter 2). This would allow to not only change the memory process, but also to significantly improve it. It would also allow to model a cold pool population dynamics, ultimately preferable.

This change in convective memory via cold pool number density may also have benefits on other systematic GCM biases of GCMs. For example, having more numerous cold pools increases the amount of precipitable water in the 1-D framework, thus potentially correcting biases in mean humidity for instance? Other biases (e.g., cloud distribution, mean humidity, radiation) could similarly be reduced by this modified cold pool scheme, which calls for further investigation and comparison with observations.

The parameters and variables presented in this work could be better constrained by observations. It would therefore be beneficial to significantly invest on observations of cold pools. Some observations of cold pools exist in 0-D (fixed stations [*Provod et al.*, 2016], ship stations [*Feng et al.*, 2015]) as well as in 2-D (drones, radars [*Rowe and Houze*, 2015; *Feng et al.*, 2015], satellites). We should make use of it to further evaluate our results.

Chapter 6

Conclusion

6.1 Summary

Convective memory can be defined as the dependence of convection on its own history, rather than just on large-scale environmental conditions. For a model, it means having a prognostic representation of processes.

In this thesis, we have introduced a framework to better study convective memory, its causes, and its consequences. Depending on whether or not processes are resolved or parameterized, they provide different types of memory. The synoptic-state memory and the macrostate memory occur through the resolved large-scale state, so that any diagnostic parameterization can aim to capture them. However, the microstate memory occurs through the unresolved subgrid structures, so that it cannot be captured without a prognostic representation of unresolved processes.

The results obtained with a Cloud-Resolving Model (CRM) showed that convective memory does exist and that it is relevant for models whose time steps are less than an hour, which is almost always the case for General Circulation Models (GCM). Importantly, we showed that convective memory is strongly enhanced by convective organisation, for which its time scale can reach up to more than a day. Physically, this stems from the fact that memory is stored in microstate structures able to persist in time, which carry some information from the past, and which are enhanced by convective organisation.

Convective memory has been found to be essentially stored in the boundary layer thermodynamic variables. This result is generally robust for all the convective organisation types studied here, even if there are some differences. In other words, memory is primarily stored in boundary layer water vapour and temperature structures, which may be captured by the boundary layer Moist Static Energy structures. In particular, there is a dominant water vapour memory which is consistent throughout this investigation.

These results support efforts to represent in a prognostic way boundary layer thermodynamic structures in GCMs, such as cold pools, thermals, downdrafts, and potentially other objects. Overall, the thesis showed it is important to represent in some way the evolution of boundary layer Moist Static Energy variance, since it is paramount for memory and organisation.

Microstate memory is the type of memory which is most problematic in GCMs, since it requires a special prognostic treatment. To isolate it from the macrostate feedbacks, we investigated the convective behaviour when the macrostate is not allowed to vary in time. In these fixed-macrostate experiments, we found that an instability of the microstate develops quickly. Depending on how accurately the macrostate profiles are held, the instability is either an exponential growth or an exponential decay.

To understand this unexpected phenomenon, we built a simple toy model of convection with memory, which turns out to be a predator-prey model: microstate heterogeneities (the predator) consume macrostate instability (the prey). The predator-prey model reproduces successfully the key characteristics of the memory behaviour analysed with the CRM, so that it is fit for the purpose of studying convective memory. In particular, under fixed-macrostate conditions, the predator-prey model also leads to an instability.

This instability phenomenon under fixed-macrostate conditions in both models shows that there is a particular kind of instability that has not been suspected yet: the instability of the microstate. This reinforces the finding that the convective microstate plays a crucial role in determining subsequent convection. Since the macrostate is known in these experiments, the instability shows that knowledge of

the large-scale state is not enough to predict convection, contrary to traditional thinking. In our experiments, a slight discrepancy in fixing the macrostate profiles can lead to a completely different behaviour (exponential growth or exponential decay). For a parameterization to be successful at predicting convection, at least on short time scales (hours, or up to one day), not only should the large-scale state be known, but the microstate history should also be taken into account.

Macrostate feedbacks on the microstate must therefore play a key role to ensure stability, either in a GCM or in the real world. This implies that the coupling between the microstate memory and the macrostate is important to hamper any convective microstate instability.

The ideas developed from the CRM results and from the predator-prey model are intended not only to bring understanding on the convective memory processes, but also to be applied to convective parameterizations in GCMs. Therefore, we used LMDZ, an atmospheric GCM which already has some prognostic representation of the microstate, through its cold pool scheme. We applied a similar perturbation method, homogenisation, in the Single-Column Model (SCM) version of LMDZ, and compared with the CRM and with the predator-prey model.

The memory in the SCM is shown to be encouraging, since the time scale and shape of the recoveries to perturbations are similar to those obtained with the CRM. However, there are also several issues. Most importantly, the SCM memory is almost fully stored in the temperature microstate, whereas the CRM showed even more memory is stored in the water vapour microstate. There is a wrong representation of the “water vapour memory”.

Based on the CRM results, memory should be improved through low-level thermodynamic structures. As a result, we attempted to improve the SCM via its cold pool scheme. In particular, we increased the cold pool number density by 100, to bring it closer to a realistic value for oceanic convection.

This change improves some aspects of memory in the modified SCM, such as the imbalance between temperature storage and water vapour storage of memory, the damping of recoveries, and the behaviour of the microstate. However, this change also deteriorates other aspects of memory. For example, the memory time scale of

precipitation, and the macrostate recoveries are not as realistic. There is a clear sensitivity of memory to the change in cold pool number density, but this does not necessarily translate into a direct improvement of the memory as a whole. One solution would perhaps be to not only modify the value of the cold pool number density, but rather to turn it into a prognostic variable, hence automatically bringing a different memory to the system.

To better understand the potential of the cold pool number density parameter in terms of memory, and its impact on large-scale properties of climate simulations, we explored in more details the sensitivity of LMDZ to this parameter.

With more numerous cold pools in the model, the SCM cold pools themselves are changed: they become less cold, less deep, and less energetic to trigger deep convection. As a result, they do not always overcome the triggering of deep convection by boundary layer thermals: there is a more balanced competition between these two processes to trigger convection.

Applying this change in cold pool number density in 3-D simulations showed that precipitation becomes more intermittent, solving a typical GCM bias which consists in raining too often. One possible interpretation is that the sensitivity of cold pool strength to the cold pool number density parameter affects memory, and therefore improves the precipitation frequency, although the link between memory and persistence is not demonstrated yet.

This shows that modifying properties controlling microstate memory can lead to improvements of large-scale properties. This should help focus attention on the role convective memory plays in the basic convective process. Therefore, this sustains the efforts to take a prognostic approach to represent unresolved processes.

6.2 Implications

6.2.1 Understanding of convection

The results suggest that the microstate should be incorporated in convective understanding and convective parameterizations. The usual thinking is that knowing the large-scale state is sufficient to predict the intensity of convection. Convection can then feed back onto the large-scale environment, leading to a coupled interaction between convection and the large-scale circulation.

However, the experiments presented in this thesis show that knowing the large-scale state is not sufficient to know the characteristics of convection, even though this is probably a necessary condition. We argue here that the microstate plays a role to determine the future evolution of a convective system. The microstate memory can partly control the development of convection, making convection dependent on its own history even for fixed large-scale conditions. So both the large-scale conditions and some measure of the microstate should be known to make a good prediction of convection. This is different from the usual thinking since it shows that the convective state influences itself, so that it introduces another degree of freedom for convection.

6.2.2 Development of GCM convective parameterizations

The results imply that parameterizations should not make the diagnostic assumption: they should not assume that there is a diagnostic relationship between convection and the large-scale environment [see subsections 5b and 5c in *Arakawa, 2004*, for a list of non-prognostic schemes]. The investigation shows that even in the worse scenarios, i.e., when convection is unorganised, there is at least a memory time scale of an hour, which is larger than the GCM time steps: the temporal resolution is such that convection life cycle cannot be neglected. When convection becomes organised, the memory time scale can be as long as a day, which means that with organised convection, it is paramount to take memory into account, even at the di-

urnal time scale. The simplest way forward is to introduce a prognostic microstate variable to capture some microstate memory.

To what extent is it detrimental to neglect microstate memory? The answer probably depends on the objectives of the model developers and model users. If the time scale of interest is much greater than one day, then memory may not be important, except if memory is proved to have an indirect effect on longer time scales (similarly to *Bony and Emanuel* [2005] or *Del Genio et al.* [2015]). Microstate memory may change some properties of the mean state, but not dramatically (Chapters 4 and 5, and other LMDZ SCM results not shown). If the interest is in the mean state, rather than on the the spatio-temporal variability, then microstate memory may also not be that important.

There may be two general methods to include microstate convective memory into a parameterization: either using a comprehensive approach, or using a simple heuristic approach. Whatever the method may be, it seems that the only way to capture memory is for the convection scheme to be prognostic. In a comprehensive approach, one needs to keep track of all processes affecting the microstate in a prognostic way. This can be done for example through an extensive representation of cold pools, thermals, and other objects leading to thermodynamic heterogeneities or Moist Static Energy structures. The risk is that one may not be able to model in an exhaustive way all the processes that lead to a prognostic behaviour, causing incomplete memory. Conversely, a heuristic approach, such as our predator-prey model or the “org” variable scheme [*Mapes and Neale*, 2011], has the advantage of simplicity since it tries to encompass all the potential phenomena into a handful of equations. However, this may be more difficult to relate to reality. The prognostic variable(s) in a heuristic approach should increase the potential for autocorrelation in time, and one can add additional stochastic terms to increase the variance of the system as well, completing the properties of such a dynamical system.

For example, in the heuristic approach, the simple *Mapes and Neale* [2011] equation with memory could be rewritten the following way:

$$\frac{d(org)}{dt} = S - \frac{org}{\tau + \alpha org} \quad (6.1)$$

where org is a dimensionless quantity representing organization, S a source term, τ a typical time scale for organization to fade away in an unorganized case (e.g. 1 h), and α a tunable parameter representing the rate of change in τ with organization (e.g. $\frac{24}{max(org)}$ h).

On the one hand, increasing GCM resolution should allow the model to resolve more processes, thus resolving more macrostate memory and limiting the need to parameterize microstate processes prognostically. Since microstate memory is dependent on the grid scale, reducing the grid spacing may help resolve more processes that were previously leading to unresolved microstate memory. But on the other hand, when GCM resolution increases, each grid box contains a smaller sample of convective cells, which means that under a dynamical forcing, individual behaviour may become prominent, which may increase the impact of memory. So it is unclear how memory would evolve with GCM grid spacing altogether.

6.2.3 Extended meaning of memory

So far, we have considered that memory was to be represented through a prognostic equation. But it may be that a more general framework could apply. Therefore, we suggest that the ultimate goal to represent memory may be to use not only the intensity of convection at the previous time step, but the intensity at many previous time steps (ranging from the two previous time steps to an infinite number of previous time steps). This type of representation of the past can be achieved via “delay differential equations”, which are of the form:

$$\frac{dx(t)}{dt} = f\left(t, x(t), x_t\right) \quad (6.2)$$

where f is an functional operator allowing to predict the change in variable x with time t , and where

$$x_t = \left\{ x(\tau) : \tau \leq t \right\} \quad (6.3)$$

x_t represents the whole trajectory of the system in the past.

One could then impose a time scale $\tau_{convection}$ representing the convective life cycles and under which the terms can be kept in f , while the history of convection

older than $\tau_{convection}$ can be forgotten.

While a prognostic equation by definition gives inertia, which is a simple form of memory, a delay differential equation builds a full memory ability, where memory does not only come from the previous time steps, but from many past time steps (e.g., from any particular time scale in the past).

Although being attractive, the idea of using delay differential equations, which look back at a non-infinitesimal past, may receive objections. To qualify the context explaining why one may have to use a variable's value further back in time than just the previous time step through delay differential equations, we may have to differentiate statistical approaches and dynamical approaches. Fundamentally, delay differential equations may be used not because the primitive equations have to look back in time by a non-infinitesimal time scale, but either (1) because the parameterization equations are based on some statistical approach to convective phenomena (e.g., after fitting a statistical model to observed data), or (2) because the parameterization's prognostic variables may not fully capture the microstate. If the scheme were to fully capture the microstate via the prognostic variable(s), one should not need to look into a past of finite time scale at all. The reason to look into a finite past is if the scheme has not properly captured the microstate so that it becomes necessary to use the past values of some variables (e.g., precipitation or other convective outcomes) in place of a proper dynamical representation of the current variables through partial differential equations. As an analogue, if one only knew the position of an object at time t it would be necessary to look at past values of the position to project the near future. But if one also knew the momentum (velocity) at time t then any past information on position would not be needed. This caveat suggests that the use of delay differential equations may require additional assessment.

6.3 Limitations

One of the main limitations is that this study only uses one CRM: WRF. It would be useful to test the results with other CRMs. Our results may also depend

on WRF model physics. So one should remain cautious about the validity of the results if other schemes were to be used in the CRM (e.g., microphysical scheme, turbulence scheme, boundary layer scheme). We tested some sensitivities to model physics choices in Chapter 2, and performances of various WRF parameterization schemes have been compared in previous studies [e.g. *Cohen et al.*, 2015], but much more remains to be tested.

The second main limitation of this thesis lies in the absence of observations. Since the CRM cannot be considered as truth, it is important to evaluate the CRM with observations. Similarly, the sensitivities of the GCM and SCM to various cold pool parameters (and in particular the cold pool number density) should be evaluated with observations, in particular in Chapters 4 and 5. In this thesis, the rare observations that are used for comparisons are from published studies about precipitation frequency. In Chapter 5, we could make use of precipitation data to compare with the sensitivity of precipitation frequency in the GCM in more details. We could also compare GCM results with observations of clouds, humidity and radiation. However, measuring the memory directly from observations (e.g., radar data) will probably be challenging and would deserve a full study.

The behaviour of convective memory could only be studied in a limited number of setups in this thesis. In particular, we only performed Radiative-Convective Equilibrium (RCE) simulations. It would be interesting to test our results either (1) when an imposed large-scale vertical velocity is added to the idealised simulations presented here, or (2) with more realistic setups, such as simulations of actual storms and quieter periods.

Our results showed the memory is essentially stored in the boundary layer (up to 700 hPa). But in the CRM simulations, which were conducted at 1 km grid spacing, we had to activate a boundary layer scheme. It would be worth repeating the homogenisation experiments at higher resolutions (e.g., 200 m) where the boundary layer scheme is not needed.

6.4 Future work

6.4.1 Need for observations

Using observations to study convective memory is not straightforward. We have little intuition of how to use existing observations to do so. The response to homogenisation, which has been our proxy for memory, cannot be used with observations. Since the definition of microstate convective memory is based on the dependence of convection on itself for given large-scale conditions, one could build a statistical database of convective states and large-scale states, and assess the amplitude of the degree of freedom of convective states for a given value of the large-scale state. This idea of building a long series of convective states and large-scale states in observations has already been used by *Davies et al.* [2013b], but here we suggest to use it to study the degree of freedom due to the convective microstate. A potential method to gather complete convective datasets may be to use radar data combined with wind profilers and perhaps lidars, from which one can estimate the convective mass flux, the thermodynamic properties and the rain rate. For the large-scale state, reanalyses may be used as a starting point.

An analysis of past, present and future microstate and macrostate conditions, composited by the present value of the macrostate, could be used to capture the time evolution of the microstate and macrostate before and after a given large-scale condition, revealing the degree of freedom from another point of view. To achieve this, radar data, reanalyses, radiosondes, and ARM station data could be used.

Existing observations could also be used to assess the realism of the GCM and its sensitivity to cold pool number density (e.g., precipitation frequency maps, PDFs of rain). To check the realism of the CRM, one could try to compare the aforementioned composites with the homogenisation recoveries.

Observations from radars and satellites may be used to assess not only cold pool temperature, water vapour, and gust winds, but also cold pool number density and cold pool fractional surface area. We could make use of available observations in 0D, 1D, 2D and 3D, although 2D and 3D observations of cold pools still remain

challenging.

6.4.2 Need for high-resolution simulations

To complete the observations, and test specific ideas, it is necessary to use high-resolution simulations. While idealised experiments provide a good setup to carry out experiments and provide general process knowledge, it would be complementary to test the validity of our results in more realistic simulations as well (e.g., simulations based on CINDY-DYNAMO, TWP-ICE, TOGA-COARE).

The more direct idealised experiments that could be conducted to follow up on the results presented in the thesis include various tests of the knowledge constructed through the thesis, ordered from the highest priority to the lowest priority:

- We could test the sensitivity of our CRM results obtained from the RCE setup to a large-scale vertical velocity forcing (ω). Different values of ω will allow to model more intense convection than in RCE, which may be relevant for real storms.
- Homogenisation experiments are strong perturbations where the existing microstate of some variables is completely removed. More realistic perturbations would be useful to replace homogenisation. For example, one may want to run three types of control run: one in RCE, one with imposed upward large-scale vertical velocity (intense deep convective case), and one with imposed downward large-scale vertical velocity (shallow convective case). Then one could extract a macrostate (mean state) and a microstate (noise, or local perturbation) in each three case. Instead of homogenising, the initial perturbation could be to swap noise regimes, i.e., swapping the microstates (without swapping the macrostates). This way, one could analyse (1) the memory of intense deep convection for a growth from shallow to intense deep convection, as well as (2) the memory of shallow convection for a decay from intense deep to shallow convection.
- Results from Chapter 2 show that the main storage of convective memory is in the boundary layer structures. As a result, we would like to repeat the

homogenisation experiments at LES resolution (e.g. 200 m) instead of 1 km resolution, allowing to dispose of the boundary layer scheme, in order to see whether the dominance of the boundary layer over the free troposphere in terms of memory storage holds.

- Instead of homogenising, we could also introduce perturbations by applying a spatial filter to the microstate. By varying the typical length scale of the low-frequency spatical filter, we could determine the horizontal scale of the processes or structures leading to memory, and compare our results with those by *Stirling and Petch* [2004] and by *Davies et al.* [2013a].
- It would be interesting to conduct an in-depth study of cold pools in the CRM control runs presented in Chapter 2. In particular, we could perform a clustering analysis of the cold pools, to analyse more precisely their geometric and thermodynamic properties, including cold pool number density and cold pool fractional surface area.
- Instead of only homogenising the direct WRF prognostic variables, one could define the perturbations on diagnostic variables, such as rain evaporation. Homogenising these diagnostic variables would have impact on various WRF prognostic variable structures, and could be used to restart the model with this new state. One could then compare processes and see whether memory can be indirectly stored in these diagnostic variables.
- We would also like to assess the sensitivity of the wind shear case results (Chapter 2) to wind shear strength and height, similarly to *Robe and Emanuel* [2001].

6.4.3 Need for low-resolution climate simulations

Low-resolution climate models are the best tool to make projections of future climate and to understand past and present global climate. They are useful to test how independent processes which we understand individually behave when all interactions are allowed. But they can also be used for simple experiments. For example, a 1D version of a GCM can be a useful testbed for convective parameterizations,

and to allow comparisons between different formulations. The 3D version is suited for attempts to assess how simple ideas behave in a fully interactive context.

The direct follow-up experiments from what was presented in the thesis include the following options, ordered from the highest priority to the lowest priority.

- To analyse aspects of the large-scale influence of sub-grid scale (microstate) properties, we would like to investigate not only the influence of cold pool number density on the rainfall frequency but also on the MJO. We could first conduct the CLIVAR MJO diagnostics on the different 3D simulations with different cold pool number density presented in Subsection 5.3.5. Changing the memory through cold pool number density may help improve the MJO.
- The next step to significantly improve the memory of the LMDZ GCM is to turn the cold pool number density parameter into a prognostic variable. This would allow to model a full cold pool population dynamics, which would then allow to advect cold pools properties more realistically from a grid cell to an adjacent one. It would also satisfy the requirement defended in this thesis that memory is best improved by adding a prognostic variable representing low-level thermodynamic variables (cold pools in this case).
- Lobotomy experiments with LMDZ would be an intriguing way to test the characteristics of memory in LMDZ and to know where the memory in LMDZ mostly comes from. This means using different versions of LMDZ that have more or less memory, and repeating the 1D pseudo-homogenisation experiments with each of them. The different versions of the model in decreasing ability for memory (increasing lobotomy) could be: (1) With prognostic cold pool number density variable, (2) With default cold pool number density parameter, (3) With 100 times larger cold pool number density parameter, (4) With partly deactivated prognostic cold pool scheme (turning any of the three cold pool prognostic variable into a diagnostic one), (5) With fully deactivated prognostic cold pool scheme. These experiments would allow to assess in which variable the LMDZ memory is mostly stored, and to find out which version of the model compares best with the CRM.
- We carried out fixed-macrostate experiments in the CRM and in the predator-

prey model, to isolate microstate memory, and to understand the basic physical process behind it (Chapter 3). It would also be useful to perform the fixed-macrostate experiments in the 1D version of LMDZ. This would allow to test whether the single-column model is able to capture the instability of the microstate. This would be a good test to verify the realism of the currently parameterized microstate.

- One could also investigate the macrostate memory in LMDZ, for example by studying the effect of a sudden large-scale imposed perturbation on convection. For example one could study the response time scale when the large-scale conditions are suddenly modified by a step-wise change, such as a dry or moist intrusion, or a change in large-scale vertical velocity forcing from zero in RCE to a non-zero value (either positive or negative). This would be useful not only in terms of memory, but also in terms of sensitivity of the parameterized convection to the large-scale forcing (steady state thinking). This may be related to *Kuang* [2010]. Note that it would be interesting to then further investigate the macrostate memory and the scheme sensitivity not only with the default model, but also with different versions of the model with more or less memory. This would mean repeating the lobotomy experiments for a macrostate perturbation instead of a microstate perturbation.
- We could use the knowledge obtained from the clustering analysis of the CRM cold pools to inform more precisely the realistic range of values for cold pool number density and cold pool fractional surface area over land and over ocean, in the tropics and in the extra-tropics. This would be useful for the 1D model development part.

6.4.4 Need for theoretical framework, and simplified models

Simplified models may be one of the most important parts of science, since they allow us to build understanding, to test and validate our ideas, or to disprove theories by comparing with observations. Comprehensive models are useful to make predictions as accurate as possible, but they are in general too difficult to comprehend. Conversely, simple models allow us to develop intuition, which can then be

used to deal with new problems or with increasingly more subtle problems. While simplified models are best tailored to understand processes, comprehensive models are best tailored to make the best predictions.

Here we have made an attempt to build a simple model for convective memory with the predator-prey model. This allowed to bring more understanding into the CRM instability. This predator-prey model could be expanded in different ways.

- Instead of using a fixed forcing by a constant evaporation E_0 , we could use a varying forcing representing the large-scale vertical velocity forcing (Ω) coming from synoptic waves or other forms of large-scale circulation patterns. This would allow to investigate the role of microstate convective memory and macrostate convective memory in a more realistic situation, where the large-scale forcing also varies.
- The predator-prey model has three equations and three variables, which means that CAPE and humidity are represented in a single variable. But the CRM experiments showed that the microstate instability only occurs when both water vapour and temperature macrostates are held fixed. Therefore, introducing a fourth equation, by separating a more temperature-based variable (e.g., CAPE or temperature itself) and a more water vapour-based variable (e.g., precipitable water, or boundary layer water vapour) could allow to conduct three types of fixed-macrostate experiments and compare with the CRM results: fixed-macrostate temperature only, fixed-macrostate water vapour only, and fixed-macrostate for both. This would allow to verify that it is the existence of at least one thermodynamic macrostate degree of freedom that prevents the instability in a coupled microstate-macrostate situation.
- One could test the behaviour of the predator-prey model with various forms of stochastic terms, and various associated PDFs.
- One could repeat the pseudo-homogenisation experiments not only in our predator-prey model, but also in the toy models developed by *Yano and Plant* [2012a] and *Davies et al.* [2009]. Are all types of models for convective memory leading to similar conclusions?

6.5 Final words: what to remember?

Figure 6.1 presents a humble attempt to summarise the meaning of macrostate memory and microstate memory in a convective parameterization, which may not capture our thinking perfectly, but still tries to convey the combined effect of microstate memory and traditional macrostate adjustment based on a diagnostic quasi-equilibrium.

The actual trajectory in Figure 6.1(b) is different from in 6.1(a), because of the introduction of microstate memory. If convection were to be diagnosed by an equilibrium with the large-scale forcing, it would only be sensitive to the recent history of the forcing. With a prognostic formulation, not only do we have non-equilibrium convection, but convection is also made sensitive to its own history. That is why these convective schemes can be said to have “convective memory”.

If one had to choose one motto for this thesis, it may be:

Keeping microstate memory
makes the model happy!

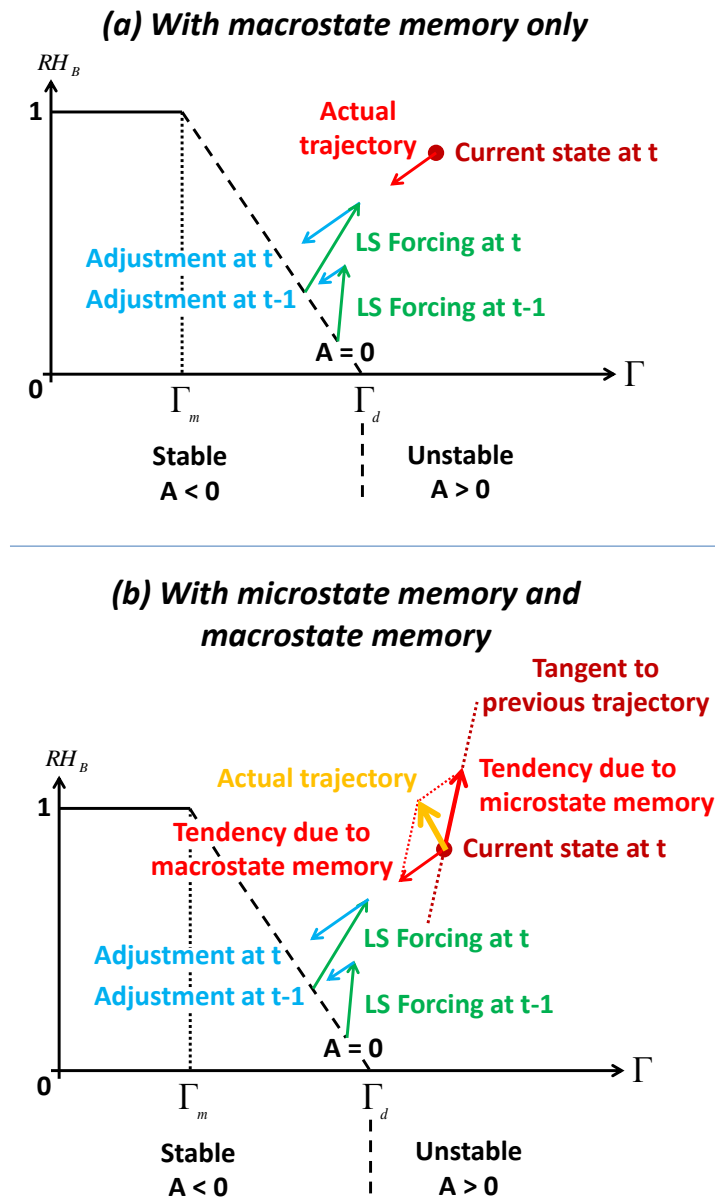


Figure 6.1 Schematics of the meaning of microstate memory and macrostate memory for (a) a parameterization which only has macrostate memory (b) a parameterization which has both microstate memory and macrostate memory. These two schematics are presented as an evolution of the quasi-equilibrium schematic presented in *Arakawa* [2004]’s figure 7 to incorporate convective memory. The x-axis is the lapse rate, the y-axis is the relative humidity of the boundary layer, and A is the cloud work function. $A > 0$ means the atmosphere is conditionally stable, and $A < 0$ conditionally unstable. The large-scale forcings at $t-1$ and at t are represented by green arrows. The resulting instantaneous adjustments (based on quasi-equilibrium or not) are the blue arrows. Note that green and red arrows are considered as vectors, so that their initial point is not important. The red dot represents the current state of the system. In (a), the actual trajectory is following a weighted mean of the adjustments at t and at $t-1$, so the macrostate at $t-1$ is remembered, which gives the system some macrostate memory. In (b), the weighted mean of the adjustments at t and $t-1$ gives a tendency due to macrostate memory, but there is also a tendency due to microstate memory, since the system now has some microstate inertia and tends to follow the tangent to its trajectory in the phase space. In this case, the actual trajectory followed by the system is the combination of both macrostate tendency and microstate tendency, as represented by the composition of the two vectors.

Bibliography

- Anber, U., S. Wang, and A. Sobel (2014), Response of atmospheric convection to vertical wind shear: Cloud-system-resolving simulations with parameterized large-scale circulation. Part I: Specified radiative cooling, *Journal of the Atmospheric Sciences*, *71*(8), 2976–2993, doi:10.1175/JAS-D-13-0320.1.
- Arakawa, A. (2004), The cumulus parameterization problem: Past, present, and future, *Journal of Climate*, *17*(13), 2493–2525, doi:10.1175/1520-0442(2004)017<2493:RATCPP>2.0.CO;2.
- Arakawa, A., and W. H. Schubert (1974), Interaction of a cumulus cloud ensemble with the large-scale environment, part I, *Journal of the Atmospheric Sciences*, *31*(3), 674–701, doi:10.1175/1520-0469(1974)031<0674:IOACCE>2.0.CO;2.
- Arneodo, A., P. Coulet, and C. Tresser (1980), Occurrence of strange attractors in three-dimensional Volterra equations, *Physics Letters*, *79A*.
- Bao, J., S. C. Sherwood, M. Colin, and V. Dixit (2017), The robust relationship between extreme precipitation and convective organization in idealized numerical modeling simulations, *Journal of Advances in Modeling Earth Systems*, *9*(6), 2291–2303, doi:10.1002/2017MS001125.
- Bechtold, P., N. Semane, P. Lopez, J.-P. Chaboureaud, A. Beljaars, and N. Bormann (2014), Representing equilibrium and nonequilibrium convection in large-scale models, *Journal of the Atmospheric Sciences*, *71*(2), 734–753, doi:10.1175/JAS-D-13-0163.1.
- Becker, T., B. Stevens, and C. Hohenegger (2017), Imprint of the convective parameterization and sea-surface temperature on large-scale convective self-

BIBLIOGRAPHY

- aggregation, *Journal of Advances in Modeling Earth Systems*, *9*(2), 1488–1505, doi:10.1002/2016MS000865.
- Bergé, P., and M. Dubois (1984), Rayleigh-Bénard convection, *Contemporary Physics*, *25*(6), 535–582, doi:10.1080/00107518408210730.
- Betts, A. K., and M. J. Miller (1986), A new convective adjustment scheme. Part II: Single column tests using GATE wave, BOMEX, ATEX and arctic air-mass data sets, *Quarterly Journal of the Royal Meteorological Society*, *112*(473), 693–709, doi:10.1002/qj.49711247308.
- Bogenschutz, P. A., A. Gettelman, H. Morrison, V. E. Larson, D. P. Schanen, N. R. Meyer, and C. Craig (2012), Unified parameterization of the planetary boundary layer and shallow convection with a higher-order turbulence closure in the Community Atmosphere Model: single-column experiments, *Geoscientific Model Development*, *5*(6), 1407–1423, doi:10.5194/gmd-5-1407-2012.
- Bogenschutz, P. A., A. Gettelman, H. Morrison, V. E. Larson, C. Craig, and D. P. Schanen (2013), Higher-order turbulence closure and its impact on climate simulations in the Community Atmosphere Model, *Journal of Climate*, *26*(23), 9655–9676, doi:10.1175/JCLI-D-13-00075.1.
- Bony, S., and K. A. Emanuel (2005), On the role of moist processes in tropical intraseasonal variability: Cloud–radiation and moisture–convection feedbacks, *Journal of the Atmospheric Sciences*, *62*(8), 2770–2789, doi:10.1175/JAS3506.1.
- Bony, S., B. Stevens, D. M. W. Frierson, C. Jakob, M. Kageyama, R. Pincus, T. G. Shepherd, S. C. Sherwood, A. P. Siebesma, A. H. Sobel, M. Watanabe, and M. J. Webb (2015), Clouds, circulation and climate sensitivity, *Nature Geosci*, *8*(4), 261–268, perspective.
- Bougeault, P., and J. F. Geleyn (1989), Some problems of closure assumption and scale dependency in the parameterization of moist deep convection for numerical weather prediction, *Meteorology and Atmospheric Physics*, *40*(1), 123–135, doi:10.1007/BF01027471.

- Bretherton, C. S., P. N. Blossey, and M. Khairoutdinov (2005), An energy-balance analysis of deep convective self-aggregation above uniform SST, *Journal of the Atmospheric Sciences*, *62*(12), 4273–4292, doi:10.1175/JAS3614.1.
- Bryan, G. H., R. Rotunno, and J. M. Fritsch (2007), Roll circulations in the convective region of a simulated squall line, *Journal of the Atmospheric Sciences*, *64*(4), 1249–1266, doi:10.1175/JAS3899.1.
- Chaboureau, J.-P., F. Guichard, J.-L. Redelsperger, and J.-P. Lafore (2004), The role of stability and moisture in the diurnal cycle of convection over land, *Quarterly Journal of the Royal Meteorological Society*, *130*(604), 3105–3117, doi:10.1256/qj.03.132.
- Chang, C.-P., Y.-T. Yang, and H.-C. Kuo (2013), Large increasing trend of tropical cyclone rainfall in Taiwan and the roles of terrain, *Journal of Climate*, *26*(12), 4138–4147, doi:10.1175/JCLI-D-12-00463.1.
- Chen, D., and P. Bougeault (1993), A simple prognostic closure assumption to deep convective parameterization: I, *Acta Meteorologica Sinica*, *1*, 1–18.
- Chepfer, H., S. Bony, D. Winker, M. Chiriaco, J.-L. Dufresne, and G. Sèze (2008), Use of CALIPSO lidar observations to evaluate the cloudiness simulated by a climate model, *Geophysical Research Letters*, *35*(15), n/a–n/a, doi:10.1029/2008GL034207, 115704.
- CLIVAR Madden-Julian Oscillation Working Group: Waliser, D., K. Sperber, H. Hendon, D. Kim, E. Maloney, M. Wheeler, K. Weickmann, C. Zhang, L. Donner, J. Gottschalck, W. Higgins, I.-S. Kang, D. Legler, M. Moncrieff, S. Schubert, W. Stern, F. Vitart, W. B., W. Wang, and S. Woolnough (2009), MJO simulation diagnostics, *Journal of Climate*, *22*(11), 3006–3030, doi:10.1175/2008JCLI2731.1.
- Cohen, A. E., S. M. Cavallo, M. C. Coniglio, and H. E. Brooks (2015), A review of planetary boundary layer parameterization schemes and their sensitivity in simulating Southeastern U.S. cold season severe weather environments, *Weather and Forecasting*, *30*(3), 591–612, doi:10.1175/WAF-D-14-00105.1.

BIBLIOGRAPHY

- Cohen, B. G., and G. C. Craig (2004), The response time of a convective cloud ensemble to a change in forcing, *Quarterly Journal of the Royal Meteorological Society*, *130*(598), 933–944, doi:10.1256/qj.02.218.
- Coppin, D., and S. Bony (2015), Physical mechanisms controlling the initiation of convective self-aggregation in a General Circulation Model, *Journal of Advances in Modeling Earth Systems*, *7*(4), 2060–2078, doi:10.1002/2015MS000571.
- Cronin, T. W. (2014), On the choice of average solar zenith angle, *Journal of the Atmospheric Sciences*, *71*(8), 2994–3003, doi:10.1175/JAS-D-13-0392.1.
- Dai, A. (2006), Precipitation characteristics in eighteen coupled climate models, *Journal of Climate*, *19*(18), 4605–4630, doi:10.1175/JCLI3884.1.
- Davies, L. (2008), Self organisation of convection as a mechanism for memory, Ph.D. thesis, University of Reading.
- Davies, L., R. S. Plant, and S. H. Derbyshire (2009), A simple model of convection with memory, *Journal of Geophysical Research: Atmospheres*, *114*(D17), n/a–n/a, doi:10.1029/2008JD011653.
- Davies, L., R. S. Plant, and S. H. Derbyshire (2013a), Departures from convective equilibrium with a rapidly varying surface forcing, *Quarterly Journal of the Royal Meteorological Society*, *139*(676), 1731–1746, doi:10.1002/qj.2065.
- Davies, L., C. Jakob, P. May, V. V. Kumar, and S. Xie (2013b), Relationships between the large-scale atmosphere and the small-scale convective state for Darwin, Australia, *Journal of Geophysical Research: Atmospheres*, *118*(20), 11,534–11,545, doi:10.1002/jgrd.50645.
- de Rooy, W. C., P. Bechtold, K. Fröhlich, C. Hohenegger, H. Jonker, D. Mironov, A. Pier Siebesma, J. Teixeira, and J.-I. Yano (2013), Entrainment and detrainment in cumulus convection: an overview, *Quarterly Journal of the Royal Meteorological Society*, *139*(670), 1–19, doi:10.1002/qj.1959.
- de Szoeke, S. P., E. D. Skyllingstad, P. Zuidema, and A. S. Chandra (2017), Cold pools and their influence on the tropical marine boundary layer, *Journal of the Atmospheric Sciences*, *74*(4), 1149–1168, doi:10.1175/JAS-D-16-0264.1.

- Del Genio, A. D., J. Wu, and Y. Chen (2012), Characteristics of mesoscale organization in WRF simulations of convection during TWP-ICE, *Journal of Climate*, *25*(17), 5666–5688, doi:10.1175/JCLI-D-11-00422.1.
- Del Genio, A. D., J. Wu, A. B. Wolf, Y. Chen, M.-S. Yao, and D. Kim (2015), Constraints on cumulus parameterization from simulations of observed MJO events, *Journal of Climate*, *28*(16), 6419–6442, doi:10.1175/JCLI-D-14-00832.1.
- Derbyshire, S. H., I. Beau, P. Bechtold, J.-Y. Grandpeix, J.-M. Piriou, J.-L. Redelsperger, and P. Soares (2004), Sensitivity of moist convection to environmental humidity, *Quarterly Journal of the Royal Meteorological Society*, *130*(604), 3055–3079.
- Donner, L. J., C. J. Seman, R. S. Hemler, and S. Fan (2001), A cumulus parameterization including mass fluxes, convective vertical velocities, and mesoscale effects: Thermodynamic and hydrological aspects in a general circulation model, *Journal of Climate*, *14*(16), 3444–3463, doi:10.1175/1520-0442(2001)014<3444:ACPIMF>2.0.CO;2.
- Emanuel, K. (1993), The effect of convective response time on WISHE modes, *Journal of the Atmospheric Sciences*, *50*(12), 1763–1776, doi:10.1175/1520-0469(1993)050<1763:TEOCRT>2.0.CO;2.
- Emanuel, K. (2005), Increasing destructiveness of tropical cyclones over the past 30 years, *Nature*, *436*(7051), 686–688, doi:10.1038/nature03906.
- Emanuel, K., A. A. Wing, and E. M. Vincent (2014), Radiative-convective instability, *Journal of Advances in Modeling Earth Systems*, *6*(1), 75–90, doi:10.1002/2013MS000270.
- Emanuel, K. A. (1991), A scheme for representing cumulus convection in large-scale models, *Journal of the Atmospheric Sciences*, *48*(21), 2313–2329, doi:10.1175/1520-0469(1991)048<2313:ASFRCC>2.0.CO;2.
- Emanuel, K. A. (1994), *Atmospheric Convection*, Oxford University Press, New York.

BIBLIOGRAPHY

- Emanuel, K. A. (1997), Overview of atmospheric convection, in *The physics and parameterization of moist atmospheric convection*, edited by R. K. Smith, pp. 1–28, Kluwer Academic Publishers.
- Emanuel, K. A., J. David Neelin, and C. S. Bretherton (1994), On large-scale circulations in convecting atmospheres, *Quarterly Journal of the Royal Meteorological Society*, *120*(519), 1111–1143, doi:10.1002/qj.49712051902.
- Emanuel, K. A., and M. Živković Rothman (1999), Development and evaluation of a convection scheme for use in climate models, *Journal of the Atmospheric Sciences*, *56*(11), 1766–1782, doi:10.1175/1520-0469(1999)056<1766:DAEOAC>2.0.CO;2.
- Feingold, G., I. Koren, T. Yamaguchi, and J. Kazil (2015), On the reversibility of transitions between closed and open cellular convection, *Atmospheric Chemistry and Physics*, *15*(13), 7351–7367, doi:10.5194/acp-15-7351-2015.
- Feng, Z., S. Hagos, A. K. Rowe, C. D. Burleyson, M. N. Martini, and S. P. de Szoeke (2015), Mechanisms of convective cloud organization by cold pools over tropical warm ocean during the AMIE/DYNAMO field campaign, *Journal of Advances in Modeling Earth Systems*, *7*(2), 357–381, doi:10.1002/2014MS000384.
- Folkens, I., T. Mitovski, and J. R. Pierce (2014), A simple way to improve the diurnal cycle in convective rainfall over land in climate models, *Journal of Geophysical Research: Atmospheres*, *119*(5), 2113–2130, doi:10.1002/2013JD020149.
- Garcia, O. E., and N. H. Bian (2003), Bursting and large-scale intermittency in turbulent convection with differential rotation, *Phys. Rev. E*, *68*, 047,301, doi:10.1103/PhysRevE.68.047301.
- Golaz, J.-C., V. E. Larson, and W. R. Cotton (2002), A PDF-based model for boundary layer clouds. Part I: Method and model description, *Journal of the Atmospheric Sciences*, *59*(24), 3540–3551, doi:10.1175/1520-0469(2002)059<3540:APBMFB>2.0.CO;2.
- Grabowski, W. W. (2004), An improved framework for superparameterization, *Journal of the Atmospheric Sciences*, *61*(15), 1940–1952, doi:10.1175/1520-0469(2004)061<1940:AIFFS>2.0.CO;2.

- Grabowski, W. W., and P. K. Smolarkiewicz (1999), CRCP: a Cloud Resolving Convection Parameterization for modeling the tropical convecting atmosphere, *Physica D: Nonlinear Phenomena*, *133*(1), 171 – 178, doi:[https://doi.org/10.1016/S0167-2789\(99\)00104-9](https://doi.org/10.1016/S0167-2789(99)00104-9).
- Grandpeix, J.-Y., and J.-P. Lafore (2010), A density current parameterization coupled with Emanuel’s convection scheme. Part I: The models, *Journal of the Atmospheric Sciences*, *67*(4), 881–897, doi:10.1175/2009JAS3044.1.
- Grandpeix, J.-Y., J.-P. Lafore, and F. Cheruy (2010), A density current parameterization coupled with Emanuel’s convection scheme. Part II: 1D simulations, *Journal of the Atmospheric Sciences*, *67*(4), 898–922, doi:10.1175/2009JAS3045.1.
- Grant, L. D., and S. C. van den Heever (2014), Microphysical and dynamical characteristics of low-precipitation and classic supercells, *Journal of the Atmospheric Sciences*, *71*(7), 2604–2624, doi:10.1175/JAS-D-13-0261.1.
- Gregory, D., J.-J. Morcrette, C. Jakob, A. C. M. Beljaars, and T. Stockdale (2000), Revision of convection, radiation and cloud schemes in the ECMWF Integrated Forecasting System, *Quarterly Journal of the Royal Meteorological Society*, *126*(566), 1685–1710, doi:10.1002/qj.49712656607.
- Grell, G. A. (1993), Prognostic evaluation of assumptions used by cumulus parameterizations, *Monthly Weather Review*, *121*(3), 764–787, doi:10.1175/1520-0493(1993)121<0764:PEOAUB>2.0.CO;2.
- Guérémy, J. F. (2011), A continuous buoyancy based convection scheme: one- and three-dimensional validation, *Tellus A*, *63*(4), 687–706, doi:10.1111/j.1600-0870.2011.00521.x.
- Hagos, S., and R. Houze (2016), Atmospheric system research. Treatment of convection in next-generation climate models: Challenges and opportunities., *Workshop report DOE/SC-ASR-16-002*, U.S. Department of Energy, Office of Science, Atmospheric System Research, <https://asr.science.energy.gov/publications/program-docs/doe-sc-asr-16-002.pdf>.

BIBLIOGRAPHY

- Held, I. M., R. S. Hemler, and V. Ramaswamy (1993), Radiative-convective equilibrium with explicit two-dimensional moist convection, *Journal of the Atmospheric Sciences*, *50*(23), 3909–3927, doi:10.1175/1520-0469(1993)050<3909:RCEWET>2.0.CO;2.
- Herold, N., L. V. Alexander, M. G. Donat, S. Contractor, and A. Becker (2016), How much does it rain over land?, *Geophysical Research Letters*, *43*(1), 341–348, doi:10.1002/2015GL066615.
- Hohenegger, C., and B. Stevens (2012), Preconditioning deep convection with cumulus congestus, *Journal of the Atmospheric Sciences*, *70*(2), 448–464, doi:10.1175/JAS-D-12-089.1.
- Holloway, C. E., A. A. Wing, S. Bony, C. Muller, H. Masunaga, T. S. L’Ecuyer, D. D. Turner, and P. Zuidema (2017), Observing convective aggregation, *Surveys in Geophysics*, doi:10.1007/s10712-017-9419-1.
- Holmes, E. E., M. A. Lewis, J. E. Banks, and R. R. Veit (1994), Partial differential equations in ecology: Spatial interactions and population dynamics, *Ecology*, *75*(1), 17–29, doi:10.2307/1939378.
- Hong, S.-Y., and J.-O. J. Lim (2006), The WRF single-moment 6-class microphysics scheme (WSM6), *Journal of the Korean Meteorological Society*, *42*(2), 129–151.
- Hourdin, F., J.-Y. Grandpeix, C. Rio, S. Bony, A. Jam, F. Cheruy, N. Rochetin, L. Fairhead, A. Idelkadi, I. Musat, J.-L. Dufresne, A. Lahellec, M.-P. Lefebvre, and R. Roehrig (2013), LMDZ5B: the atmospheric component of the IPSL climate model with revisited parameterizations for clouds and convection, *Climate Dynamics*, *40*(9), 2193–2222, doi:10.1007/s00382-012-1343-y.
- Houze, R. A. (1977), Structure and dynamics of a tropical squall-line system, *Monthly Weather Review*, *105*(12), 1540–1567, doi:10.1175/1520-0493(1977)105<1540:SADOAT>2.0.CO;2.
- Houze, R. A. (2004), Mesoscale convective systems, *Reviews of Geophysics*, *42*(4), n/a–n/a, doi:10.1029/2004RG000150.

- Hu, Q., and D. A. Randall (1995), Low-frequency oscillations in radiative-convective systems. Part II: An idealized model, *Journal of the Atmospheric Sciences*, *52*(4), 478–490, doi:10.1175/1520-0469(1995)052<0478:LFOIRC>2.0.CO;2.
- Jakob, C. (2014), Going back to basics, *Nature Climate Change*, *4*, 1042 EP –.
- Jeevanjee, N., and D. M. Romps (2013), Convective self-aggregation, cold pools, and domain size, *Geophysical Research Letters*, *40*(5), 994–998, doi:10.1002/grl.50204.
- Jiang, X., D. E. Waliser, P. K. Xavier, J. Petch, N. P. Klingaman, S. J. Woolnough, B. Guan, G. Bellon, T. Crueger, C. DeMott, C. Hannay, H. Lin, W. Hu, D. Kim, C.-L. Lappen, M.-M. Lu, H.-Y. Ma, T. Miyakawa, J. A. Ridout, S. D. Schubert, J. Scinocca, K.-H. Seo, E. Shindo, X. Song, C. Stan, W.-L. Tseng, W. Wang, T. Wu, X. Wu, K. Wyser, G. J. Zhang, and H. Zhu (2015), Vertical structure and physical processes of the Madden-Julian oscillation: Exploring key model physics in climate simulations, *Journal of Geophysical Research: Atmospheres*, *120*(10), 4718–4748, doi:10.1002/2014JD022375, 2014JD022375.
- Jiménez, P. A., J. Dudhia, J. F. González-Rouco, J. Navarro, J. P. Montávez, and E. García-Bustamante (2012), A revised scheme for the WRF surface layer formulation, *Monthly Weather Review*, *140*(3), 898–918, doi:10.1175/MWR-D-11-00056.1.
- Jones, T. R., and D. A. Randall (2011), Quantifying the limits of convective parameterizations, *Journal of Geophysical Research: Atmospheres*, *116*(D8), n/a–n/a, doi:10.1029/2010JD014913.
- Kain, J. S., and J. M. Fritsch (1990), A one-dimensional entraining/detraining plume model and its application in convective parameterization, *Journal of the Atmospheric Sciences*, *47*(23), 2784–2802, doi:10.1175/1520-0469(1990)047<2784:AODEPM>2.0.CO;2.
- Khouider, B., and A. J. Majda (2006), Multicloud convective parametrizations with crude vertical structure, *Theoretical and Computational Fluid Dynamics*, *20*(5), 351–375, doi:10.1007/s00162-006-0013-2.

BIBLIOGRAPHY

- Koren, I., and G. Feingold (2011), Aerosol–cloud–precipitation system as a predator–prey problem, *Proceedings of the National Academy of Sciences*, *108*(30), 12,227–12,232, doi:10.1073/pnas.1101777108.
- Krishnamurti, T. N., R. Krishnamurti, A. Simon, A. Thomas, and V. Kumar (2016), A mechanism of the MJO invoking scale interactions, *Meteorological Monographs*, *56*, 5.1–5.16, doi:10.1175/AMSMONOGRAPHS-D-15-0009.1.
- Kuang, Z. (2010), Linear response functions of a cumulus ensemble to temperature and moisture perturbations and implications for the dynamics of convectively coupled waves, *Journal of the Atmospheric Sciences*, *67*(4), 941–962, doi:10.1175/2009JAS3260.1.
- Langhans, W., and D. M. Romps (2015), The origin of water vapor rings in tropical oceanic cold pools, *Geophysical Research Letters*, *42*(18), 7825–7834, doi:10.1002/2015GL065623, 2015GL065623.
- Langhans, W., J. Schmidli, O. Fuhrer, S. Bieri, and C. Schar (2013), Long-term simulations of thermally driven flows and orographic convection at convection-parameterizing and cloud-resolving resolutions, *Journal of Applied Meteorology and Climatology*, *52*(6), 1490–1510, doi:10.1175/JAMC-D-12-0167.1.
- Legras, B. (updated 2016), Moist convective instability and organisation of convection, or circulation générale et météorologie, Lecture notes for Masters M2 OACOS. <http://www.lmd.ens.fr/legras/>.
- Liu, W. T., W. Tang, and P. P. Niiler (1991), Humidity profiles over the ocean, *Journal of Climate*, *4*(10), 1023–1034, doi:10.1175/1520-0442(1991)004<1023:HPOTO>2.0.CO;2.
- Lord, S. J., W. C. Chao, and A. Arakawa (1982), Interaction of a cumulus cloud ensemble with the large-scale environment. Part IV: The discrete model, *Journal of the Atmospheric Sciences*, *39*(1), 104–113, doi:10.1175/1520-0469(1982)039<0104:IOACCE>2.0.CO;2.
- Lothon, M., B. Campistron, M. Chong, F. Couvreux, F. Guichard, C. Rio, and E. Williams (2011), Life cycle of a mesoscale circular gust front observed by a C-

- band Doppler radar in West Africa, *Monthly Weather Review*, *139*(5), 1370–1388, doi:10.1175/2010MWR3480.1.
- Mapes, B., and R. Neale (2011), Parameterizing convective organization to escape the entrainment dilemma, *Journal of Advances in Modeling Earth Systems*, *3*, 20 pp., doi:10.1029/2011MS000042, art. M06004.
- Mapes, B., R. Milliff, and J. Morzel (2009), Composite life cycle of maritime tropical mesoscale convective systems in scatterometer and microwave satellite observations, *Journal of the Atmospheric Sciences*, *66*(1), 199–208, doi:10.1175/2008JAS2746.1.
- Mapes, B. E. (1997), Equilibrium vs. activation control of large-scale variations of tropical deep convection, in *The physics and parameterization of moist atmospheric convection*, edited by R. K. Smith, pp. 321–358, Kluwer Academic Publishers.
- Marsham, J. H., and D. J. Parker (2006), Secondary initiation of multiple bands of cumulonimbus over southern Britain. II: Dynamics of secondary initiation, *Quarterly Journal of the Royal Meteorological Society*, *132*(617), 1053–1072, doi:10.1256/qj.05.152.
- Marsham, J. H., M. Hobby, C. J. T. Allen, J. R. Banks, M. Bart, B. J. Brooks, C. Cavazos-Guerra, S. Engelstaedter, M. Gascoyne, A. R. Lima, J. V. Martins, J. B. McQuaid, A. O’Leary, B. Ouchene, A. Ouladichir, D. J. Parker, A. Saci, M. Salah-Ferroudj, M. C. Todd, and R. Washington (2013), Meteorology and dust in the central Sahara: Observations from Fennec supersite-1 during the June 2011 Intensive Observation Period, *Journal of Geophysical Research: Atmospheres*, *118*(10), 4069–4089, doi:10.1002/jgrd.50211.
- Masunaga, H. (2012), Short-term versus climatological relationship between precipitation and tropospheric humidity, *Journal of Climate*, *25*(22), 7983–7990, doi:10.1175/JCLI-D-12-00037.1.
- Masunaga, H., and Y. Sumi (2017), A toy model of tropical convection with a moisture storage closure, *Journal of Advances in Modeling Earth Systems*, *9*(1), 647–667, doi:10.1002/2016MS000855.

BIBLIOGRAPHY

- Miller, M., and M. Moncrieff (1983), The use and implementation of dynamical cloud models in a parametrisation scheme for deep convection, in *Proc. Workshop on Convection in Large-Scale Numerical Models, Reading, UK, ECMWF*, pp. 33–65.
- Miyamoto, Y., Y. Kajikawa, R. Yoshida, T. Yamaura, H. Yashiro, and H. Tomita (2013), Deep moist atmospheric convection in a subkilometer global simulation, *Geophysical Research Letters*, *40*(18), 4922–4926, doi:10.1002/grl.50944.
- Moncrieff, M. W. (1981), A theory of organized steady convection and its transport properties, *Quarterly Journal of the Royal Meteorological Society*, *107*(451), 29–50, doi:10.1002/qj.49710745103.
- Moncrieff, M. W. (1992), Organized convective systems: Archetypal dynamical models, mass and momentum flux theory, and parametrization, *Quarterly Journal of the Royal Meteorological Society*, *118*(507), 819–850, doi:10.1002/qj.49711850703.
- Moorthi, S., and M. J. Suarez (1992), Relaxed Arakawa-Schubert. A parameterization of moist convection for general circulation models, *Monthly Weather Review*, *120*(6), 978–1002, doi:10.1175/1520-0493(1992)120<0978:RASAPO>2.0.CO;2.
- Morcrette, C. J., K. A. Browning, A. M. Blyth, K. E. Bozier, P. A. Clark, D. Ladd, E. G. Norton, and E. Pavelin (2006), Secondary initiation of multiple bands of cumulonimbus over southern britain. I: An observational case-study, *Quarterly Journal of the Royal Meteorological Society*, *132*(617), 1021–1051, doi:10.1256/qj.05.151.
- Moseley, C., C. Hohenegger, P. Berg, and J. O. Haerter (2016), Intensification of convective extremes driven by cloud-cloud interaction, *Nature Geoscience, advance online publication*, 748–752, doi:10.1038/ngeo2789, letter.
- Muller, C., and S. Bony (2015), What favors convective aggregation and why?, *Geophysical Research Letters*, *42*(13), 5626–5634, doi:10.1002/2015GL064260, 2015GL064260.
- Muller, C. J., and I. M. Held (2012), Detailed investigation of the self-aggregation

- of convection in cloud-resolving simulations, *Journal of the Atmospheric Sciences*, *69*(8), 2551–2565, doi:10.1175/JAS-D-11-0257.1.
- Nober, F. J., and H. F. Graf (2005), A new convective cloud field model based on principles of self-organisation, *Atmospheric Chemistry and Physics*, *5*(10), 2749–2759, doi:10.5194/acp-5-2749-2005.
- Ooyama, K. (1969), Numerical simulation of the life cycle of tropical cyclones, *Journal of the Atmospheric Sciences*, *26*(1), 3–40, doi:10.1175/1520-0469(1969)026<0003:NSOTLC>2.0.CO;2.
- Oueslati, B., and G. Bellon (2013), Convective entrainment and large-scale organization of tropical precipitation: Sensitivity of the CNRM-CM5 hierarchy of models, *Journal of Climate*, *26*(9), 2931–2946, doi:10.1175/JCLI-D-12-00314.1.
- Pan, D.-M., and D. D. A. Randall (1998), A cumulus parameterization with a prognostic closure, *Quarterly Journal of the Royal Meteorological Society*, *124*(547), 949–981, doi:10.1002/qj.49712454714.
- Panchev, S., and T. Spassova (2005), Simple general atmospheric circulation and climate models with memory, *Advances in Atmospheric Sciences*, *22*(5), 765–769, doi:10.1007/BF02918720.
- Park, S. (2014), A unified convection scheme (UNICON). Part I: Formulation, *Journal of the Atmospheric Sciences*, *71*(11), 3902–3930, doi:10.1175/JAS-D-13-0233.1.
- Parodi, A., and K. Emanuel (2009), A theory for buoyancy and velocity scales in deep moist convection, *Journal of the Atmospheric Sciences*, *66*, 3449–3463, doi:10.1175/2009JAS3103.1.
- Peters, K., C. Jakob, L. Davies, B. Khouider, and A. J. Majda (2013), Stochastic behavior of tropical convection in observations and a multcloud model, *Journal of the Atmospheric Sciences*, *70*(11), 3556–3575, doi:10.1175/JAS-D-13-031.1.
- Piriou, J.-M., J.-L. Redelsperger, J.-F. Geleyn, J.-P. Lafore, and F. Guichard (2007), An approach for convective parameterization with memory: Separating micro-

BIBLIOGRAPHY

- physics and transport in grid-scale equations, *Journal of the Atmospheric Sciences*, *64*, 4127–4139, doi:10.1175/2007JAS2144.1.
- Provod, M., J. H. Marsham, D. J. Parker, and C. E. Birch (2016), A characterization of cold pools in the West African Sahel, *Monthly Weather Review*, *144*(5), 1923–1934, doi:10.1175/MWR-D-15-0023.1.
- Qian, L., G. S. Young, and W. M. Frank (1998), A convective wake parameterization scheme for use in general circulation models, *Monthly Weather Review*, *126*(2), 456–469, doi:10.1175/1520-0493(1998)126<0456:ACWPSF>2.0.CO;2.
- Randall, D., and D. Pan (1993), Implementation of the Arakawa-Schubert cumulus parameterization with a prognostic closure, in *The Representation of Cumulus Convection in Numerical Models*, edited by K. Emanuel and D. Raymond, Meteorological Monographs, American Meteorological Society, Boston, MA, doi: https://doi.org/10.1007/978-1-935704-13-3_11.
- Randall, D., Q. Hu, K.-M. Xu, and S. Krueger (1994), Radiative-convective disequilibrium, *Atmospheric Research*, *31*(4), 315 – 327, doi:[http://dx.doi.org/10.1016/0169-8095\(94\)90006-X](http://dx.doi.org/10.1016/0169-8095(94)90006-X).
- Randall, D., M. Khairoutdinov, A. Arakawa, and W. Grabowski (2003), Breaking the cloud parameterization deadlock, *Bulletin of the American Meteorological Society*, *84*(11), 1547–1564, doi:10.1175/BAMS-84-11-1547.
- Randall, D., M. Branson, M. Wang, S. Ghan, C. Craig, A. Gettelman, and J. Edwards (2013), A Community Atmosphere Model with superparameterized clouds, *Eos, Transactions American Geophysical Union*, *94*(25), 221–222, doi: 10.1002/2013EO250001.
- Randall, D. A. (2013), Beyond deadlock, *Geophysical Research Letters*, *40*(22), 5970–5976, doi:10.1002/2013GL057998, 2013GL057998.
- Raymond, D. J. (1995), Regulation of moist convection over the West Pacific Warm Pool, *Journal of the Atmospheric Sciences*, *52*(22), 3945–3959, doi:10.1175/1520-0469(1995)052<3945:ROMCOT>2.0.CO;2.

- Raymond, D. J., and M. J. Herman (2011), Convective quasi-equilibrium reconsidered, *Journal of Advances in Modeling Earth Systems*, *3*(3), n/a–n/a, doi:10.1029/2011MS000079, m08003.
- Raymond, D. J., and Željka Fuchs (2009), Moisture modes and the Madden–Julian Oscillation, *Journal of Climate*, *22*(11), 3031–3046, doi:10.1175/2008JCLI2739.1.
- Rio, C., and F. Hourdin (2008), A thermal plume model for the convective boundary layer: Representation of cumulus clouds, *Journal of the Atmospheric Sciences*, *65*(2), 407–425, doi:10.1175/2007JAS2256.1.
- Rio, C., F. Hourdin, J.-Y. Grandpeix, and J.-P. Lafore (2009), Shifting the diurnal cycle of parameterized deep convection over land, *Geophysical Research Letters*, *36*(7), n/a–n/a, doi:10.1029/2008GL036779, l07809.
- Rio, C., J.-Y. Grandpeix, F. Hourdin, F. Guichard, F. Couvreux, J.-P. Lafore, A. Fridlind, A. Mrowiec, R. Roehrig, N. Rochetin, M.-P. Lefebvre, and A. Idelkadi (2013), Control of deep convection by sub-cloud lifting processes: the ALP closure in the LMDZ5B general circulation model, *Climate Dynamics*, *40*(9), 2271–2292, doi:10.1007/s00382-012-1506-x.
- Robe, F. R., and K. A. Emanuel (2001), The effect of vertical wind shear on Radiative-Convective Equilibrium states, *Journal of the Atmospheric Sciences*, *58*(11), 1427–1445, doi:10.1175/1520-0469(2001)058<1427:TEOVWS>2.0.CO;2.
- Rochetin, N., F. Couvreux, J.-Y. Grandpeix, and C. Rio (2014a), Deep convection triggering by boundary layer thermals. Part I: LES analysis and stochastic triggering formulation, *Journal of the Atmospheric Sciences*, *71*(2), 496–514, doi:10.1175/JAS-D-12-0336.1.
- Rochetin, N., J.-Y. Grandpeix, C. Rio, and F. Couvreux (2014b), Deep convection triggering by boundary layer thermals. Part II: Stochastic triggering parameterization for the LMDZ GCM, *Journal of the Atmospheric Sciences*, *71*(2), 515–538, doi:10.1175/JAS-D-12-0337.1.
- Romps, D. M. (2011), Response of tropical precipitation to global warming, *Journal of the Atmospheric Sciences*, *68*(1), 123–138, doi:10.1175/2010JAS3542.1.

BIBLIOGRAPHY

- Romps, D. M., and Z. Kuang (2010), Do undiluted convective plumes exist in the upper tropical troposphere?, *Journal of the Atmospheric Sciences*, *67*(2), 468–484, doi:10.1175/2009JAS3184.1.
- Rooney, G. G. (2015), Descent and spread of negatively buoyant thermals, *Journal of Fluid Mechanics*, *780*, 457–479, doi:10.1017/jfm.2015.484.
- Rotunno, R., J. B. Klemp, and M. L. Weisman (1988), A theory for strong, long-lived squall lines, *Journal of the Atmospheric Sciences*, *45*(3), 463–485, doi:10.1175/1520-0469(1988)045<0463:ATFSSL>2.0.CO;2.
- Rowe, A. K., and R. A. Houze (2015), Cloud organization and growth during the transition from suppressed to active MJO conditions, *Journal of Geophysical Research: Atmospheres*, *120*(19), 10,324–10,350, doi:10.1002/2014JD022948, 2014JD022948.
- Rozbicki, J. J., G. S. Young, and L. Qian (1999), Test of a convective wake parameterization in the single-column version of CCM3, *Monthly Weather Review*, *127*(6), 1347–1361, doi:10.1175/1520-0493(1999)127<1347:TOACWP>2.0.CO;2.
- Satoh, M., T. Matsuno, H. Tomita, H. Miura, T. Nasuno, and S. Iga (2008), Nonhydrostatic icosahedral atmospheric model (NICAM) for global cloud resolving simulations, *Journal of Computational Physics*, *227*(7), 3486 – 3514, doi:https://doi.org/10.1016/j.jcp.2007.02.006, predicting weather, climate and extreme events.
- Schlemmer, L., and C. Hohenegger (2014), The formation of wider and deeper clouds as a result of cold-pool dynamics, *Journal of the Atmospheric Sciences*, *71*(8), 2842–2858, doi:10.1175/JAS-D-13-0170.1.
- Schlemmer, L., and C. Hohenegger (2016), Modifications of the atmospheric moisture field as a result of cold-pool dynamics, *Quarterly Journal of the Royal Meteorological Society*, *142*(694), 30–42, doi:10.1002/qj.2625.
- Sherwood, S. C., D. Hernández-Deckers, M. Colin, and F. Robinson (2013), Slippery thermals and the cumulus entrainment paradox, *Journal of the Atmospheric Sciences*, *70*(8), 2426–2442, doi:10.1175/JAS-D-12-0220.1.

- Singh, M. S., and P. A. O’Gorman (2014), Influence of microphysics on the scaling of precipitation extremes with temperature, *Geophysical Research Letters*, *41*(16), 6037–6044, doi:10.1002/2014GL061222.
- Skamarock, W., J. Klemp, J. Dudhia, D. Gill, D. Barker, M. Duda, X.-Y. Huang, and W. Wang (2008), A description of the Advanced Research WRF version 3. NCAR technical note, *Tech. rep.*, NCAR/TN-475+STR, doi:10.5065/D68S4MVH.
- Stephens, G. L., T. L’Ecuyer, R. Forbes, A. Gettleman, J.-C. Golaz, A. Bodas-Salcedo, K. Suzuki, P. Gabriel, and J. Haynes (2010), Dreary state of precipitation in global models, *Journal of Geophysical Research: Atmospheres*, *115*(D24), n/a–n/a, doi:10.1029/2010JD014532, d24211.
- Stevens, B. (2007), On the growth of layers of nonprecipitating cumulus convection, *Journal of the Atmospheric Sciences*, *64*, 2916–2931, doi:10.1175/JAS3983.1.
- Stevens, B., and S. Bony (2013), What are climate models missing?, *Science*, *340*(6136), 1053–1054, doi:10.1126/science.1237554.
- Stirling, A. J., and J. C. Petch (2004), The impacts of spatial variability on the development of convection, *Quarterly Journal of the Royal Meteorological Society*, *130*(604), 3189–3206, doi:10.1256/qj.03.137.
- Stratton, R. A., and A. J. Stirling (2012), Improving the diurnal cycle of convection in GCMs, *Quarterly Journal of the Royal Meteorological Society*, *138*(666), 1121–1134, doi:10.1002/qj.991.
- Sun, Y., S. Solomon, A. Dai, and R. W. Portmann (2006), How often does it rain?, *Journal of Climate*, *19*(6), 916–934, doi:10.1175/JCLI3672.1.
- Tan, J., C. Jakob, and T. P. Lane (2013), On the identification of the large-scale properties of tropical convection using cloud regimes, *Journal of Climate*, *26*(17), 6618–6632, doi:10.1175/JCLI-D-12-00624.1.
- Tan, J., C. Jakob, W. B. Rossow, and G. Tselioudis (2015), Increases in tropical rainfall driven by changes in frequency of organized deep convection, *Nature*, *519*(7544), 451–454, letter.

BIBLIOGRAPHY

- Tiedtke, M. (1989), A comprehensive mass flux scheme for cumulus parameterization in large-scale models, *Monthly Weather Review*, *117*(8), 1779–1800, doi:10.1175/1520-0493(1989)117<1779:ACMFSF>2.0.CO;2.
- Tobin, I., S. Bony, and R. Roca (2012), Observational evidence for relationships between the degree of aggregation of deep convection, water vapor, surface fluxes, and radiation, *Journal of Climate*, *25*(20), 6885–6904, doi:10.1175/JCLI-D-11-00258.1.
- Tobin, I., S. Bony, C. E. Holloway, J.-Y. Grandpeix, G. Sèze, D. Coppin, S. J. Woolnough, and R. Roca (2013), Does convective aggregation need to be represented in cumulus parameterizations?, *Journal of Advances in Modeling Earth Systems*, *5*(4), 692–703, doi:10.1002/jame.20047.
- Tompkins, A. M. (2000), The impact of dimensionality on long-term cloud-resolving model simulations, *Monthly Weather Review*, *128*(5), 1521–1535, doi:10.1175/1520-0493(2000)128<1521:TIODOL>2.0.CO;2.
- Tompkins, A. M. (2001a), Organization of tropical convection in low vertical wind shears: The role of cold pools, *Journal of the Atmospheric Sciences*, *58*(13), 1650–1672, doi:10.1175/1520-0469(2001)058<1650:OOTCIL>2.0.CO;2.
- Tompkins, A. M. (2001b), Organization of tropical convection in low vertical wind shears: The role of water vapor, *Journal of the Atmospheric Sciences*, *58*(6), 529–545, doi:10.1175/1520-0469(2001)058<0529:OOTCIL>2.0.CO;2.
- Tompkins, A. M., and G. C. Craig (1998), Radiative-convective equilibrium in a three-dimensional cloud-ensemble model, *Quarterly Journal of the Royal Meteorological Society*, *124*(550), 2073–2097, doi:10.1002/qj.49712455013.
- Tompkins, A. M., and A. G. Semie (2017), Organization of tropical convection in low vertical wind shears: Role of updraft entrainment, *Journal of Advances in Modeling Earth Systems*, pp. n/a–n/a, doi:10.1002/2016MS000802.
- Torri, G., and Z. Kuang (2016), Rain evaporation and moist patches in tropical boundary layers, *Geophysical Research Letters*, *43*(18), 9895–9902, doi:10.1002/2016GL070893, 2016GL070893.

- Torri, G., Z. Kuang, and Y. Tian (2015), Mechanisms for convection triggering by cold pools, *Geophysical Research Letters*, *42*(6), 1943–1950, doi:10.1002/2015GL063227, 2015GL063227.
- Trenberth, K. E., and Y. Zhang (2018), How often does it really rain?, *Bulletin of the American Meteorological Society*, *99*(2), 289–298, doi:10.1175/BAMS-D-17-0107.1.
- Trenberth, K. E., Y. Zhang, and M. Gehne (2017), Intermittency in precipitation: Duration, frequency, intensity, and amounts using hourly data, *Journal of Hydro-meteorology*, *18*(5), 1393–1412, doi:10.1175/JHM-D-16-0263.1.
- Tsai, W.-M., and C.-M. Wu (2017), The environment of aggregated deep convection, *Journal of Advances in Modeling Earth Systems*, *9*(5), 2061–2078, doi:10.1002/2017MS000967.
- Wang, S., and A. H. Sobel (2011), Response of convection to relative sea surface temperature: Cloud-resolving simulations in two and three dimensions, *Journal of Geophysical Research: Atmospheres*, *116*(D11), n/a–n/a, doi:10.1029/2010JD015347.
- Wang, S., A. H. Sobel, and J. Nie (2016), Modeling the MJO in a cloud-resolving model with parameterized large-scale dynamics: Vertical structure, radiation, and horizontal advection of dry air, *Journal of Advances in Modeling Earth Systems*, *8*(1), 121–139, doi:10.1002/2015MS000529.
- Wang, W., C. Bruyère, M. Duda, J. Dudhia, D. Gill, M. Kavulich, K. Keene, H.-C. Lin, J. Michalakes, S. Rizvi, X. Zhang, J. Berner, and K. Smith (2014), Weather Research and Forecasting ARW version 3 modeling system user’s guide, *Tech. rep.*, NCAR/Mesoscale and Microscale Meteorology Division.
- Wang, Y., and C.-C. Wu (2004), Current understanding of tropical cyclone structure and intensity changes – a review, *Meteorology and Atmospheric Physics*, *87*(4), 257–278, doi:10.1007/s00703-003-0055-6.
- Willett, M. R., and M. A. Whitall (2017), A simple prognostic based convective entrainment rate for the Unified Model: description and tests, *Tech. Rep. Forecasting Research Technical Report No 617*, Met Office.

BIBLIOGRAPHY

- Wing, A. A., and K. A. Emanuel (2014), Physical mechanisms controlling self-aggregation of convection in idealized numerical modeling simulations, *Journal of Advances in Modeling Earth Systems*, *6*(1), 59–74, doi:10.1002/2013MS000269.
- Wing, A. A., K. Emanuel, C. E. Holloway, and C. Muller (2017), Convective self-aggregation in numerical simulations: A review, *Surveys in Geophysics*, pp. 1–25, doi:10.1007/s10712-017-9408-4.
- Yano, J.-I. (2014), Basic convective element: bubble or plume? A historical review, *Atmospheric Chemistry and Physics*, *14*(13), 7019–7030, doi:10.5194/acp-14-7019-2014.
- Yano, J.-I., and R. Plant (2012a), Finite departure from convective quasi-equilibrium: periodic cycle and discharge-recharge mechanism, *Quarterly Journal of the Royal Meteorological Society*, *138*(664), 626–637, doi:10.1002/qj.957.
- Yano, J.-I., and R. S. Plant (2012b), Convective quasi-equilibrium, *Reviews of Geophysics*, *50*(4), n/a–n/a, doi:10.1029/2011RG000378, rG4004.
- Yano, J.-I., M. Bister, v. Fuchs, L. Gerard, V. T. J. Phillips, S. Barkidija, and J.-M. Piriou (2013), Phenomenology of convection-parameterization closure, *Atmospheric Chemistry and Physics*, *13*(8), 4111–4131, doi:10.5194/acp-13-4111-2013.
- Zhang, C. (2005), Madden-Julian Oscillation, *Reviews of Geophysics*, *43*(2), n/a–n/a, doi:10.1029/2004RG000158, rG2003.
- Zhang, G., and N. A. McFarlane (1995), Sensitivity of climate simulations to the parameterization of cumulus convection in the Canadian Climate Centre general circulation model, *Atmosphere-Ocean*, *33*(3), 407–446, doi:10.1080/07055900.1995.9649539.
- Zuidema, P., G. Torri, C. Muller, and A. Chandra (2017), A survey of precipitation-induced atmospheric cold pools over oceans and their interactions with the larger-scale environment, *Surveys in Geophysics*, doi:10.1007/s10712-017-9447-x.

Appendices

Appendix A

Defining convective memory

A.1 Several ways of defining convective memory

Convective memory is not such a common phrase. To give intuition, convective memory can be viewed as the persistence of clouds in time. So it is related to cloud life cycle [*Davies et al.*, 2009]. If clouds tend to remain similar over time, then there is a strong convective memory. To be more precise, we define convective memory as the similarity between a current convective state and previous convective states. If it takes time for a shallow convective state to evolve into a deep convective state, there is more convective memory.

For further explanation on convective memory, let us focus on what it means for a numerical model. All numerical models live in a discretized world. Current Global Climate Models (GCM) have typical horizontal resolutions of the order of 100km, which makes it too coarse to resolve convective processes. Inside a single GCM grid cell, many processes that are relevant for convection are happening in reality. Because they take place in what would be seen as a unique GCM grid cell, they are said to occur at sub-grid scales. We will refer to them as micro-scale processes, or as the “microstate”. The GCM grid cell itself is simply seen by the GCM as a vertical profile. We can refer to this as the local effect, or the GCM grid cell processes, or the macro-scale processes, or else as the “macrostate”. Finally, some processes require the interaction between several GCM grid cells (dynamics, Rossby waves, Hadley cell,

etc...). We refer to these as large-scale processes, or “synoptic state”. Memory can arise from each of these 3 scales. So we can distinguish between microstate memory arising for the micro-scale structures, macrostate memory arising from the macro-scale structures, and synoptic state memory arising from synoptic-scale structures (see figure in the main text).

Most parameterization developments focus on understanding the relationship between the microstates of convection, and the macrostate of the atmosphere [Davies *et al.*, 2013b]. But we think it is also valuable to take into account fluctuations in the microstate for a given macrostate. This is what convective memory at small-scale is about.

A mathematical equivalent of the above definition of memory with similarity can be based on conditional probability. Convective memory is a measure of how much convection depends on its own history, rather than just depending on current “environmental” or external conditions (i.e. larger scale conditions).

First, one should select a length scale λ . At each time t , let us define a measure of the convective state $C(\lambda, t)$ and a measure of the “environmental” variables $\xi(\lambda, t)$. Now statistics based on Probability Distribution Functions (PDF) can be made with varying t . Convective memory is the dependence of the PDF of the convective state $C(\lambda)$ on its own history, for given environmental conditions $\xi(\lambda, t)$. If convection had no memory, the convective state $C(\lambda, t_0)$ would be conditionally independent from earlier convection $C(\lambda, t) \forall t < t_0$, for a given environmental state $\xi(\lambda, t_0)$.

Another definition of convective memory can be built upon the idea of non-equilibrium convection [Davies *et al.*, 2013a; Bechtold *et al.*, 2014]. Convection is a response of the atmosphere to solar forcing. If we had equilibrium convection, convection would be in phase with the solar forcing, and convective precipitation would peak around midday. In this case, there would be an instantaneous equilibrium between convection and its forcing. Because of the late trigger of deep convection in daytime, the response of convection is out of phase: this is non-equilibrium convection. Even though non-equilibrium convection is thought to be true, most parameterizations still rely on the assumption of quasi-equilibrium convection [Arakawa,

2004], following the pioneering convection scheme by *Arakawa and Schubert* [1974]. This long-standing issue in modern parameterizations has been mentioned by many studies, such as *Davies et al.* [2009]; *Raymond and Herman* [2011]; *Bechtold et al.* [2014].

The diurnal cycle issue relates to convective memory, because the more memory there is in the system, the more convection is delayed relatively to its forcing.

Convective memory gives more time coherence to cloud systems, which is likely to mean more spatial coherence to cloud systems. So convective memory is suspected to be intrinsically related to convective organisation.

A.2 A statistical definition of convective memory

This statistical approach on convective memory relates to conditional probability. With memory, the probability of the current state is different if it comes after one atmospheric state or another. In other words, when there is a thunderstorm with cold pools, it is likely that the next state of the atmosphere will also be a thunderstorm. And this is more likely than if we just had clear-sky conditions. That means the probability of the current convective state given the past states is different from the (raw) probability of the current state. If $C_{s,1}(t)$ is the convective state labeled 1 (for example thunderstorm) at instant t , and $C_{s,2}(t)$ is the convective state labeled 2 (for example precipitating cumulus) at instant t , and if $P(C_{s,1}(t) | C_{s,2}(t-1))$ is a conditional probability of the convective state 1 at instant t , given convective state 2 at instant $t-1$, we can express the conditional probability of the current convective state given a past convective state with Bayesian probability:

$$P(C_{s,1}(t) | C_{s,2}(t-1)) = \frac{P(C_{s,1}(t) \cap C_{s,2}(t-1))}{P(C_{s,2}(t-1))} \quad (\text{A.1})$$

If there were no memory, then the probabilities would not be conditional to the

previous states of the atmosphere, so that:

$$P\left(C_{s,i}(t) \mid C_{s,j}(t-1)\right) = P\left(C_{s,i}(t)\right) \quad \forall (i,j) \text{ convective states} \quad (\text{A.2})$$

This leads to a statistical way of defining a non-dimensional memory (M_{stat}), in which memory is an image of the difference between the conditional probability in the real system, and the conditional probability that we would have if there were no memory (the latter is given by equation A.2). As we want the memory to be non-negative, we use a square of that difference. Let N_i be the number of convective states we have. Thus, we can define:

$$M_{stat}(t) = \frac{1}{N_i^2} \sum_{i,j \text{ convective states}} \left(P(C_{s,i}(t) \mid C_{s,j}(t-1)) - P(C_{s,i}(t)) \right)^2 \quad (\text{A.3})$$

In this definition, the dimensionless convective memory M_{stat} is non-negative, and less than 1, which is sensible.

With this definition, if there is no “memory” (i.e. if $M_{stat} = 0$), convection only depends on environmental conditions – large-scale conditions. And as convective parameterizations don’t usually carry prognostic variables representing the sub-grid scale structures to compute the convective state, GCMs do not have convective memory in this sense.

Appendix B

Exploring convective self-aggregation with various WRF setups: what controls self-aggregation?

It is not straightforward to control how self-aggregation occurs in Cloud-resolving Models. In Chapter 2, we wanted to investigate different types of convective organisation. In particular, this implied to find ways to obtain self-aggregation or unorganised convection with the WRF model. The reference setup we used in WRF led to unorganised convection. Therefore we had to find a method to generate self-aggregation. We tried 16 different setups, all in Radiative-Convective Equilibrium (RCE) with fixed Sea Surface Temperature (SST) in WRF. The 10 most important ones are presented on Figure B.1.

These experiments show that increasing the domain size, increasing the SST, or decreasing the resolution only marginally help foster self-aggregation. Conversely, the turbulence scheme and the microphysical scheme play a key role in generating self-aggregation. With the 3D Turbulent Kinetic Energy (TKE) turbulence scheme available in WRF [*Skamarock et al.*, 2008; *Wang et al.*, 2014], there is unorganised convection in the RCE state. But the 3D Smagorinsky scheme allows self-aggregation to form. The physical mechanism behind this problem has been

APPENDIX B. EXPLORING CONVECTIVE SELF-AGGREGATION WITH VARIOUS WRF SETUPS: WHAT CONTROLS SELF-AGGREGATION?

explained by *Tompkins and Semie* [2017]. In essence, the 3D Smagorinsky scheme leads to more efficient horizontal mixing, which acts as a negative feedback on convective updrafts, making convection more difficult to occur. Favourite locations for convection are therefore preferentially chosen by a system which has to overcome a larger mixing-related barrier. Consequently, the 3D Smagorinsky scheme strongly favours self-aggregation.

Although this has never been reported before, the role of the microphysical scheme is also important to allow for self-aggregation. With the WSM6 scheme, self-aggregation is much more unlikely than with Thompson microphysics or Morrison microphysics. We speculate this may be related either (1) to precipitation efficiency, or (2) to the double-moment or single-moment character of the scheme. Further analysis would be required to determine the physical mechanisms explaining this sensitivity of self-aggregation to the microphysics.

With Morrison microphysics, vortices are expelled from the convective core, as seen on Figure B.1, although the RCE runs have no Coriolis force. This is an unexpected results by comparing with self-aggregated cases presented in the literature. Our result is consistent with the fact that the Morrison scheme tends to produce more clouds than other WRF microphysical schemes, so that cirrus clouds created by the self-aggregated core may persist longer. But the formation of relative vorticity remains to be explained.

The most aggregated state is obtained by combining the Thompson microphysical scheme and the 3D Smagorinsky turbulence scheme, with a coarser resolution. Since we wish to keep a finer resolution throughout the CRM experiments presented in the thesis, we used the Thompson and 3D Smagorinsky schemes for the self-aggregated case in Chapter 2. Note that shifting back to WSM6 microphysics is less detrimental for self-aggregation than shifting back to 3D TKE turbulence, as seen by comparing the 3-km resolution runs number 0180 and 0184 in Figure B.1. This may imply that the turbulence scheme has a more important role on self-aggregation than the microphysical scheme, even though we have also shown that both matter.

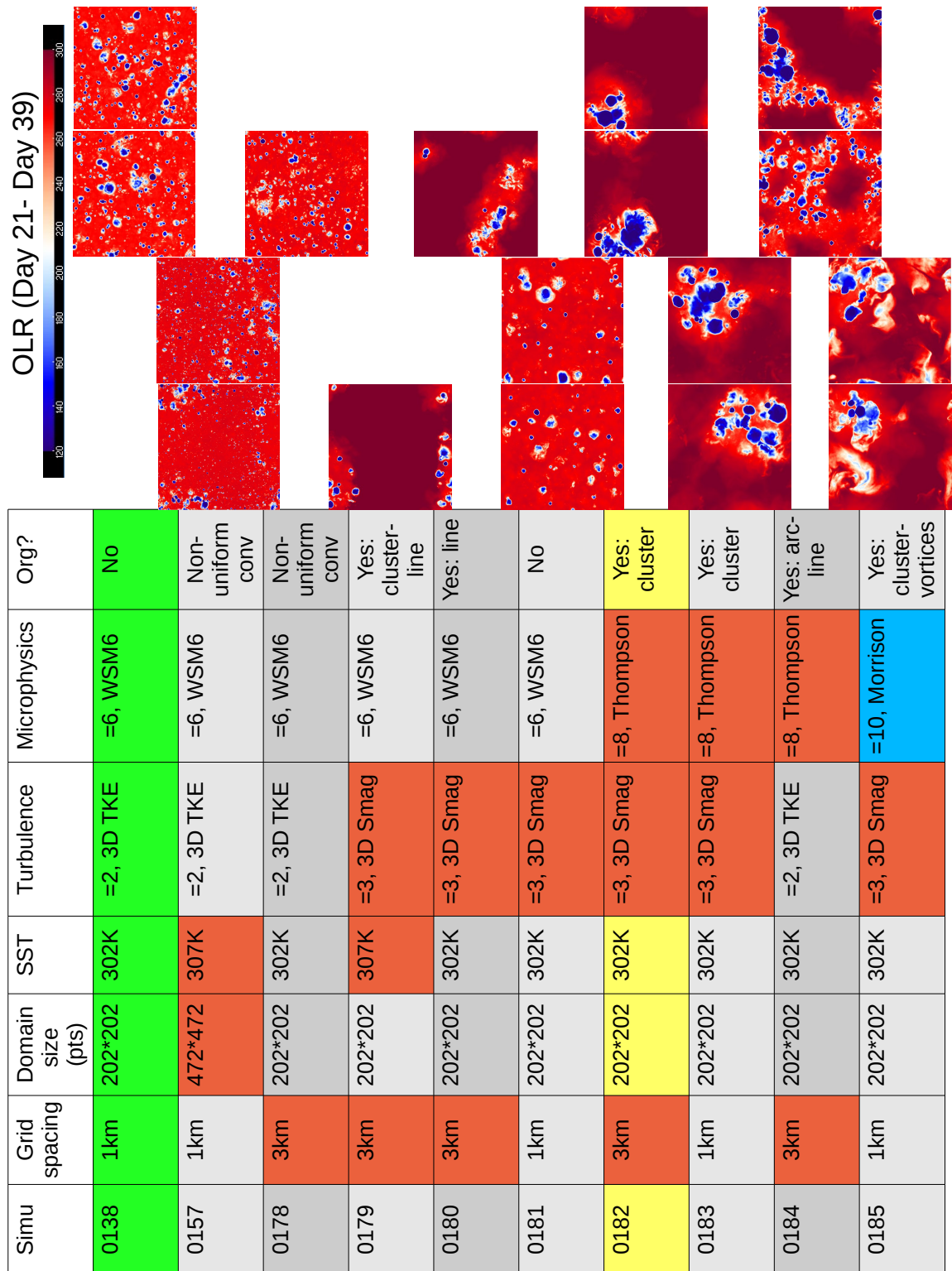


Figure B.1 Table of various WRF setups and their impact on self-aggregation. Each setup (each row) is defined by its grid spacing, domain size, Sea Surface Temperature (SST), turbulence scheme, microphysical scheme, as specified by the columns. The impact on convective organisation is (1) measured by two Outgoing Longwave Radiation (OLR) snapshots on the right-hand side: after 21 days of simulation, and after 39 days, and (2) summarised by a subjective comment in the last column. The two OLR snapshots for each setup are placed in staggered rows, either slightly more to the right, or slightly more to the left: the results for each setup are always horizontally aligned. Green highlighting shows the reference unorganised setup used in the whole thesis (e.g. Chapter 2). Red or blue highlighting indicates changes to this reference setup. Yellow highlighting indicates the most aggregated setup.

Appendix C

Statistics of water vapour, in particular for the transformation from dry to humid states

In Chapter 3, we tried to hold the domain-mean values (macrostate) of temperature, water vapour, and horizontal winds fixed in time, through a strong nudging method. However, this led to an instability of convection. In the process of trying to find an alternative method to keep the macrostate fixed but without triggering the instability, we tried to apply the nudging terms only on points which were not too humid, in order not to increase or decrease water vapour in saturated parts of the domain and in parts of the domain close to saturation. The idea was to avoid creating additional phase changes (liquid to gas, or gas to liquid) by the strong nudging terms. To achieve this, we had to analyse in a statistical way the water vapour structures from the RCE unorganised control run analysed throughout the thesis. An analysis of these statistical properties is presented here, notably the differences between the Probability Distribution Function (PDF) of water vapour mixing ratio in dry parts of the domain and humid parts of the domain, for various atmospheric levels.

The PDF of water vapour for the driest mean situations (domain-mean water vapour less than the 10th percentile) and the PDF for the most humid mean situations (domain-mean water vapour greater than the 90th percentile) are almost the

APPENDIX C. STATISTICS OF WATER VAPOUR, IN PARTICULAR FOR THE TRANSFORMATION FROM DRY TO HUMID STATES

same (Figure C.1). This implies that there is little difference in the statistics of the water vapour microstate with the RCE fluctuations. This result is confirmed by the fact that the value of the 10th percentile and the value of the 90th percentile are hardly distinguishable. Surprisingly, at many levels, the highest value of the water vapour PDF is larger in dry situations than in humid situations. This suggests that even if the mean situation is dry, there can exist some intensely humid points.

The skewness of the PDFs seems to evolve monotonically from a negative value near the surface to a positive value near the tropopause (Figure C.1). Near the surface, humid values seem to be normal and extreme values tend to be dry. This may come from the influence of dry downdrafts created by convection. In the high troposphere, we observe the opposite: dry values are the norm, while extremes values tend to be humid. This may stem from the influence of detrainment from deep convection. The critical altitude where the skewness of the PDFs becomes zero seems to be around 850 hPa. This is higher than the cloud base (~ 940 hPa), but is probably lower than shallow cloud top.

The variance of the water vapour PDF is much lower in terms of temporal evolution than in terms of spatial evolution. Indeed, the PDF of domain-mean water vapour evolving in time is much more peaked than the PDF of local values in either dry mean situations or humid mean situations (Figure C.2). This result is valid at all vertical levels, even though the PDF of domain-mean water vapour becomes larger in the higher troposphere. This means that the microstate is not easily perturbed by the RCE fluctuations: the RCE fluctuations may be negligible, in particular in the lower troposphere.

Computing the difference between the PDF for humid situations and the PDF for dry situations shows that the evolution of the PDF peak is as expected: shifted towards larger values of water vapour in more humid situations (Figure C.3).

To better understand what is necessary to bring for the dry conditions to become humid conditions, we define a transformation function $dq_{vapour}(q)$. It is built as the difference between the water vapour in dry situations (when the domain-mean water vapour is smaller than the 10th percentile) and the water vapour in humid situations (when the domain-mean water vapour is greater than the 90th percentile).

It is a function of q , the water vapour mixing ratio. To define the transformation function in a unique way, we rank the water vapour mixing ratio obtained based from small to large, thus constructing a list. We do so independently in each of the two situations. The transformation function is simply the difference between these two lists. For example, this function explains by how much water vapour the 10th percentile of the humid situation exceeds the 10th percentile of the dry situation.

The transformation function mostly takes positive values, as expected for a transformation from dry situations to humid situations, although there are negative values away from the water vapour PDF peak as well. The shape of the function is not simple, but it tends to always have a linearly decreasing part over a large range of values around the PDF peak. This implies that the relatively drier points of the dry situation gain more water vapour than the relatively more humid points, when it is transformed into a humid situation. It suggests a slight reduction of the microstate heterogeneities in a humid situation. Above the sub-cloud layer, there tends to be a secondary peak in the transformation function, making the situation non-monotonous. At some vertical levels, the function may look like the letter “W”. There is a large spread near the extreme values in some cases, which is not surprising. Overall, this shows that it is possible to find a statistical relationship between the microstate attached with dry states and the one attached with humid states.

PDF of 2D water vapour fields for mean >90th percentile and mean <10th percentile, at different pressure levels

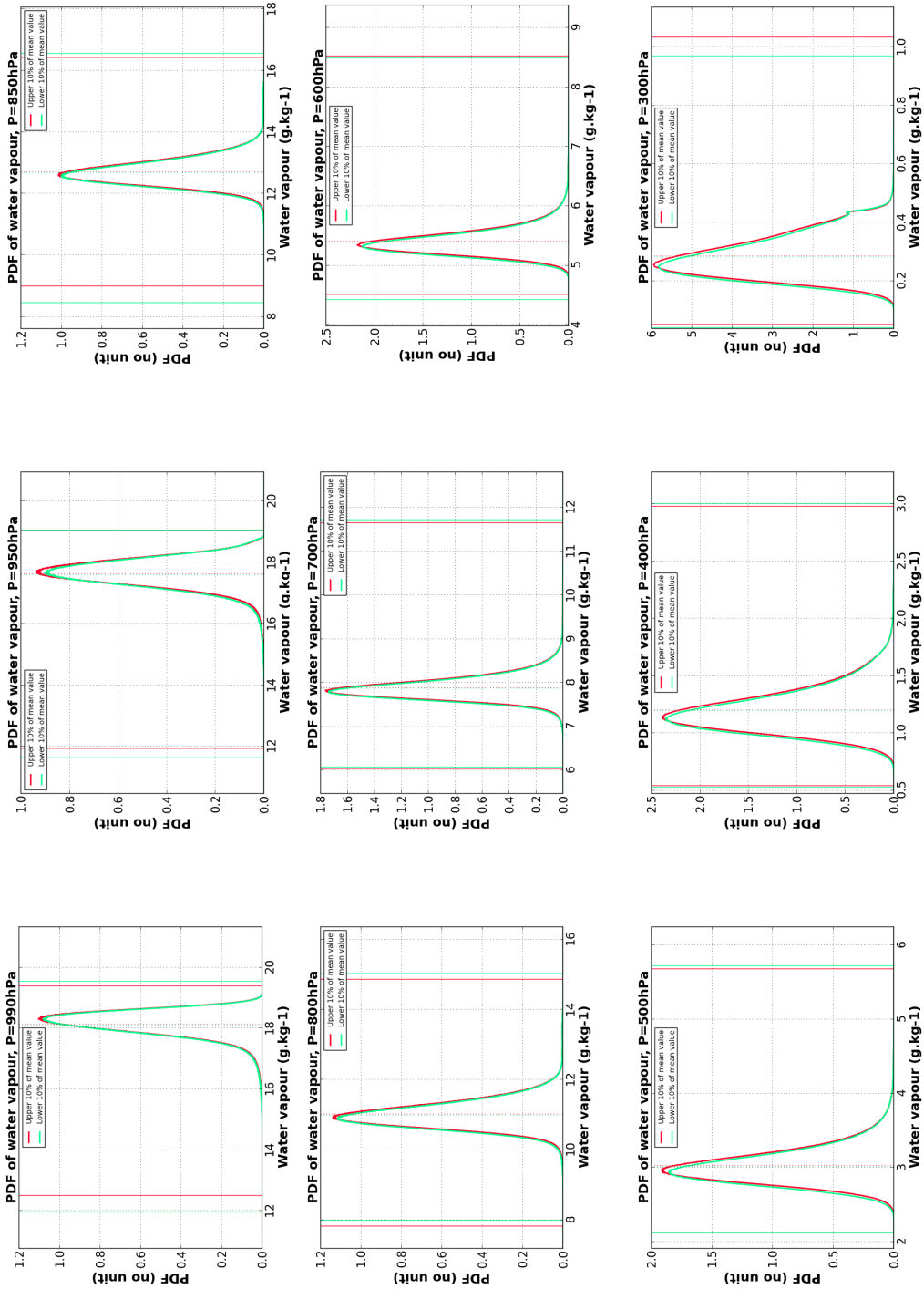


Figure C.1 PDFs of water vapour fields at different pressure levels (different panels), for all instants when the horizontal mean is higher than the 90th percentile (red) or lower than the 10th percentile (green) of the time series (based on the last 50 days of RCE unorganised control run). The vertical solid red (resp. green) lines indicate the minimum and maximum values of the water vapour fields when the mean is higher than the 90th percentile (resp. when the mean is lower than the 10th percentile). The vertical dotted red (resp. green) lines show the value of the 90th percentile (resp. 10th percentile) of the time series of horizontal mean water vapour (in practice they are almost co-located). The scales on the x-axis (water vapour range) and y-axis (normalised PDF) are different in each panel.

PDF of 2D water vapour fields for mean > 90th percentile and mean < 10th percentile, at different pressure levels

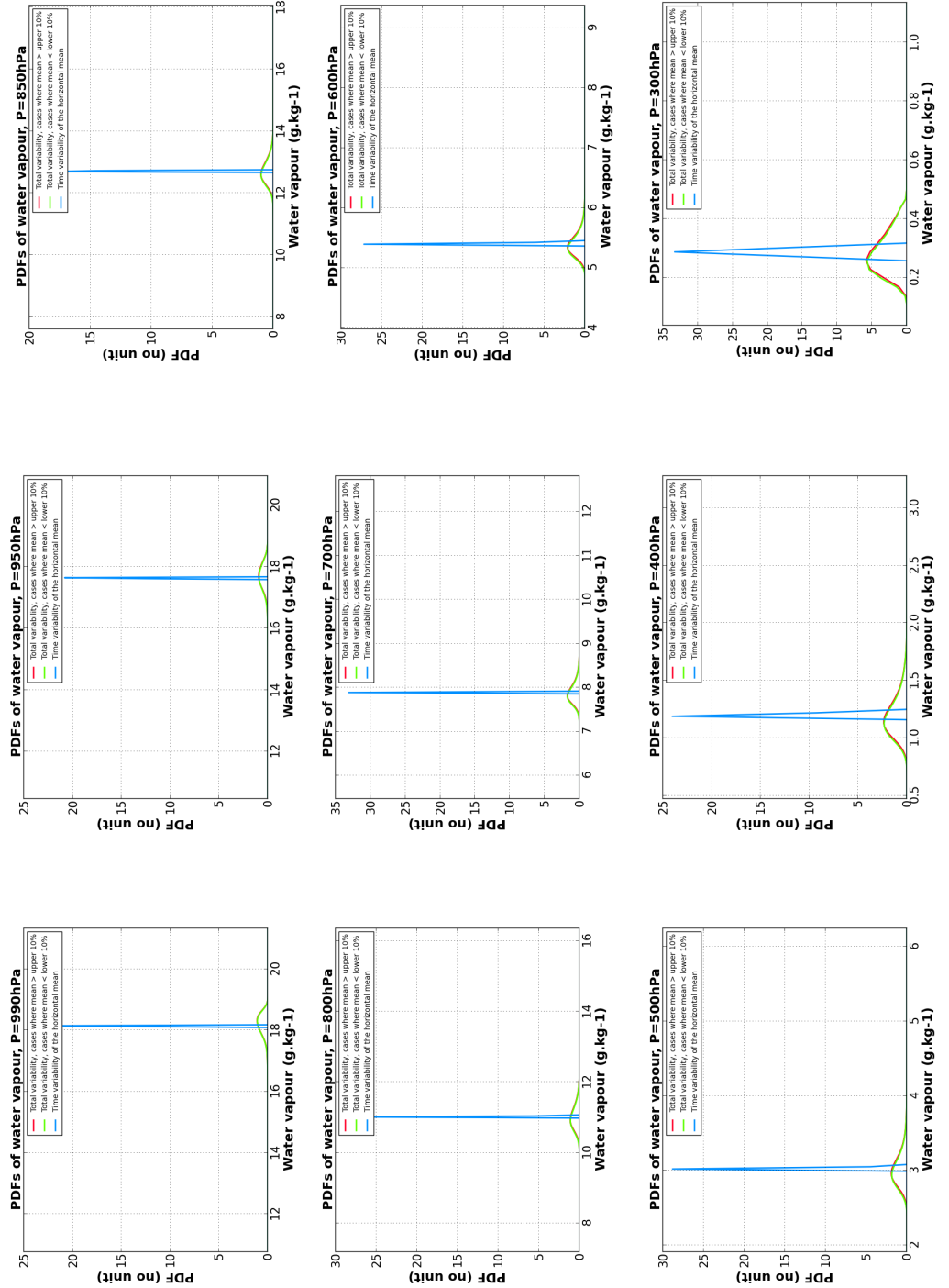


Figure C.2 PDFs of water vapour fields at different pressure levels, based on the last 50 days of RCE unorganised control run. The red and green PDFs are the same as on Figure C.1. The blue PDF is calculated on the time series of the horizontal mean water vapour mixing ratio at that pressure level. The horizontal mean does not vary much with time compared to the spatial variations.

Difference between PDF of 2D water vapour fields for mean >90th percentile and mean <10th percentile, at different pressure levels

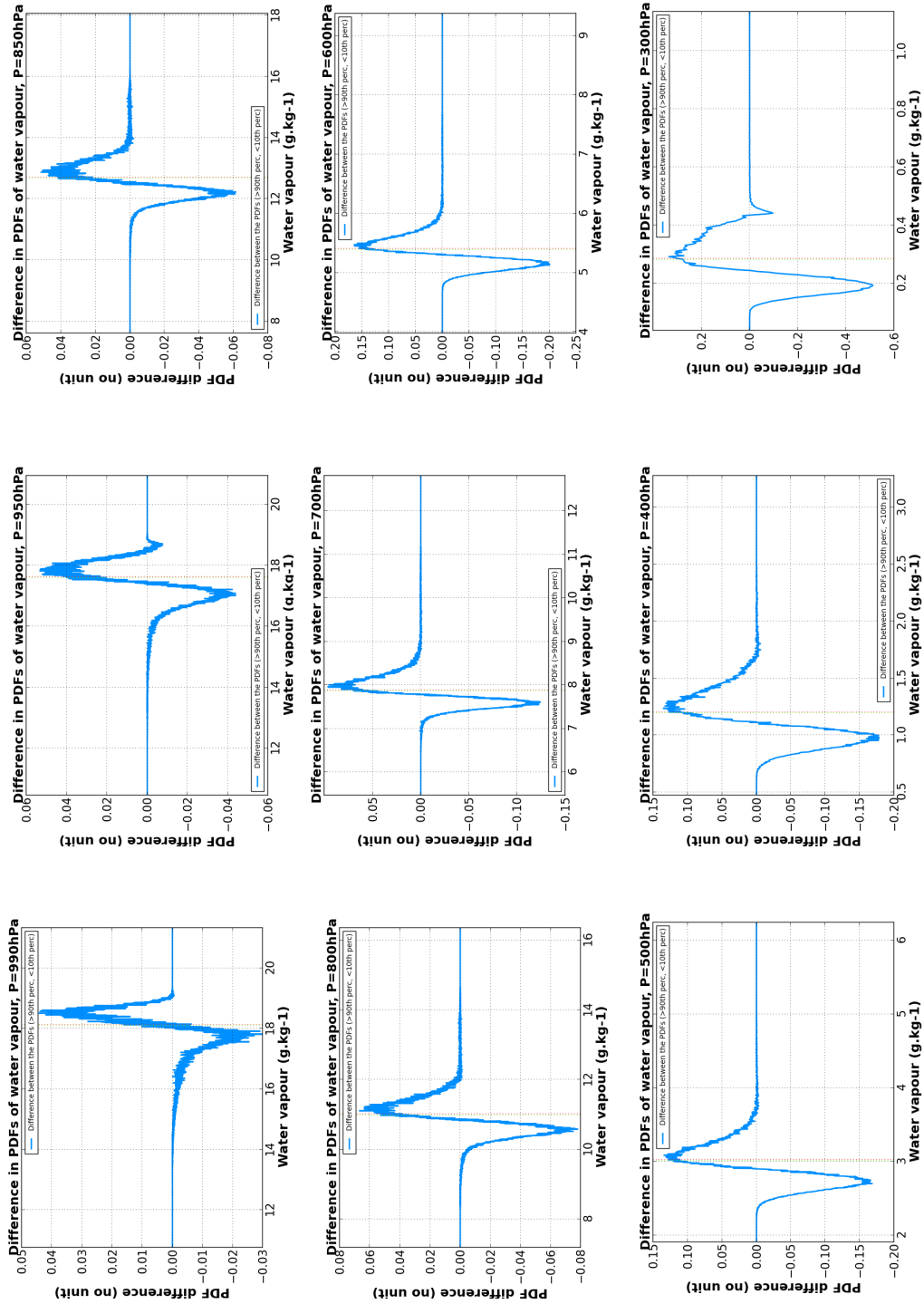


Figure C.3 Difference between the two PDFs of water vapour mixing ratio field, calculated for all instants when the horizontal mean is higher than the 90th percentile on the one hand, and when the horizontal mean is lower than the 10th percentile on the other hand, at different pressure levels (based on the last 50 days of RCE unorganised control run). In other words, it is the difference between the red and the green PDFs from Figure C.1. The number of bins we choose to compute the PDFs influences somewhat the amount of noise that appears.

$dq_vapor(q)$ transforming the mean dry states (<10th perc.)
to the mean humid states (>90th perc.)

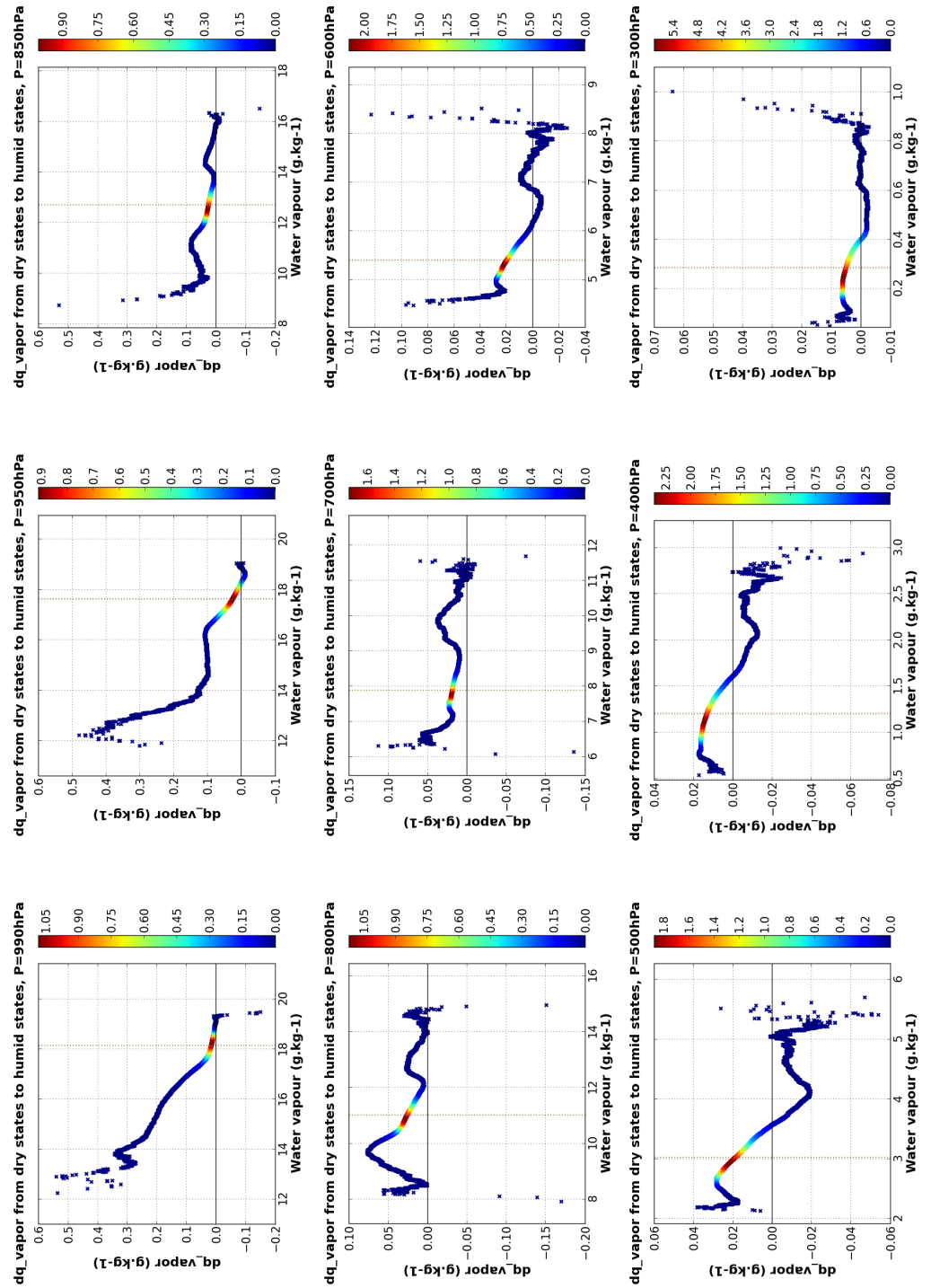


Figure C.4 Transformation function $dq_vapor(q)$ to go from the relatively "dry" states (x,y,t variations for a mean value <10th percentile) to the relatively "humid" states (x,y,t variations for a mean value >90th percentile). The x,y,t variations were used to build two single-dimension ordered lists, one for the dry states and one for the humid states. dq_vapor represents the difference between the humid ordered list and the dry ordered list of points. The x-axis q is the mean water vapour mixing ratio between the values in the two ordered lists. This was done at different pressure levels (different panels). The colours indicate the PDF of the x-axis, so that the density of points in the scatter plots becomes obvious. Thus, the transformation function is just an abstract representation of a shift from an equilibrated 2D dry state to an equilibrated 2D humid state.

Appendix D

Table of homogenisation experiments performed in WRF in Chapter 2

Table D.1 List of homogenisation experiments performed in 3D on different variables: "single" set impact and "double" set impact. The model is restarted from different horizontally homogenised conditions.

<i>Simulation</i>	<i>Homogenised variables</i>	<i>Type of experiment</i>
3D-CONTROL		
3D-Blank	<i>none</i>	
3D- u	3D winds (u,v,w) u	single set
3D- q_v	water vapour mixing ratio q_v	single set
3D- θ	potential temperature θ	single set
3D- q_{cond}	all condensates (q_c, q_r, q_i, q_s, q_g)	single set
3D- $q_v + \theta$	water vapour mixing ratio q_v , and potential temperature θ	double set
3D- u + θ	3D winds (u,v,w), and potential temperature θ	double set
3D- u + q_v	3D winds (u,v,w), and water vapour mixing ratio q_v	double set

APPENDIX D. TABLE OF HOMOGENISATION EXPERIMENTS PERFORMED IN WRF

Table D.2 List of 3D homogenisation experiments performed by layers. The sub-cloud layer corresponds to the layer between the surface and 940hPa (600m). Mid layer refers to the layer between 940hPa and 700hPa. And high layer refers to the layer between 700hPa and the tropopause.

<i>Simulation</i>	<i>2D or 3D</i>	<i>Homogenised variables</i>	<i>Homogenised layer</i>
3D-Qvap+Theta	3D	q_v, θ	All
Qvap+Theta-Subc	3D	q_v, θ	sub-cloud
Qvap+Theta-Mid	3D	q_v, θ	mid
Qvap+Theta-High	3D	q_v, θ	high
Qvap+Theta-1st	3D	q_v, θ	1st model layer
3D-Theta	3D	θ	All
Theta-Subc	3D	θ	sub-cloud
Theta-Mid	3D	θ	mid
Theta-High	3D	θ	high
3D-Qvap	3D	q_v	All
Qvap-Subc	3D	q_v	sub-cloud
Qvap-Mid	3D	q_v	Mid
Qvap-High	3D	q_v	High

Table D.3 List of 3D homogenisation experiments on layers performed on specific areas of the domain. When homogenisation is performed only *below* the mean values: the horizontal mean is computed for each variable, at each vertical level, and only the values *below* the mean are averaged out together, values *above* the mean are left untouched. When homogenisation is performed only *above* the mean values, the same process applies but on values *above* each horizontal mean.

<i>Simulation</i>	<i>2D or 3D</i>	<i>Homogenised variables</i>	<i>Homogenised layer</i>	<i>Specific areas?</i>
Qvap+Theta-Subc	3D	q_v, θ	sub-cloud	
Qvap+Theta-Subc-be	3D	q_v, θ	sub-cloud	below mean values only
Qvap+Theta-Subc-ab	3D	q_v, θ	sub-cloud	above mean values only
Theta-Subc	3D	θ	sub-cloud	
Theta-Subc-be	3D	θ	sub-cloud	below mean values only
Theta-Subc-ab	3D	θ	sub-cloud	above mean values only
Qvap-Subc	3D	q_v	sub-cloud	
Qvap-Subc-be	3D	q_v	sub-cloud	below mean values only
Qvap-Subc-ab	3D	q_v	sub-cloud	above mean values only

Table D.4 List of homogenisation experiments performed in 2D. The model is restarted from different horizontally homogenised conditions.

<i>Simulation</i>	<i>2D or 3D</i>	<i>Homogenised variables</i>	<i>Type of experiment</i>
2D-Ctrl	2D		
2D-Blank	2D	<i>none</i>	
2D-U	2D	U	Single set
2D-UVW	2D	U, V, W	Single set
2D-Qvap	2D	q_v	Single set
2D-Theta	2D	θ	Single set
2D-HyMet	2D	q_c, q_r, q_i, q_s, q_g	Single set
2D-Base	2D	U, V, W, q_v	Additional impact to base
2D-Base+Theta	2D	U, V, W, q_v, θ	Additional impact to base
2D-Base+HyMet	2D	U, V, W, $q_v, q_c, q_r, q_i, q_s, q_g$	Additional impact to base
2D-Base+PH	2D	U, V, W, q_v, ϕ	Additional impact to base
2D-Base+MU	2D	U, V, W, q_v, μ_d	Additional impact to base
2D-Base+TKE	2D	U, V, W, q_v , TKE	Additional impact to base
2D-Base+Theta+HyMet	2D	U, V, W, $q_v, \theta, q_c, q_r, q_i, q_s, q_g$	Maximum effects
2D-AllProg	2D	U, V, W, $q_v, \theta, q_c, q_r, q_i, q_s, q_g, \phi, \mu_d$, TKE	Maximum effects

